UNIVERSITY of TASMANIA

Targeting microtubule alterations in axon degeneration and Alzheimer's disease

by

Kelsey Hanson

BBiotechMedRes (Hons)

Submitted in fulfilment of the requirement for the

Degree of Doctor of Philosophy

Wicking Dementia Research and Education Centre

University of Tasmania

15th February 2019

COPYRIGHT STATEMENT

This thesis contains no material which has been accepted for a degree or diploma by the Institute or any other University or institution, except by way of background information duly acknowledged in the thesis, and to the best of my knowledge and belief no material previously published or written by another person except where due acknowledgement is made in the text of the thesis, nor does the thesis contain any material that infringes copyright.

Kelsey Hanson

STATEMENT OF AUTHORITY OF ACCESS

Kelsey Hanson

STATEMENT OF CO-AUTHORSHIP

The following people and institutions contributed to the publication of work undertaken as part of this thesis:

Candidate: Kelsey A. Hanson, Wicking Dementia Research and Education Centre, University of Tasmania

Author 2: Nan Tian, Wicking Dementia Research and Education Centre, University of Tasmania

Author 3: James C. Vickers, Wicking Dementia Research and Education Centre, University of Tasmania

Author 4: Anna E. King, Wicking Dementia Research and Education Centre, University of Tasmania

Publication entitled: **The HDAC6 inhibitor trichostatin A acetylates microtubules and protects axons from excitotoxin-induced degeneration in a compartmented culture model**

Part of the work presented in this thesis (chapter 4 and 5) has been published for publication, and the PDF is included in appendix 8.3.

The candidate (75%) was the primary author and contributed to laboratory work, data analysis and manuscript preparation. Author 2 (10%) assisted with data collection, and development of the project. Author 3 (5%) contributed to the conception and development of the project and author 4 (10%) contributed to the conception and development of the project and assisted with data interpretation. All authors contributed to manuscript refinement and presentation.

We the undersigned agree with the above stated "proportion of work undertaken" for each of the above published (or submitted) peer-reviewed manuscripts contributing to this thesis:

Signed:_____

Associate Professor Anna King,	Professor Ben Canny
Primary supervisor	Head of School
Wicking Dementia Research and Education Centre	School of Medicine
Date: 15.02.2019	Date: 21/02/2019

STATEMENT OF ETHICAL CONDUCT

The research associated with this thesis abides by the international and Australian codes on human and animal experimentation, the guidelines by the Australian Government's Office of the Gene Technology Regulator and the rulings of Safety, Ethics and Institutional Biosafety Committees of the University.

Kelsey Hanson

PUBLICATION CONTRIBUTIONS DURING CANDIDATURE

Kelsey Hanson, Nan Tian, James Vickers, and Anna King (2018) The HDAC6 inhibitor trichostatin A acetylates microtubules and protects axons from excitotoxin-induced degeneration in a compartmented culture model. *Frontiers in Neuroscience*. 12: 872

Adele Woodhouse, Carmen M Fernandez-Martos, Rachel AK Atkinson, **Kelsey Hanson**, Jessica M Collins, Aidan O'Mara, Nico Terblanche, Marcus Skinner, James C Vickers and Anna E King (2018) Repeat propofol anesthesia does not exacerbate plaque deposition or synapse loss in the APP/PS1 transgenic mouse model of Alzheimer's disease. *BMC Anesthesiology*. 18:47

Anna King, Anna Brain, **Kelsey Hanson**, Justin Dittmann, James Vickers and Carmen Fernandez-Martos (2018) Disruption of leptin signalling in a mouse model of Alzheimer's disease. *Metabolic Brain Disease*. 33(4): 1097-1110

SUMMARY

Microtubules are a key cytoskeletal element within the axon, which provide structure, shape and polarity to the neuron. They are important in numerous cellular processes, as they provide the platform for intracellular transport; moving organelles and secretory vesicles to synaptic terminals and are a major constituent for cell division. Disruption to microtubules has been implicated in a number of neurodegenerative diseases including Alzheimer's disease (AD), Parkinson's disease and amyotrophic lateral sclerosis, which involve progressive loss of structure and function of neurons, leading to neuronal death in different regions of the nervous system. Although each of these diseases display different symptoms, some features may be shared across neurodegenerative diseases, such as axon degeneration, an active cellular process which can be initiated in pathological conditions resulting in synaptic impairment. Microtubule alterations have been implicated in mechanisms of axon degeneration. However, the alterations to microtubules in pathological conditions and the potential of modulating microtubules as a therapeutic target is currently unrealised. This thesis has examined the effect of microtubule stabilisation in a mouse model of AD and has investigated the changes to microtubules and microtubule-associated proteins within the axon following an excitotoxic insult, a pathological mechanism involved in several neurodegenerative diseases and injury. To examine microtubule alterations following excitotoxic insult, a compartmented primary mouse neuronal cell culture model was utilised and live imaging was used to monitor axon degeneration. Examination of alterations to microtubule associated proteins (MAPs) demonstrate that levels of tau and CRMP2 were significantly ($p<0.05$) increased after excitotoxic insult, but MAP1B levels were unchanged. Modifying the phosphorylation state of MAPs, using the PP2A inhibitor sodium selenate, which regulates their binding to microtubules, did not significantly affect the degeneration of axons. Examination of microtubule post-translational modifications demonstrated significantly ($p<0.05$) decreased

acetylated tubulin levels, specifically in axons, whereas tyrosinated tubulin levels were unchanged. Trichostatin A, an HDAC6 inhibitor, was used in vitro to determine whether preventing loss of acetylated tubulin protects against axon degeneration. Primary cortical neurons treated with trichostatin A had significantly ($p<0.05$) increased acetylated tubulin levels within axons. Furthermore, live imaging results confirmed that neurons treated with trichostatin A had significantly ($p<0.05$) decreased axon degeneration following an excitotoxic insult. Previous studies have demonstrated a positive effect of microtubule stabilisation in mouse models of tau pathology. However, AD involves deposition of amyloid plaques in addition to tau pathology and the effect of microtubule stabilisation on amyloid and axon pathology in AD models is unknown. Therefore, an AD mouse model of amyloid deposition, the APP/PS1 mouse model was treated with the microtubule stabilising agent, epothilone D to determine the effect on plaque deposition, dystrophic neurite pathology and synapse alterations. Behavioural testing demonstrated significant changes in tests associated with anxious activity in APP/PS1 mice following epothilone D treatment. Biochemical analysis demonstrated that epothilone D had effects on the cytoskeleton with a significant ($p<0.05$) decrease in levels of phosphorylated neurofilaments in both the neocortex and hippocampus. However, epothilone D did not alter amyloid deposition or neurite dystrophy within the mouse neocortex. Together these results suggest that microtubule instability may be a key factor in axon degeneration pathways, and pharmacological manipulation of microtubules is a promising therapeutic target to prevent axon degeneration.

ACKNOWLEDGEMENTS

Firstly, I would like to express my sincere gratitude to my primary supervisor Associate Professor Anna King for her continuous support of my PhD study and related research, for her patience, motivation and immense knowledge. Her guidance helped me in all the time of research and writing of my thesis. I could not have imaging having a better supervisor and mentor for my PhD candidature.

I would also like to thank the rest of my PhD supervisory team: Professor James Vickers and Dr Carmen Fernandez-Martos for their insightful comments and encouragement, and also for teaching me laboratory techniques, which without, I would be unable to complete my research.

My sincere thanks also goes to Dr Rachel Atkinson, Dr Kimberly Stuart, Dr Nan Tian, Dr Jessica Collins, Dr Sharn Perry, Dr Jenna Ziebell, Dr Jacqueline Leung and Graeme McCormack who provided me with support which made it possible to conduct this research.

I thank my fellow Wicking PhD students for the stimulating discussions and the endless fun we have had in the last four years.

Last but not least I would like to thank my wonderful family: my parents and my sister for their unwavering support throughout writing this thesis and my life in general.

TABLE OF CONTENTS

ABBREVIATIONS

Adenosine diphosphate	ADP
Adenosine triphosphate	ATP
Alpha tubulin acetyltransferase 1	αTAT1
α-amino-3-hydroxy-5-methyl-4-isoxazolepropionic acid	AMPA
Alzheimer's disease	AD
Apolipoprotein E	APOE
Amyloid Precursor Protein	APP
Beta amyloid	Aβ
Calcium	Ca^{2+}
Ca^{2+}/calmodulin-dependent protein kinase II	CaMKII
Central Nervous System	CNS
Collapsin response mediator protein	CRMP
Cyclin-dependent kinase 1	cdk1
Cyclin-dependent kinase 5	cdk5
Cytosolic carboxypeptidase 1	CCP1
Cytosolic carboxypeptidase 5	CCP5
Enzyme-linked immunosorbent assay	ELISA
Delta-tubulin	Δ2
Epothilone D	Epo D
Food and Drug Administration	FDA
Glycogen synthase kinase 3 beta	GSK3β
Guanosine triphosphate	GTP
Histone deacetylase 6	HDAC6
Ionized calcium binding adaptor molecule 1	Iba1
Kainic acid	KA
Kilo daltons	kDa
Microtubule-associated protein	MAP
Microtubule-associated protein 1A	MAP1A
Microtubule-associated protein 1B	MAP1B
Microtubule-associated protein 2	MAP2
Mild cognitive impairment	MCI
Mitogen-activated extracellular signal-regulated kinase	MAPK
N-methyl-D-aspartate	NMDA
Neurofilament light protein	NFL

Phosphorylated neurofilament protein	SMI312
Plus-end tracking proteins	+TIPs
Post-translational modification	PTM
Presenilin 1	PS1
Protein phosphatase 2	PP2A
Sirtuin 2	SIRT2
Standard Error Mean	SEM
Trichostatin A	TSA
Tubulin-tyrosine ligase	TTL
Tubulin-tyrosine ligase-like protein 6	TTLL6
Wallerian-like degeneration slow	Wlds
Wildtype	WT

Chapter 1

Literature Review

1 LITERATURE REVIEW

1.1 MICROTUBULES AS A THERAPEUTIC TARGET IN ALZHEIMER'S DISEASE AND NEURODEGENERATION

1.1.1 Introduction

Microtubules are part of the cytoskeleton and are vital to maintaining cellular function as they determine cell polarity, and are involved in gene expression and regulation, cell division and axon transport. They play an essential role in the development of the nervous system, where the dynamics of tubulin are fine-controlled by associated proteins. Alterations to microtubules have been documented in several neurodegenerative diseases and injury. In particular, their role in axon degeneration has been well-reported (Dubey et al., 2015; Tang-Schomer et al., 2010), although the mechanisms of microtubule alterations are less clear. Recent evidence has suggested that microtubules may be an important therapeutic target in Alzheimer's disease (AD) and other neurodegenerative conditions, particularly those involving axon degeneration (Eira et al., 2016; Pachima et al., 2016; Zhang et al., 2018). This thesis examines the potential of microtubules as a therapeutic target in AD and axon degeneration.

1.2 TARGETING MICROTUBULES IN ALZHEIMER'S DISEASE

1.2.1 Alzheimer's disease

Alzheimer's disease is a progressive neurodegenerative disease with an increasing prevalence across the global population (Qiu et al., 2009). Alzheimer's disease was first described in 1907 and in the 100 years hence, little progress has been made in understanding the driving mechanisms of the disease. Familial AD accounts for <10% of AD cases, however, there is a

large genetic component to sporadic AD with the apolipoprotein E (APOE)-e4 allele being the strongest known genetic risk factor, and drives the early development of the disease (Liu et al., 2013). Other risk factors for developing sporadic AD frequently seen in people over 65 years of age, are age-related alterations to the brain, such as atrophy (Habes et al., 2016), inflammation and reactive oxygen species (Kaur et al., 2015; Manoharan et al., 2016; Wyss-Coray and Rogers, 2012). Brain injuries have also been proposed to increase AD risk (Lye and Shores, 2000).

Alzheimer's disease pathology, particularly neurofibrillary pathology, follows a specific pattern of development in brain regions, initiating in the transentorhinal region and distributing toward the hippocampus and the occipito-temporal region (Braak et al., 2006). It is unclear why particular regions are more vulnerable to pathology early in disease, whilst other regions are unaffected until very late in disease progression, although it is suggested that areas of high plasticity are more at risk (Arendt et al., 1998). On an anatomical level, AD is characterised by shrinkage of hippocampal and cerebral regions, especially posterior cortical areas (Serrano-Pozo et al., 2011). On a cellular level, AD is characterised by two major pathological hallmarks: amyloid plaque pathology and tau neurofibrillary tangles (Alzheimer, 1907).

1.2.2 Pathology and treatment of Alzheimer's disease

The pathological hallmarks of AD mainly involve abnormal protein aggregation which disrupts normal function of the brain. Whilst the two main pathological hallmarks are amyloid beta (Aβ) plaques and tau neurofibrillary tangles, other features also present, include dystrophic neurites, synapse loss, and gliosis (Serrano-Pozo et al., 2011; Spires-Jones and Hyman, 2014). There is considerable debate about what triggers the progression of these types

of pathology and how they are linked. Current hypotheses propose amyloid deposition and tau alterations as the drivers of neurodegeneration in AD and most therapeutic agents are based on targeting amyloid and tau pathology, although more work is needed to identify the events occurring in early stages of disease. Since the initiating events usually occur before clinical onset of symptoms, these early changes are difficult to define and may require use of biomarkers.

Although numerous clinical trials targeting several different cellular mechanisms have been conducted, there are currently no disease modifying therapeutics for AD and the only US Food and Drug Administration (FDA)-approved drugs for AD provide symptom relief and include memantine and the cholinesterase inhibitors; tacrine, donepezil, rivastigmine, and galantamine (Anand et al., 2014; Folch et al., 2016). They act by modifying neurotransmitter levels, by decreasing acetylcholine breakdown, and therefore enhancing cholinergic neurotransmission.

Amyloid pathology

The amyloid cascade hypothesis, one of the most postulated theories of AD pathogenesis, proposes that amyloid deposition is the main driver of disease onset and progression (Hardy and Higgins, 1992). This hypothesis advocates that pathological changes associated with AD occur downstream of extracellular Aβ accumulation. The hypothesis is supported by research which has focused on therapeutic strategies, which target amyloid pathology (Barage and Sonawane, 2015; Fernandez et al., 2014; Kim et al., 2007; Selkoe and Hardy, 2016) and familial genetics cases. The amyloid cascade hypothesis is also supported by the APOE risk genes, which is thought to play a role in clearance of Aβ (Robert et al., 2017; Verghese et al.,

2013). The presence of amyloid plaques is used to confirm diagnosis on post-mortem examination, making amyloid deposition a defining feature of AD.

Amyloid plaque deposition is thought to result from altered cleavage of the transmembrane amyloid precursor protein (APP) by beta (BACE1) and gamma secretases. The normal role of APP is not completely known but it is thought to regulate synapse formation and play a role in neuroprotection and neuroplasticity (Plummer et al., 2016; Priller et al., 2006). Beta amyloid is the 40-42 kDa peptide cleavage product of APP, which is deposited into the extracellular space and aggregates to form Aβ plaques (Glenner and Wong, 1984). Mice deficient in BACE1 have a normal phenotype and abolished Aβ generation (Luo et al., 2001; Yan et al., 2014). Beta amyloid, in either of its soluble or insoluble forms is likely involved in toxicity or physical stress to neurons (Liu et al., 2004b; Zhang et al., 2012b). The cellular site of the cleavage of APP is unclear, although it is thought to occur at several sites within the cell. Secretase cleavage of APP occurs mostly within the Golgi complex or the plasma membrane, but the BACE1 cleavage may be localised mainly to endosomes (Koo and Squazzo, 1994; Lammich et al., 1999). It has been hypothesised that the time spent in specific cellular locations can affect APP processing into Aβ peptides, suggesting that alterations in cellular transport processes, including microtubule-dependent transport, can affect Aβ production (Gotz et al., 2006). Another potential cause of amyloid plaque deposition is reduced clearance of Aβ. The clearance of Aβ can be through non-enzymatic or enzymatic mechanisms (Yoon and Jo, 2012). Non-enzymatic pathways include microglial phagocytosis whereas enzymatic pathways, such as neprilysin, are directly involved in the clearance process (Yoon and Jo, 2012).

Beta amyloid is also removed into the cerebrospinal fluid (CSF) through the glymphatic system, and normal levels of Aβ in CSF are 8.3% (Bateman et al., 2006). Although familial

AD is likely associated with altered Aβ production, it is hypothesised that sporadic AD results from reduced clearance rates (Lee and Landreth, 2010; Weller et al., 2000).

Therapeutics targeting amyloid pathology

Due to the amyloid cascade hypothesis, amyloid pathology is the most investigated therapeutic target for AD (Beyreuther and Masters, 1991; Hardy and Higgins, 1992; Selkoe, 1991) with strategies targeting both the decreased production and increased clearance of Aβ from the brain. There have been a number of high profile immunotherapy trials in recent years using antibodies to enhance the clearance of Aβ including Aducanumab (Sevigny et al., 2016), Solanezumab (Doody et al., 2014; Siemers et al., 2016) and Bapineuzumab (Ketter et al., 2017; Salloway et al., 2014; Vandenberghe et al., 2016). Each of these drugs target different forms or epitomes of Aβ. Although some efficacy for amyloid removal has been shown, to date, there is no convincing data demonstrating an effect on cognitive decline (Fiala et al., 2018; Mo et al., 2017).

Beta-secretase inhibitors are another therapeutic strategy that have been proposed to block the abnormal cleavage pathway of APP, therefore decreasing Aβ production and reducing disease progression (Menting and Claassen, 2014). In mouse model studies of AD, BACE1 inhibitors reduce Aβ pathology and rescue cognitive decline (Ghosh and Osswald, 2014), however in clinical trials for both AD patients and pre-symptomatic AD patients, concerns about the toxicity of β-secretase inhibitors due to links with cardio toxicity and inhibition of cytochrome enzymes have been raised (Vassar, 2014).

It has also been proposed that therapeutic intervention could be provided to protect against the potential downstream effects of amyloid pathology (discussed below) including neuron,

synapse and axon loss. Microtubule manipulation is a possible target for this type of intervention. For example, microtubule stabilisation could protect against transport impairment and axon pathology (Varidaki et al., 2018). Similarly, microtubule stabilisation could be used to protect vulnerable synapses (Zajkowski et al., 2015). More specifically, tau-dependent microtubule severing by TTLL6 and spastin induces synaptic damage by Aβ oligomers (Zempel et al., 2013), suggesting that amyloid toxicity is able to cause alterations to microtubules, which can lead to synaptic damage. Dysregulation of microtubule stability also impairs connectivity in primary neuronal networks (Verstraelen et al., 2017).

The lack of success in targeting Aβ in AD has led to the pursuit of other therapeutic targets such as tau pathology. The role of tau pathology in the amyloid cascade hypothesis is currently unclear.

Tau pathology

Tau, another key hallmark of AD, is a MAP, which promotes assembly and stability of microtubules (Kadavath et al., 2015; Prezel et al., 2018). In disease states, tau becomes hyperphosphorylated and can form intracellular accumulations known as neurofibrillary tangles. Several diseases/disorders result from different types of tauopathies, including Down syndrome, Pick's disease, and frontotemporal dementia (Iqbal et al., 2010). Tau is encoded by the *Mapt* gene and can undergo alternative splicing to form numerous isoforms, which can either have a 3 or 4 microtubule binding domain (3-repeat and 4-repeat tau) in their C-terminus. The 3-repeat and 4-repeat isoforms alter the capacity of tau to bind to microtubules. In disease, tau's affinity for microtubules may be reduced by altered expression of the 3-repeat isoform, or abnormal phosphorylation by cyclin-dependent kinase 5 (cdk5) and glycogen synthase kinase-3-beta (GSK-3β; Engmann and Giese, 2009; Sengupta et al., 2006).

Dissociated tau forms intracellular aggregates, potentially leading to microtubule depolymerisation or altered microtubule dynamics. Altered tau may lead to impaired intracellular transport and loss of synaptic function. Tau pathology is more closely associated with clinical cognitive decline in AD than amyloid pathology, justifying further analysis as a target for therapeutic intervention (Bi et al., 2011; Pedersen and Sigurdsson, 2015; Sigurdsson, 2016).

Therapeutics targeting tau pathology

Similar to amyloid-based therapeutics, some tau-based treatment strategies also focus on immunotherapy to promote clearance of aggregated tau from the brain. Currently, Phase I clinical trials are being performed, testing both active and passive forms of tau antibodies (Medina, 2018; West et al., 2017).

Tau antibodies have been developed to interact with both extracellular and intracellular tau. Extracellular tau is more likely to be successfully cleared, but to prevent the secretion and further spread of tau, intracellular tau may be the most important target (Sigurdsson, 2016), thus the epitope target and charge of the antibody is of importance to gain entry into target cells. In animal tauopathy models, a passive immunisation approach targeting different epitopes of tau, showed success in reducing tau pathology (Ittner et al., 2015). Furthermore, some progress has been made in overcoming limitations of immunotherapy, such as hindrances of delivering larger-sized antibodies to the brain, using scanning ultrasound, which enhances the delivery of antibodies across the blood brain barrier (Nisbet et al., 2017). However, it is important to consider the potential toxicity of immunisation, as cytotoxic T-cell responses have been enhanced through immunotherapy (Rosenmann et al., 2006).

Other tau-based therapies include inhibition of tau phosphorylation (Castro and Martinez, 2000), blocking tau aggregation (Wischik et al., 2014), and enhancing tau degradation (Lee et al., 2015). Alternatively, it has been proposed that the downstream effects of tau loss could be targeted through stabilising the microtubules themselves (Ballatore et al., 2010; Brunden et al., 2014).

Other pathological alterations in AD

In addition to the key pathological features of AD, there are a number of other pathological changes which are thought to be downstream effects of amyloid and tau pathology. A particular prominent pathology in AD is the presence of dystrophic neurites, which are swollen and distorted axons or dendrites present predominantly around fibrillar Aβ plaques (Dickson et al., 1999). In disease, it has been shown using an APP/PS1 mouse model, that neurons which contain neurofilament-triplet proteins are more vulnerable to dystrophic neurite pathology than other neuronal types (Mitew et al., 2013b). Neurochemically, dystrophic neurites have been suggested to predominantly contain either neurofilament, tau, or chromogranin A (Dickson et al., 1999). Similar pathology is also observed in other neurodegenerative diseases, including amyotrophic lateral sclerosis and multiple sclerosis (Vickers et al., 2009).

Dystrophic neurites have been identified surrounding plaques, which are sites of microtubule disruption and increased BACE1 cleavage of APP and Aβ generation (Kandalepas et al., 2013). Live cell imaging of primary neurons exposed to Aβ42 oligomers showed extensive microtubule disruption and inhibited anterograde and retrograde trafficking (Sadleir et al., 2016), suggesting this could be a mechanism of dystrophic neurite formation and highlights the potential role for impaired axonal transport in exacerbation of amyloid pathology. Of note,

formation of dystrophic neurites is highly plastic, as a study using live two-photo imaging of two amyloidosis mouse models demonstrated a high turnover of dystrophic neurites around plaques (Blazquez-Llorca et al., 2017).

Synapse loss is another pathological feature observed in both AD animal models and human AD cases. Synapse loss is thought to correlate more strongly with the loss of cognitive function than tau or amyloid pathology, and therefore is an important target for therapeutic intervention (Terry et al., 1991). Glutamatergic synapses are particularly vulnerable to loss with a relative sparing of GABAergic synapses in the disease (Mitew et al., 2013a). It is currently unclear whether the loss of synapses is associated with the presence of dystrophic neurites, which could cause a dying back of the distal axon terminals, or whether it is unrelated to axonal degeneration. The loss of neurites and synapses may be responsible for the loss of brain volume in disease (Baron et al., 2014; Crews and Masliah, 2010; Dickson et al., 1999; Heneka et al., 2010; Praprotnik et al., 1996; Terry et al., 1991; Wu et al., 2010).

1.2.3 Pathological mechanisms in Alzheimer's disease

Alterations in neurotransmission

Altered neurotransmission, particularly alterations to cholinergic and glutamatergic signalling, is thought to be a key driver of cognitive decline in AD. Acetylcholine is a neurotransmitter involved in memory and learning and is decreased in AD patients, along with a loss of cholinergic neurons (Francis, 2005). Excitatory glutamatergic synapses and inhibitory GABAergic synapses have also been studied in AD. Neuronal damage is thought to arise from overactivation of N-methyl-d-aspartate (NMDA) receptors by glutamate (Francis, 2005). Furthermore, expression of functional glutamate transporters and α-amino-3-hydroxy-5-methyl-4-isoxazolepropionic acid (AMPA)/kainate-type glutamate receptors

were increased in AD mice (Peters et al., 2009). Kainate receptors mediate post-synaptic depolarisation and modulate the release of GABA and glutamate. Kainate receptors have many interactors, which interact with different specific sub-units of the receptor. For example, PSD95 interacts with GluK2 and GluK5 which alters receptor function by reducing desensitisation (Garcia et al., 1998). However, glutamatergic neurotransmission via kainate receptors have been implicate in several neurodegenerative diseases and brain disorders, such as epilepsy (Li et al., 2010; Falcón-Moya et al., 2018) and schizophrenia (Benes et al., 2001). Most of the excitatory transmission in the brain occurs via AMPA receptors, however in disease, AMPA receptor function is altered (Chang et al 2012). For example, altered AMPA receptors allow excessive calcium into neurons, causing cytotoxicity and neuron death in amyotrophic lateral sclerosis (Chang et al., 2012). However, decreased AMPA activation and synapse loss can lead to altered excitatory transmission and seizure activity, common in AD (Vossel et al., 2017). Recent research has shown that disrupted default neuronal networks may cause impaired memory (Li et al., 2014). GABAergic alterations may also be enhanced to negate excitotoxicity, and therefore disrupt overall neuronal network function (Li et al., 2014). The post-synaptic membrane is dense with NMDA receptors, and in AD, excessive presynaptic glutamate release and decreased re-uptake may contribute to slow excitotoxicity, contrasting to that of rapid excitotoxicity associated with stroke or epilepsy.

Therapeutics targeting neurotransmission alterations

There are several therapeutic options available to modulate alterations in neurotransmission in AD. Acetylcholine inhibitors are currently the main effective treatment that are safe to use to reduce some of the cognitive symptoms exhibited in AD (Anand et al., 2014; Folch et al., 2016). Although they do not alter the course of AD, the cholinesterase inhibitors tacrine, donepezil, rivastigmine, and galantamine, along with the NMDA receptor agonist, are the

only drugs approved by the FDA to treat AD symptoms (Anand et al., 2014; Folch et al., 2016). Several other strategies currently being investigated including other NMDA receptor antagonists (Olivares et al., 2012) and GABAergic modulation (Nava-Mesa et al., 2014). Other therapeutics for AD are reviewed (Chiang and Koo, 2014).

Inflammation

Reactive glial cells are present in the brains of AD patients, leading to the proposal that the inflammatory response may relate to the development, progression or protection against AD pathology. Microglia, one of the main glial cells involved in AD inflammation (Dickson, 1999; Heneka et al., 2010), can recruit astrocytes, which increases the neuroinflammatory response to Aβ (Heneka et al., 2010).

Microglial cells are part of the innate immune system within the central nervous system (CNS) and act as the first line of defence against amyloid pathology (Ransohoff and Brown, 2012; Solito and Sastre, 2012). In the early stage of AD progression, microglia are thought to play a protective role in promoting clearance of Aβ, however, in later stages of AD, microglia are no longer protective as they produce pro-inflammatory cytokines (Hickman et al., 2008). Microglia have been shown to react to Aβ plaques through the expression of cytokines and neurotoxins, which cause them to migrate around the Aβ plaques (Baron et al., 2014; El Khoury et al., 1996; Meda et al., 1995). Microglia also interact with the forms of Aβ in different ways, as soluble forms of Aβ are taken up by macropinocytosis, whereas fibrillar forms of Aβ interact with the cell surface innate immune receptor complex, stimulating phagocytosis (Lee and Landreth, 2010). As the inflammatory response influences the activation of microglia, it subsequently regulates the ability of microglia to degrade Aβ.

Microglia migration toward plaques has been shown occurs in both human AD and animal AD models (Baron et al., 2014; Dickson, 1999; Hickman et al., 2008; Perlmutter et al., 1990; Yoshiyama et al., 2007). In APP/PS1 mouse models, microglia have been demonstrated to move quickly to surround Aβ plaques and thereafter recruit more microglia if the plaque volume becomes greater (Bolmont et al., 2008). These processes are likely to be microtubule-dependent and therefore could be affected by microtubule-stabilising drugs. However, the role of glial cells in AD has been debated and whether inflammation in AD is neuroprotective by creating a barrier between plaques and neurons, or harmful by contributing to neural damage, is currently unclear (Heneka et al., 2010). If neuroinflammation does contribute to the progression of AD pathology, it may become a potential therapeutic target, by the use of anti-inflammatory drugs (Heneka et al., 2010). Furthermore, in some animal model studies, microglial activation has been shown to precede amyloid plaques and tau neurofibrillary tangles formation (Griffin et al., 1989; Heneka et al., 2005), whilst clinical PET studies have shown inflammation changes in a third of mild cognitive impairment (MCI) cases (Cagnin et al., 2001; Okello et al., 2009), leading to a suggestion that inflammation may be an upstream driver of disease.

Effect of microtubule therapeutics on AD pathology

It is currently unclear how altering microtubules could affect AD pathology. Changing microtubule dynamics could potentially affect amyloid plaque deposition, due to axonal transport impairment. If amyloid plaque deposition is altered via targeting microtubules, the downstream effects from amyloid pathology also have the potential to be altered. Microtubule stabilisation could also protect against neurite dystrophy formation and loss of synapses due to increased stability of the axon via stabilised microtubules.

1.3 TARGETING MICROTUBULES IN AXON DEGENERATION

1.3.1 Mechanisms of axon degeneration

Axon loss is present in several neurodegenerative diseases, including amyotrophic lateral sclerosis, Huntington's disease and Parkinson's disease (Lingor et al., 2012; Liu et al., 2012; Salvadores et al., 2017). Axonal and synaptic loss cause major circuitry dysfunction, which leads to significant clinical changes in people with neurodegenerative disease. Axonal and synaptic loss is promoted by axon degeneration, which occurs through specific pathways that are independent of cell death (Cusack et al., 2013; Geden and Deshmukh, 2016; Neukomm and Freeman, 2014; Wang et al., 2012).

1.3.2 Normal function of axon degeneration

Axon degeneration mechanisms, as well as being a consequence of neurodegeneration, can have normal biological functions within the nervous system that are associated with plasticity. For example, during development of the nervous system, neurons extend axons to more targets than are required for normal adulthood function. These excess projections are removed via programmed neurite removal, resulting in the programmed loss of synapses and processes (Yuan et al., 2003) to establish functional organisation of the circuitry (Low and Cheng, 2006). This synaptic pruning includes both axons and dendrites and involves apoptotic pathways including caspase activation as well as removal of debris by nearby glial cells.

To observe the molecular mechanisms of axon pruning, Drosophila has been used as a model (Yu and Schuldiner, 2014). In the Drosophila mushroom body, a brain structure implicated in learning and memory, there is considerable remodelling of axons and dendrites (Watts et

al., 2003) where microtubule and neurofilament degradation has been implicated in the initial stages of axon removal (Watts et al., 2004). Activation of caspases is also involved in developmental pruning (Cusack et al., 2013; Erturk et al., 2014; Simon et al., 2012). In addition to large-scale pruning of axonal processes, small-scale axon pruning can occur to fine-tune subsets of axonal terminals. This small-scale pruning does not involve removal of cellular debris, but rather a retraction of the axoplasm (Low and Cheng, 2006). This suggests that more than one axon removal process has evolved. A similar progression of events has been documented in Wallerian degeneration in vertebrates (Zhai et al., 2003).

1.3.3 Wallerian degeneration

A well-investigated alternative to development axonal pruning, frequently implicated in neuronal injury, is Wallerian degeneration (Conforti et al., 2014). Wallerian degeneration is the degeneration of the axon following a severing event, leading to disruption of the distal regions of the axon. Our understanding of Wallerian degeneration comes from the discovery of the mutant *slow Wallerian degeneration* (*Wld*^{S}) mouse, where severed axons, distal to the injury site, were observed to survive for several weeks, rather than the maximum of 48 hours that occurs in wildtype mice (Coleman and Freeman, 2010; Lunn et al., 1989). This led to the understanding that the axonal compartment can survive without the cell body.

Wallerian degeneration is initiated by a cutting or a crushing of the axon, followed by disintegration and clearance of the axon distal to the injury site (Freeman, 2014). Within an hour of the sever, a calcium influx is localised to the severed ends of the axon, leading to retraction of both ends. Following a lag period of several hours, a second calcium influx occurs throughout the severed distal end of the axon, which initiates fragmentation and disintegration of the cytoskeleton and is followed by clean-up with glial cells (Wang et al.,

2012). The amount of time for Wallerian degeneration to occur varies between neuron types and is slower in the CNS than in the peripheral nervous system (Mietto et al., 2015; Qin et al., 2012; Vargas and Barres, 2007). An important distinction between axonal pruning and Wallerian degeneration is the activation of caspases, which is absent in Wallerian degeneration.

1.3.4 Axon degeneration in disease

The mechanisms by which axon degeneration occurs in disease are currently unclear, although it is known that most diseases involving axon degeneration are not associated with frank axon severing. One way to investigate this is to examine the effects of specific pathological insults on the axon in order to determine targets for axon protection. One pathological insult that is implicated in a number of neurodegenerative diseases including AD (Hynd et al., 2004; Ong et al., 2013) and ALS (King et al., 2016; Van Den Bosch et al., 2006) is excitotoxicity. Excitotoxicity has been postulated to be one of the key pathological mechanisms of AD, potentially through alterations to calcium signalling (Fujiwara et al., 2012).

Excitotoxicity occurs through excessive stimulation of excitatory neurotransmitters (Carriedo et al., 1996), and can be modelled through application of agonists of glutamate receptors, such as kainic acid (agonist of kainate and AMPA receptors) and NMDA. Kainic acid has been shown to induce excitotoxicity *in vitro* (Hosie et al., 2012; King et al., 2013). Post-synaptic kainate receptors are excitatory, but pre-synaptic kainate receptors are inhibitory as they modulate the release of GABA (Cossart et al., 2001). Kainic acid has also been shown to increase production of reactive oxygen species, further causing oxidative damage (Layton and Pazdernik, 1999).

Excitotoxicity has been postulated as a potential cause of axon degeneration in disease and injury (Hynd et al., 2004). Although Wallerian degeneration does not activate the caspase pathway, models of excitotoxic-induced axon degeneration *in vitro* have been shown to activate axonal caspase 3 (King et al., 2013; Uribe et al., 2012), although it is not known if the intrinsic or extrinsic caspase pathway is involved. This suggests some differences between excitotoxin-induced axon degeneration and Wallerian degeneration. Excitotoxicity causes disruption of the cytoskeleton leading to axon fragmentation, axonal swelling and beading (Hosie et al., 2012; McCarran and Goldberg, 2007). Furthermore, stabilising microtubules with taxol has been shown to prevent axon fragmentation (King et al., 2013). It is currently unclear which changes to microtubules result in axon degeneration, such as that induced by excitotoxicity.

1.4 MICROTUBULES AS A THERAPEUTIC TARGET

In order to understand how to target microtubules therapeutically, a detailed understanding of their structure and function is needed.

1.4.1 Structure of microtubules

The cytoskeleton is a network of interlinking structures which provide and aid cells with shape, polarity, movement and cell division. Microtubules were first visualised by transmission electron microscopy (Fawcett and Porter, 1954; Manton and Clarke, 1952). Microtubules are a dynamic cytoskeletal element essential for normal cellular function. They are hollow cylinders of 25 nm diameter and are polarised molecules, composed of alpha- and beta-tubulin subunits, which were originally proposed as a homodimer model of alpha/alpha

and beta/beta tubulin (Mohri, 1968), but were later shown to be a heterodimer (Nogales et al., 1998). This heterodimer structure is vital as it greatly increases the ability of tubulin to polymerise to form microtubules.

1.4.2 Polymerisation and nucleation

Polymerisation is the process where free tubulin subunits are integrated to form microtubule protofilaments which require guanosine triphosphate (GTP) binding. Nucleation is the process of microtubule polymerization *de novo*. Nucleation of microtubules only occurs at the centrosomes at the centre of the cell, which are capable of nucleating hundreds of microtubules (Job et al., 2002). The 'plus'-ends of microtubules grow outwardly towards the periphery of the cell. The centrosome constantly sends out new microtubules, as microtubules are continually being depolymerised. Another type of tubulin, gamma tubulin ring complex, aids in nucleation by acting as a template for tubulin heterodimers, creating a 13 protofilament base for the growing microtubule (Dammermann et al., 2003). The gamma tubulin ring acts as a cap for the non-growing 'minus'-end and provides stability (Moritz et al., 2000). After tubulin subunits have been polymerised, they are covalently linked together to form a rigid microtubule structure. Tubulin subunits are more likely to be added to the plus-end of microtubules, where polymerisation rates are higher (Brouhard and Rice, 2014).

1.4.3 Dynamic instability and GTP hydrolysis

Microtubule function heavily relies upon their ability to easily assemble and disassemble. The continuous process of microtubule growth and shrinkage is dynamic instability (Burbank and Mitchison, 2006). Dynamic instability is a tightly-regulated process dependent on GTP hydrolysis and interactions with MAPs (Bowne-Anderson et al., 2013). The rate of

microtubule polymerisation is proportional to free tubulin levels. Binding GTP and Mg^{2+} are essential for microtubule assembly and stability. When GTP binds to beta-tubulin, it binds to the exchangeable (E) site, is hydrolysed to guanosine diphosphate (GDP) and creates a change in confirmation causing instability of the microtubule (Nogales et al., 1998). The GTP binding site on alpha-tubulin is the non-exchangeable (N) site. The role of the Mg^{2+} cation is highly important for the structural integrity of microtubules (Menéndez et al., 1998). During GTP hydrolysis, Mg^{2+} binds to the same site on the heterodimer. Heterodimers will either bind 1 or 2 Mg^{2+} cations, depending on the state of GTP hydrolysis. If the N-site of the alpha-tubulin binds GTP and the E-site of beta-tubulin binds GDP (after hydrolysis) then a Mg^{2+} cation will bind at the N-site (Alushin et al., 2014). However, if GTP is bound on both alpha- and beta-tubulin subunits, then another Mg^{2+} cation will bind at the E-site. The Mg^{2+} at the N-site controls stability of the heterodimer, whereas the Mg^{2+} at the E-site controls the stability of the microtubule. When the polymerisation rate of microtubules is higher than the rate of GTP hydrolysis of beta-tubulin, it results in a GTP cap on the carboxyl-end of the microtubule. This causes a higher affinity between tubulin with GTP than GDP, therefore the GTP cap stimulates further microtubule growth. A GTP cap can stabilise a microtubule by preventing depolymerisation of that microtubule (Horio et al., 2014). The loss of a GTP cap results in rapid disassembly of the microtubule, due to GTP hydrolysis to GDP. Normally, GTP hydrolysis of tubulin allows microtubules to depolymerise as it breaks the bonds between the tubulin subunits. Delayed GTP hydrolysis after the tubulin polymerisation results in a GTP cap (Bowne-Anderson et al., 2013). When free tubulin levels fall below a critical concentration threshold, rapid shrinkage of the microtubule at the plus-end occurs, which has been proposed to be caused by the loss of the GTP cap (Bowne-Anderson et al., 2013). This is because dissociation of GTP bound to tubulin in turn exposes the GDP bound to tubulin, causing microtubule instability and shrinkage. When microtubule disassembly occurs rapidly,

protofilaments curve due to a conformational change of GDP bound to beta-tubulin (Horio et al., 2014). GDP-bound heterodimers form a ring shape, which differs to the straight shape of heterodimers with GTP bound, giving the protofilaments their straight shape. Most of the neuronal microtubules in axons are stabilised, however, many factors such as PTMs and MAPs influence microtubule stability (Kadavath et al., 2015; Song et al., 2013).

1.5 POST-TRANSLATION MODIFICATIONS OF MICROTUBULES

1.5.1 Post-translational modifications influence dynamics

Microtubule stability is highly dependent on PTMs of its tubulin subunits, as they influence protein binding, as bound proteins can increase stability to aid in microtubule function. Tubulin can be modified in its soluble dimer form or polymerised as a microtubule. Most PTMs are acquired on the carboxyl-terminal of tubulin after polymerisation, except for acetylation of alpha-tubulin. Some PTMs are exclusive to one type of tubulin, such as acetylation, however, microtubule PTMs can also enhance binding of severing proteins (Song and Brady, 2015; Wloga and Gaertig, 2010), which have increased activity in neurodegenerative disease (Brunden et al., 2017; Sharp and Ross, 2012; Sudo and Baas, 2011). Post-translational modifications can be altered by pharmacological intervention and therefore can be used as potential therapeutic targets. For a summary of PTMs refer to Table 1.1.

1.5.2 Acetylation of microtubules

Acetylation is currently the only known PTM which occurs inside the lumen of microtubules. Acetylation of alpha-tubulin is the only known acetylation process to occur on polymerised microtubules, suggesting it is marker of microtubule age as they are more stable and resistant

Type of modification	Type of tubulin	Enzymes	Description	Site
Acetylation	alpha, assembled microtubules	Forward: αTAT1 Reverse: HDAC6 SIRT2	addition of acetyl group	lysine 40 of α-tubulin
Detyrosination / Δ2 / Δ3 / Tyrosination	alpha, assembled microtubules, tyrosination on tubulin heterodimers	Forward: CCP1,4,6 Reverse: TTL	removal of C-terminal tyrosine removal of penultimate glutamate from detyrosinated α-tubulin	terminal tyrosine on CTT of α-tubulin CTT of α-tubulin
Glutamylation / Polyglutamylation	alpha beta, assembled microtubules	Forward: TTLL4,5,7 TTLL1,6,11,13 Reverse: CCP5 CCP1,4,6	addition of one or more glutamates as a side chain	multiple glutamates in the primary sequence of CTTs of α- and β-tubulin
Glycylation / Polyglycylation	alpha beta, assembled microtubules	Forward: TTLL3,8 TTLL10	addition of one or more glycine as a side chain	multiple glutamates in the primary sequence of CTTs of α- and β-tubulin
Phosphorylation	alpha beta, unpolymerised tubulin dimer	Forward: Cdk1 PSK Syk	addition of phosphate group	serine 172 of β-tubulin
βΔ4	beta	Unknown	removal of amino acids EDEA from the C-terminus	C-terminal of β-tubulin

Table 1.1 Microtubule post-translational modifications

A summary of the microtubule PTMs with a description of the type of tubulin and the enzymes and sites involved in each modification.

to turnover (Portran et al., 2017). However, it is unclear whether acetylated tubulin is the outcome of stabilised microtubules, or is a process required to stabilise microtubules. Acetylation is the transference of an acetyl group from acetyl Co-enzyme A to lysine 40 of alpha-tubulin by acetyltransferase 1 (αTAT1**;** Li and Yang, 2015). Deacetylation or removal of the acetyl group from lysine 40 is catalysed by histone deacetylase 6 (HDAC6) and sirtuin 2 (SIRT2; Janke and Montagnac, 2017). It has been proposed that HDAC6 can inhibit microtubule growth because of its deacetylating activity (Asthana et al., 2013), but this is debated (Zilberman et al., 2009). However, acetylation has been proposed to induce microtubule severing as it enhances the binding of severing enzymes. Katanin, a severing enzyme, has been shown to have enhanced severing activity on acetylated-rich microtubules (Sudo and Baas, 2010). Supporting the view that acetylation is a result of microtubule stabilisation, αTAT1 has a higher rate of acetylation on assembled microtubules, rather than tubulin dimers (Kull and Sloboda, 2014). In contrast, αTAT1 has been shown to destabilise microtubules independently of its acetylating role (Kalebic et al., 2013), although there are no changes in the structural architecture of deacetylated and acetylated microtubules (Howes et al., 2014). Acetylated microtubules are also resistant to nocodazole, which alters microtubule polymerisation (Xie et al., 2010; Xu et al., 2017).

1.5.3 Tyrosination of microtubules

Tyrosination is another type of PTM which directly affects tubulin. Alpha-tubulin is tyrosinated and forms a heterodimer with beta-tubulin before being assembled into microtubules. After microtubule assembly, tyrosinated tubulin eventually becomes detyrosinated (Kumar and Flavin, 1981). Thus, detyrosination is a marker of microtubule stabilisation and microtubule age. Detyrosination is produced by cytosolic carboxypeptidase 1 (CCP1) and the reverse process is generated by the enzyme tubulin tyrosine ligase (TTL).

Detyrosinated alpha-tubulin can undergo a second round of detyrosination, known as △2 (Vu et al., 2017). This process removes the terminal glutamic acid residue, however, as this process is not reversible, the tubulin heterodimers with this PTM are unable to be reused, making them another marker of microtubule age.

In some forms of degeneration, microtubules are possibly converted back to a state of tyrosination and therefore more vulnerable to depolymerisation. The enzyme responsible for detyrosination, TTL is increased in injured axons and results in axon retraction (Song et al., 2015). Microtubules, particularly in axons, have two major domains of varying degrees of stabilisation. The labile domain located at the plus-end of the microtubule is highly tyrosinated and acetylated, despite the connection with acetylation and stable microtubules. In mitosis, interphase microtubules which are detyrosinated (glutamylated tubulin) are more resistant to high concentrations of nocodazole than tyrosinated tubulin (Kreis, 1987). Detyrosination has also been demonstrated to stabilise microtubules (Peris et al., 2009). Detyrosination of alpha-tubulin is protective against depolymerisation of microtubules by kinesin-13 (a motor protein). Overall, the distal axon is mostly tyrosinated due to its role in outgrowth, whereas the proximal axon is mostly detyrosinated to stabilise the axon. When detyrosinated tubulin has a glutamate residue at the carboxyl-terminal, it becomes glutamylated tubulin.

1.5.4 Glutamylation of microtubules

Glutamylation is a PTM which enhances the severing activity of microtubules. In this case, severing activity is used for microtubule outgrowth, as glutamylation is the main regulator of the microtubule-severing enzyme, spastin (Valenstein and Roll-Mecak, 2016). Glutamylation is a polymodification as it has side chains branching from the glutamic acid residue from the

C-terminal tail. Glutamylation is catalysed by a similar enzyme to detyrosination, TTL-like proteins, whereas deglutamylation is catalysed by CCP5.

Polyglutamylation increases MAPs binding to microtubules, including motor proteins, thus playing an important role in regulation of binding of proteins such as MAP1A, MAP1B, MAP2 and kinesin, but not tau (Bonnet et al., 2001). Polyglutamylation has been shown to occur on 50% of neuronal alpha-tubulin on glutamate 445 and can also be found on both tyrosinated and detyrosinated tubulin. Tau is closely linked to glutamylating enzymes, because in disease, mis-sorting of tau occurs, localising to the dendrites, which in turn induces mis-localisation of TTLL6 to the dendrites (Zempel and Mandelkow, 2015).

1.5.5 Phosphorylation of microtubules

Phosphorylation is thought to only occur on beta-tubulin by cdk1 kinase. Phosphorylation inhibits assembly of tubulin subunits into microtubules (Fourest-Lieuvin et al., 2006), however, alpha-tubulin phosphorylation on a tyrosine residue, has been demonstrated to prevent tubulin being incorporated into microtubules (Ley et al., 1994). In general, insight into phosphorylated microtubules is limited, especially in neurons.

There are a variety of kinases which phosphorylate tubulin, including insulin receptor kinase (Kadowaki et al., 1985; Wilden and Kahn, 1994). Pharmacological manipulation can also influence tubulin phosphorylation, as taxol can promote phosphorylation, whereas nocodazole decreases tubulin phosphorylation (Fourest-Lieuvin et al., 2006; Song et al., 2015).

1.6 MICROTUBULE-ASSOCIATED PROTEINS

Microtubule-associated proteins bind to multiple sites on tubulin and stabilise microtubules by cross-bridging multiple tubulin subunits and promote stability by suppressing tubulin dissociation. As described above, most MAPs binding to microtubules are modulated by phosphorylation. For a summary of MAPs refer to Table 1.2.

Tau is a neuronal MAP protein encoded by the *Mapt* gene on chromosome 17 and can undergo alternative splicing to form several different isoforms. During development, 3-repeat tau, is primarily expressed, while 4-repeat tau, is predominantly expressed in adulthood (D'Souza and Schellenberg, 2000; Malmanche et al., 2017). Tau is thought to promote microtubule stability, as the C-terminal of tau binds to tubulin subunits, with the 4-repeat tau isoform showing a higher affinity for microtubules than the 3-repeat tau (Goedert et al., 1989). Similarly, phosphorylation of tau also affects the capacity of tau to bind to microtubules. Phosphorylation at Ser262, Ser293, Ser324 and Ser365 decreases the capacity of tau to bind to microtubules (Drewes et al., 1995).

Tau phosphorylation of Tyr18 has been suggested to have a role in regulation of axonal transport (Cox et al., 2016; Kanaan et al., 2012). Phosphorylation of these tyrosine sites of tau are also associated with tau's capacity to aggregate. Importantly, tau is an inhibitor of HDAC6, therefore, it promotes microtubule stability (Perez et al., 2009). Phosphorylation of tau is regulated by various kinases, mainly by serine/threonine kinase. Like kinases, phosphatases, such as serine/threonine-specific protein phosphates 2A (PP2A), also play a role in tau regulation. Phosphorylation at sites serine 262 and 356, in turn activate other kinases GSK3β and cdk5, which have other roles in disease progression.

Type of protein	Isoforms	Molecular Weight (kDa)	Function
MAP1	MAP1A MAP1B	300 255	neural development; stabilisation of microtubules in axons and dendrites
MAP2	MAP2A MAP2B MAP2C MAP2D	280 200 70 42	neural development; stabilisation of microtubules in dendrites; signal transduction; early neural development
MAP4	multiple	210	promotes microtubule assembly
Tau	HMW-tau tau 4R/2N tau 4R/0N tau 3R/0N	55-62	neural development; stabilisation of microtubules in axons; axonal transport
CRMP2	CRMP2A CRMP2B	62	axon guidance; neuronal growth cone; cell migration

Table 1.2 Proteins associated with microtubules

A summary of the MAPs with a description of the known isoforms and their function when bound to microtubules.

MAP1A and MAP1B are structural MAPs, whose interaction with tubulin is modulated by polyglutamylation (Bonnet et al., 2001). MAP1A and MAP1B are expressed from different genes, from chromosomes 2 and 13 respectively (Halpain and Dehmelt, 2006). MAP2 does not compete with MAP1 binding to tubulin, suggesting they have different binding sites and function (Noble et al., 1989), although previous research has shown the opposite (Kuznetsov et al., 1984). MAP2, also a structural MAP, has three main isoforms expressed in neurons, MAP2A, MAP2B and MAP2C. Phosphorylation of MAP1B influences its microtubule-binding capacity. MAP1B is highly expressed during development, perhaps due to its role in neurite outgrowth, which is also regulated by phosphorylation (Scales et al., 2009). In addition, MAP1B is also important for axonal plasticity (Bouquet et al., 2004). MAP2B is expressed in development and in adulthood, whereas MAP2C is expressed mainly during neuronal development and MAP2A expression levels are up-regulated during adulthood (Burgoyne and Cumming, 1984; Doll et al., 1993; Ferhat et al., 2009; Nunez, 1988). MAP2 is located in the cell body and dendrites (Dehmelt and Halpain, 2005).

In addition to structural MAPs, some MAPs are involved in promoting microtubule assembly. Collapsin response mediator proteins (CRMPs) are MAPs that bind to microtubules to promote assembly via their C-terminal (Fakata et al., 2002; Niwa et al., 2017). CRMPs are regulated by phosphorylation and are expressed from five genes, with many isoforms. Importantly, CRMP2 localises to the distal part of growing axons, where it mediates tubulin dimers to the ends of growing microtubules (Arimura et al., 2005). Phosphorylated CRMP2 loses affinity for tubulin heterodimers resulting in reduced microtubule growth and increased axonal retraction. Therefore, CRMP2 binds and stabilises microtubule plus-ends and promotes axon growth (Niwa et al., 2017), along with CRMP4 (Khazaei et al., 2014; Tan et al., 2015). CRMP2 is observed in neurofibrillary tangles in AD (Soutar et al., 2009). CRMP2 is also involved in transporting vesicles by acting as an adaptor for kinesin 1 motor protein

for anterograde transport vesicles (Encalada et al., 2011; Reis et al., 2012). It is hypothesised that it also acts in this way for retrograde transport vesicles for dynein motor proteins (Arimura et al., 2009). CRMP2 interacts with NMDA receptors and the Na^+/Ca^+ exchanger and regulates their functional activity (Brustovetsky et al., 2014). CRMP2 binding to microtubules is influenced by microtubule-stabilising drugs taxol and epothilone B as they displace CRMP2 (Lin et al., 2011).

Motor proteins

Kinesins are microtubule motor proteins which transport cargo anterogradely along the axon, mainly transporting mitochondria and synaptic vesicles containing neurotransmitters (Encalada et al., 2011). Structurally, kinesin has light chains which mainly bind cargo, although some cargo may bind to the carboxyl terminal of the heavy chains. The globular unit of kinesin has a binding site for microtubules and one for binding adenosine triphosphate (ATP). Hydrolysis and release of adenosine diphosphate (ADP) makes a conformational change to microtubule-binding domains. When lysine 40 of alpha-tubulin is acetylated, kinesin-1 can bind to microtubules (Reed et al., 2006). Therefore, increased acetylation of microtubules results in increased requirement of kinesin-1 and another motor protein, dynein.

Microtubule severing enzymes

Microtubule-severing enzymes, spastin and katanin are ATPases, although it is unknown how these severing enzymes bind to microtubules. Severing enzymes are required for normal cell function as they release newly polymerised microtubules to be transported to axons and dendrites for neurite outgrowth (Vemu et al., 2018). If severing occurs in a stable region of a microtubule, it results in two separate microtubules, however, if a severing event occurs in a labile region, it is more likely to result in depolymerisation. Katanin and spastin are the most

commonly known severing enzymes and preferably bind to stable regions of microtubules. Spastin is associated with enhanced axonal branching formation (Yu et al., 2008). A loss of spastin results in reduced axonal length and reduced formation of axonal branches. Differing from katanin, spastin accumulates more at the site of branching formation, however, in the absence of spastin, axonal branches continue to form. Polyglutamylated microtubules are also more susceptible to spastin severing (Lacroix et al., 2010). It is possible that spastin also influences other cytoskeletal elements such as actin filaments, because axonal branching requires actin filaments and microtubules. There are no microtubule modifications which are resistant to severing by spastin, however, axons with a lack of tau undergo more axonal branching independent of spastin being present (Yu et al., 2008). Spastin potentially has a role in nucleation of microtubules and it is hypothesised that spastin along with fidgetin releases microtubules from the centrosome. Fidgetin, another ATPase severing enzyme, severs microtubules particularly at the minus-end and promotes degeneration in dendrites after injury (Tao et al., 2016).

The severing activity of katanin is highly influenced by tau, however, spastin severing activity is unchanged in the presence or absence of tau (Sudo and Baas, 2010). Generally, MAPs influence severing enzyme activity, whilst microtubule PTMs influence severing enzyme binding. MAP4 inhibits katanin severing activity, whilst tau activates katanin via the tau microtubule-binding domains, where it is phosphorylated to become activated (Sudo and Baas, 2011; Zempel and Mandelkow, 2015). Tau can therefore also inhibit katanin microtubule severing, since tau in disease enhances katanin microtubule severing as tau is no longer able to inhibit katanin through phosphorylation (Qiang et al., 2006). Katanin also enhances microtubule growth by severing the microtubule at the centrosome (Bailey et al., 2015). Katanin is highly important for axonal outgrowth because if it or gamma-tubulin is

inhibited, no new microtubules are released from the centrosome and transported along the axon.

Mutations to MAPs in neurodegenerative disease

Mutations of MAPs have been implicated in neurodegenerative disease. A mutated form of spastin has been found in hereditary spastic paraplegia (HSP; Errico et al., 2002; Yabe et al., 2002). A spontaneous mouse mutation of MAP1A, mm2719, causes tremors, ataxia and loss of cerebellar Purkinje neurons due to abnormal focal swellings disrupting the axon initial segment morphology (Liu et al., 2015b). Tau mutations have been widely reported in several neurodegenerative diseases, including sporadic AD, Pick's disease and progressive supranuclear palsy (as reviewed by Goedert and Jakes, 2005; Goedert and Spillantini, 2001; Wolfe, 2009). There are currently more than ten *MAPT* mutations that have been reported in familial cases of progressive supranuclear palsy, which are mainly located in exon 10 and its splicing region, which mainly produces 4-repeat tau (Rohrer et al., 2011; Stanford et al., 2000). Mutations to tau have also been identified in frontotemporal dementia (FTD) cases, which result in hyperphosphorylation of tau and assembly into filaments, causing subsequent cell death (Rizzu et al., 1999). MAP11, whose function is currently unknown, has been shown to co-localise with alpha-tubulin during mitosis. Truncating mutations of MAP11 cause microcephaly in both humans and in zebrafish models (Perez et al., 2019). Mutations to microtubule motor proteins have also been identified. Kif5A is an isoform on kinesin-1, with 23 separate mutations being identified in patients with HSP. These mutations have reduced catalytic and mechanical activities, with motility significantly reduced (Jennings et al., 2017). In Drosophila models, mutations in kinesin have been shown to cause motor neuron disease phenotypes by disrupting fast axonal transport (Kurd and Saxton, 1996). Mutations to

MAP1B cause extensive white matter deficits (Walters et al., 2018). Together this suggests that altered microtubule cytoskeleton can be a driver of neurodegenerative disease.

1.6.1 Summary of post-translational modifications and microtubule-associated proteins interactions

Microtubules are dynamic molecules, a property that is essential to fulfil their necessary function. This dynamic property is enabled through their PTMs and interactions with MAPs, either by promoting stability or instability. Furthermore, PTMs and MAPs also influence each other's binding to microtubules and MAPs can also undergo their own PTMs, such as phosphorylation, which can prevent their binding to microtubules. Microtubules can be manipulated through pharmacological intervention. In disease, changes to the level of PTMs and dissociation of MAPs can occur, altering microtubule stability. There are several interactions between microtubules functions, such as axonal transport, and MAPs, which are implicated in AD pathology as well as other neurodegenerative diseases and injury.

1.7 MICROTUBULE ALTERATIONS IN DISEASE AND INJURY

1.7.1 Introduction

Microtubule alterations have been reported in many diseases and injury conditions, including microtubule loss in AD (Cash et al., 2003; Jean and Baas, 2013). In stretch injury models, microtubules disassembly is one of the earliest events in axon degeneration (Tang-Schomer et al., 2010). Several studies have shown that microtubule alterations precede axon degeneration, although microtubule alterations in axon degeneration are relatively uncharacterised. Alterations to microtubules can be manipulated by microtubule-stabilising

drugs and have shown to be protective. However, changes to microtubules are currently unknown, but promoting microtubule stability has been shown to prevent axon loss by excitotoxic-induced axon degeneration (King et al., 2013).

Microtubule post-translational modifications in disease and injury

Microtubule PTMs have been reported in several neurodegenerative disease models. Glutamylation is increased in the hippocampi of a model of kainic acid-induced epileptic seizures as well as in AD patients, particularly in the CA3 region (Vu et al., 2017), although other studies suggest a decrease (Zhang et al., 2015a). Excessive polyglutamylation of tubulin has been shown to cause neurodegeneration and impair neuronal transport (Magiera et al., 2018). Likewise, tyrosination and detyrosination levels have been documented to be reduced in brains of AD patients. After injury, increased tyrosinated tubulin is required to promote axon regeneration, suggesting loss of tyrosination during injury (Song et al., 2015). Similarly, increased acetylated tubulin is required to rescue axonal transport in a model of Parkinson's disease (Godena et al., 2014) and in a tauopathy mouse model (Mao et al., 2017), suggesting a loss of acetylation during neurodegenerative disease.

1.7.2 MAPs in disease and injury

Tau in neurodegenerative disease

A number of alterations to tau in AD have been reported, including abnormal phosphorylation by cyclin-dependent kinase (cdk5) and glycogen synthase kinase-3-beta (GSK3β), as well as altered splicing in favour of the 3-repeat isoform, all of which are thought to reduce its affinity for microtubules and affect microtubule stability (Mietelska-Porowska et al., 2014). More recently, studies suggest that tau acetylation, which alters tau function, depending on which lysine is acetylated (Guo et al., 2017), may be altered in AD. Acetylation at Lys174 has been

shown to occur early in AD disease progression and results in cognitive deficits *in vivo* (Min et al., 2015), potentially through mis-localisation to the dendrites and disruption of AMPA receptors (Guo et al., 2017). Tau acetlyation may also be involved in FTD as lowering total levels of tau and acetylated tau at Lys174 in a PS19 FTD mouse model using a NSAID treatment, salsalate, rescued memory deficits and prevented hippocampal atrophy (Min et al., 2015). However, other lysine sites when acetylated may be protetive by preventing tau phosphorylation and are reduced in AD brains (Cook et al., 2014; Mietelska-Porowska et al., 2014). Ubiquitination of tau has also been suggested to be affected by acetylation of tau, as 11 acetylation sites are also ubiquitination sites, which suggests that degradation of tau is affected by acetylation (Morris et al., 2015). In addition, GSK3β is known to phosphorylate tau and promote tangle-like morphology (Rankin et al., 2007). Tau and another MAP, CRMP2, have the same kinases which act upon them, suggesting that they are part of a similar pathway and may both be affected in disease conditions. In tau knockout mouse models, a lack of tau protected mice from kainic-acid induced seizures (Pallo et al., 2016), and tau has also been shown to exacerbate excitotoxic brain damage in a stroke mouse model (Bi et al., 2017). However, the exact alterations that occur to tau during excitotoxicity are unknown. Aside from the changes to isoform expression, tau exon splicing, and tau to microtubule interactions, the alterations to tau remain unclear in neurodegenerative disease.

MAP1 and MAP2 in neurodegenerative disease

Like tau, MAP1B has been reported to be hyperphosphorylated in AD (Gong and Iqbal, 2008; Wang et al., 2001) and is present in sites of neurofibrillary degeneration in AD patients (Ulloa et al., 1994). Furthermore, MAP1A and MAP1B proteolysis was observed after Aβ-induced activation of caspase 3 and calpain (Fifre et al., 2006). Neuronal deficiency of MAP1B,

results in structural presynaptic deficiencies and altered presynaptic physiology (Bodaleo et al., 2016).

In models of NMDA-induced excitotoxicity, loss of MAP2 from the apical dendrites was observed (Hoskison et al., 2007; Hoskison and Shuttleworth, 2006). Similarly, loss of MAP2 immunoreactivity was reported prior to neuronal cell loss in rodent brain injury models (Huh et al., 2004), particularly in the hippocampus (Taft et al., 1992) and levels of MAP2 have been shown to fluctuate in a diffuse brain injury model immediately post-injury and up to 10 days after (Papa et al., 2017).

Collapsin response mediator proteins in neurodegenerative disease

CRMP2 plays a major protective role in acute axon degeneration, as a calcium influx after a lesion activates calpain which then cleaves CRMP2, and impairs axon transport (Zhang and Koch, 2017). In models over-expressing CRMP2, proximal axons were protected in acute axon degeneration (Zhang and Koch, 2017). CRMP2 was also altered in models of excitotoxicity and over-expression of CRMP2 has also been shown to aggravate NMDA-induced injury (Yin et al., 2013). CRMP2 has been proposed as a therapeutic target in neurodegenerative disease through its ability to regulate microtubule stability through a similar mechanism to tau (Hensley and Kursula, 2016). When CRMP2 is dephosphorylated, it facilitates axonogenesis (Voronkov et al., 2011).

1.7.3 Phosphorylation of microtubule associated proteins

Tau phosphorylation

Phosphorylation of MAPs is involved in stability of microtubules. In disease, several MAPs become hyperphosphorylated, most notably tau, become hyperphosphorylated, which leads

to their pathological function (Ma et al., 2017). As such, targeting protein phosphorylation has become a proposed therapeutic in AD (Gong and Iqbal, 2008; Voronkov et al., 2011) and has led to reducing tau-based synaptic toxicity (Ma et al., 2017). In the current literature, sodium selenate has shown to mitigate tau pathology in AD models (van Eersel et al., 2010) via targeting the phosphatase PP2A.

Phosphorylation of other MAPs

In addition to tau, other MAPs become phosphorylated and pathological in AD. Dendritic MAP2, is phosphorylated in disease and alters cytoskeletal function (Sánchez et al., 2000), as it has a role in nucleation and stabilisation of microtubules, neuronal processes outgrowth and synaptic plasticity. When MAP2 becomes hyperphosphorylated it dissociates from microtubules, increasing dynamic instability (Illenberger et al., 1996). Similarly, CRMP2 is hyperphosphorylated in AD, which is a feature not common to other neurodegenerative diseases (Williamson et al., 2011) and is one of the earliest events in AD progression in AD patients and in AD mouse models (Cole et al., 2007; Soutar et al., 2009).

Other microtubule modifications in neurodegenerative disease

In addition to alterations to microtubule PTMs, other microtubule-associated changes are implicated in disease and injury. For example, mutations to presenilin have been shown to impair kinesin-based axonal transport (Gunawardena et al., 2013; Pigino et al., 2003). Acetylated microtubules are also more susceptible to katanin severing, particularly in the axon, where microtubules are more stable, due to their acetylation (Sudo and Baas, 2010). Tau bound to axonal microtubules, renders them less sensitive to katanin activity, thus the loss of microtubule-associated tau in neurodegenerative disease, makes them vulnerable to severing (Sudo and Baas, 2011).

1.8 PHARMACOLOGICAL MANIPULATION OF MICROTUBULES

1.8.1 Microtubule stabilisation as a therapeutic

Microtubule-stabilising drugs have been proposed as a therapy for AD and other neurodegenerative diseases with axonal transport impairments (Ballatore et al., 2012; Trojanowski et al., 2005). Reduced microtubule stability is an early pathological change in response to Aβ toxicity, likely a result of tau hyperphosphorylation. In addition, the destabilisation of microtubules is implicated in axon degeneration (Tang-Schomer et al., 2010). There are a number of ways that microtubule stabilisation can be targeted. Firstly, there are microtubule-stabilising agents that bind directly to microtubules and can promote stability of microtubules and prevent them from depolymerising (Yu et al., 2013). Research into drugs that bind to the same site as tau, such as taxanes and epothilones, has demonstrated their effects in reducing pathology in tauopathy mouse models (Bakota and Brandt, 2016; Brunden et al., 2010; Erez et al., 2014; Zhang et al., 2012a). However, it is unknown whether binding by these agents cause a conformational change to microtubules which promotes stability. Alternatively, drugs that can target PTMs of tubulin such as acetylation and glutamylation, as well as MAPs such as tau, may promote stability and are also attractive targets for intervention.

An important feature of any drug for neurodegenerative disease is that it must be able to cross the blood brain barrier. Many microtubule-stabilising drugs were first used to treat cancers by causing cell cycle arrest, so while they may have been developed for human use, their ability to access the CNS needs to be determined. Taxanes and epothilones are two of the two main classes of microtubule-stabilising agents, however their properties differ. Taxol has

poor permeability to the blood brain barrier, whereas epothilone B and D have been shown to cross the blood brain barrier and are a potential therapeutic for AD.

1.8.2 Microtubule modifying drugs

Taxol

Taxol was first isolated from *Taxus brevifolia* in 1971 and was identified as an anti-leukemic and anti-tumour drug (Wani et al., 1971). It is now known that it enhances microtubule assembly and length, as well as stabilising microtubules (Parness and Horwitz, 1981; Schiff and Horwitz, 1981). Taxol has been found to assemble tubulin subunits of microtubules in the absence of GTP or MAPs, such as tau (Schiff and Horwitz, 1981). Without taxol, in *in vitro* preparations, tubulin is predominantly in the depolymerised state, however, with the addition of taxol, polymerisation increases, along with GTP hydrolysis (Hamel et al., 1981). When GTP is absent, tubulin still forms microtubule structures when taxol and MAPs are present (Hamel et al., 1981). Taxol binds to tubulin polymers between the 'M-loop' and the 'central helix' of beta-tubulin (Amos and Lowe, 1999; Nogales et al., 1999). A number of studies have investigated the therapeutic potential of taxol in injury models to the brain, spinal cord and peripheral nerves. In a needle stick model of acute damage to the somatosensory cortex, taxol was an effective therapeutic agent to protect against neurodegeneration by reducing neurite loss via microtubule stabilisation of axons (Adlard et al., 2000). As taxol improves axonal elongation, the potential of taxol to improve axon regeneration of neurons following injury has also been investigated. In adult rats with a dorsal hemisection spinal cord injury, taxol treatment increased the number of axons regenerating, and increased axon outgrowth (Hellal et al., 2011). Moreover, when taxol was administered prior to axon stretch injury *in vitro*, it delayed axon degeneration was delayed compared to untreated injured axons (Tang-Schomer et al., 2010). Taxol restored facial nerve function after nerve crush injury in

Wistar rats, through the stabilisation of microtubules, which was evaluated through motor function and the degree of axonal branching (Grosheva et al., 2008). Furthermore, taxol administration to an optic nerve crush injury site, allowed axon regeneration past the lesion area because of microtubule stabilisation (Sengottuvel et al., 2011). At spinal cord lesions sites in rodents, microtubule stabilisation promoted axonal growth, and increased levels of detyrosinated and acetylated tubulin, at the lesion site of the spinal cord in rodents (Ruschel et al., 2015), suggesting that axon growth may have been due to the reduction of scar tissue, which contains axon growth-inhibitory factors (Ruschel et al., 2015), although astrogliosis was shown to be unaffected by microtubule stabilisation treatment. The effect of microtubule-stabilising agents on glial cells has not been extensively investigated in disease models. The effects of taxol have also been studied in a T44 tau mouse model where fast axonal transport was improved, and microtubule density and detyrosinated tubulin levels increased (Zhang et al., 2005).

Epothilones

Another family of microtubule-stabilising agents, epothilones, have similar characteristics and mechanisms to taxol, although they are able to cross the blood brain barrier (Bollag et al., 1995). Epothilone, originally an anti-tumour drug, is produced by the gram-negative bacteria *Sorangium cellulosum*, and has undergone both phases I and II clinical trials (Beer et al., 2007; Bollag et al., 1995; Konner et al., 2012). Taxol and epothilones have a similar structure and bind to beta-tubulin at a common site (Cheng et al., 2008). Like taxol, epothilone, has been shown to prevent microtubule disassembly when calcium is present. Taxol and epothilone also reduce the amount of tau bound to microtubules, suggesting that these drugs also compete with tau (Mukhtar et al., 2014; Ross et al., 2004). Due to their success in treating cancer, epothilones are being investigated as a treatment for

neurodegenerative diseases. As Parkinson's disease shares some pathological features with AD, epothilone D was shown to reduce microtubule defects and increase detyrosinated microtubules in dopaminergic neurons in a mouse model of Parkinson's disease (Cartelli et al., 2013). In a mouse model of schizophrenia, epothilone D was also shown to improve short-term memory, suggesting that epothilone D may affect synapses in the hippocampus (Andrieux et al., 2006). Some research has suggested that the effectiveness of treatment with epothilone B depends on the type and age of the neuron (Jang et al., 2016). Many mouse models of varying neurodegenerative diseases have shown successful microtubule stabilisation, resulting in reduced pathology. For example, amyloid plaque pathology may be hindered by microtubule stabilisation, as APP is transported along microtubules in the same compartment as its cleaving enzymes (Kamal et al., 2001), and that loss of microtubules may cause altered processing of APP, leading to possible increased Aβ production (Busciglio et al., 1995). Therefore, stabilisation of microtubules with taxanes or epothilones could potentially alter APP processing by preventing microtubule depolymerisation. Epothilone D has increased microtubule density in axons, decreased axonal dystrophy and reduced cognitive defects in a PS19 mouse model of frontotemporal lobar degeneration (Zhang et al., 2012a). Tau acetylation leads to destabilisation of the axon initial segment cytoskeleton and leads to mis-localisation of tau to the somatodendritic compartment. The axon initial segment provides a barrier from the axon and the somatodendritic compartment and allows retention of axonal proteins. Cytoskeletal proteins Ankyrin G and βIV-spectrin, which are part of the axon initial segment, are reduced in AD and are associated with increased tau acetylation in tau transgenic mouse models. However, in primary neuronal cultures, epothilone D treatment restored the axon initial segment barrier function, preventing tau from being mis-localised (Sohn et al., 2016). Another type of microtubule-stabilising agent, NAPVSIPQ (Bassan et al., 1999) has been shown to reduce tau pathology and enhance cognitive function (Matsuoka et

al., 2008). Epothilones may also have an effect on mobility of glial cells, such as microglia, due to over-stabilisation of the cytoskeleton. One study demonstrated that epothilone B attenuated microglia activation through redistributing the cytoskeleton, causing morphological transition and suppressed expression of pro-inflammatory factors such as interleukin-1β and tumour necrosis factor-α (Yu et al., 2018). This suggests that epothilones may not alter mobility of microglia, but can have an effect on morphology. Epothilone D also had a similar effect in an in vitro model of multiple system atrophy. Epothilone D was shown to reduce microglial-mediated transport of alpha synuclein by inhibiting cytoskeletal dynamics (Valdinocci et al., 2018).

HDAC6 inhibitors

Another microtubule-stabilising agent which has been postulated as a therapeutic is trichostatin A (Simões-Pires et al., 2013). Trichostatin A inhibits the de-acetylating enzyme HDAC6, responsible for deacetylation, therefore promoting acetylation (Liu et al., 2015a). Research has shown that HDAC6 inhibition by use of trichostatin A or tubastatin A in neurodegenerative mouse models, have rescued axonal transport and locomotor deficits (Benoy et al., 2018; Godena et al., 2014) and neurite outgrowth (Hasan et al., 2013). Several HDAC6 inhibitors such as tubastatin A and tubacin have been used as a treatment in various diseases, including Japanese encephalitis virus (Lu et al., 2017), lymphoproliferative disease (Cosenza and Pozzi, 2018) and Charcot-Marie-Tooth disease (Benoy et al., 2018). Axonal transport has been shown to be restored after treatment with trichostatin A (Godena et al., 2014). In an APP/PS1 mouse model, with a knock-out of HDAC6, Aβ-induced deficits in mitochondrial trafficking were rescued (Govindarajan et al., 2013).

PP2A agonists

Sodium selenate is an agonist to PP2A, enhancing phosphatase activity. Serine/threonine-specific PP2A is a major phosphatase implicated in tau dephosphorylation and is reduced in protein and mRNA levels and activity in the AD brain (van Eersel et al., 2010; Vogelsberg-Ragaglia et al., 2001). Altered expression of PP2A is also correlated with AD pathology (Sontag and Sontag, 2014). Sodium selenate acts upon the phosphatase, thereby stabilising the tau-PP2A complex, and reducing hyperphosphorylated tau (Shultz et al., 2015). In a tauopathy mouse model, mice treated with sodium selenate had reduced levels of both phosphorylated tau and total tau levels in both the hippocampus and amygdala compared with controls (Corcoran et al., 2010). The TAU441 mice also exhibited significantly improved spatial learning and memory. Sodium selenate is currently undergoing a Phase II clinical trial for mild-moderate AD (Malpas et al., 2016). More recently, sodium selenate has been used to treat hyperexcitability in mouse models of Lafora disease, where some motor and memory deficits were ameliorated and neurodegeneration and the glial response were reduced (Sánchez-Elexpuru et al., 2017). Other AD pathology has been reduced with sodium selenate treatment, where in a 3xTg-AD mouse model, sodium selenate repressed amyloid beta formation, via the Wnt/β-catenin signalling pathway (Jin et al., 2017).

Developing microtubule-modifying drugs as therapeutics for neurodegenerative disease

Microtubule stabilisation has been successful in treating many forms of cancer, as it causes cell cycle arrest at G_2/M transition phase (Fanale et al., 2015; Rohrer Bley et al., 2013; Zhao et al., 2016). Microtubule stabilisation as a therapeutic has undergone many phase I and II clinical trials to treat solid tumours, lymphoma, malignancies, metastatic prostate cancer and advanced colorectal cancer. (Beer et al., 2007; Eng et al., 2004; Holen et al., 2004; Konner et al., 2012; Rubin et al., 2005; Spriggs et al., 2003).

Although these studies suggest that microtubule stabilisation with taxol, epothilone D or trichostatin A may be protective in a number of conditions, the use of taxol and epothilones as anti-cancer drugs has shown adverse side effects such as neutropenia, fatigue, nausea, dizziness as well as abdominal pain, when high doses of epothilone D were administered (Bedard et al., 2010; Holen et al., 2004). In addition, administration of these drugs can cause peripheral neuropathy. Most doses required to cause cell cycle arrest in cancer are approximately 100 mg/m^2 weekly, however these doses are considered to be relatively high compared to only a low dose needed for neurodegenerative disease (Cartelli et al., 2013; Ruschel et al., 2015). A number of clinical studies using epothilone as a microtubule-stabilising drug have demonstrated that these toxic effects are dose-dependent and when used at a lower dosage, the side effects are minimised (Fumoleau et al., 2007). Importantly, the concentrations of taxol or epothilone required to stabilise microtubules in axons or to promote axon regeneration are much lower than those required to prevent division of cancer cells (Brunden et al., 2012).

1.9 PROJECT SUMMARY AND AIMS

Microtubules are a key modifiable structural component of the neuron, essential to their many functions. Alteration to microtubules and associated proteins have been implicated in a number of neurodegenerative diseases and linked to neurodegeneration and neuronal dysfunction, particularly that relating to the axon. Modifying microtubules has been postulated as a therapeutic target, particularly in AD, which currently has no effective treatment. In this regard, clinical trials that reduced pathological features of AD such as amyloid deposition have been unable to reduce clinical symptoms. A key feature of many

neurodegenerative diseases is axon degeneration or the breakdown of axons following pathological insult such as excitotoxicity. Axonal transport impairment can lead to axon degeneration and previous research has shown that stabilising microtubules may protect against axon fragmentation following pathological insult, suggesting microtubules may be an important target for therapeutic intervention of axon degeneration. Furthermore, microtubule alterations, such as those occurring in AD through tau abnormalities, may lead to axonal loss and neurodegeneration (Roy et al., 2005; Stokin and Goldstein, 2006; Trojanowski et al., 2005) and that axon transport failure may be a primary mechanism in AD (Stokin et al., 2005).

Although microtubule alterations have been implicated in disease and postulated as a therapeutic target, limited research has focused on defining the alterations to microtubules that need to be targeted in disease. Furthermore, since modifying microtubules is likely to have downstream effects on cellular processes, it is important to determine their capacity to protect cellular structures but also to alter other pathological features of disease such as the amyloid plaques of AD. This thesis seeks to increase understanding of microtubule alterations following pathological insults, specifically excitotoxicity, and the effect of the microtubule-stabilising drug epothilone D on the amyloid-related alterations in the AD brain.

Aim 1: To determine *in vivo* if the microtubule-stabilising agent epothilone D could be a viable therapy for AD

The role of microtubules in AD has been previously explored, however, most microtubule-based strategies have been limited to determining the effect in tauopathy mouse models. The effects on other AD-based pathology including amyloid plaques, dystrophic neurons and synapses has not been determined. Epothilone D is a microtubule-stabilising drug that crosses the blood brain barrier, increases microtubule density, and has been trialled in humans,

although the human AD trial was terminated. Therefore, the first aim was to explore the effect of epothilone D in an amyloid mouse model of AD to determine if microtubule stabilisation can affect AD pathology.

Aim 2: To determine alterations to microtubule PTMs in neurons and their axons following kainic acid-induced excitotoxicity *in vitro* and investigate whether inhibiting these alterations prevents axon degeneration

Microtubule alterations have been described during axon degeneration, however the exact alterations to microtubules are relatively unknown. By modelling axon degeneration with an excitotoxic insult such as kainic acid, applied to primary cultured rodent neurons, microtubule alterations during excitotoxicity can be examined. Therefore, the second aim was to determine which PTMs are altered during kainic acid-induced axon degeneration in primary mouse cortical neurons. To determine microtubules alterations, specifically in axons, a compartmentalised microfluidic chamber was used to separate axons from the somatodendritic compartment and allow compartmented treatments and protein harvest.

Aim 3: To determine alterations to MAPs in neurons and their axons following kainic acid-induced excitotoxicity *in vitro* and investigate whether inhibiting MAP phosphorylation prevents axon degeneration

MAPs which bind to microtubules can modify their function and alterations to MAPs have the capacity to promote axonal stability or destruction. MAP binding to microtubules can also be influenced by microtubule PTMs and microtubule-stabilising drugs. Therefore, the third

aim was to determine whether MAPs are altered during axon degeneration, or if dephosphorylation of MAPs prevents axon degeneration, potentially through stabilising the microtubule network. As in aims 2, primary cortical neuron cultures grown in compartmented microfluidic chambers were used to determine changes to MAPs.

Chapter 2

Methods

2 METHODS

2.1 MICE

All experiments and procedures were approved by the University of Tasmania Animal Ethics Committee and were in accordance with the Australian Guidelines for the Care and Use of Animals for Scientific Purposes under the ethics A13471 and A16041 for the 12-month-old APP/PS1 mice cohort experiments, and ethics A12780, A15121 and A17530 for cell culture experiments. All experimental procedures utilised male (for APP/PS1 cohort experiments) or female (for cell culture experiments) mice. Male $APP_{SWE}/PS1_{dE9}$ (APP/PS1) on a C57BL/6 background (Jankowsky et al., 2001) and wildtype littermates mice were used in the first study of this thesis. Differences between male and female mice on the B6 congenic line have been reported, as males have been shown to develop amyloid plaques more rapidly than females (Ordóñez-Gutiérrez et al., 2015), therefore only male mice were used in this study. Mice were housed in optiMICE cages with a minimum of 3 mice in a cage on a 12-hour light cycle and had access to food ad libitum. Mice were provided with minimal enrichment consisting of an igloo, tissue and a stick.

2.2 IN VIVO EPOTHILONE D TREATMENT

Epothilone D (AbCam, ab143616, Lot#APN14287-1-1) treatment was prepared in 100% DMSO (Sigma Aldrich, D4540, Lot#RNBF1056) to a stock of 10 $mgmL^{-1}$ and vehicle was 100% DMSO and diluted to a working stock of 1 $mgmL^{-1}$. Twelve-month-old $APP_{SWE}/PS1_{dE9}$ (Jankowsky et al., 2001) mice and wildtype littermates received weekly treatment of 2 mg/kg epothilone D (as previously shown by Brunden et al., 2010) of either epothilone D or vehicle (5% DMSO) delivered by intraperitoneal (IP) injection for 12 weeks. The maximum volume

delivered IP was 70 µL. Behavioural testing was performed post-treatment. Mice had weight monitored weekly to assess any detrimental health effects.

2.3 BEHAVIOURAL TESTING

Epothilone D used in cancer trials can have detrimental effects on health (Argyriou et al., 2011; Konner et al., 2012). Therefore, mice were weighed weekly from 12 months old and behavioural testing was performed at 15-months of age to assess short-term memory, anxiety and movement of mice at 15-months of age. The following tests were used; open field, spontaneous Y-maze, Barnes maze and marble burying, with the distance and velocity travelled also being recorded (n = 9=10 mice per group). All tests except the marble burying test were analysed using EthoVision XT (Noldus). Each test was performed in the same position in the room with black opaque curtains surrounding the testing area for the duration of the test, under 200 lux lighting conditions.

2.3.1 Habituation

Habituation was performed a week prior to starting behavioural testing. Habituation involved placing mice in their home cages in the behaviour testing room for one hour in the same lighting conditions as testing conditions. Habituation was performed for five consecutive days.

2.3.2 Marble burying

The marble burying test was used to measure anxiety as mice should want to bury foreign objects. In this study, marble burying was examined as a behavioural measure as differences

in marble burying have been recorded in APP/PS1 mice (Kim et al., 2012; Koivisto et al., 2016). Mice were placed in an OptiMICE cage with 5cm deep bedding and 6 evenly-spaced marbles. Mice were allowed to explore the cage for 30 minutes. After this time mice were removed and an image was acquired from above and from the side. From the images, the number of marbles that were at least 75% buried were recorded (Figure 2.1; (Angoa-pérez et al., 2013; Deacon, 2006).

2.3.3 Open field

An open field test is used to measure general movement and anxiety of mice, which aids in analysing performance on other behavioural and cognitive tests. Mice were allowed to explore a square box (30cm x 30cm) for 10 minutes and were recorded from a camera position above the box, under 200 lux lighting conditions. As mice have an aversion to open areas, the amount of time a mouse spends in the centre of the box relative to the outside of the box was calculated as a measure of anxiety (Figure 2.1; Brownlow et al., 2013; Ferguson et al., 2013).

2.3.4 Spontaneous alternation Y maze

Due to rodent's natural instinct to explore new areas, the Y-maze was used to assess short-term spatial memory in APP/PS1 and wildtype littermates. The Y-maze was situated in dim lighting conditions (200 lux) surrounded by black curtains to control for different spatial cues. The arms of the Y-maze measured 75 mm x 400 mm. Mice were placed in the centre and allowed explore the Y-maze for eight minutes, where mice rely on their ability to remember which arm they have explored immediately before and should therefore alternate exploring arms. Mice were recorded from above and the order of the arms that the mice entered were recorded and analysed (Figure 2.1; Miedel et al., 2017). The percentage of spontaneous alteration entries was calculated by:

A

MARBLE BURYING

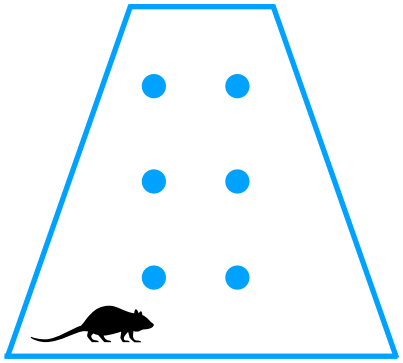

x1 trial

30 mins

B

OPEN FIELD

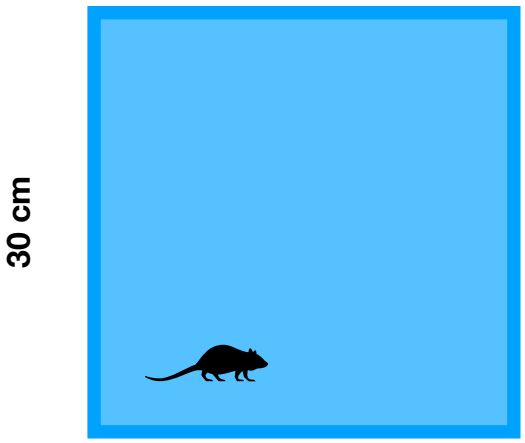

x1 trial

10 mins

C

SPONTANEOUS Y MAZE

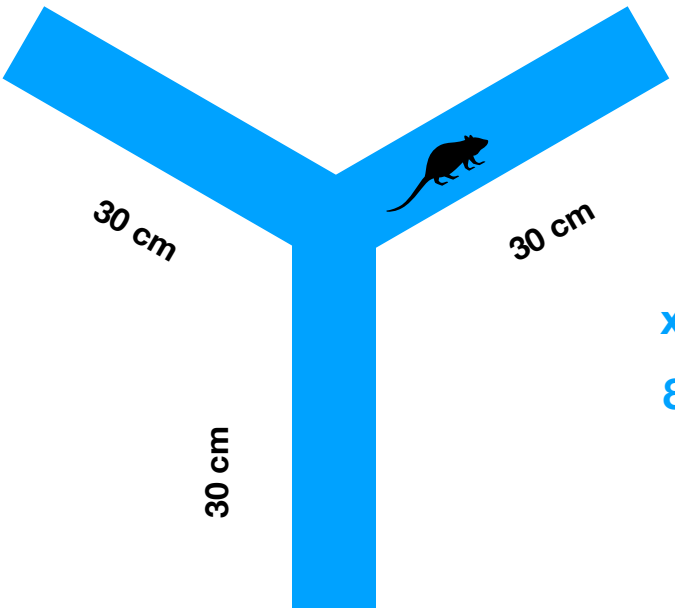

x1 trial

8 mins

Figure 2.1 Marble burying, open field and spontaneous alternation Y maze paradigms

(A) The marble burying test was performed in OptiMICE cages with 5cm of fresh bedding in the bottom of the cage. Six marbles were placed evenly within the cage and the mice were places into the cage with the marbles. The cage was placed behind black opaque curtains which surrounded the cages, under 200 lux lighting conditions. The mice were left in the cage for 30 minutes. (B) The open field test arena is a 30cm x 30cm white box, with black opaque curtains surrounding the arena. The test was performed for 10 minutes in 200 lux lighting conditions. (C) The Y maze test arena was a 30cm long, 10cm wide, and 15cm deep white box in a Y shape. Each test was performed for 8 minutes behind black opaque curtains under 200 lux lighting conditions.

$$Percentage\ alteration = \left(\frac{\#\ of\ alternations}{total\ \#\ of\ triads}\right) \times\ 100$$

Where, the number of triads = total entries -2, and the alternations are scored as a triad (set of three numbers) containing all three numbers (arm 1, arm 2 and arm 3).

2.3.5 Barnes maze

This test measures long-term memory over a period of five days. The Barnes maze arena was set up with curtains surrounding the testing area as described above. Images of a square, circle, arrow and triangle were attached to the curtains around the edge. The initial stages of this test are the training phases, which is followed by the testing phase. For training: on day one, mice were allowed three minutes on the Barnes Maze and shown the escape box at the end of the trial. On day two, mice had three trials on the Barnes Maze where they were allowed to explore the maze until they found the escape box or until three minutes had passed, at which stage the mice were showed the escape box. On day three, mice had two trials on the Barnes Maze. On day four, mice were not tested. For testing: day five was the test day where mice had one trial on the Barnes Maze for three minutes. The time until mice entered the escape box and the time spent in the quadrant of the escape box were measured (Figure 2.2, 2.5; Pitts, 2018; Rosenfeld and Ferguson, 2014).

2.4 TISSUE PREPARATION

Following treatment, mice were terminally anaesthetised with sodium pentobarbitone (140 mg/kg) and transcardially perfused with 4% paraformaldehyde (PFA) for histochemical

A

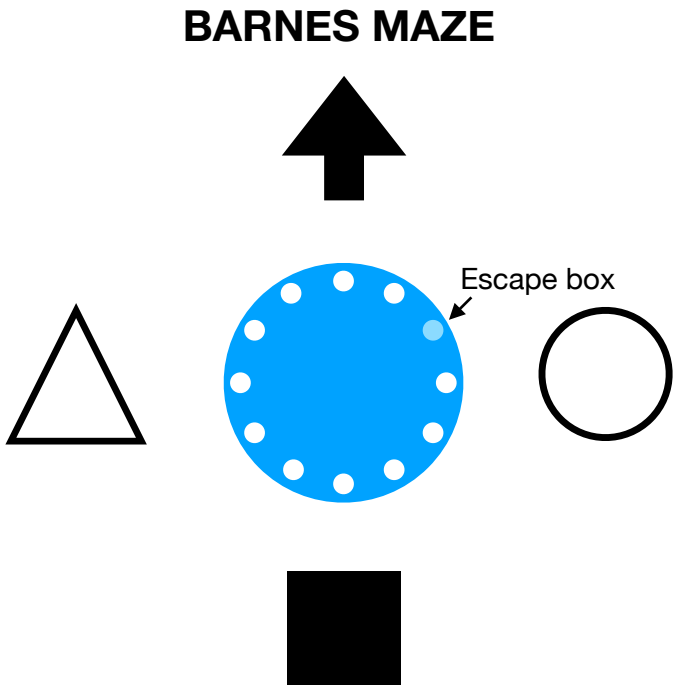
BARNES MAZE
Escape box

B

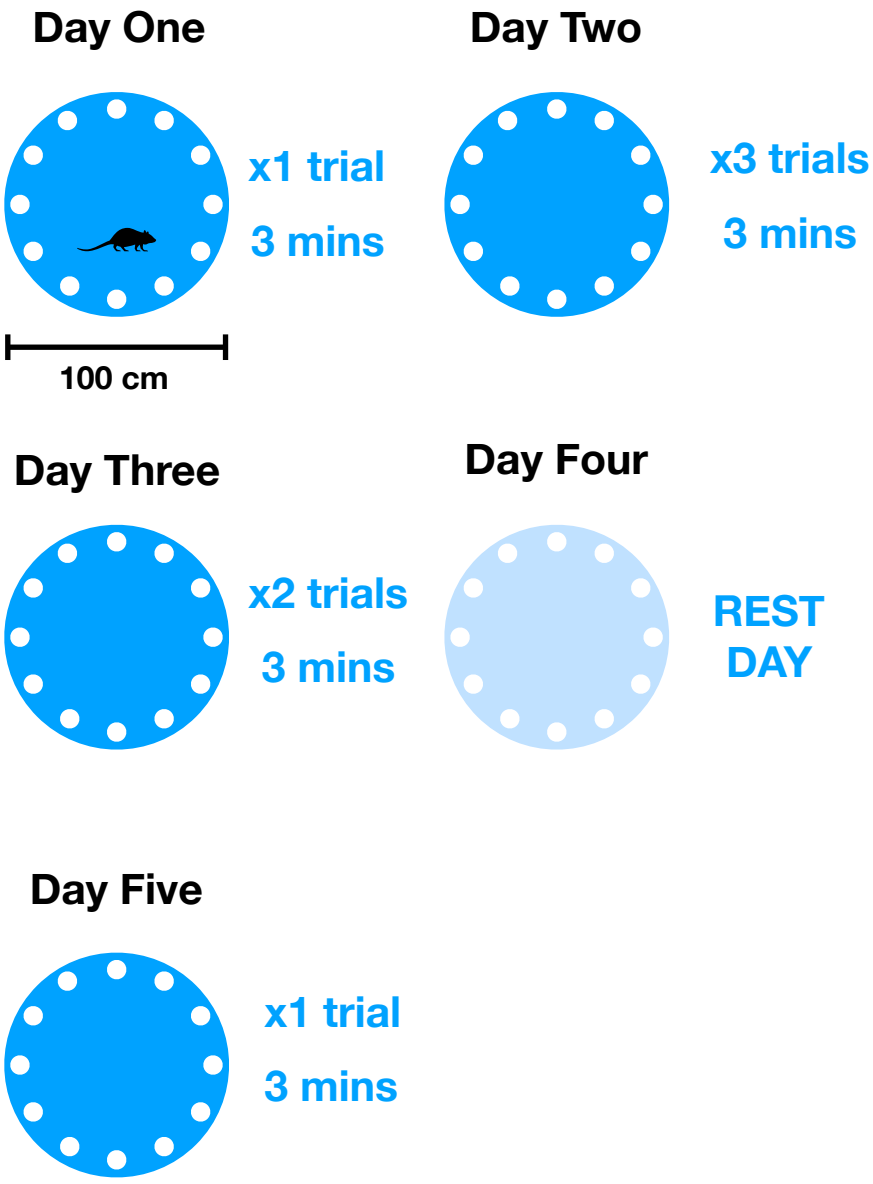
Day One
x1 trial
3 mins
100 cm
Day Two
x3 trials
3 mins
Day Three
x2 trials
3 mins
Day Four
REST
DAY
Day Five
x1 trial
3 mins

Figure 2.2 Barnes maze paradigm

(A) **Barnes maze set up:** The Barnes maze test arena was a white 100cm diameter circular platform with X holes, one of which contained the escape hatch. The platform was placed behind black opaque curtains and maintained under 200 lux lighting conditions. Visual cues (arrow, triangle, circle and square) were printed on A4 paper and attached to the curtains every 90º around the Barnes maze. (B) **Trial parameters used:** The training phase was performed from day one to day three with a rest day was on day four of testing. Day five was the probe trial testing day, where only one trial was performed. Each trial lasted either for three minutes, or until the mouse had entered the escape box.

analysis or with 0.01 M PBS for Western blot analysis. Brains were post-fixed overnight in PFA at 4ºC for 24 hours and stored in PBS azide (0.02% sodium azide in 0.01 M PBS) for histological analysis or snap frozen in liquid nitrogen for biochemical analysis. For Western blot analysis, brains were immediately dissected into cortex, hippocampus, and rest of brain and were snap frozen in liquid nitrogen and stored at -80ºC prior to use.

Tissue preparation for histochemical analysis

Prior to sectioning, brains were cryoprotected through sequential treatment in 18% sucrose and 30% sucrose (in 0.01 M PBS azide) for 24 hours each. For analysis, tissue was serially sectioned on a coronal plane at 40 µm at -15ºC on a cryostat from bregma 2 to -3 for analysis (Figure 2.3).

Tissue preparation for biochemical analysis (details of protein extraction and measurement)

Frozen brain tissue was transferred into 350 µL of RIPA buffer (Sigma Aldrich) containing protease (cOmplete™ Mini Protease Inhibitor Cocktail tablets, Roche) and phosphatase inhibitors (Phosphatase Inhibitor Cocktail, A.G. Scientific) and homogenised using an UltraTurrax. Homogenates were mixed for 30 minutes at 4ºC followed by centrifugation at 13,000 rpm for 20 minutes at 4ºC. The supernatant was transferred to a clean eppendorf tube and the pellet discarded. Protein concentration was determined using a Bradford assay as per the manufacturer's protocol (BioRad Protein Assay, BioRad). Protein samples were stored at -80ºC.

A

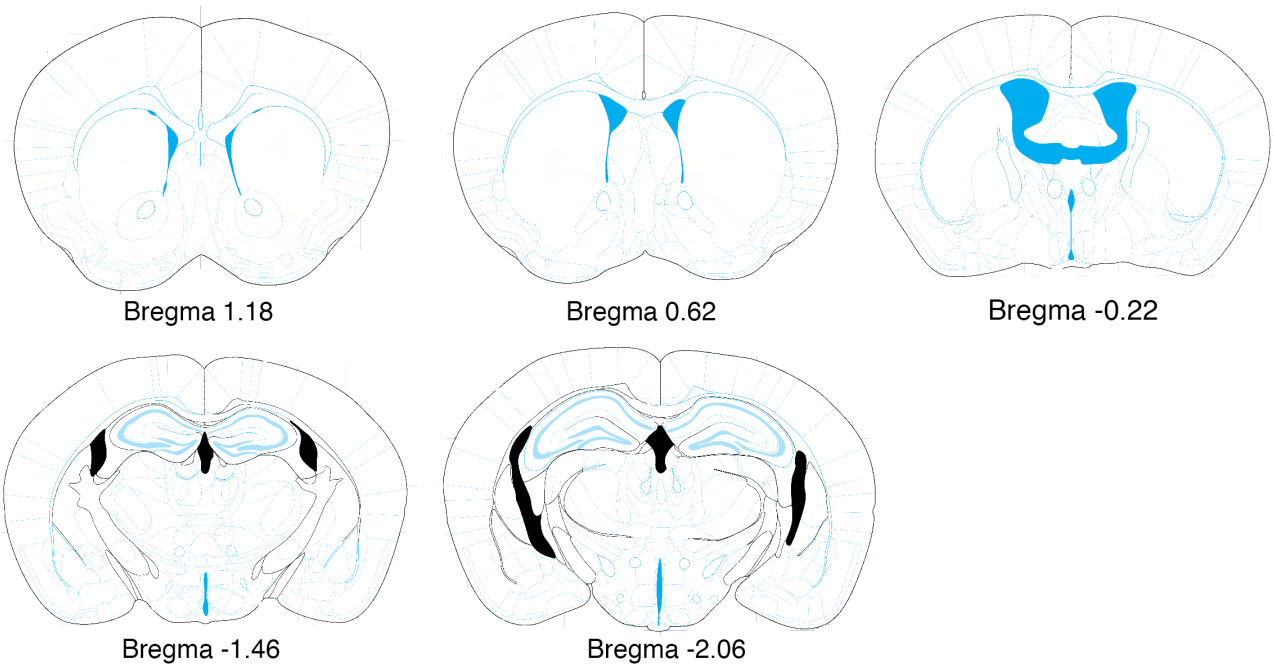

Figure 2.3 Coronal sections used from bregma 1.18 to -2.06

(A) Schematic to show coronal sections used for immunohistochemical analysis from bregma 1.18 to -2.06.

2.5 IMMUNOHISTOCHEMISTRY

2.5.1 Indirect fluorescent immunohistochemistry

Brain sections were mounted onto slides, prior to being washed three times with tris-buffered saline (TBS-T; 0.3% Triton X, Sigma Aldrich) at 10-minute intervals at room temperature. Sections were blocked for 1 hour in 10% horse serum (Sigma Aldrich) in TBS-T, followed by overnight incubation with combinations of mouse monoclonal and rabbit polyclonal primary antibodies (See Table 2.1) diluted in 1% horse serum in TBS-T at 4ºC. Sections were washed in TBS-T and incubated with species and isotype specific fluorescent secondary antibodies (See Table 2.2) diluted at 1:500 in 1% horse serum in TBS-T for 2 hours. Sections were washed in TBS-T followed by DAPI (1:10,000) staining for 5 minutes to stain nuclei. Finally, the sections were washed in TBS before slides were coverslipped with immu-mounting medium (Thermo Scientific).

2.5.2 Thioflavin-S staining

Thioflavin S (Sigma Aldrich) staining was used to determine Aβ plaque load, which labels fibrillar and dense-core plaques composed of Aβ with a β-pleated sheet confirmation. Brain sections were mounted onto slides prior to incubation in thioflavin S solution (0.125% thioflavin S in 60% absolute ethanol and 40% 0.01 M TBS) for 5 minutes at room temperature. Sections were then washed twice in 50%/50% absolute ethanol/0.01 M TBS for 1 minute each followed by 3 10-minute washes in 0.01 M TBS. Immunohistochemistry was then performed as above.

2.5.3 Confocal microscopy

Confocal images were taken on a spinning disk confocal Nikon TE- 2000 inverted microscope with a Yokagawa CSU-22 confocal scanning unit and a Hamamatsu C9100-02 EMCCD camera with a 40x objective using Velocity (PerkinElmer) software for image capture.

2.5.4 Dystrophic neurite population quantitative analysis

To quantitate the dystrophic neurite load surrounding individual plaques in APP/PS1 epothilone D and vehicle-treated mice (n=7-8 per group), two coronal sections were immunolabelled with an antibody against phosphorylated neurofilament protein (SMI312), which labels distinct populations of dystrophic neurites, and stained with thioflavin S to label fibrillar plaques. Dystrophic neurites images were imaged using a spinning disk confocal microscope at 40x objective. Plaques were randomly selected between layers II – V in the cortex using the following criteria: between 10 μm – 30 μm in diameter, single plaques (not multilobed). A total of 10 isolated plaques per section were selected from layers 2, 3 or 4 of the cortex. Using Adobe Illustrator, 40 μm was measured from the edge of the plaque, to determine the region of interest, where the number, the average size and the dystrophic neurite load was measured (Figure 2.4 A). The dystrophic neurite load was determined by the following:

$$Dystrophic\ neurite\ load = \left(\frac{the\ total\ area\ of\ the\ dystrophic\ neurites}{the\ total\ area\ of\ the\ region\ of\ interest}\right) \times 100$$

Table 2.1 Primary antibodies

Name	Species	Immunogen / Immunoreactivity	Application	Concentration	Company	Catalogue Number
GAPDH	M IgG1	Glyceraldehyde-3-phosphate dehydrogenase	WB	1:5000	Millipore	MAB374
SMI312	M IgG1	Phosphorylated neurofilament / axons	IHC WB	1:1000 1:2000	Covance	SMI312R
Synaptophysin	R	Synaptophysin / pre-synaptic vesicle marker	IHC WB	1:200 1:1000	Millipore	AB9272
VGLUT1	M IgG1	Anti-Vesicular Glutamate Transporter 1	WB	1:1000	Millipore	MAB5502
Acetylated Tubulin	M IgG2b	Acetylated tubulin	IHC WB ELISA	1:1000 1:1000 1:1000	Sigma Aldrich	T7451
Tyrosinated Tubulin	R	KLH-conjugated linear peptide corresponding to human tyrosinated alpha tubulin	ELISA	1:1000	Millipore	ABT171
MAP1B	M IgG1	Neuronal marker, MAP1B	ELISA	1:1000	Abcam	AB3095
MAP2	M IgG1	Clone AP20	ELISA IHC WB	1:1000 1:500	Millipore	MAB3418
Iba1	R	Ionised calcium binding adaptor molecule 1 / labels microglia	IHC	1:1000	WAKO	019-19741

M = mouse, R = rabbit, IHC = immunohistochemistry, WB = Western blotting

Table 2.2 Secondary antibodies for immunohistochemistry

Emission (nm)	Reactivity	Species	Concentration	Company	Catalogue Number
Alexa 488	M IgG1	G	1:1000	Molecular Probes	A-21121
Alexa 594	M IgG	G	1:1000	Molecular Probes	A-32742
Alexa 488	R IgG	G	1:1000	Molecular Probes	A-11034
Alexa 594	R IgG	G	1:1000	Molecular Probes	A-11037

M = mouse, R = rabbit, G = goat

2.5.5 Synapse quantitation

Alterations in synaptic boutons were examined by immunolabelling coronal tissue sections from vehicle-treated APP/PS1 and wildtype mice with an antibody against synaptophysin, which is a presynaptic protein present at the majority of synapses and frequently used in synapse quantitation (Fernandez-Martos et al., 2015). Immunolabelling was performed in three coronal sections per mouse. To quantitate synaptic puncta, 10 random evenly-spaced areas were selected throughout the neocortex from the rhinal fissure to the midline, from layers 2-5. During imaging, the researcher was blinded to genotype of the tissue. From these images, synaptic bouton density and the number of synapses was measured.

Previous studies suggest that synaptic puncta are reduced around plaques in APP/PS1 mice (Fernandez-Martos et al., 2015). Plaque-associated synaptic puncta were quantitated for 10 plaques per section from 3 coronal sections per mouse. Plaques sized 10 µm – 30 µm were imaged throughout the neocortex to measure synaptic bouton density. A mask was made to determine the region of interest. The number of synapses per plaque, bouton size and density within 40 µm distance from the edge of the plaque was quantitated (Figure 2.4 B).

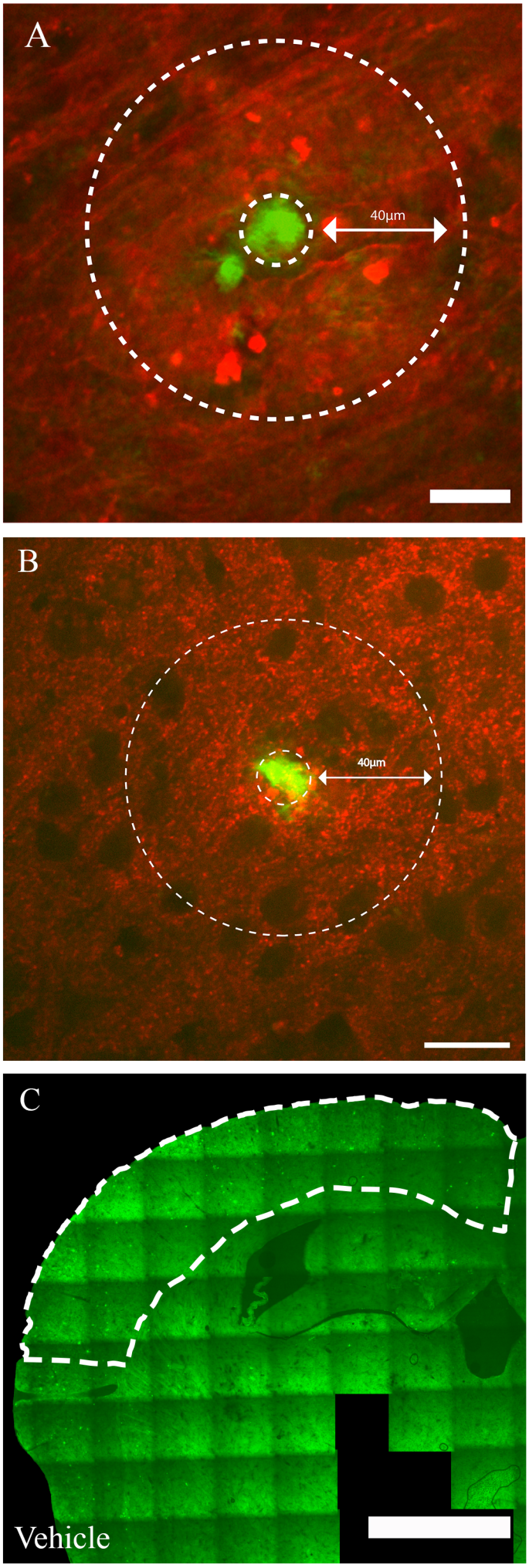
A
40µm
B
40µm
C
Vehicle

Figure 2.4 Analysis methods of dystrophic neurites, synapses and plaques

Representative images to show analysis of (A) dystrophic neurites was performed from plaques sized 10 nm – 30 nm. Dystrophic neurites were assessed from the edge of the plaque to a 40 μm region from the edge. Analysis of (B) synapses was performed from the edge of the plaque to a 40 μm region from the edge. Analysis of (C) plaque load from the midline of the cortex to the rhinal fissure. Scale bar for (A, B) = 30 μm. Scale bar for (C) = 400 μm.

2.5.6 Plaque load quantitative analysis

Plaque load analysis was performed in 5 evenly spaced (approximately 800 µm – 1000 µm apart) 40 µm cortical sections, taken from bregma 2 to -3 from each animal (n=7-8 per group). Whole cortices were imaged using a spinning disk confocal microscope at 20x objective. Plaques were assessed in a region of interest from the midline of the cortex to the rhinal fissure (Figure 2.4 C). Images were taken from the midline to the rhinal fissure, as this enables the same area to be consistently imaged throughout the brain sections selected. Plaque stain signal intensities were classified using ImageSURF (O'Mara et al., 2018). The Random Forest Segmenter removes human bias from thresholding positive immunohistochemical signal. Classified images were then analysed in Fiji using the analyse particles function to quantitate plaque load from the midline to the rhinal fissure of the cortex. The number of plaques, the average size and the plaque load were calculated and recorded. The plaque load was determined by the following:

$$Plaque\ load = \left(\frac{the\ total\ area\ of\ the\ plaques}{the\ total\ area\ of\ the\ region\ of\ interest}\right) \times 100$$

2.5.7 Microglia qualitative analysis

Microglia were qualitatively assessed between genotype and treatment to determine if the glial response is altered during amyloidosis pathology and with epothilone D treatment. Immunolabelling with Iba1 for microglia was performed in four coronal sections per mouse. Specific regions throughout the cortex where blindly qualitatively compared for any difference between groups. In particular, sections from bregma 0.22 were used for qualitative assessment.

2.5.8 Microglia quantitative analysis

Microglia were quantitatively assessed between genotype and treatment to determine if the glial response is altered during amyloidosis pathology and with epothilone D treatment. Immunolabelling with Iba1 for microglia was performed in three coronal sections per mouse. A specific region from the midline of the cortex to the rhinal fissure was investigated to determine microglia cell density. Positive immunohistochemical signal from images classified using the ImageSURF plugin in Fiji then analysed in using the analyse particles function to quantitate microglia cell density. The microglia cell density was determined by the following:

$$Microglia\ cell\ density = \left(\frac{the\ total\ area\ of\ the\ microglia}{the\ total\ area\ of\ the\ region\ of\ interest}\right) \times 100$$

2.6 WESTERN BLOT

Semi-quantitatively Western blot analysis was performed to determine the level of proteins in APP/PS1 mice and wildtype littermates with either epothilone D or vehicle treatment.

2.6.1 Gel electrophoresis and Western Blot

Denatured protein samples (20µg for tissue and 25µg for cultured cells) were electrophoresed into Bolt® 4-12% Bis-Tris gels (Invitrogen), transferred to PVDF membrane (Bio-Rad). Membranes were probed overnight with primary antibodies (See Table 2.1) including anti-synaptophysin (1:1000 rabbit, Millipore AB9272), anti-VGLUT (1:1000 mouse, Millipore

MAB5502) and anti-phosphorylated neurofilament protein (SMI312; 1:2000 mouse, Covance SMI312R). The corresponding anti-rabbit or anti-mouse horseradish peroxidase (HRP) conjugated secondary antibody (See Table 2.3; 1:7000, DAKO) was used as previously described (Fernandez-Martos et al., 2015). GAPDH (1:5000 mouse, Millipore MAB374) was used as a loading control. Bands were visualised with enhanced chemiluminescence (ECL) solution-Luminata Forte Western HRP substrate (Millipore) and images acquired with a Chemi-Smart 5000 Imaging System (Vilber Lourmat) equipped with Chemi-Capt 5000 software. Band intensity was measured as the integrated intensity using Fiji software. Each value was calculated as a percentage of the standard sample run between gels. Sample numbers were as documented in individual chapter results.

Table 2.3 Secondary antibodies for Western blotting

Name	Reactivity	Species	Concentration	Company	Catalogue Number
Anti-Mouse Immunoglobulins/HRP	M	G	1:7000	DAKO	P044701-2
Anti-Rabbit Immunoglobulins/HRP	R	G	1:7000	DAKO	P044801-2

M = mouse, R = rabbit, G = goat

2.7 CELL CULTURE

2.7.1 Microfluidic chamber and culture tray preparation

For experiments probing axons specifically, neurons were grown in compartmented microfluidic chambers (Figure 2.5; 450 µm long, 10 µm wide and 3 µm high barrier grooves, Xona Microfluidics), which allows fluidic isolation of cells from the axon (Taylor et al., 2006). For other experiments, neurons were grown directly in 24-well culture trays. Microfluidic chambers were sterilised in 70% ethanol for 10 minutes and allowed to dry under sterile conditions. Chambers were attached to sterile 22mm^2 coverslips. Culture wells and microfluidic chambers were treated with 5% poly-L-lysine (Sigma Aldrich) in Hank's Balanced Salt Solution (HBSS) overnight. Poly-L-lysine was removed and replaced with an initial neuron plating media consisting of neurobasal medium (Gibco), 2% B27 supplement (Gibco), 10% fetal calf serum (Gibco), 0.5 mM glutamine, 25 mM glutamate and 1% antibiotic/antimycotic (Gibco). Chambers and culture trays were incubated at 37ºC prior to plating of the neurons.

2.7.2 Cortical primary cell culture

Mouse cortical neuron cultures were prepared as previously described (King et al., 2013). Neocortical tissue was dissected from C57Bl/6 embryonic day 15.5 (E15.5) mouse embryos. Heads were kept on ice during dissection to prevent tissue degradation. Cortices were removed using a dissecting microscope (Leica), dissociated from the meningeal layers and transferred to 5 mL Hanks Balanced Salt Solution (HBSS, Gibco). Tissue was incubated with

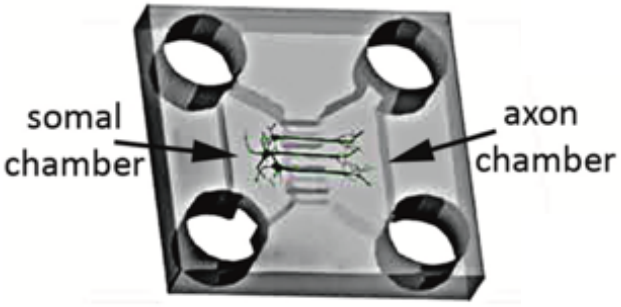
somal
chamber
axon
chamber

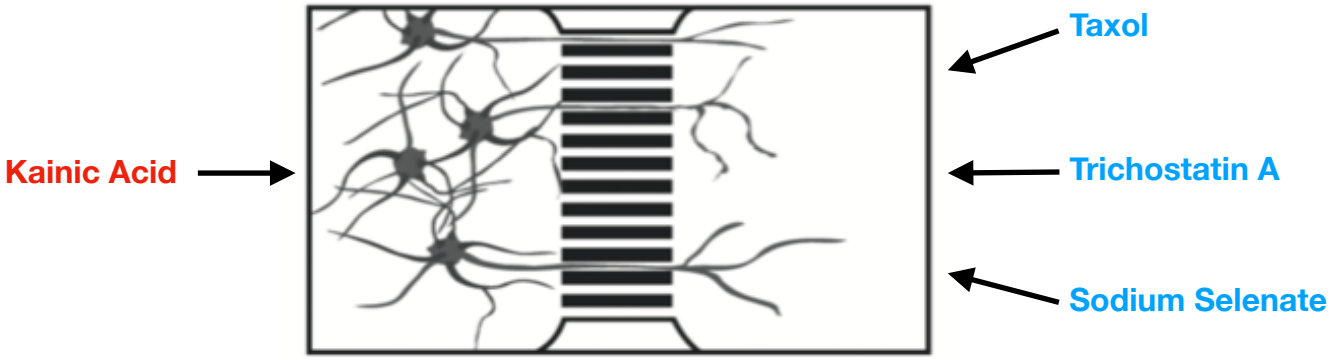
Kainic Acid
Taxol
Trichostatin A
Sodium Selenate

Figure 2.5 Compartmentalised treatment in microfluidic chamber

(A) Schematic to show design of the microfluidic chambers used in this thesis. The two compartments (axonal and somal) are separated by microgrooves (450 µm long, 10 µm wide and 3 µm high, Xona Microfluidics), which allows fluidic isolation of cells from the axon. Treatments such as taxol, trichostatin A and sodium selenate were added to the axonal compartment, whereas kainic acid was added to the somatodendritic compartment, so the axon remains unexposed to the excitotoxin.

0.0125% trypsin in HBSS for 4 minutes at 37ºC followed by removal of HBSS and replaced with 1 mL of initial plating media (Neurobasal media (Gibco) containing 2% B27 supplement, 0.5 mM glutamine, 25 μM glutamate, 10% fetal calf serum and 1% antibiotic/antimycotic. Cell viability and density was assessed using a trypan blue exclusion assay. For microfluidic chamber cultures, initial plating media was removed from the wells of chambers and 20 μL of cells ($2x10^5$ cells/mL) were plated onto one side of the microfluidic chamber. Cells were allowed to adhere to the coverslip surface for 30 minutes prior to filling chambers with initial plating media. For tray-only cultures, $2x10^5$ cells/mL were loaded into wells with previously loaded initial plating media and gently shaken to evenly distribute cells. Cells were incubated at 37ºC overnight before removal of initial media and replacement with subsequent plating media, with no fetal calf serum and glutamate. Cells were grown for 10 days *in vitro* (DIV) at 37ºC in 5% CO_2, a timepoint which corresponds to dense axonal growth in the axon compartment of microfluidic chambers (Hosie et al., 2012; Millet and Gillette, 2012).

At 1-day *in vitro* initial plating media was removed and replaced with subsequent plating media, with no fetal calf serum and glutamate. Cells were grown for 10 days at 37ºC before being fixed with 4% paraformaldehyde in fume hood and agitated for 30 minutes at room temperature.

2.7.3 Western blotting and ELISA protein extraction

For Western blotting and ELISA analysis, cells were harvested from both microfluidic chambers and culture wells. Culture media was removed and cells were rinsed with cold HBSS. Cells were harvested using RIPA buffer with protease (cOmplete™ Mini Protease

Inhibitor Cocktail tablets, Roche) and phosphatase inhibitors (Phosphatase Inhibitor Cocktail, A.G. Scientific). For culture wells, cells were collected using a cell scraper (Falcon) and transferred to an eppendorf tube. For chambers axons were harvested from the axon chamber by using RIPA buffer as stated above, where axons were pooled from 2-4 chambers per treatment. Once collected, tubes were mixed on a shaker for 30 minutes at 4ºC before being centrifuged at 4ºC for 15 minutes at 13,000 rpm. Supernatant was transferred to new eppendorf tube and stored at -80ºC until further use.

2.8 *IN VITRO* MODEL OF EXCITOTOXICITY

2.8.1 Pharmacological manipulation and excitotoxic modelling

To model excitotoxicity *in vitro* neurons in either microfluidic chambers or growing in culture wells were with 0 µM, 10 µM, 25 µM, 35 µM, 50 µM and 100 µM of kainic acid (Sigma Aldrich, K0250, Lot#SLBD1491V) or vehicle (DMSO; Sigma Aldrich, Lot#RNBF1056) for 0.5 hours, 1 hour, 3 hours, 6 hours and 18 hours. Kainic acid was added directly to the culture wells or to the somatodendritic side of the chambers. The microtubule-stabilising agent taxol (Calbiochem, 580556, Lot#B66835) was prepared in DMSO and used at 10 $ngmL^{-1}$ and 100 $ngmL^{-1}$ and added to the axonal compartment of chambers. To alter microtubule acetylation, trichostatin A (TSA; Sigma Aldrich, T8552, Lot#026M4036V) was used to inhibit de-acetylating enzyme HDAC6. TSA was diluted in DMSO and added to the axonal compartment of chambers or directly to the culture wells. To dephosphorylate microtubule-associated proteins, sodium selenate was used at 100 µM (Sigma Aldrich, 288675, Lot#BCBT2170) dissolved in DMSO and was added to the axonal compartment of chambers.

2.8.2 Cell viability assay

Cell viability was assessed using alamarBlue® viability assay (Bio-Rad), which is a resazurin-based solution which is a non-toxic, cell permeable compound. Living cells reduce resazuring to resorufin, which is red in colour and highly fluorescent, where changes are detected by either absorbance (detected at 570 and 600 nm) or fluorescence (using an excitation between 530–560 and an emission at 590 nm). Cells were incubated with 10% alamarBlue® in subsequent media for 2 hours in dark at 37ºC. 50 µL of alamarBlue® in subsequent media was removed and added to a 96-well flat-bottomed plate. Plate fluorescence was read at excitation 570 nm and emission at 585 nm. Viability was determined as a percentage of untreated control cells.

2.8.3 Live-imaging of microfluidic chambers and quantification of axon degeneration *in vitro*

To determine the amount of axon fragmentation and loss following treatments, microfluidic cultures were imaged on a Nikon TiE live cell microscope, with chambers maintained at 37ºC. Imaging was performed from the axon side of microfluidic chambers both prior to any treatment and 18h following treatment to allow analysis of axonal changes. Images were acquired using 40× objective lens over the axonal side of the chamber. A quantitative measure of axonal degeneration was obtained from five random regions of interest (200 × 200 µm) in the axonal chamber, at least 40 µm away from the microgrooves. Identical regions were imaged before and after treatment. Axons were scored as degenerating by a blinded observer (criteria used: axons must be able to be identified isolated from any bundles that are present and must display fragmenting with at least three sections missing along the axon and/or contain two or more swellings along the axon). Axon degeneration was calculated by

counting degenerated axons. A degeneration index (DI) was determined by the following equation.

$$DI = \left(\frac{\left(\frac{axons\ degenerated\ before}{axons\ degenerated\ after} \right)}{total\ number\ of\ axons} \right) \times 100$$

The percentage degeneration refers to the percentage of axons the have degenerated after treatment, compared to the total number of axons before treatment. Total numbers of axons in the images were also quantitated. The percentage degeneration refers to the percentage of axons the have degenerated after treatment, compared to the total number of axons before treatment. In these experiments, 35 µM, 50 µM, and 100 µM of kainic acid were also analysed in the cell culture using live-imaging, however the axons were too degenerated to be able to target therapeutically.

2.8.4 ELISA to analyse cell culture samples

Relative amounts of specific proteins were determined using ELISAs prepared in house. Extracted samples were centrifuged at 13,000 rpm for 1 minute. 50 µL of samples diluted at 1:300 in coating buffer (approximately 4 µg of protein) were added to 96-well plate and incubated overnight at 4ºC in order to bind the protein to the well. For the standard curve, samples were serially diluted at 1:100, 1:200, 1:400, 1:800 and 1:1600 in coating buffer and 50 µL was added to 96-well plate and incubated overnight at 4ºC. Plates were washed with washing buffer (0.05% tween-20, Sigma Aldrich; in 0.01 M PBS) 5 times and plates were dabbed onto paper towel in between each wash. 100 µL blocking buffer was added to each well and incubated at 37ºC for 30 minutes. Plates were washed 5 times with washing buffer. Detecting antibodies (See Table 2.1) were diluted in blocking buffer and 50 µL was added to

wells and incubated for 1 hour at room temperature. Plates were washed 5 times with washing buffer. 50 µL of species-specific HRP secondary antibody (See Table 2.3) was diluted in blocking buffer at 1:2000 and added to wells and incubated at room temperature for 45 minutes. Plates were washed 5 times with washing buffer. 50 µL of room temperature tetramethylbenzidine (TMB) substrate was added to each well for 15 minutes. The reaction was stopped with 50 µL of 0.1 M H_2SO_4. Plate was read using a plate reader (SpectraMax Plus 384 Absorbance Reader, Molecular Devices) at 450 nm. Sample absorbance was averaged from each duplicate. A standard curve was produced from the serially diluted samples from the absorbance and protein concentration from a Bradford assay. Sample protein concentration was determined from the standard curve. An average from the control samples were obtained and expressed as 100% with samples expressed as a percentage of the control.

2.8.5 Western blotting and ELISA protein extraction

For Western blotting and ELISA analysis, cells were harvested from both microfluidic chambers and culture wells. Culture media was removed and cells were rinsed with cold HBSS. Cells were harvested using RIPA buffer with protease (cOmplete™ Mini Protease Inhibitor Cocktail tablets, Roche) and phosphatase inhibitors (Phosphatase Inhibitor Cocktail, A.G. Scientific). For culture wells, cells were collected using a cell scraper (Falcon) and transferred to an eppendorf tube. For chambers axons were harvested from the axon chamber by using RIPA buffer as stated above, where axons were pooled from 2-4 chambers per treatment. Once collected, tubes were mixed on a shaker for 30 minutes at 4ºC before being centrifuged at 4ºC for 15 minutes at 13,000 rpm. Supernatant was transferred to new eppendorf tube and stored at -80ºC until further use.

2.8.6 Western blot to analyse cell culture sample

Western blot was performed on cell culture samples as previously discussed in section 2.6.1. Briefly, membranes were incubated overnight with primary antibody acetylated tubulin (1:1000 mouse, Sigma Aldrich T7451). The corresponding goat anti-mouse HRP conjugated secondary antibody (1:7000, DAKO P0447) was used as previously described (King et al., 2018). GAPDH (1:5000 mouse, Millipore MAB374) was used as a loading control.

2.9 IMMUNOCYTOCHEMISTRY

Cell cultures were fixed with 4% PFA for 30 minutes at room temperature. PFA was removed, cells rinsed with three washes of PBS and chambers were removed from coverslips. Fixed coverslips were incubated with PBS-T (0.3% triton-X100) diluent for 15 minutes with agitation. Primary antibodies were diluted in 0.01 M PBS and incubated overnight at 4ºC (See Table 2.1). Primary antibodies were removed and rinsed with three PBS washes. Secondary antibodies (See Table 2.2) were diluted in 0.01 M PBS for 2 hours at room temperature with agitation. Secondary antibodies were removed and rinsed with three PBS washes. Coverslips were mounted onto slides (Livingston International with mounting media; DAKO).

2.10 STATISTICAL ANALYSIS

Kolmogorov-Smirnov normality test was used to determine if the values from each group had a Gaussian distribution. Unpaired parametric t-tests were used to assess analysis between vehicle and epothilone D treated APP/PS1 tissue, and one-way ANOVAs using multiple comparison tests were used to compare treatment groups with the controls using GraphPad PRISM 6.0C. Differences for ELISA and axon degeneration counts were evaluated using

one-way ANOVA, with Tukey's post-hoc test for multiple comparisons between groups. For kainic acid live-imaging experiments two coverslips from five separate culture days were analysed. For trichostatin A live-imaging experiments, 1-2 coverslips from four separate culture days were analysed. For whole cell kainic acid ELISAs, three coverslips per treatment from four separate culture days were used. For whole cell trichostatin A ELISAs, three coverslips per treatment from five separate culture days were used. For axon-only kainic acid ELISAs, cells were pooled from 2-3 chambers per treatment from four separate culture days. For axon-only trichostatin A ELISAs, cells were pooled from 2-3 chambers per treatment from five separate culture days. All statistical analysis and graphs were prepared in GraphPad Prism (v6.1). All analysis was performed with the researcher blinded to treatment and genotype. Values were reported as means ± standard error of the mean (SEM), with differences considered significant at $p<0.05$ Further details of statistical analysis are provided in results chapters. For details of n and statistical analysis for each result refer to Table 8.1, Table 8.2, Table 8.3.

Chapter 3

The effect of epothilone D on amyloid and axonal pathology in 12-15 month-old APP/PS1 mice

3 THE EFFECT OF EPOTHILONE D ON AMYLOID AND AXONAL PATHOLOGY IN 12-15 MONTH-OLD APP/PS1 MICE

3.1 INTRODUCTION

3.1.1 Microtubules as a therapeutic target in AD

Pathological alterations to the MAP tau are a key feature of AD and closely correlate with cognitive decline. Microtubules provide structural support to the axon and provide the tracks of axonal transport. Microtubule function relies heavily upon the dynamic ability to rapidly grow and shrink. It has been proposed that a loss of the normal function of tau, results in microtubule depolymerisation, impaired axonal transport and reduced axonal structural stability (Dubey et al., 2008; Mandelkow et al., 2003; Stamer et al., 2002). Thus, a potential strategy to maintain neuronal connectivity in AD is microtubule stabilisation through pharmacological manipulation (Trojanowski et al., 2005).

3.1.2 Microtubule stabilisation drugs in neurodegenerative disease

Microtubule-stabilising agents have been successfully used as a cancer treatments and many are FDA approved (Bollag et al., 1995; Fumoleau et al., 2007; Holen et al., 2004; Konner et al., 2012; Rubin et al., 2005). Microtubules have two major binding sites for drugs that stabilise microtubules; the taxol site and the laulimalide site (Zhao et al., 2016). Taxanes and epothilones are the two main classes of microtubule-stabilising drugs which bind to the taxane site (Nogales et al., 1995; Rao et al., 1999; Snyder et al., 2001). The blood brain barrier creates a major obstacle for treatment of neurodegenerative disease and must be considered in selecting therapeutics. Epothilone B and D in particular are known to cross the blood brain barrier (Brunden et al., 2010; Jang et al., 2016; Varidaki et al., 2018), suggesting that these stabilising agents have potential for treatment in neurodegenerative disease. Previous studies

have directly investigated the potential of microtubule-stabilising drugs, including epothilone D, to reduce microtubule depolymerisation and rescue degeneration in tauopathy mouse models (Brunden et al., 2010; Cheng et al., 2008; Zhang et al., 2005, 2012a). Zhang and others found increased levels of acetylated tubulin, a marker of stable microtubules, after epothilone D administration in the PS19 tauopathy mouse model (Zhang et al., 2012a). Furthermore, they observed a significant decrease in axonal dystrophy and an increase in microtubule density in the optic nerve after epothilone D compared to vehicle treatment. These results also translated to improved cognitive performance in the Y maze and Barnes maze.

In addition to tauopathy, microtubule stabilisation using taxanes or epothilones has been investigated as a therapeutic target in other disorders that involve axon degeneration. In particular, spinal cord injury is associated with several downstream neural mechanisms which ultimately lead to axon degeneration. Microtubule stabilisation has been shown to affect regeneration, axon degeneration, glial response after injury and dendritic spine plasticity (Dubey et al., 2015; Hellal et al., 2011; Ruschel et al., 2015; Sengottuvel and Fischer, 2011).

3.1.3 Potential effects of microtubule stabilisation on AD pathology

If microtubule stabilising drugs are to be investigated as a potential therapeutic in AD, we need to understand their effects on pathological disease processes. The link between Aβ, the other key feature of AD, and microtubule stability has been established. According to the amyloid hypothesis, Aβ alterations are proposed to drive alterations to microtubules, by tau-independent (Pianu et al., 2014) and tau-dependent pathways (Gotz et al., 2001; King et al., 2006; Lewis et al., 2001; Rapoport et al., 2002; Roberson et al., 2007). However, the effect of microtubule stabilisation on amyloid plaque deposition is unclear. Amyloid beta is derived

from the cleavage of APP, which is transported along microtubules in the same compartment as its cleaving enzymes (Kamal et al., 2001). It has been proposed that during axon degeneration and simultaneous microtubule breakdown that APP processing is altered, leading to possible increased Aβ production (Busciglio et al., 1995). Therefore, stabilisation of microtubules with taxanes or epothilones could potentially alter APP processing by preventing microtubule depolymerisation.

Dystrophic neurites have been identified at sites of microtubule disruption (Sadleir et al., 2016). Microtubule stabilisation has potential to rescue dystrophic neurite pathology. Epothilone B has been shown to rescue neuritic dystrophy in MN9D cells after 6-hydroxyDA-induced cytotoxicity in a culture model of Parkinson's disease (Yu et al., 2018). In addition to amyloid and tau pathology, AD cases have substantial gliosis in the brain. In mouse models of amyloidosis, increased gliosis occurs by 6 months of age (Kamphuis et al., 2012). Microglia have also been observed to surround plaques, proposed as an attempt to block toxicity and clear plaques (Bolmont et al., 2008), however the interaction of astrocytes and plaques is still debated (Galea et al., 2015; Kraft et al., 2013; Lopez-Rodriguez et al., 2018; Perez-Nievas and Serrano-Pozo, 2018). The role of MAPs in glial activation and migration suggest that altering microtubules could affect these inflammatory processes (Hellal et al., 2011).

In summary, microtubule stabilisation has been investigated as a protective strategy against axon degeneration resulting from tau pathology, however, the effect of microtubule stabilisation on other pathological features of AD, such as amyloid deposition and glial activation, remain unclear. This is important to consider in investigating microtubule stabilisation as a therapeutic target for AD. In the current study, the effect of epothilone D,

used at concentrations shown in previous studies to affect axonal pathology, was investigated on AD pathology in a mouse model of amyloidosis.

The mouse model used for this study was the $APP_{SWE}/PS1_{dE9}$ mouse model (Jankowsky et al., 2001). This model overexpresses humanised APP with the Swedish mutation, and PS1 with a deletion in exon 9 of PS1 (both identified in familial AD cases), under the mouse prion protein promoter. This model develops amyloidosis, due to enhanced catalytic activity of APP by gamma secretase, which accelerates the deposition rate of Aβ, producing a higher ratio of Aβ-42 than the less toxic Aβ-40. By combining these mutations as a double transgenic mouse model, the pathology of AD is rapidly accelerated, allowing observation of changes to pathology within the mouse brain. The $APP_{SWE}/PS1_{dE9}$ mice used in this study develop amyloid plaques in the cortical and hippocampal regions of the brain from 4-6 months of age. Plaques are frequently surrounded by dystrophic neurites and a substantial glial response is present. Tau pathology is absent from this model allowing direct examination of the effect of amyloid on downstream pathological alterations. The effect of a weekly dose of 2 mg/kg epothilone D (Brunden et al., 2010) from 12-15 months of age, when substantial plaque pathology is present, was examined on amyloid plaques, as well as closely-related brain changes such as dystrophic neurites, astrocyte proliferation and cognition. This age group was chosen as it is representative of a treatment strategy occurring following diagnosis of AD.

3.1.4 Study outline

In the current study, an amyloidosis mouse model of AD, the $APP_{SWE}/PS1_{dE9}$ (Jankowsky et al., 2001), was used to examine the effect of a weekly dose of 2 mg/kg epothilone D at 12-

months of age for 12 weeks. The effects of epothilone D on cognition, dystrophic neurites, synapse loss, amyloid deposition and inflammation were examined.

3.2 METHODS

3.2.1 Ethics and mice

Male $APP_{SWE}/PS1_{dE9}$ (APP/PS1) on a C57BL/6 background (Jankowsky et al., 2001) and wildtype littermates mice were used in this study (see section 2.1).

3.2.2 Epothilone D treatment

Epothilone D (AbCam Lot#APN14287-1-1) was dissolved in DMSO (Sigma Aldrich, Lot#RNBF1056) to a concentration of 100 mg/mL. Twelve-month old APP/PS1 and wildtype littermate controls received weekly treatment of either epothilone D or equivalent volume of DMSO vehicle treatment, intraperitoneally (IP) injected at 2 mg/kg dose (Brunden et al., 2010) for 12 weeks (see section 2.2).

3.2.3 Behavioural, cognitive and weight analysis

Mice were weighed weekly from 12 months old and cognitive testing was performed at 15-months of age. The following tests were used; open field, spontaneous Y-maze, Barnes maze and marble burying and were recorded using EthoVision XT (Noldus; see section 2.3).

3.2.4 Tissue preparation

Following epothilone D treatment, mice were terminally anaesthetised with sodium pentobarbitone (140 mg/kg) and were transcardially perfused with 0.1 M phosphate buffered saline (PBS) for Western blot analysis or with 4% paraformaldehyde (PFA) for histochemical analysis. Tissue was prepared for either molecular analysis or immunohistochemical analysis as outlined in Materials and Methods section 2.4. Amyloid plaque deposition, synaptic loss,

and dystrophic neurites were all analysed in cortical and hippocampal regions of brain tissue using methods outlined in section 2.5.

3.2.5 Protein extraction for molecular analysis

Protein extraction was performed as outlined in Material and Methods section 2.4. Briefly, snap-frozen cortical and hippocampal tissue were homogenised with an UltraTurrax using RIPA buffer with protease and phosphatase inhibitors. Protein concentration was determined using a Bradford assay as per the manufacturer's protocol.

3.2.6 Western blotting

Methods are outlined in Materials and Methods section 2.6. Briefly, membranes were incubated overnight with primary antibodies, anti-synaptophysin (1:1000 rabbit, Millipore), anti-VGLUT (1:1000 mouse, Millipore) and anti-phosphorylated neurofilament protein (SMI312; 1:2000 mouse, Covance). Bands were visualised with enhanced chemiluminescence (ECL) solution-Luminata Forte Western horseradish peroxidase (HRP) substrate (Millipore) and images acquired with a Chemi-Smart 5000 Imaging System (Vilber Lourmat) equipped with Chemi-Capt 5000 software. Band intensity was measured as the integrated intensity using Fiji software. Each value was calculated as a percentage of the standard sample run between gels.

3.2.7 Immunohistochemistry

Immunohistochemical methods are outlined in Material and Methods section 2.5. For immunohistochemical analysis, sections were mounted on slides prior to washing with PBS and blocking with 10% horse serum. Tissue was incubated overnight with primary antibodies

(Table 2.1) in 0.3% triton-X100 followed by incubation with corresponding species-specific secondary antibodies (Table 2.2), in PBS for two hours in the dark. Slides were coverslipped with DAKO mounting media.

3.2.8 Confocal microscopy

Confocal images were taken on a spinning disk confocal Nikon TE- 2000 inverted microscope with a Yokagawa CSU-22 confocal scanning unit and a Hamamatsu C9100-02 EMCCD camera with a 40x objective using Velocity software for image capture.

3.2.9 Plaque load quantitative analysis

Whole cortices were imaged using a spinning disk confocal microscope at 20x objective. Plaque stain signal intensities were classified using ImageSURF (O'Mara et al., 2018). The number of plaques, the average size and the plaque load were calculated and recorded (see section 2.5.4).

3.2.10 Dystrophic neurite quantitative analysis

Dystrophic neurites images were captured using a spinning disk confocal microscope at 40x objective. Plaques were randomly selected between layers II – V in the cortex using the following criteria: between 10 μm – 30 μm in diameter, single plaques (not multilobed). The number, the average size and the dystrophic neurite load was measured (see section 2.5.5).

3.2.11 Synapse quantitative analysis

Alterations in synaptic boutons were examined by immunolabelling coronal tissue sections from vehicle-treated APP/PS1 and wildtype mice with an antibody against synaptophysin.

Immunolabelling was performed in three coronal sections per mouse. Synaptic bouton density and the number of synapses were measured. Synapses around plaques were also quantitated for the number of synapses per plaque, bouton size and density within 40 μm distance from the edge of the plaque (see section 2.5.6).

3.2.12 Microglia qualitative analysis

Microglia were qualitatively assessed between genotype and treatment to determine if the glial response is altered during amyloidosis pathology and with epothilone D treatment. Immunolabelling with Iba1 for microglia was performed in two coronal sections per mouse. Specific regions throughout the cortex where blindly qualitatively compared for any difference between groups, in particular, sections from bregma 0.22 were assessed (see section 2.5.7).

3.2.13 Microglia quantitative analysis

Microglia were quantitatively assessed between genotype and treatment to determine if the glial response is altered during amyloidosis pathology and with epothilone D treatment. Immunolabelling with Iba1 for microglia was performed in three coronal sections per mouse. A region of interest from the midline of the cortex to the rhinal fissure was quantitatively compared for any difference between groups (see section 2.5.8).

3.2.14 Statistical analysis

All statistical analyses were performed in GraphPad PRISM 6.0C. Kolmogorov-Smirnov normality test was used to confirm that the values from each group had a Gaussian distribution. All analyses were performed with the researcher blinded to treatment and

genotype and $p<0.05$ was considered significant. Values are expressed as means and standard error of the mean. For a list of all statistical analyses performed, see section 8.1.

3.3 RESULTS

3.3.1 Epothilone D treatment did not produce any detrimental health effects

To determine if APP/PS1 mice and wildtype littermates had any detrimental health effects following either epothilone D or vehicle treatment, mice were weighed weekly from the onset of treatment. During twelve weeks of treatment there were no significant difference in weights between genotype or treatment (Figure 3.1 A).

3.3.2 Effect of epothilone on behavioural and cognitive measures

At the end of the treatment period, mice underwent behavioural and cognitive testing to determine if genotype or treatment caused any difference in anxiety, short-term memory (one hour), and spatial memory (over a period of five days). During each test, distance and velocity were also measured to determine if epothilone D treatment affected motor performance as this would affect the outcome of the behaviour and cognitive testing.

The marble burying test was performed to measure changes in behaviour. After spending 30 minutes in an OptiMICE cage with 6 evenly spaced marbles (example image in Figure 3.2 A), there was no difference in marble burying for either genotype or treatment (Figure 3.2 A).

Mice were then assessed in the open field test, which can be used to measure both movement and anxiety. In the 10 minutes that mice were placed in the arena, two-way ANOVA demonstrated a significant effect of genotype on velocity and distance. Tukey's post hoc test demonstrated that while epothilone D had no effect on distance travelled and velocity relative

to vehicle treated mice of the same genotype, the epothilone D treated APP/PS1 mice travelled significantly further, and at a greater velocity than their wildtype counterparts.

A

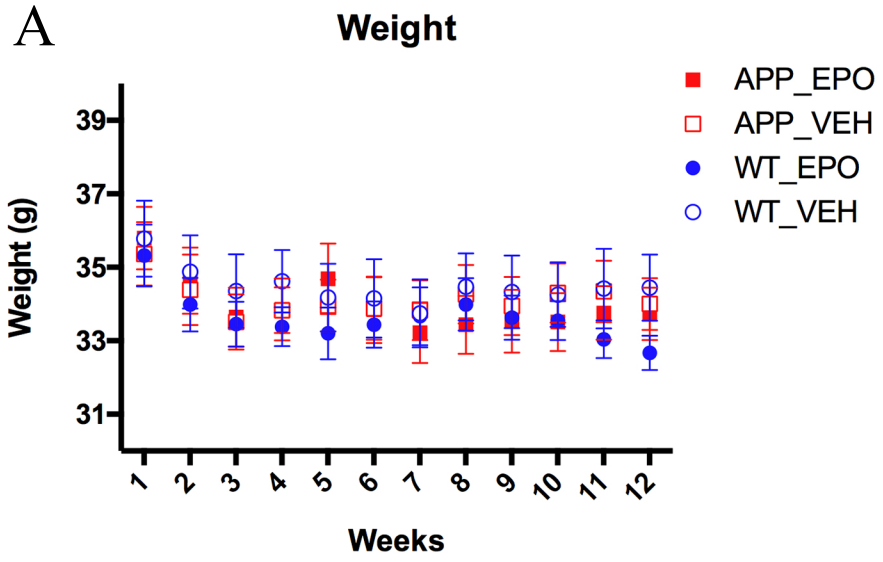
Weight
APP_EPO
APP_VEH
WT_EPO
WT_VEH
Weight (g)
39
37
35
33
31
1
2
3
4
5
6
7
8
9
10
11
12
Weeks

Figure 3.1 The effect of epothilone D treatment on weight in APP/PS1 mice

(A) Bar graph to show average weights of APP/PS1 (APP, red) and wildtype (WT, blue) mice prior to weekly treatment of 2 mg/kg epothilone D (EPO) or vehicle DMSO (VEH) for 12 weeks. There were no significant differences in the weights of animals between groups. Data represented as mean ± SEM.

A

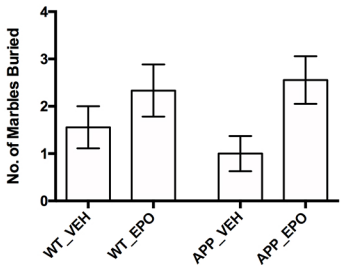
Marble Burying
No. of Marbles Buried
0
1
2
3
4
WT_VEH
WT_EPO
APP_VEH
APP_EPO

B

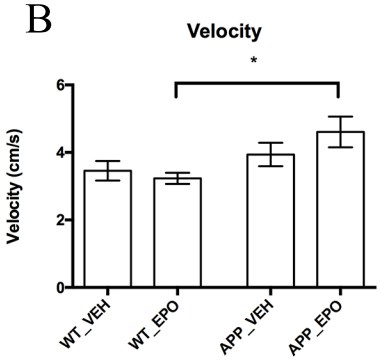
Velocity
*
Velocity (cm/s)
0
2
4
6
WT_VEH
WT_EPO
APP_VEH
APP_EPO

C

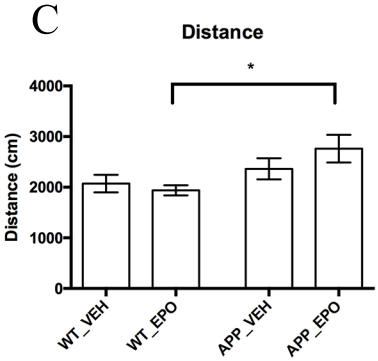
Distance
*
Distance (cm)
0
1000
2000
3000
4000
WT_VEH
WT_EPO
APP_VEH
APP_EPO

D

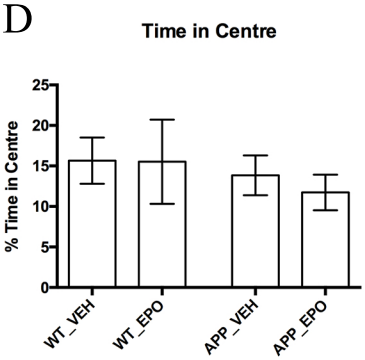
Time in Centre
% Time in Centre
0
5
10
15
20
25
WT_VEH
WT_EPO
APP_VEH
APP_EPO

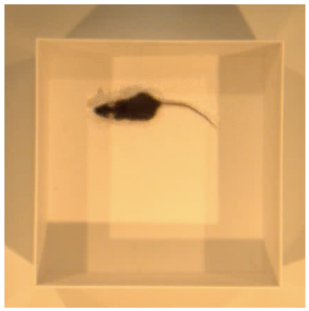

E

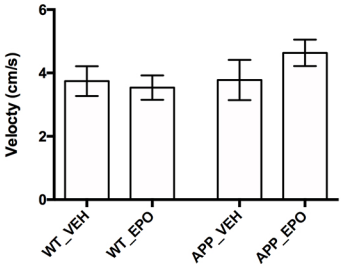
Velocity
Velocty (cm/s)
0
2
4
6
WT_VEH
WT_EPO
APP_VEH
APP_EPO

F

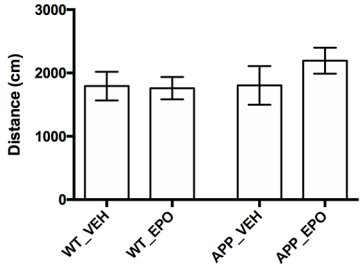
Distance
Distance (cm)
0
1000
2000
3000
WT_VEH
WT_EPO
APP_VEH
APP_EPO

G

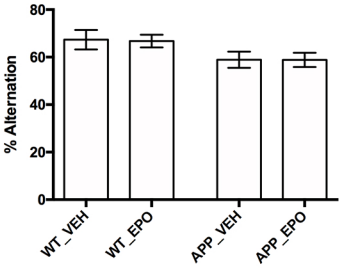
Y-Maze Spontatneous Alternation
% Alternation
0
20
40
60
80
WT_VEH
WT_EPO
APP_VEH
APP_EPO

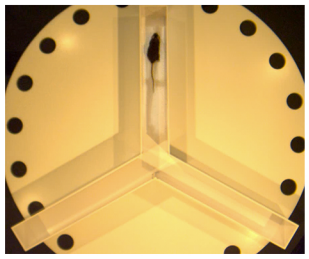

Figure 3.2 The effect of epothilone D treatment on behaviour and cognition in APP/PS1 mice

APP/PS1 (APP) and wildtype (WT) epothilone D (EPO) and vehicle DMSO (VEH) treated mice were tested for anxiety, motor behaviour and cognition using the marble burying test (A), open field (B-D) and Y-maze (E-G).

The number of marbles buried by mice did not depend on animal genotype or treatment (A). Picture representation of the marble burying task (right). APP/PS1 epothilone D treated mice moved at a faster velocity (B) and over a greater distance (C) in the open field arena than wildtype epothilone D treated mice. (D) The time spent in the centre of the arena did not differ between genotype or treatment groups. Picture representation of the open field task (right). APP/PS1 and wildtype mice had no difference in velocity (E), or distance travelled (F) in the Y-maze arena, regardless of treatment. There was no difference in the Y-maze spontaneous arm alternation between groups (G). Picture representation of the spontaneous alteration Y-maze task (right). Bar graph represents mean ± SEM *$p < 0.05$ relative to control.

There was no significant difference in the time the mice spent in the centre, regardless of genotype or treatment (Figure 3.2 B-D).

Cognitive function was assessed using Barnes maze and spontaneous alternation in Y maze tests. There were no differences in velocity, distance or alternating entry in the Y maze (Figure 3.2 E-G). No cognitive differences were detected between genotypes, and short-term memory was not affected by epothilone D treatment in the Barnes maze (Figure 3.3 A-H).

3.3.3 Epothilone D treatment had no effect on dystrophic neurites surrounding plaques

Dystrophic neurites filled with neurofilaments, cellular organelles or lysosomes are a frequent finding surrounding amyloid plaques in AD (Figure 3.4 A, B). The cause of dystrophic neurite formation is unclear, but may result from an interaction of amyloid on the cytoskeleton. I investigated whether stabilising microtubules with epothilone D, affected neurofilament positive dystrophic neurite formation. Sections were immunolabelled with an antibody against phosphorylated neurofilament (SMI312). Dystrophic neurites were examined surrounding individual plaques (between 10 μm – 30 μm) and numbers and size were quantitated in an area of 40 μm distance from the edge of the plaque, according to our published protocols (Fernandez-Martos et al., 2015). There was no difference in the number or size of phosphorylated neurofilament-labelled dystrophic neurite particles around plaques (Figure 3.4 C, D). Similarly, there was no difference in the area occupied by dystrophic neurites (Figure 3.4 E).

3.3.4 Epothilone D treatment reduced phosphorylated neurofilament in the mouse neocortex and hippocampus

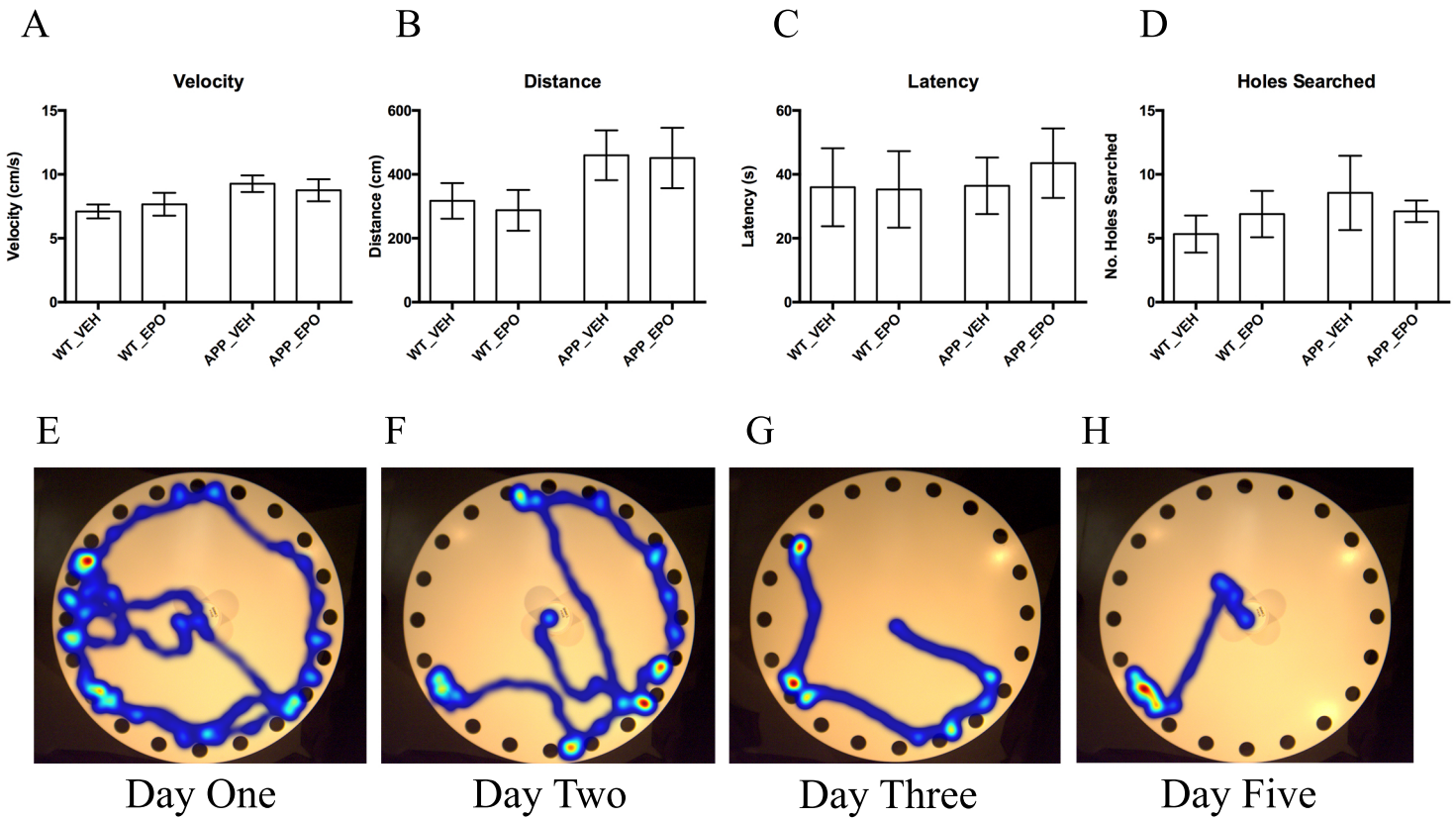
A
Velocity
Velocity (cm/s)
15
10
5
0
WT_VEH
WT_EPO
APP_VEH
APP_EPO
B
Distance
Distance (cm)
600
400
200
0
C
Latency
Latency (s)
60
40
20
D
Holes Searched
No. Holes Searched
E
F
G
H
Day One
Day Two
Day Three
Day Five

Figure 3.3 The effect of epothilone D treatment on cognition in APP/PS1 mice

APP/PS1 (APP) and wildtype (WT) epothilone D (EPO) and vehicle (VEH) treated mice were testing using the Barnes maze test.

APP/PS1 and wildtype mice had no difference in (A) velocity or (B) distance travelled in the Barnes maze, regardless of treatment. The (C) latency of mice to find the escape hole and the (D) number of holes searched in error had no differences between groups on day five of testing (probe trial). Data from training days had no significant difference between treatment groups. Representative heatmap images to show areas of the Barnes maze explored over (E) day one, (F) day two, (G) day three and (H) day 5 (probe trial), with similar profiles for each group. Bar graph represents mean ± SEM *$p < 0.05$ relative to control.

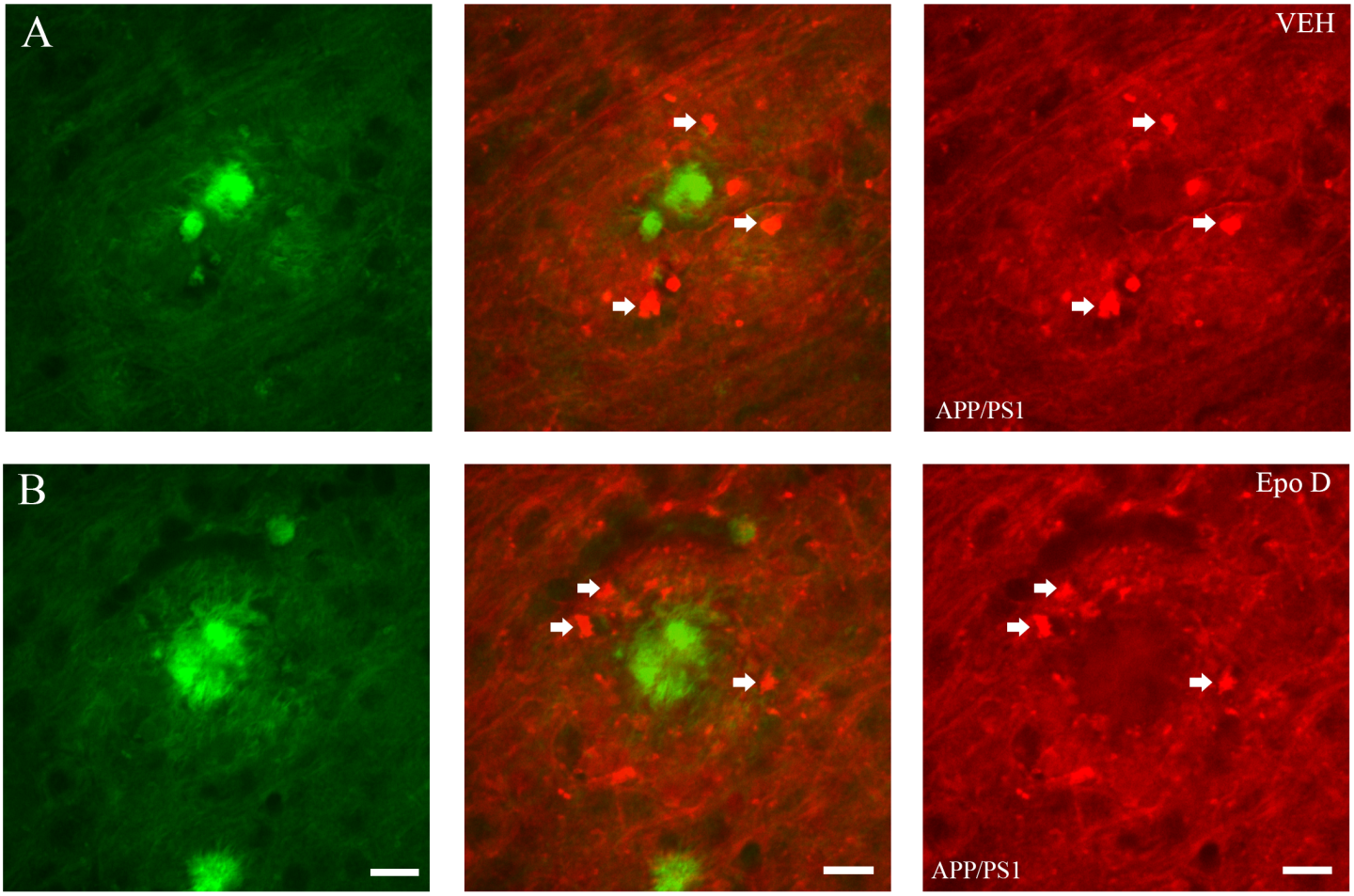
A
VEH
APP/PS1
B
Epo D
APP/PS1

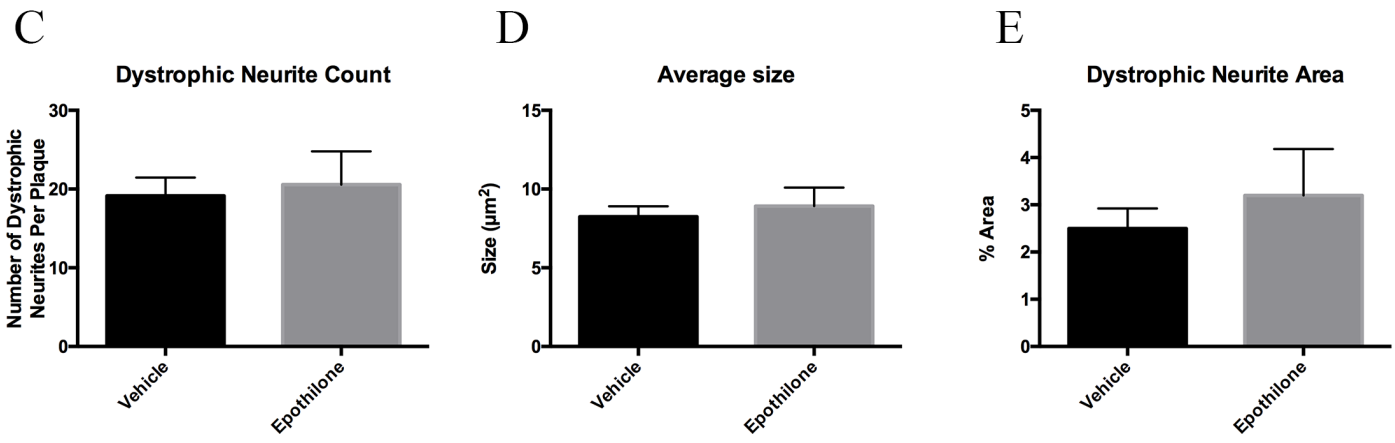
C
Dystrophic Neurite Count
Number of Dystrophic Neurites Per Plaque
30
20
10
0
Vehicle
Epothilone
D
Average size
Size (µm²)
15
10
5
0
Vehicle
Epothilone
E
Dystrophic Neurite Area
% Area
5
4
3
2
1
0
Vehicle
Epothilone

Figure 3.4 Axonal pathology in epothilone D treated 15-month-old APP/PS1 mice

Dystrophic neurites were assessed in APP/PS1 mice treated with vehicle DMSO or epothilone D. Representative images of thioflavin S (green) stained amyloid plaques surrounded by phosphorylated neurofilament immunolabelled dystrophic neurites (SMI312; red) in APP/PS1 mice cortices treated with either (A) vehicle or (B) epothilone D. White arrows indicate dystrophic neurite swellings. Graphs to show (C) the average number of dystrophic neurite particles surrounding a plaque, (D) the average size of the dystrophic neurite particles, and (E) the percentage area occupied by dystrophic neurites within a 40 μm radius of the plaque. There was no difference between treatment groups. Bar graph represents mean ± SEM *$p < 0.05$ relative to control. Scale bar = 14μm.

Since epothilone D binds to microtubules, I postulated that it may have an effect on the cytoskeleton of neurons or glial cells. The effect of epothilone D was examined on phosphorylated neurofilaments (SMI312 antibody) as well as acetylation of microtubules, in the neocortex and hippocampus through Western blotting. Previous studies have indicated that epothilone D may affect microtubule acetylation (Brunden et al., 2011). In the current study, Western blotting analysis demonstrated that in both wildtype and APP/PS1 mice, epothilone D treatment significantly decreased phosphorylated neurofilament compared to vehicle treated mice and this was consistent in the neocortical tissue as well as the hippocampus (Figure 3.5 A, B). Despite using a similar concentration of epothilone D that was used in previous studies, acetylation of microtubules was not affected by epothilone D treatment in either genotype (Figure 3.5 C).

3.3.5 Epothilone D treatment did not affect numbers of synaptic puncta

Microtubule stability is important for synapse and spine stability (Bodaleo et al., 2016; Maas et al., 2009; Merriam et al., 2013) therefore I examined the density of synaptophysin-labelled synaptic puncta in the neocortex in the mice cohort. Synaptic puncta were examined in plaque-free areas of APP/PS1 and wildtype mice neocortices (Figure 3.6 A) as well as surrounding individual plaques (40 µm from plaque edge; Figure 3.6 E) in APP/PS1 mice. There were no significant ($p>0.05$) differences found in the average number of synapses per micrometre, the average size of synaptic boutons or synaptic load between wildtype and APP/PS1 mice in plaque-free areas with or without treatment (Figure 3.6 B-D). There was no difference found in the average number of synapses per micrometre, the average size of the synaptic boutons, or synaptic load around plaques with epothilone D treatment relative to vehicle in APP/PS1 mice (Figure 3.6 F-H).

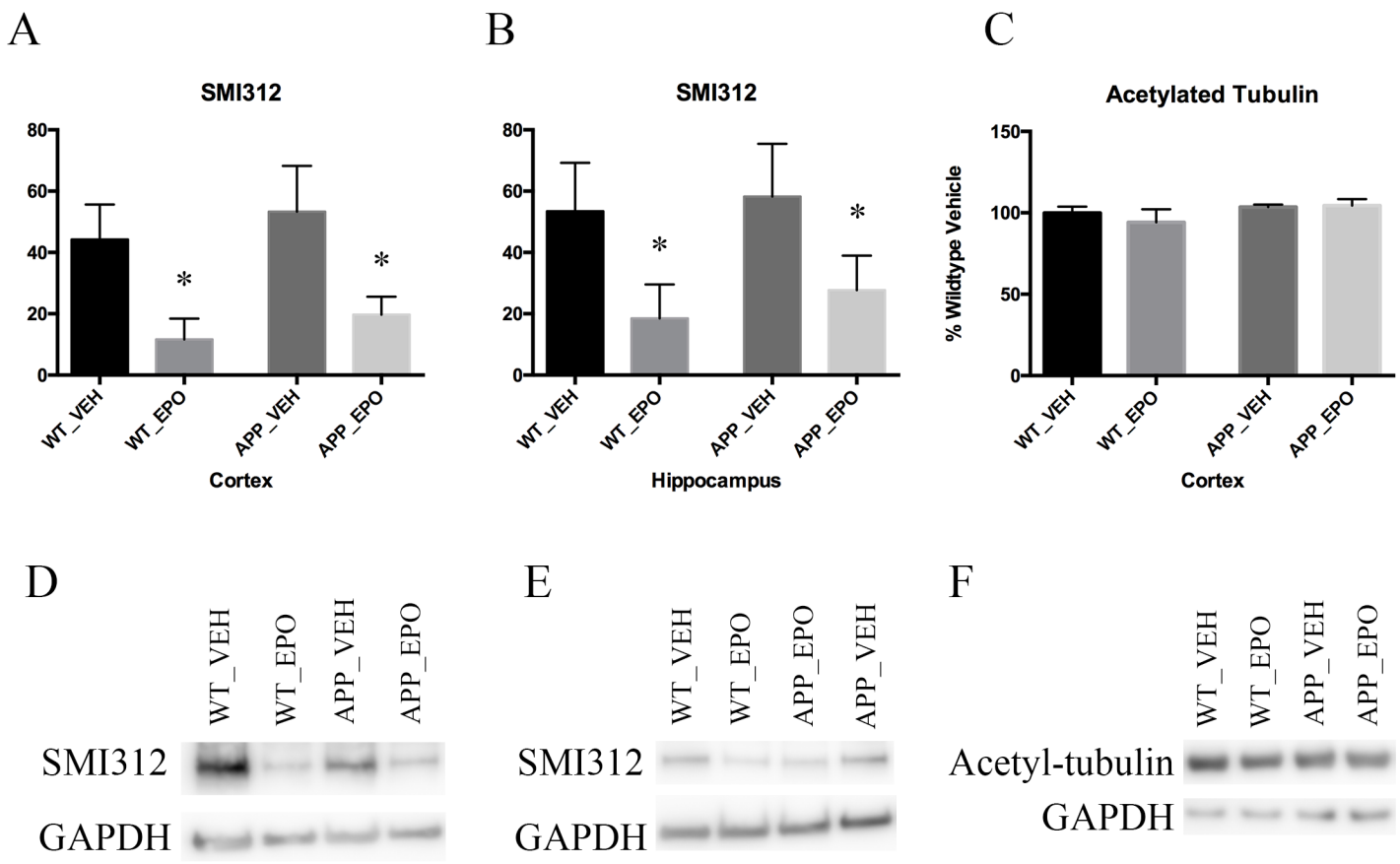
A
SMI312
80
60
40
20
0
*
*
WT_VEH
WT_EPO
APP_VEH
APP_EPO
Cortex
B
SMI312
80
60
40
20
0
*
*
WT_VEH
WT_EPO
APP_VEH
APP_EPO
Hippocampus
C
Acetylated Tubulin
% Wildtype Vehicle
150
100
50
0
WT_VEH
WT_EPO
APP_VEH
APP_EPO
Cortex
D
WT_VEH
WT_EPO
APP_VEH
APP_EPO
SMI312
GAPDH
E
WT_VEH
WT_EPO
APP_EPO
APP_VEH
SMI312
GAPDH
F
WT_VEH
WT_EPO
APP_VEH
APP_EPO
Acetyl-tubulin
GAPDH

Figure 3.5 Effect of epothilone D on phosphorylated neurofilaments and acetylation of microtubules

Western blot analysis of phosphorylated neurofilament (SMI312) levels in the (A) cortex and (B) hippocampus of APP/PS1 and wildtype (WT) mice treated with vehicle (VEH) or epothilone D (EPO). There were significant differences in epothilone D treated APP/PS1 and wildtype mice compared to vehicle treated mice in both the cortex and hippocampus. Western blot analysis of (C) acetylated tubulin in the cortex of APP/PS1 and wildtype mice treated with epothilone D and vehicle and showed no significant difference between groups. Images of representative blots incubated with SMI312 and GAPDH as a housekeeping control for (D) cortex and (E) hippocampus and (F) acetylated tubulin in the cortex. Bar graph represents mean ± SEM *$p < 0.05$ relative to control.

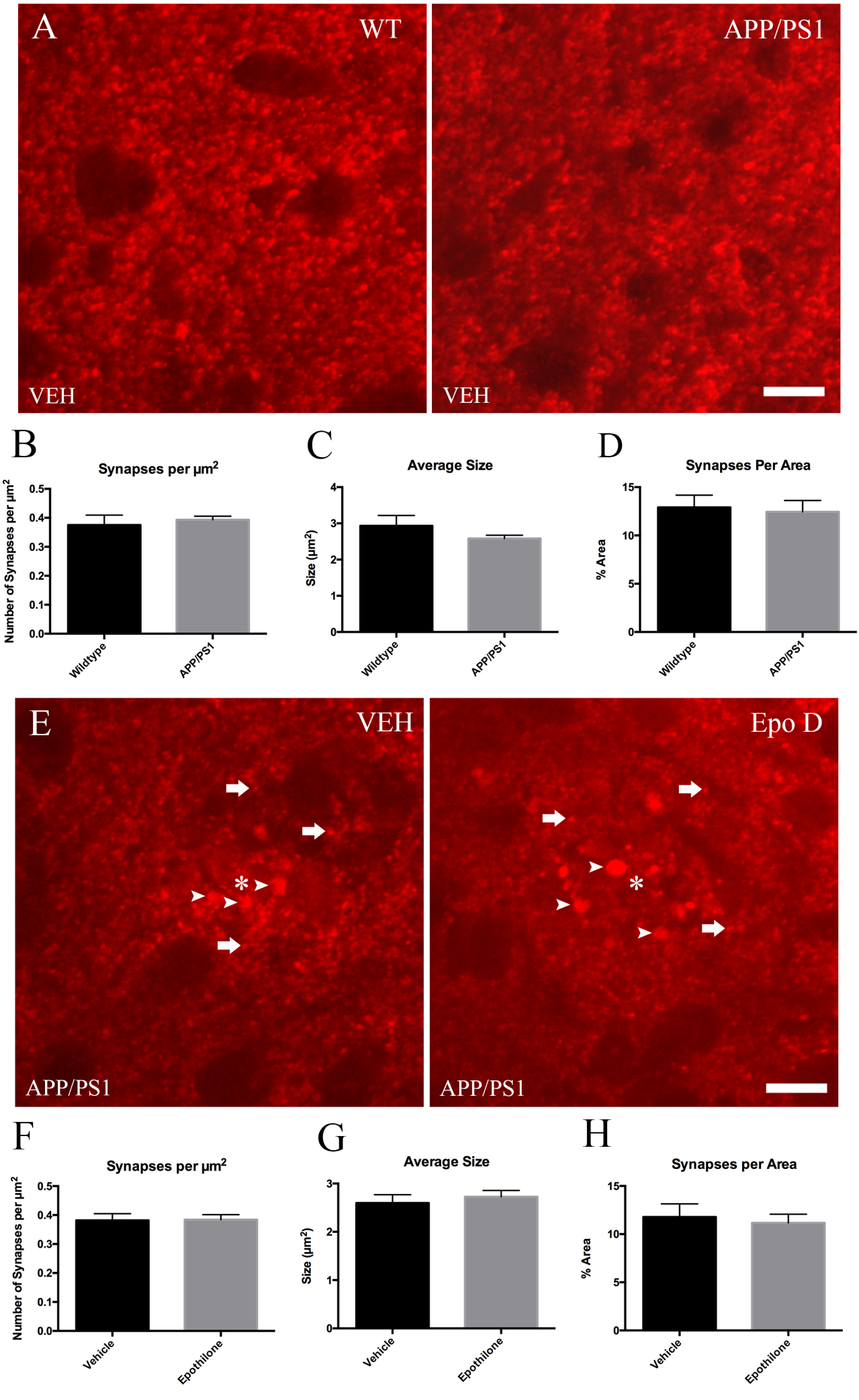
A
WT
APP/PS1
VEH
VEH
B
Synapses per µm²
Number of Synapses per µm²
0.5
0.4
0.3
0.2
0.1
0.0
Wildtype
APP/PS1
C
Average Size
Size (µm²)
4
3
2
1
0
Wildtype
APP/PS1
D
Synapses Per Area
% Area
15
10
5
0
Wildtype
APP/PS1
E
VEH
Epo D
APP/PS1
APP/PS1
F
Synapses per µm²
Number of Synapses per µm²
0.5
0.4
0.3
0.2
0.1
0.0
Vehicle
Epothilone
G
Average Size
Size (µm²)
3
2
1
0
Vehicle
Epothilone
H
Synapses per Area
% Area
15
10
5
0
Vehicle
Epothilone

Figure 3.6 Synapse pathology in epothilone D treated 15-month-old APP/PS1 mice

Synaptophysin immunolabelled tissue was used to quantitate synapses in the cortex of vehicle treated APP/PS1 and wildtype (WT) mice to determine if there were any baseline differences in synapses between genotypes. (A) Representative images of synaptophysin-labelled vehicle-treated mice cortices of wildtype and APP/PS1 mice. Graphs to show the (B) number of synapses per μm^2, (C) average size of synaptic boutons, and (D) synapse load (defined as the percentage area occupied by synaptic boutons) in wildtype and APP/PS1 mice. There were no differences in genotypes for any of the measures.

Synapses were quantitated in APP/PS1 mice treated with vehicle and epothilone D to determine if epothilone D treatment affects synaptic density. (E) Representative images of synaptophysin-labelled synaptic boutons (arrows) around plaques in APP/PS1 mice cortices treated with either vehicle or epothilone D. Note the presence of synaptophysin labelled dystrophic neurites around plaques (arrow head) which were excluded from the analysis by size exclusion. Graphs to show (F) the number of synapses per μm^2, (G) the average size of synaptic boutons, and (H) the synaptic load in APP/PS1 mice treated with vehicle or epothilone D. There were no differences between the treatment groups. Bar graph represents mean ± SEM *$p < 0.05$ relative to control. Scale bar = 14 μm. * = indicates presence of plaque.

Neocortical and hippocampal regions were also assessed for protein expression levels of pre-synaptic markers synaptophysin and VGLUT1 using Western blotting as an indicator of synaptic alterations (Micheva et al., 2010). No differences were found between genotypes or treatment groups (Figure 3.7 A-H).

3.3.6 Epothilone D treatment and amyloid pathology

To determine whether epothilone D treatment affected plaque deposition, coronal sections (n = 5 sections per animal evenly spaced between bregma -2 and bregma 2) were stained with thioflavin S. Number and load (defined as the percentage of plaques per region of interest) of fibrillar plaques were quantitated in the neocortex from the midline to the rhinal fissure. Epothilone D treatment had no significant ($p>0.05$) effect on the average number of plaques per area, average plaque size, or amyloid plaque load in APP/PS1 mice (Figure 3.8 A-E).

3.3.7 Epothilone D treatment and microglia

To determine whether epothilone D treatment affected morphology of microglia in the neocortex, analysis was performed of Iba1 immunolabelled sections (on 2 sections per mouse at bregma 0.22). Qualitative analysis showed a presence of microglia throughout the cortex of all groups. Qualitatively, wildtype mice had more hyper-ramified and bushy microglia compared to APP/PS1 mice, which tended to have more amoeboid microglia present, suggestive of an activated phenotype (Figure 3.9 A-E). Qualitatively, epothilone D did not affect microglia morphology. Quantitative analysis showed no difference in the microglia cell density throughout the cortex of vehicle and epothilone D treated APP/PS1 mice (Figure 3.9 F).

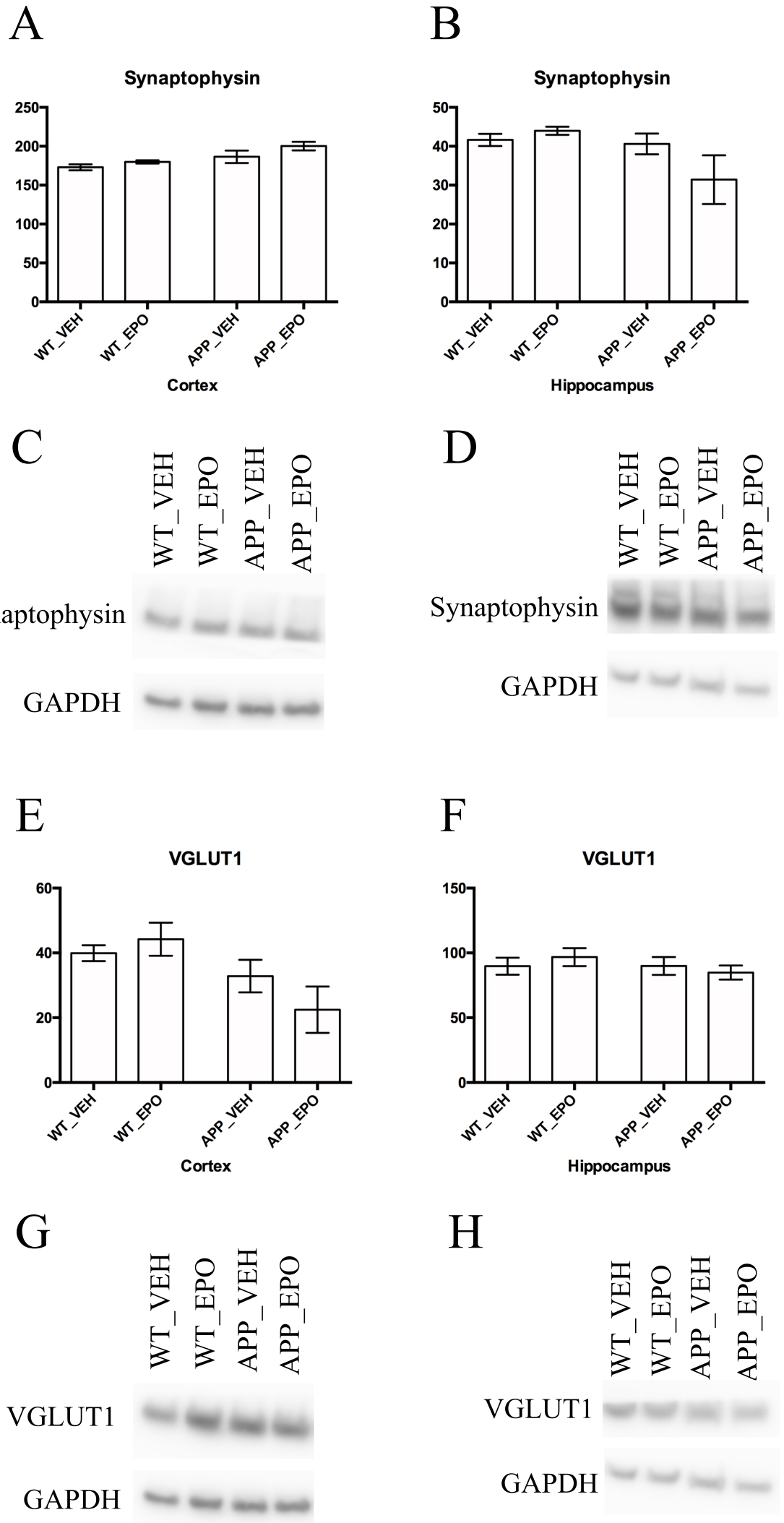
A
Synaptophysin
250
200
150
100
50
0
WT_VEH
WT_EPO
APP_VEH
APP_EPO
Cortex
B
Synaptophysin
50
40
30
20
10
0
WT_VEH
WT_EPO
APP_VEH
APP_EPO
Hippocampus
C
WT_VEH
WT_EPO
APP_VEH
APP_EPO
Synaptophysin
GAPDH
D
WT_VEH
WT_EPO
APP_VEH
APP_EPO
Synaptophysin
GAPDH
E
VGLUT1
60
40
20
0
WT_VEH
WT_EPO
APP_VEH
APP_EPO
Cortex
F
VGLUT1
150
100
50
0
WT_VEH
WT_EPO
APP_VEH
APP_EPO
Hippocampus
G
WT_VEH
WT_EPO
APP_VEH
APP_EPO
VGLUT1
GAPDH
H
WT_VEH
WT_EPO
APP_VEH
APP_EPO
VGLUT1
GAPDH

Figure 3.7 Western blot analysis of synapses in epothilone D treated 15-month-old APP/PS1 mice

Graphs to show Western blot quantification of synaptophysin levels in (A) cortex and (B) hippocampus, relative to wildtype vehicle housekeeping GAPDH (at 100%). There was no difference between groups. Images of representative blots for synaptophysin and GAPDH for (C) cortex and (D) hippocampus. Graphs to show Western blot quantification of VGLUT1 levels in (E) cortex and (F) hippocampus, relative to wildtype vehicle housekeeping GAPDH (at 100%). There was no difference between groups. Images of representative blots for synaptophysin and GAPDH for (G) cortex and (H) hippocampus. Synaptophysin and VGLUT1 were incubated on the same blot, where GAPDH was used as a housekeeping control for both synaptophysin and VGLUT1. Bar graph represents mean ± SEM.

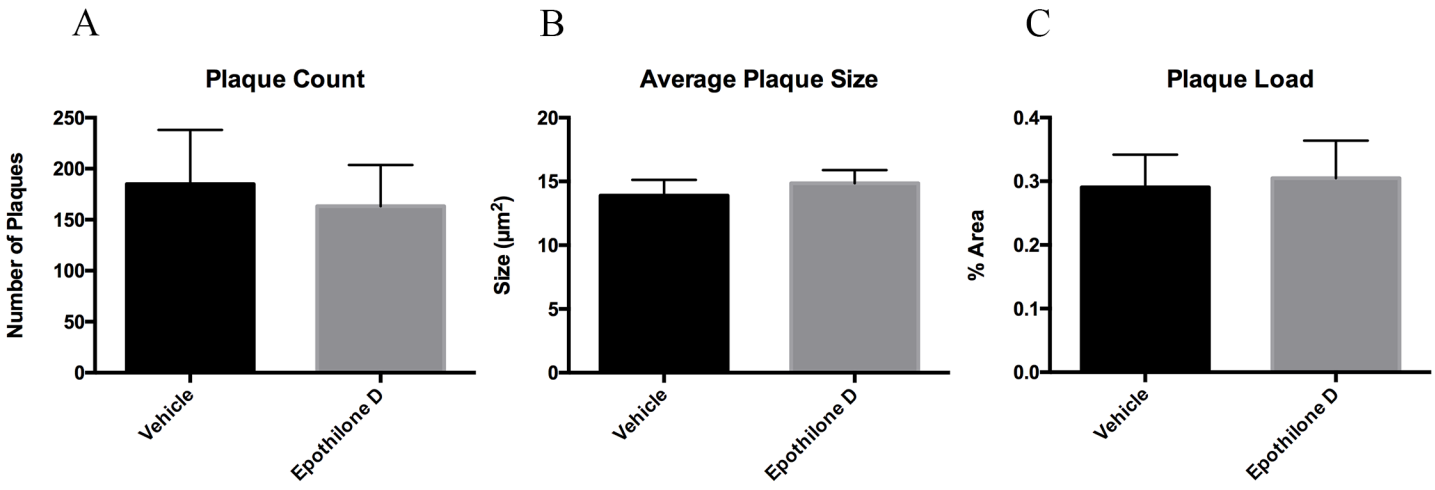
A
Plaque Count
Number of Plaques
250
200
150
100
50
0
Vehicle
Epothilone D
B
Average Plaque Size
Size (μm²)
20
15
10
5
0
Vehicle
Epothilone D
C
Plaque Load
% Area
0.4
0.3
0.2
0.1
0.0
Vehicle
Epothilone D

Figure 3.8 Amyloid pathology in epothilone D and vehicle treated 15-month-old APP/PS1 and wildtype mice

Graphs to show (A) the number of plaques per area, (B) the average plaque size and (C) the plaque load (defined as the area occupied by plaques) in the neocortex. There was no difference between treatment groups. Bar graphs represents mean ± SEM *$p < 0.05$ relative to control.

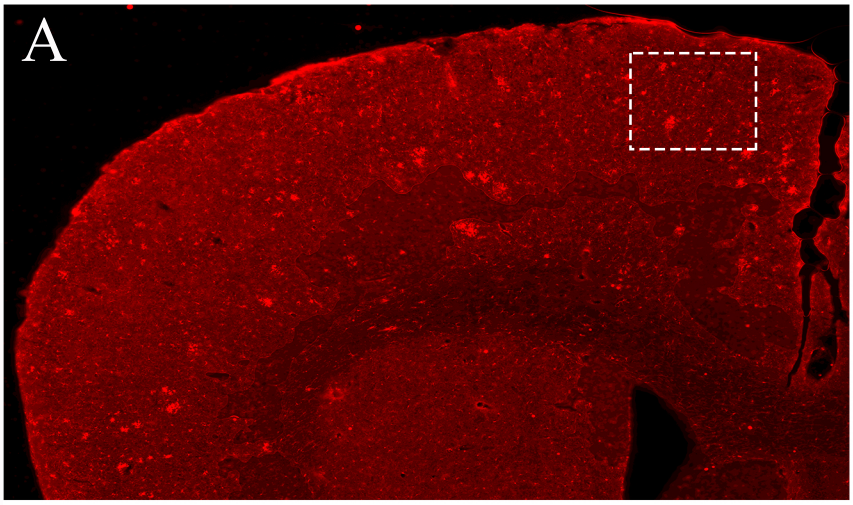
A

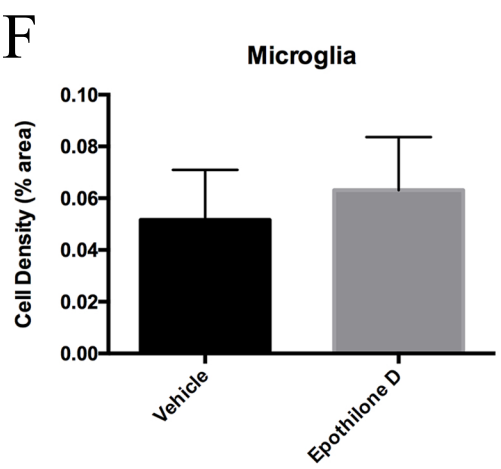
F
Microglia
Cell Density (% area)
0.10
0.08
0.06
0.04
0.02
0.00
Vehicle
Epothilone D

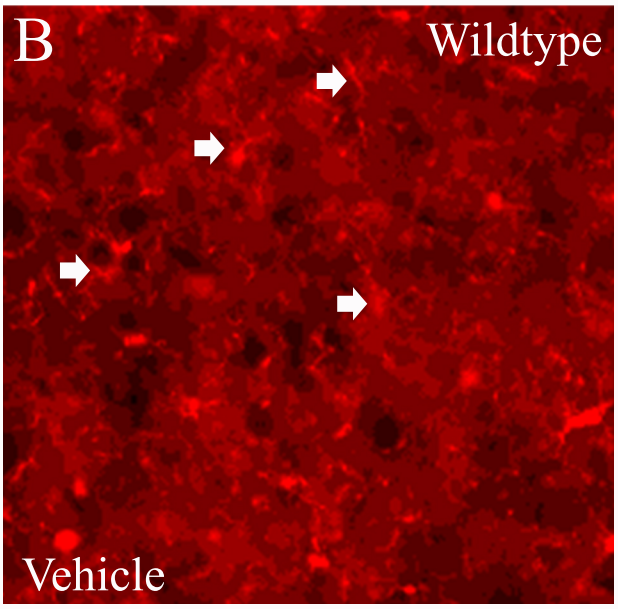
B
Wildtype
Vehicle

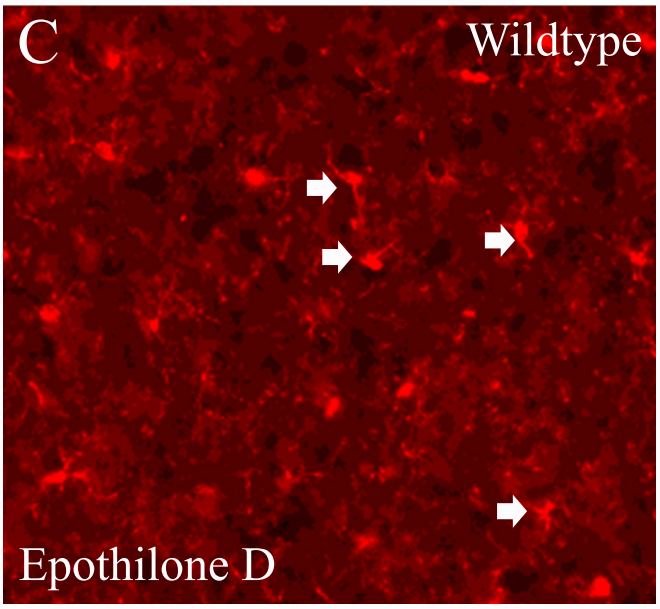
C
Wildtype
Epothilone D

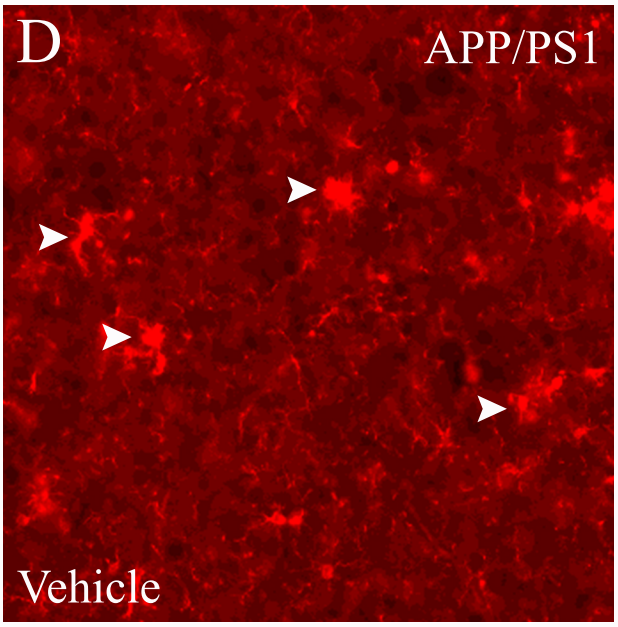
D
APP/PS1
Vehicle

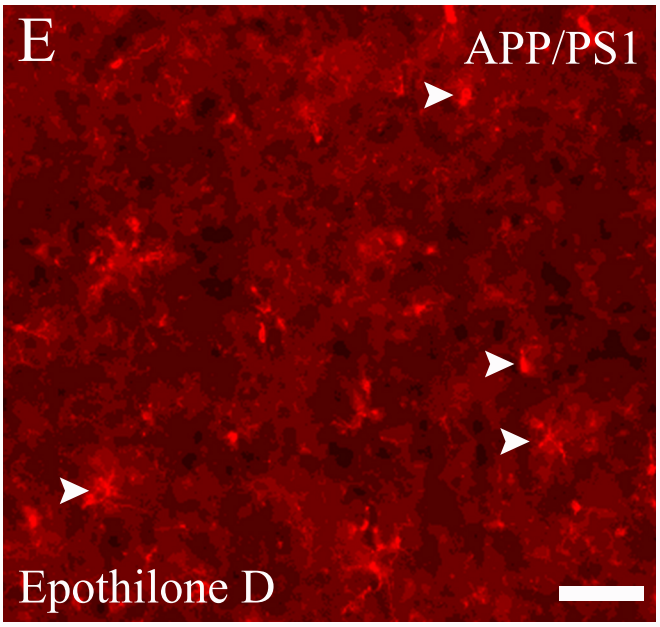
E
APP/PS1
Epothilone D

Figure 3.9 Microglia in epothilone D treated 15-month-old APP/PS1 and wildtype mice

Microglia labelled with Iba1 were assessed qualitatively in APP/PS1 and wildtype mice treated with epothilone D or vehicle. Representative image to show (A) region of interest for qualitative assessment of microglia. Representative images of microglia in (B) wildtype vehicle treated mice (C) wildtype epothilone D treated mice (D) APP/PS1 vehicle treated mice and (D) APP/PS1 epothilone D treated mice. Arrows indicate hyper-ramified and bushy microglia with long and thin processes, and arrow heads indicate amoeboid microglia with short, thick processes. (F) Graph to show microglia cell density in the cortex of APP/PS1 mice treated with either vehicle or epothilone D. Bar graphs represents mean ± SEM. Scale bar = 30μm.

3.4 DISCUSSION

A primary aim of this study was to investigate the therapeutic potential of microtubule stabilisation with drugs such as epothilone D as a treatment for AD, by examining the effect on behavioural and cognitive outcomes, Aβ deposition, synaptic loss, and axonal dystrophy in the APP/PS1 mouse model of AD (Mitew et al., 2013a). Previous research has demonstrated that epothilone D reduces axon and tau pathology whilst increasing microtubule density in tauopathy mouse models (Brunden et al., 2010; Zhang et al., 2018). Following on from this research, this study aimed to determine whether epothilone D treatment has effects on other pathological alterations in AD such as amyloid deposition and dystrophic neurite formation in an amyloid mouse model; the APP/PS1 mouse. As epothilone D had the potential to alter behavioural and cognitive outcomes, memory and anxiety were also assessed using several cognitive tests. This study demonstrated that weight, short-term, spatial and long-term memory were not affected by epothilone D, however epothilone D did have an effect on some behavioural measures in APP/PS1 mice, compared to vehicle treatment, including velocity and distance travelled in the open field test. Furthermore, although epothilone D altered the composition of the cytoskeleton, with a decrease in phosphorylated neurofilament, it did not have any significant beneficial or adverse effects on the pathological features of AD measured in this study.

3.4.1 Microtubule stabilisation with epothilone D affected mouse behaviour and cognition in APP/PS1 mice

This thesis demonstrated that epothilone D did not have any effects on the weight of the mice suggesting no general detrimental effects on health. Similarly, memory function was unaltered by the treatment. In this study, no baseline differences were detected between the APP/PS1 mice and the wildtype mice with vehicle treatment as has been reported in previous

studies (Jankowsky and Zheng, 2017), meaning that there was no deficit to correct. However, this study still demonstrated that epothilone D did not adversely affect cognition supporting its use as a therapeutic. Marble burying is used to measure anxiety by many researchers (Bahi and Dreyer, 2012; Homma and Yamada, 2009; Kim et al., 2012; Taylor et al., 2017), although the interpretation of the results is of much debate (Lazic, 2015; Njung'e and Handley, 1991). Marble burying behaviour does not show habituation after repeated testing, indicating that it is not a learning process, and has also been reported that the behaviour does not differ by gender (Homma and Yamada, 2009). Some suggest that rodents have a tendency to bury harmful objects, although other studies have reported that if the objects make them more anxious, it is more likely that they will avoid the objects (Broekkamp et al., 1986; De Boer and Koolhaas, 2003; Nicolas et al., 2006; Thomas et al., 2009). This study showed no differences between genotype or treatment in marble burying activity.

Overall, the results of the behavioural testing suggest that epothilone D may be having subtle effects in the APP/PS1 mice only, but further research would need to be done to determine the pathways effected.

3.4.2 Epothilone D treatment altered the neuronal cytoskeleton

Treatment with epothilone D significantly decreased phosphorylated neurofilament protein, immunolabelled with SMI312, in both wildtype and APP/PS1 mice. A limitation of the current study is that it is currently unclear whether altered phosphorylated neurofilament protein is due to altered total neurofilament protein levels or to an altered phosphorylation state of neurofilaments as total neurofilament was not investigated and this will need to be performed in future studies. Aggregation of neurofilaments is a common marker of neurodegenerative disease (Liu et al., 2004a) and results from altered levels or

phosphorylation state of neurofilaments (Dale and Garcia, 2012; Yuan and Nixon, 2016). Previous research has examined the relationship between microtubules and neurofilaments in mice with a knockout of the neurofilament light protein (NFL), which is a core component of the neurofilament triplet protein and results in altered axonal expression of neurofilaments (Millecamps et al., 2007). It has been shown that neurofilament depletion increased microtubule density and improved microtubule dynamics (Yadav et al., 2016). Similar studies have shown that knockout of NFL in mouse cultured dorsal root ganglion neurons, depletes axonal neurofilaments and increases both fast axonal transport and mitochondria transport (Perrot and Julien, 2010), which are microtubule dependent processes. Furthermore, NFL depletion in mouse models of motor neuron disease have increased microtubule stability and delayed axon degeneration (Bömmel et al., 2002; Martin et al., 2002; Selvaraj et al., 2012; Yadav et al., 2016). As epothilone D was found to reduce phosphorylated neurofilament protein in this study, it provides proof of concept that epothilone D was having an effect on the cytoskeleton in this cohort, despite the lack of altered microtubule acetylation in this study, unlike the study by Brunden and colleagues (Brunden et al., 2011), which used the same concentration of the drug. The reason for the differences is unclear, but may be due to technological differences, such as the site of injections. Alternatively, as acetylated tubulin is a marker of long-lived microtubules, it may be that in these 15-month old animals, acetylated tubulin levels are already high and therefore less affected by epothilone D. This may suggest that new microtubules could be more vulnerable to dystrophic neurite pathology and it would be of interest to investigate dystrophic neurites in younger APP/PS1 mice. There is limited research about the interactions of epothilone D and phosphorylated neurofilament. Epothilone D could possibly affect phosphorylated neurofilament by increasing microtubule stability, thereby making neurofilaments redundant, however the mechanism by which microtubules and neurofilaments interact is not known. From the current study, the concentration of

epothilone D required to cause a change to prevent further axonal dystrophy, such as dystrophic neurite formation, may be much higher, and more in line with doses to treat cancers, which cause cell cycle arrest.

3.4.3 Epothilone D did not alter neurofilament immunoreactive dystrophic neurite formation despite alterations to phosphorylated neurofilament

Dystrophic neurites are damaged neural processes within the cortex of AD patients, and in AD mouse models, which frequently surround amyloid plaques. These plaques are termed neuritic plaques (Vickers et al., 1996). Neurofilament labelling with SMI312 antibody has previously been reported to visualise dystrophic neurites (Fernandez-Martos et al., 2015; Masliah et al., 1993). In the current study, neurofilament-labelled dystrophic neurites were assessed by immunohistochemical analysis. Dystrophic neurites were present surrounding amyloid plaques in this cohort, in line with other studies (Adlard et al., 2000; Spires-Jones and Hyman, 2014). However, immunohistochemical analysis showed no difference in number or size of dystrophic neurite particles labelled with SMI312. Since the current study administered epothilone D at a timepoint after formation of many dystrophic neurites, epothilone D may be unable to alter neurite dystrophy once formed. It is less clear whether epothilone D is able to prevent formation of new dystrophic neurites as the disease progresses and new amyloid plaques continue to grow. Further analysis of the timing of dystrophic neurite formation in this mouse model would aid in determining a timepoint for examining this. Previous work in this mouse model demonstrated that there is an increased plaque load between 12 and 15 months of age, however an analysis of dystrophic neurite formation over this timepoint has not been performed. It would be of interest in future studies to also examine the effect of epothilone D at earlier timepoints where plaque load increases and potentially dystrophic neurite formation are more dynamic.

The results of this thesis suggest that any strategy to reduce phosphorylated neurofilament is unlikely to rescue dystrophic neurites. A previous study has examined whether loss of neurofilament light protein (NFL), which reduces axonal neurofilament levels had an effect on dystrophic neurites (Fernandez-Martos et al., 2015). This study demonstrated that NFL deficiency significantly ($p<0.05$) increased neocortical dystrophic neurite pathology. Further examination of the changes to specific neurofilament triplet proteins and their phosphorylation state following epothilone D treatment would aid in an understanding of the mechanisms by which dystrophic neurite pathology is affected by neurofilament. It has previously been shown that the microtubule and neurofilament cytoskeleton are closely linked and alteration in one could result in compensation of the other (Liu et al., 2012).

3.4.4 Epothilone D did not affect synapses

In this study the effect of epothilone D on axons was further investigated by examining pre-synaptic terminals in the neocortex. No difference in synaptic density or size was present in any treatment group or genotype. Since there was no difference in presynaptic puncta in plaque-free areas between vehicle treated wildtype and APP/PS1 mice, this suggests that there is no synapse loss in this model, in the age and cortical areas examined, as suggested by other studies (Hong et al., 2016; Wirths and Bayer, 2010). However, some researchers report synapse loss in the hippocampus of this mouse model (Alonso-Nanclares et al., 2013; Da Silva et al., 2016; Gengler et al., 2010; Salazar et al., 2017). One study has showed that oligomeric Aβ surrounding plaques does contribute to excitatory synapse loss in the APP/PS1 mouse model, however the age range of these mice varied from 8-13 months (Koffie et al., 2009). Other research is in line with the results of the current study, demonstrating that dense core plaques do not accentuate synapse loss in brains of AD patients (Masliah et al., 1990),

although results may be dependent on the specific markers analysed and the analysis technique. Overall the current study demonstrates that epothilone D at the levels used in this project does not damage synaptic connections.

Previous reports have suggested that epothilone D does have the capacity to rescue synapse loss in other models that exhibit synaptic degeneration. For example, in a STOP-null mouse model of schizophrenia, epothilone D treatment increased synaptic vesicle pools and improved synaptic plasticity in glutamatergic neurons and improved cognition (Andrieux et al., 2006). However, consistent with the results from the current study, epothilone D has no effect on pre-synaptic terminal synapses at the neuromuscular junction (Clark et al., 2018; Dubey et al., 2015).

3.4.5 Epothilone D did not affect fibrillar amyloid deposition

A potential effect of microtubule stabilisation targeting tau pathology in AD is an effect on Aβ production. APP is transported via fast anterograde transport to the axon terminal. A link between APP transportation and amyloid processing has been suggested since APP, β-secretase and presenilin 1 may be transported together via fast anterograde transport (Brunholz et al., 2012; Kamal et al., 2001; Lazarov et al., 2005; Rodrigues et al., 2012). The authors of this study demonstrated that processing of APP occurs within its compartment during transport along axons, resulting in production of the toxic Aβ peptide (Kamal et al., 2001). This suggests that alterations in transport could drive APP processing along the amyloidogenic pathway, creating more amyloid deposits. To investigate potential effects of altered transport through microtubule stabilisation on amyloid processing, fibrillar plaque load was examined. The current data shows no difference in plaque load following epothilone D treatment, suggesting that microtubule stability may not affect amyloid deposition. While

epothilone B has been reported to exhibit both beneficial and detrimental effects in animal models, which is dependent on the drug concentration, the type of neuron, and the age of neurons (Jang et al., 2016), the data presented from the current study suggest that epothilone D is unlikely to have adverse effects on amyloid if used as a treatment strategy to protect against tau pathology.

3.4.6 Epothilone D and microglia

Microglia were qualitatively assessed to determine if genotype or epothilone D treatment affected morphology of microglia. Microglia were present throughout the cortex in all treatment groups. Wildtype mice treated with either vehicle or epothilone D had hyper-ramified and bushy microglia. In APP/PS1 mice, amoeboid microglia were present regardless of vehicle or epothilone D treatment. An increase in microglia in an APP/PS1 mouse model has previously been reported (Holland et al., 2018; Manocha et al., 2016).

There are a number of limitations which need to be considered in this study. One limitation is that the APP/PS1 model is limited to amyloidosis-driven pathology, and drives amyloid pathology through a specific pathway. Therefore, this model may not represent sporadic disease. Another limitation of is study is that the actual concentration of epothilone D in the brain is unknown, and as the acetylated tubulin results show, it suggests that there is less than in previous studies. One concentration and one timepoint was investigated in the current study, but future studies could investigate higher concentrations of epothilone D, such as 3 mg/mL, and early timepoints could be examined, such as 6 months, when amyloid plaques are developing within the cortex and hippocampus. An unexpected outcome of this study was that synapses changes were not detected between genotypes in vehicle treated mice. Another limitation of this study is the use of male mice only. Future studies could also further

investigate astrocytes and microglia, by assessing morphology and density within the neocortex and hippocampus.

3.4.7 Conclusion

In conclusion, the results presented here provide evidence that epothilone D treatment does not further exacerbate APP/PS1 pathology, including amyloid plaques and neurite dystrophy. However, epothilone D treatment does significantly reduce phosphorylated neurofilament in both the neocortex and hippocampus. Although studies have shown changes to synapse loss around plaques, there were no changes detected in synapses in this mouse model at the age examined. Importantly, the low doses (2 mg/kg) of epothilone D appeared safe as weight and cognitive testing was unchanged to the vehicle-treated mice.

Chapter 4

Targeting microtubule post-translational modifications in excitotoxin-induced axon degeneration

4 TARGETING MICROTUBULE POST-TRANSLATIONAL MODIFICATIONS IN EXCITOTOXIN-INDUCED AXON DEGENERATION

4.1 INTRODUCTION

4.1.1 Introduction

The previous chapter demonstrated that epothilone D treatment caused some alterations to the cytoskeleton and had minor effects on behaviour but did not affect the key pathological features of the APP/PS1 mouse model. Previous studies suggest that epothilone D can protect against tau pathology. Together these results suggest that targeting microtubules to stabilise their structure could be an effective intervention to prevent axon degeneration without adverse effects on other types of pathology in neurodegenerative disease. Axon degeneration and microtubule breakdown are reported in several neurodegenerative diseases, however the relationship between microtubule depolymerisation and axon degeneration, particularly as it relates to neurodegenerative disease, is not clearly understood.

Axon degeneration is reported, not only in several neurodegenerative diseases, but also in acquired forms of brain injury, and can occur independently of cell death (Lingor et al., 2012). The best described mechanisms of axon degeneration are axonal pruning, which occurs during development and Wallerian degeneration, which occurs following axon severing (Coleman, 2005; Coleman and Freeman, 2010). In contrast, the cellular process underlying axon degeneration in a range of neurodegenerative diseases and following brain injury are less understood and are unlikely to be linked to direct axonal severing, but rather to a gradual series of biochemical changes following specific disease-associated pathological insults.

4.1.2 Excitotoxin-induced axon degeneration

One such pathological insult, excitotoxicity, is a result of excessive stimulation by the excitatory neurotransmitter glutamate, leading to increased intracellular calcium and a cascade of harmful calcium-dependent events (Dong et al., 2009). Excitotoxic mechanisms have been implicated in AD, traumatic brain injury, stroke, and amyotrophic lateral sclerosis, which all undergo some form of axon degeneration (as reviewed by Gibson and Bromberg, 2012; Lai et al., 2014; Lewerenz and Maher, 2015). Previous studies in compartmentalised cultured cortical neurons have shown that excitotoxic insult directed to the neuronal soma results in fragmentation of the unexposed axon (Hosie et al., 2012). This was significantly attenuated by treatment of the axons with the microtubule stabilising drug, taxol, implicating microtubule disruption in the breakdown of the axon (King et al., 2013).

4.1.3 Microtubule post-translational modifications

As described in section 1.4, microtubule are highly dynamic polymers of alpha- and beta-tubulin. Their ability to undergo rapid changes in polymerisation state (termed dynamic instability) is essential for their function and is controlled by the binding of MAPs as well as by their PTMs (Horio et al., 2014). The microtubule disruption that occurs following excitotoxin exposure and leads to axon degeneration could result from depolymerisation, potentially relating to changes to PTM or from altered MAP binding. However, microtubule PTMs and MAP binding are not independent, as the binding capacity of some MAPs can be influenced by microtubule PTMs (Howes et al., 2014). Understanding the specific changes that occur to microtubules following an excitotoxic insult could help in directing therapeutics to protect axons and maintain nerve cell connectivity in neurodegenerative disease. In this chapter I focus on examining alterations to microtubule PTMs following an excitotoxic insult. PTMs of microtubules include glutamylation, tyrosination and acetylation. Acetylation, glutamylation and detyrosination are associated with stable microtubules, whereas

tyrosination is associated with unstable and more dynamic areas of microtubules (Uchida and Shumyatsky, 2016). Thus, microtubule PTMs may be a potential target for therapeutic intervention. In this regard, drugs targeting acetylation such as histone deacetylase 6 (HDAC6) inhibitors have been investigated for the treatment of depression, cancer, stroke, environmental stress and Huntington's disease (Brindisi et al., 2016, 2018; Ceccacci and Minucci, 2016; Dompierre et al., 2007; Jochems et al., 2014; Lazo-Gómez et al., 2013; Rao et al., 2017; Simões-Pires et al., 2013; Wang et al., 2016).

4.1.4 Microfluidic chambers as a model to study excitotoxin-induced axon degeneration

Microtubules are present in all cell types and there may be cell-type specific responses to excitotoxin exposure. Therefore, in order to investigate microtubule alterations in neurons and more specifically in axons, it is necessary to be able to separate out these specific compartments and an appropriate model is needed. Primary neuron cultures derived from rodents can be grown in isolation of other cell types and can be grown in compartmented microfluidic chambers. These multicompartment culture chambers allow for fluidic isolation of neuronal processes from their cell bodies, thereby allowing for pharmacological manipulation on isolated parts of the neuron (Taylor et al., 2006). Therefore, microfluidic chambers are ideal to investigate axon degeneration and the associated mechanisms.

Axonal growth within the microgrooves of microfluidic chambers is well-documented (Taylor et al., 2005), whereby at 7 DIV, axons have extended into the axonal compartment of the chamber, while dendrites remain isolated to the somal compartment, even up to 14 DIV, a timepoint between 10-14 DIV also corresponds to an established mature glutamate receptor phenotype (Taylor et al., 2005). Therefore, in the current study, axons were grown to 10 DIV to allow for both axonal growth and mature receptor phenotype. Furthermore, excitotoxicity

by continuous stimulation of NMDA and AMPA/kainite stimulation has been implicated in several neurodegenerative diseases, including AD, Huntington's disease, Parkinson's disease and amyotrophic lateral sclerosis (as reviewed in (Dong et al., 2009; Van Den Bosch et al., 2006). NMDA receptors have high Ca^{2+} permeability and conductance properties and continuous stimulation leads to a cascade of events resulting in caspase activation and cellular toxicity (Fan and Raymond, 2007; Ikonomidou et al., 2000; Jung et al., 2009; Ndountse and Chan, 2009). AMPA-type glutamate receptors have been implicated in excitotoxicity and are also highly permeable to Ca^{2+}. Stimulation of NMDA and AMPA receptors has been implicated in excitotoxin-induced axon degeneration (Wang et al., 2006, 2008). However, mechanisms of toxicity may differ between disease and little is known about how each contributes to axon degeneration. In this thesis, kainic acid toxicity through modulating AMPA/kainite receptors was investigated. This model has been well-characterised (King et al., 2013; Wang et al., 2005; Zhu et al., 2011). Although glutamate receptors are present throughout the neuron (Hosie et al., 2012), the majority are present on the somatodendritic compartment, therefore, using microfluidic chambers allows for targeted exposure to the somatodendritic compartment, while changes to the unexposed axon are observed.

4.1.5 Study outline

In this study, alterations of microtubule PTMs were examined after excitotoxic-induced axon degeneration. Microtubule breakdown occurs in axon degeneration, although mechanisms of microtubule alterations are unknown. Kainic acid has been previously used *in vitro* to induce excitotoxicity, resulting in axon degeneration. In this model, primary cortical cultures at 10 DIV, grown either on coverslips or in microfluidic chambers, were treated with kainic acid. Microtubule PTMs were examined using ELISA and immunocytochemical techniques. Live-imaging techniques were utilised to measure the degree of axon degeneration in cells treated

with kainic acid. After microtubule alterations were characterised, the potential of microtubule stabilising agents was investigated to determine if they prevent axon degeneration.

4.2 METHODS

4.2.1 Ethics and mice

All experiments and procedures were approved by the University of Tasmania Animal Ethics Committee (A12780, A15121 and A17530) and were in accordance with the Australian Guidelines for the Care and Use of Animals for Scientific Purposes. C57Bl/6 mice were used for cell culture experiments (see section 2.1).

4.2.2 Primary cortical cell culture

Mouse cortical neuron cultures were prepared as previously described (King et al., 2013). Cortical neurons were prepared from embryonic day 15.5 (E15.5) C57Bl/6 mice. Cortices were and transferred to 5 mL Hanks Balanced Salt Solution (HBSS, Gibco). Trypsin (0.0125%) was added for 5 minutes at 37ºC, followed by removal of HBSS and replaced with 1 mL of initial plating media and mechanically triturated with a 1 mL pipette. Cells were plated either into the soma compartment of microfluidic chambers or directly into the wells of poly-L-lysine coated culture plates. Cells were allowed to adhere to the coverslip (Livingstone) at 37ºC for 30 minutes prior to adding initial plating media to the chambers. Cells were incubated at 37ºC overnight before initial media was replaced with subsequent media with no fetal calf serum and glutamate. Cells were grown to 10 days *in vitro* (DIV) at 37ºC in 5% CO_2 (see section 2.7.1, 2.7.2).

4.2.3 Pharmacological manipulation

Cells were treated with 0 µM, 10 µM, or 25 µM of kainic acid (Sigma Aldrich, Lot#SLBD1491V) in DMSO (Sigma Aldrich, Lot#RNBF1056) at 10 DIV. Cells grown in 12-well plates or the soma compartment of microfluidic chambers were exposed to kainic

acid for 1 hour, 6 hours and 18 hours. For a set of experiments cells were treated with trichostatin A. Cells at 10 DIV in 12-well plates or axonal compartment of microfluidic chambers were treated with 10 nM or 100 nM trichostatin A (Sigma Aldrich, Lot#026M4036V) for 2 hours before 6 hours of kainic acid exposure. The health of cells was determined using an alamarBlue® assay. For a set of experiments cells were treated with taxol (Calbiochem, Lot#B66835). For all pharmacological manipulations, vehicle controls were performed and are reported. No significant difference was found in any measure for vehicles to untreated cells (see section 2.8.1, 2.8.2).

4.2.4 Live cell imaging and quantitation of axonal degeneration

Microfluidic cultures were imaged on a Nikon TiE live cell microscope, with chambers maintained at 37ºC. Imaging was performed prior to treatment and 18 hours following treatment. Axonal side of the microfluidic chambers were imaged using 40x objective lens in identical regions before and after treatment. Axon degeneration was calculated by counting degenerated axons (see section 2.8.3).

4.2.5 ELISA analysis of microtubule post-translational modifications

Cells were harvested with RIPA buffer with protease and phosphatase inhibitors. Samples were diluted at 1:300 in 50 µL bicarbonate/carbonate coating buffer (AbCam), added to 96-well plate and incubated overnight at 4ºC. For the standard curve, protein samples were serially diluted at 1:100, 1:200, 1:400, and 1:800. A blank and no primary control were included to correct for ELISA results. ELISA plates were incubated with detecting antibodies (acetylated tubulin 1:500 mouse, Sigma Aldrich; tyrosinated tubulin 1:500 rabbit, Millipore; see section 2.8.4).

4.2.6 Western blot analysis of microtubule post-translational modifications

Axons were harvested with RIPA buffer with protease (cOmplete™ Mini Protease Inhibitor Cocktail tablets, Roche) and phosphatase inhibitors (Phosphatase Inhibitor Cocktail, A.G. Scientific), with protein pooled from 2-4 chambers per treatment group. Membranes were incubated overnight with primary antibody acetylated tubulin (1:1000 mouse, Sigma Aldrich). Bands were visualised with enhanced chemiluminescence (ECL) solution-Luminata Forte Western horseradish peroxidase (HRP) substrate (Millipore) and images acquired with a Chemi-Smart 5000 Imaging System (Vilber Lourmat) equipped with Chemi-Capt 5000 software (see section 2.8.5).

4.2.7 Immunocytochemistry

Immunocytochemistry was performed as previously described in section 2.9. After fixation cultures were blocked in diluent and incubated with primary antibody acetylated tubulin (1:1000 mouse, Sigma Aldrich).

4.2.8 Statistical analysis

Differences for ELISA and axon degeneration counts were evaluated using one-way ANOVA, with Tukey's post-hoc test for multiple comparisons between groups. For kainic acid live-imaging experiments two coverslips on five separate culture days were analysed. For trichostatin A live-imaging experiments, 1-2 coverslips from four separate culture days were analysed. For whole cell kainic acid ELISAs, three coverslips per treatment from four separate culture days were used. For whole cell trichostatin A ELISAs, three coverslips per treatment from five separate culture days were used. For axon-only kainic acid ELISAs, cells were pooled from 2-3 chambers per treatment from four separate culture days. For axon-only trichostatin A and taxol ELISAs, cells were pooled from 2-3 chambers per treatment from

five separate culture days. All statistical analysis and graphs were prepared in GraphPad Prism (v6.1). Values were reported as means ± standard error of the mean (SEM), with differences considered significant at $p<0.05$. For a list of all statistical analyses performed, see section 8.2.

4.3 RESULTS

4.3.1 Model of excitotoxin-induced axon degeneration

To establish an acute model of excitotoxin-induced axon degeneration, mouse cortical neurons were grown to 10 DIV either on poly-L-lysine coated culture trays or in microfluidic chambers. At this timepoint, there is robust growth of axons in the axon compartment of microfluidic chambers and the neurons are mature enough to express glutamate receptors and respond to an excitotoxic insult with a calcium influx (unpublished data by Dr Nan Tian). Previous research in our laboratory has used a relatively high concentration of kainic acid to induce axon degeneration. Therefore, I first determined whether axon degeneration occurred at lower concentrations of kainic acid. Microfluidic chambers allow compartmentalised separation of axons from the somatodendritic compartment, which permits treatment to be applied to the somatodendritic compartment and the effects examined on the axons. Neurons were exposed to 0 μM, 10 μM and 25 μM kainic acid in the somatodendritic compartment for 18 hours. Live-imaging of axons was performed immediately prior to and post-treatment to determine a degeneration index (detailed in section 2.8). Axon loss was significantly increased ($p<0.05$) at 25 μM kainic acid compared to control (Figure 4.1 A). Axonal degeneration at both 10 μM and 25 μM kainic acid was significantly increased ($p<0.05$) compared to control (Figure 4.1 B). A time-course of axon degeneration was established over 18 hours (Figure 4.1 C, D).

4.3.2 Microtubule alterations after excitotoxin-induced axon degeneration

The previous experiment determined that axon degeneration and axon loss were present at 18 hours post exposure to excitotoxin. To look at early changes to microtubules that could

contribute to axon degeneration, changes to microtubule PTMs were next determined following 25 μM kainic acid exposure at 1 and 6 hours. Primary mouse cortical neurons were

A

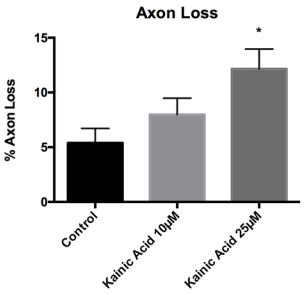

B

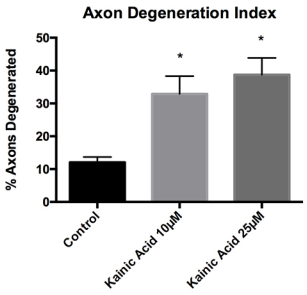

C

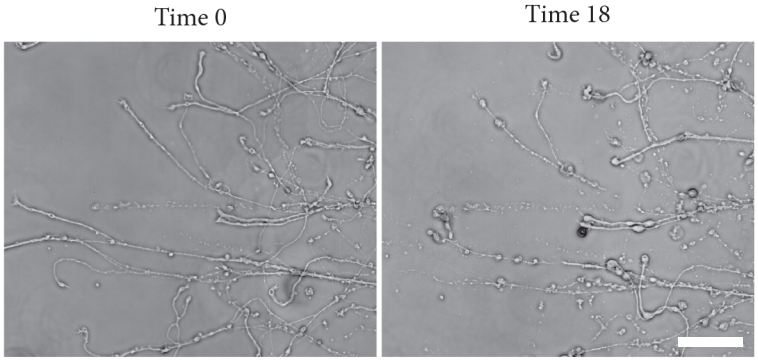

D

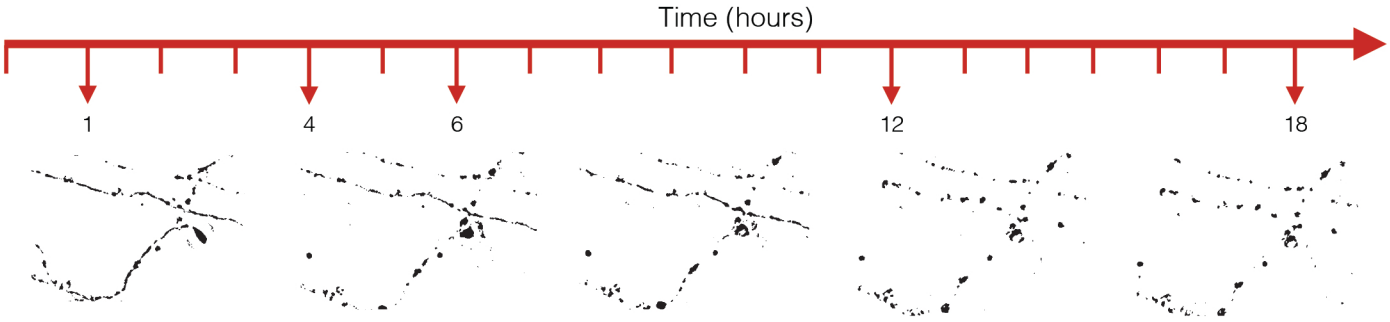

1 hour	4 hours	6 hours	12 hour	18 hours
Axon terminals move rapidly	Blebbing starts to occur	Dying back occurs Small fragmentation	Axon mostly blebbed Secondary neurites all fragmented	No axon movement All axons blebbed, fragmented
~ Acetylated ~ Tyrosinated		↓ Acetylated ~ Tyrosinated		~ Acetylated ~ Tyrosinated
↑ Tau		↑ Tau		

Figure 4.1 Axon degeneration and loss in microfluidic chambers after kainic acid treatment

Live-imaging of the axonal compartment of microfluidic chambers. For analysis images were taken of identical areas before and after treatment. Quantitation was performed for (A) axon loss and (B) axon degeneration index 18 hours after treatment with 10 μM or 25 μM kainic acid. Axon loss was significantly increased ($p<0.05$) relative to control following exposure to 25 μM kainic acid, but not 10 μM kainic acid. The axon degeneration index was significantly increased ($p<0.05$) relative to control following either 10 μM or 25 μM doses of kainic acid. (C) Representative images to show axons at 0 hours and 18 hours after treatment with 25 μM kainic acid. (D) Representative axon image showing a timeline of changes to axons from 1 hour to 18 hours following exposure to 25 μM kainic acid. Bar graph represents mean ± SEM *$p < 0.05$ relative to control. Scale bar = 50 μm.

grown on 12-well culture trays to 10 DIV and were exposed to 25 µM kainic acid for up to 6 hours. Protein was harvested from the cells at 1 and 6 hours. ELISA analysis of neurons demonstrated that, at 1 hour after 25 µM kainic acid treatment, acetylated and tyrosinated tubulin levels were unchanged, compared to vehicle control (Figure 4.2 A, B). At 6 hours after 25 µM kainic acid treatment acetylated tubulin levels were significantly ($p<0.05$) decreased (Figure 4.2 A), while tyrosinated tubulin levels were unchanged (Figure 4.2 B). To confirm that these changes were present in axon, primary neurons were grown in compartmented chambers to 10 DIV and the somatodendritic compartment exposed to 25 µM kainic acid and protein harvested from the axon compartment at 6 hours post exposure. ELISA analysis confirmed the results found in whole neurons with a significant decreased ($p<0.05$) in axonal acetylated tubulin at 6 hours post kainic acid (Figure 4.2 C) with no change in tyrosinated tubulin (Figure 4.2 D). Western blot analysis of acetylated tubulin levels in axons confirmed this was also significantly ($p<0.05$) decreased (Figure 4.2 E).

As acetylated tubulin was significantly decreased after kainic acid treatment, analysis of acetylated tubulin was performed using immunocytochemical labelling after 0, 1 or 6 hours of 100 µM kainic acid. Qualitative analysis demonstrated that initially without kainic acid, acetylated tubulin labelling is bright with no fragmentation present, demonstrating that the axon is still intact (Figure 4.2 F). However, after 1 hour, immunolabelling is less intense, and fragmentation and beading is observed in the acetylated tubulin labelling (Figure 4.2 G). At 6 hours, intensity of immunohistochemistry appears further decreased and more fragmentation is observed (Figure 4.2 H). Overall, qualitative analysis suggests that 100 µM kainic acid reduced intensity of acetylated tubulin immunoreactivity.

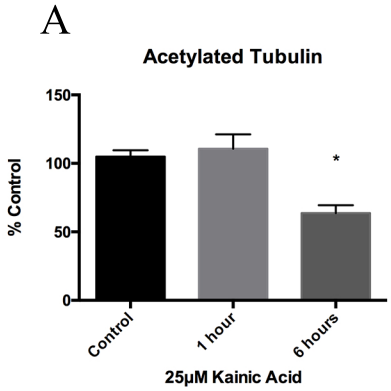
A
Acetylated Tubulin
% Control
150
100
50
0
*
Control
1 hour
6 hours
25μM Kainic Acid

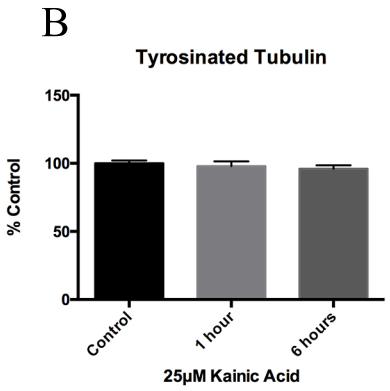
B
Tyrosinated Tubulin
% Control
150
100
50
0
Control
1 hour
6 hours
25μM Kainic Acid

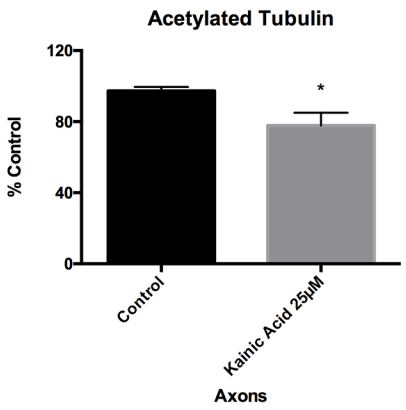
C
Acetylated Tubulin
% Control
120
80
40
0
*
Control
Kainic Acid 25μM
Axons

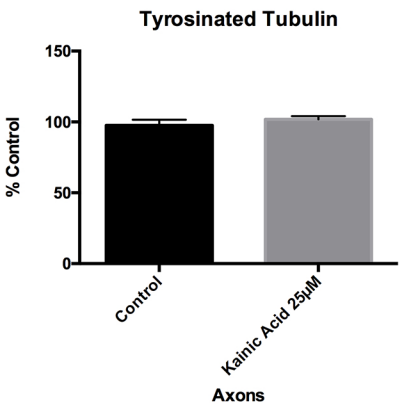
D
Tyrosinated Tubulin
% Control
150
100
50
0
Control
Kainic Acid 25μM
Axons

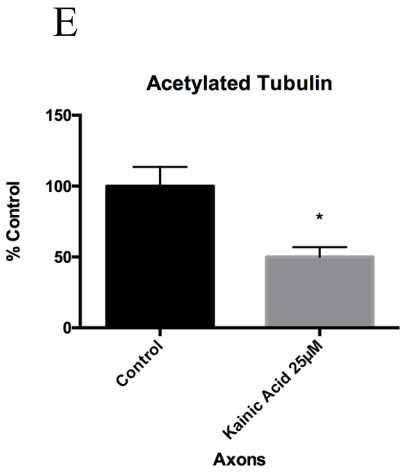
E
Acetylated Tubulin
% Control
150
100
50
0
*
Control
Kainic Acid 25μM
Axons

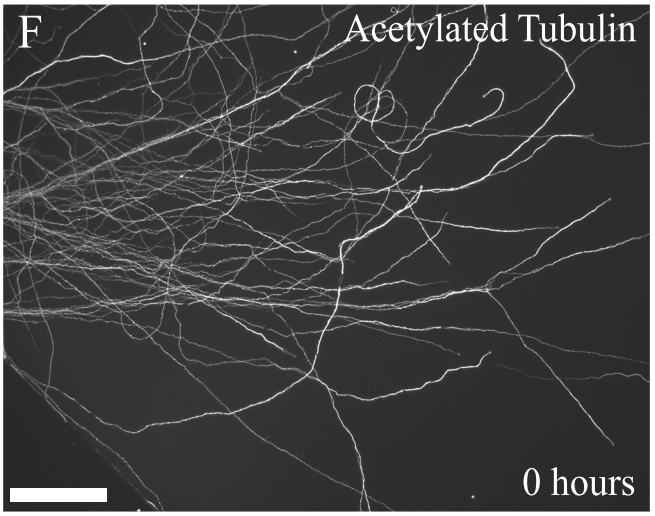
F
Acetylated Tubulin
0 hours


G
1 hour

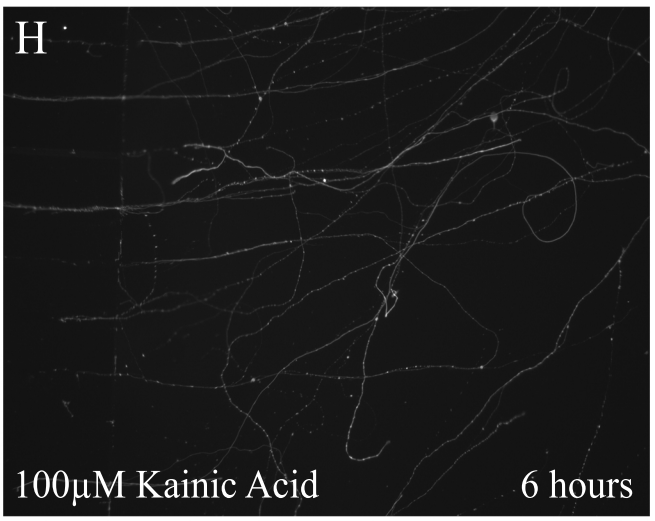
H
100μM Kainic Acid
6 hours

Figure 4.2 Changes to microtubule PTMs after kainic acid treatment

Changes to microtubule PTMs were investigated in whole cultured cortical neurons as well as isolated axons in microfluidic chambers after treatment with 25 μM kainic acid. ELISA analysis of neurons at 1 and 6 hours after 25 μM kainic acid treatment showed (A) a significant decrease ($p<0.05$) in acetylated tubulin levels after 6 hours whereas (B) tyrosinated tubulin levels were unchanged compared to control. ELISA analysis of isolated axons at 6 hours post treatment with 25 μM kainic acid demonstrated (C) significantly decreased ($p<0.05$) levels of acetylated tubulin, at this timepoint relative to control. Axonal levels of (D) tyrosinated tubulin were unchanged compared to control. To confirm the effect of 25 μM kainic acid on acetylated tubulin in axons Western blot analysis was performed (E) demonstrating a significant decrease ($p<0.05$). Representative images of axons grown in microfluidic chambers immunolabelled with acetylated tubulin after (F) 0 hours, (G) 1 hour and (H) 6 hours of 100 μM kainic acid treatment. Bar graph represents mean ± SEM *$p < 0.05$ relative to control. Scale bar = 50 μm, scale bar for panel F = 30 μm.

4.3.3 The effect of trichostatin A on microtubules

Since the data showed significantly reduced acetylated tubulin levels in the axon after 25 µM kainic acid treatment (Figure 4.2), it was hypothesised that promoting microtubule acetylation could rescue these changes and prevent axon degeneration. To promote microtubule acetylation, the drug trichostatin A was used to inhibit the de-acetylating enzyme HDAC6.

Firstly, the concentration of trichostatin A required to promote acetylation in primary mouse cortical cultures was determined. Primary cortical neurons were grown to 10 DIV in 12-well trays and treated with 2 concentrations of trichostatin A which were selected based on published literature (Moreira et al., 2003; Rahman et al., 2003; Williams et al., 2011). Protein was harvested at 2 hours post-treatment. ELISA analysis demonstrated that acetylated tubulin levels after 10 nM and 100 nM trichostatin A were significantly ($p<0.05$) increased compared to vehicle control at 2 hours post-treatment (Figure 4.3 A). There was no significant difference in the levels of acetylated tubulin between the two concentrations of trichostatin A, suggesting a threshold effect. To determine whether trichostatin A had any detrimental effects on the neurons, cell viability was tested using an alamarBlue® cell viability assay, which measures cell proliferation. This demonstrated that 10 nM and 100 nM trichostatin A did not significantly affect cell health different compared to vehicle treated cultures. However, cells treated with higher doses (250 nM and 500 nM) of trichostatin A had significantly reduced ($p<0.05$) cell health compared to vehicle control (Figure 4.3 B). Cell viability was also tested after treatment with trichostatin A (10 nM and 100 nM) in the presence of kainic acid and there was no significant difference compared to the vehicle control for any treatment concentration (Figure 4.3 C).

A

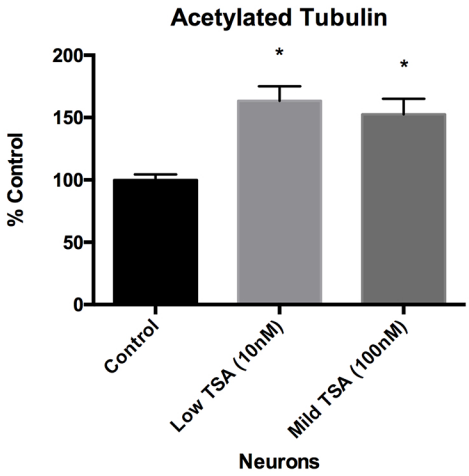
Acetylated Tubulin
% Control
200
150
100
50
0
*
*
Control
Low TSA (10nM)
Mild TSA (100nM)
Neurons

B

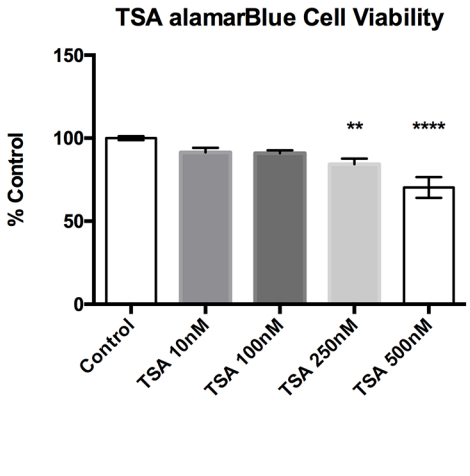
TSA alamarBlue Cell Viability
% Control
150
100
50
0
**
****
Control
TSA 10nM
TSA 100nM
TSA 250nM
TSA 500nM

C

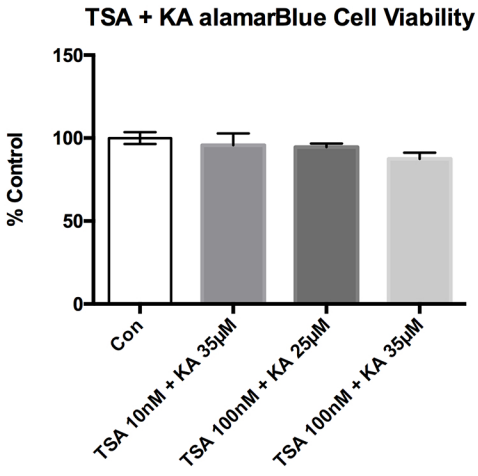
TSA + KA alamarBlue Cell Viability
% Control
150
100
50
0
Con
TSA 10nM + KA 35μM
TSA 100nM + KA 25μM
TSA 100nM + KA 35μM

Figure 4.3 Effect of trichostatin A on microtubule acetylation following kainic acid treatment

(A) Levels of acetylated tubulin were examined after treatment of whole neurons with the HDAC6 inhibitor trichostatin A. ELISA analysis to show significantly ($p<0.05$) increased acetylated tubulin after both 10 nM and 100 nM trichostatin A treatment in neurons. (B) Cell viability in neurons was determined using an alamarBlue® assay after treatment with varying concentrations of trichostatin A for two hours. 10 nM and 100 nM trichostatin A resulted in no loss in cell viability compared to control, however cell viability was significantly ($p<0.05$) decreased after both 250 nM and 500 nM trichostatin A, compared to control. (C) Cell viability of neurons was determined after treatment with kainic acid for 6 hours in the presence of trichostatin A. Trichostatin A (10 nM or 100 nM) was applied 2 hours before kainic acid treatment. There was no difference in cell viability compared to control (untreated cells), for any of the treatments.

4.3.4 Trichostatin A and microtubule alterations after excitotoxicity

It was next determined whether HDAC6 inhibition by trichostatin A, at non-toxic doses, could rescue acetylated tubulin following excitotoxin exposure. Neuronal cells grown on 12-well trays and the axonal compartment of microfluidic chambers were pre-treated with low (10 nM) trichostatin A for 2 hours prior to exposure to 25 μM kainic acid for 6 hours, after which time protein was harvested from the neurons. ELISA analysis demonstrated that 10 nM trichostatin A restored acetylated tubulin levels after kainic acid exposure, as compared to vehicle control (Figure 4.4 A). To confirm these changes in axons, neurons were grown in microfluidic chambers and the axons were pre-treated with 10 nM trichostatin A for 2 hours prior to exposure of the somatodendritic compartment to 25 μM kainic acid for 6 hours. ELISA analysis was performed on harvested axons and demonstrated that axonal acetylated tubulin levels were significantly decreased, after kainic acid exposure (similar to previous results) and significantly increased after trichostatin A. After combined treatment acetylated tubulin levels were unchanged from vehicle control (Figure 4.4 B). Western blot analysis of harvested axons also demonstrated that 10 nM trichostatin A restored acetylated tubulin levels after excitotoxicity in axons (Figure 4.4 C, D), confirming the ELISA analysis. Tyrosinated tubulin levels in both the neurons (Figure 4.5 A) and axons (Figure 4.5 B) were unchanged after combined trichostatin A and kainic acid treatment, when compared to control levels.

4.3.5 Effect of trichostatin A on axon degeneration

After demonstrating acetylated tubulin levels in axons following excitotoxic injury are restored by treatment with trichostatin A, it was next determined if trichostatin A treatment following excitotoxin exposure was also protective against axonal degeneration at 18 hours post treatment. Neurons were grown in microfluidic chambers and axons exposed to 10 nM and 100 nM trichostatin A for 2 hours prior to somatodendritic treatment with 25 μM kainic

A

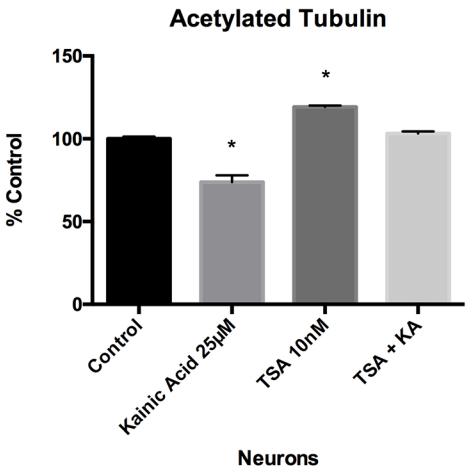
Acetylated Tubulin
% Control
150
100
50
0
*
*
Control
Kainic Acid 25μM
TSA 10nM
TSA + KA
Neurons

B

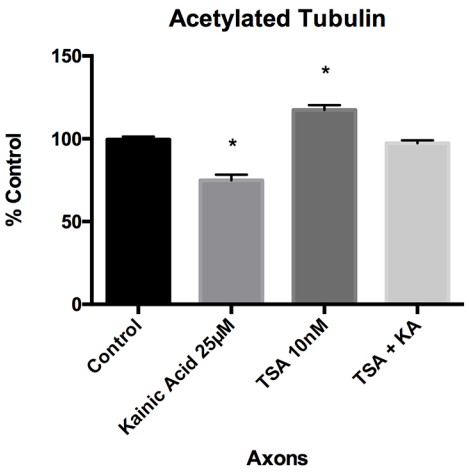
Acetylated Tubulin
% Control
150
100
50
0
*
*
Control
Kainic Acid 25μM
TSA 10nM
TSA + KA
Axons

C

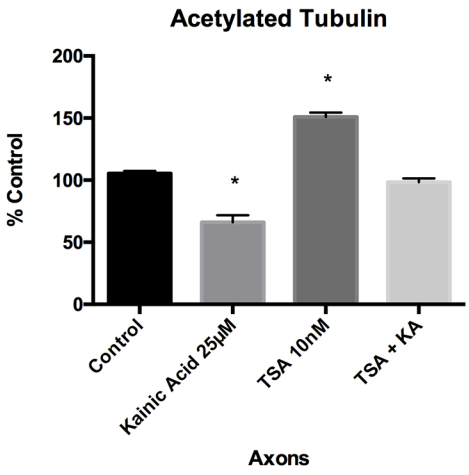
Acetylated Tubulin
% Control
200
150
100
50
0
*
*
Control
Kainic Acid 25μM
TSA 10nM
TSA + KA
Axons

D

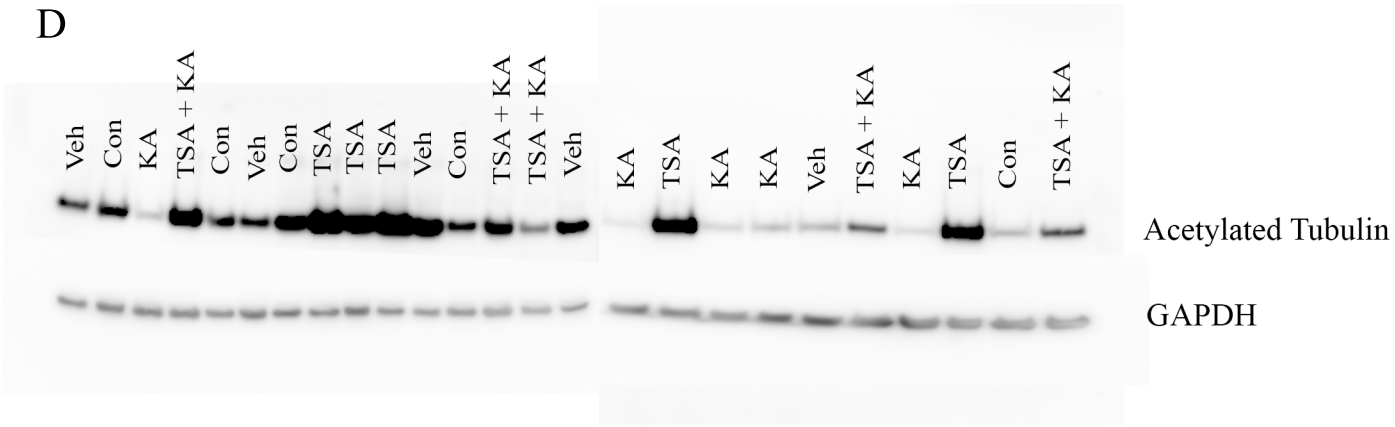
Veh
Con
KA
TSA + KA
Con
Veh
Con
TSA
TSA
TSA
Veh
Con
TSA + KA
TSA + KA
Veh
KA
TSA
KA
KA
Veh
TSA + KA
KA
TSA
Con
TSA + KA
Acetylated Tubulin
GAPDH

Figure 4.4 Effect of trichostatin A on microtubule acetylation following kainic acid treatment

(A) Levels of acetylated tubulin were quantitated in whole neurons following six hours of kainic acid treatment in the presence of trichostatin A (applied two hours prior to kainic acid). ELISA analysis demonstrated a significant decrease ($p<0.05$) in acetylated tubulin levels after 6 hours of kainic acid treatment, a significant increase ($p<0.05$) in acetylated tubulin after 2 hours of 10 nM trichostatin A. Acetylated tubulin levels in neurons treated with kainic acid in the presence of trichostatin A were not significantly different from control. (B) Levels of acetylated tubulin were quantitated in axons following six hours of kainic acid treatment applied to the somatodendritic compartment of microfluidic chambers in the presence of trichostatin A (applied to axons two hours prior to kainic acid). ELISA analysis demonstrated a significant increase ($p<0.05$) in acetylated tubulin after 2 hours of 10 nM trichostatin A. Acetylated tubulin levels in neurons treated with kainic acid in the presence of trichostatin A were not significantly different from control. (C) To confirm the effect of 10 nM trichostatin A on acetylated tubulin in axons, Western blot analysis was performed demonstrating a significant increase in axonal acetylated tubulin following 10 nM trichostatin A and no significant difference in combined trichostatin A and kainic acid compared to control ($p<0.05$). (D) Representative Western blot used for quantitation of (C). Bar graph represents mean ± SEM *$p < 0.05$ relative to control.

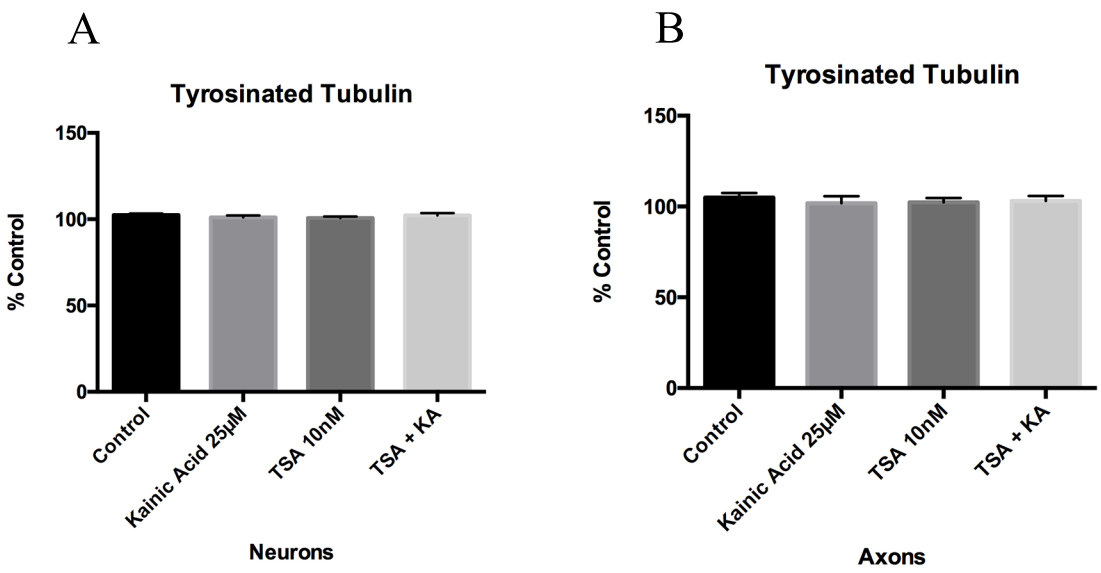
A
Tyrosinated Tubulin
% Control
150
100
50
0
Control
Kainic Acid 25μM
TSA 10nM
TSA + KA
Neurons
B
Tyrosinated Tubulin
% Control
150
100
50
0
Control
Kainic Acid 25μM
TSA 10nM
TSA + KA
Axons

Figure 4.5 Effect of trichostatin A on microtubule tyrosination following kainic acid treatment

(A) Levels of tyrosinated tubulin were examined after treatment of whole neurons with the HDAC6 inhibitor trichostatin A. ELISA analysis demonstrated no difference in tyrosinated tubulin after 10 nM trichostatin A treatment for 2 hours or 25 μM kainic acid for 6 hours. (B) Levels of tyrosinated tubulin were examined after treatment of isolated axons with trichostatin A. ELISA analysis demonstrated that tyrosinated tubulin levels were unchanged in any treatment group, relative to control. Bar graph represents mean ± SEM *$p < 0.05$ relative to control. TSA; trichostatin A, KA; kainic acid.

acid. Axon degeneration was quantitated from images acquired from identical regions of the coverslip, before and 18 hours after kainic acid treatment. In the presence of 10 nM and 100 nM trichostatin A, axon loss (Figure 4.6 A) and axon degeneration (Figure 4.6 B) were significantly reduced ($p<0.05$) after exposure to 25 μM kainic acid. Live-imaging demonstrated that trichostatin A prevented axons from degenerating following kainic acid treatment (Figure 4.6 D-G).

4.3.6 Taxol and microtubule post translational modifications after excitotoxicity

The above results demonstrated the microtubule acetylating agent, trichostatin A altered microtubule PTMs, and protected axons from degenerating. Previous studies have also demonstrated an axonal protective effect of the microtubule stabilising agent, taxol following kainic acid exposure in a similar model (King et al., 2013). Thus, in this thesis I further investigated the effect of taxol on microtubule PTMs following kainic acid exposure. Primary mouse cortical neurons were grown in microfluid chambers to 10 DIV and the axonal compartment of microfluidic chambers was pre-treated with 10ng taxol for 2 hours prior to exposure of the somatodendritic compartment to 25 μM kainic acid, followed by harvest of the axonal proteins at 6 hours. ELISA analysis demonstrated that both 10ng taxol alone and combined taxol and kainic acid treatment restored acetylated tubulin levels in axons after kainic acid exposure, as compared to vehicle control in axons (Figure 4.7 A). However, 10ng of taxol also significantly decreased ($p<0.05$) tyrosinated tubulin levels in axons, compared to vehicle, both in the presence and absence of kainic acid (Figure 4.7 B).

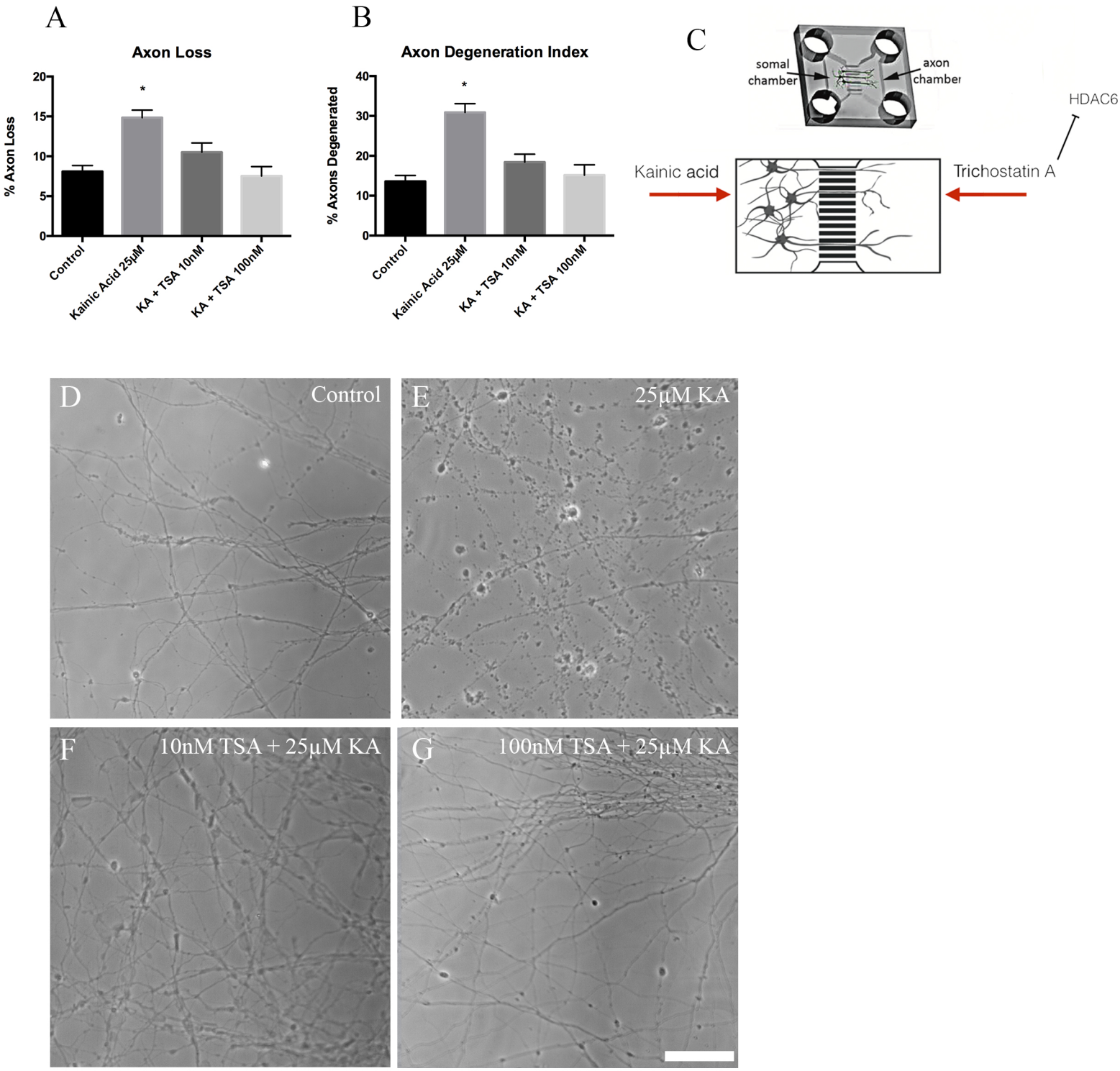
A
Axon Loss
% Axon Loss
20
15
10
5
0
*
Control
Kainic Acid 25μM
KA + TSA 10nM
KA + TSA 100nM
B
Axon Degeneration Index
% Axons Degenerated
40
30
20
10
0
*
Control
Kainic Acid 25μM
KA + TSA 10nM
KA + TSA 100nM
C
somal chamber
axon chamber
HDAC6
Kainic acid
Trichostatin A
D
Control
E
25μM KA
F
10nM TSA + 25μM KA
G
100nM TSA + 25μM KA

Figure 4.6 Axon degeneration and axon loss after kainic acid treatment in the presence of trichostatin A

Degenerating and lost axons were quantitated from live images of the axonal compartments of microfluidic chambers following 25 μM kainic acid treatment in the presence of axonal trichostatin A (10 nM or 100 nM). Both (A) axon loss and (B) axon degeneration were significantly increased ($p<0.05$) with 25 μM kainic acid treatment, however, these effects were rescued by treatment with either concentration of trichostatin A. In the presence of trichostatin A, axonal loss and degeneration were not significantly different from controls. (C) Schematic showing where each treatment was applied to the microfluidic chambers. Representative images of axons for (D) control, (E) 25 μM kainic acid, (F) 10 nM trichostatin A + 25 μM kainic acid and (G) 100 nM trichostatin A + 25 μM kainic acid. Bar graph represents mean ± SEM *$p < 0.05$ relative to control. Scale bar = 50 μm. TSA; trichostatin A, KA; kainic acid.

A

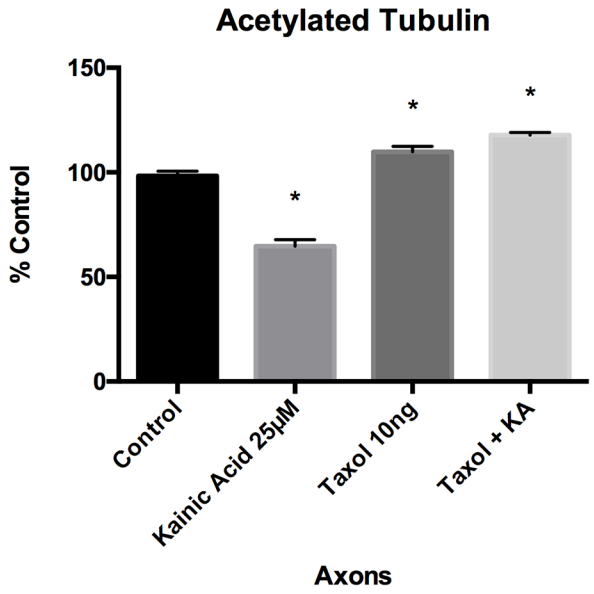
Acetylated Tubulin
150
100
50
0
% Control
*
*
*
Control
Kainic Acid 25μM
Taxol 10ng
Taxol + KA
Axons

B

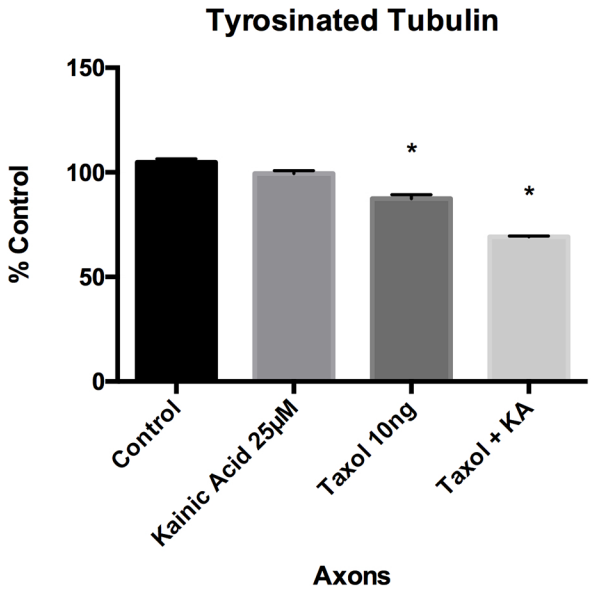
Tyrosinated Tubulin
150
100
50
0
% Control
*
*
Control
Kainic Acid 25μM
Taxol 10ng
Taxol + KA
Axons

Figure 4.7 The effect of taxol on microtubule PTMs

Changes to microtubule PTMs were investigated in isolated axons after treatment with 10ng taxol in the presence or absence of 25 µM kainic acid. ELISA analysis of axons showed (A) significantly decreased ($p<0.05$) acetylated tubulin after 6 hours of 25 µM kainic acid exposure. After taxol and combined taxol with kainic acid treatment, acetylated tubulin was significantly increased ($p<0.05$) compared to control levels. ELISA analysis of axons showed (B) unchanged levels of tyrosinated tubulin after 6 hours of 25 µM kainic acid exposure. However, after 10ng taxol, and combined taxol and kainic acid treatment, tyrosinated tubulin was significantly decreased ($p<0.05$) compared to control levels. Bar graph represents mean ± SEM *$p < 0.05$ relative to control.

4.4 DISCUSSION

Understanding the mechanisms underlying the relationship between microtubule alterations and axon degeneration can potentially lead to a better understanding of neurodegenerative changes linked to excitotoxicity. The current study investigated whether excitotoxin-induced axon degeneration caused alterations in the PTMs of microtubules and whether inhibition of these biochemical changes to the cytoskeleton can protect axons.

The main finding of this study was that, following excitotoxin exposure, there were significant decreases to acetylated tubulin by six hours after treatment, both in the whole neuron and more specifically within the axon. It is currently unclear whether loss of tubulin acetylation in the current project results from increased deacetylation or from decreased acetylation. Furthermore, downstream processes following kainic acid exposure that result in loss of acetylation are currently not known but will be the subject of future investigations. In the current study, treatment with trichostatin A prevented decreases in acetylated tubulin levels after kainic acid exposure, consequently reducing axonal fragmentation and axon loss, suggesting that tubulin deacetylation is a key event in excitotoxin induced axon degeneration.

There are three key enzymes involved in microtubule acetylation levels. The major enzyme involved in tubulin acetylation state in mammals is alpha-tubulin acetyltransferase 1 (αTAT1; Coombes et al., 2016). There are two enzymes involved in deacetylation, histone deacetylase 6 (HDAC6) and sirtuin 2 (SIRT2; Seto and Yoshida, 2014). In this study, I chose to therapeutically target HDAC6 inhibition using the drug, trichostatin A, which has previously been investigated in motor neuron degeneration (Lazo-Gómez et al., 2013; Yoo and Ko, 2011) and used to treat retinal degenerative diseases (reviewed in Zhang et al., 2015b). HDAC6 is one of a family of histone deacetylases. There are 18 HDAC enzymes, divided

into 4 classes in humans that use either zinc or NAD^+ dependent mechanisms to deacetylate the lysine substrate. HDACs are substrate-specific and are subject to a range of controlling mechanisms, including PTMs and protein to protein interactions (Seto and Yoshida, 2014). Trichostatin A is a non-specific HDAC6 inhibitor, which inhibits class I and class II HDACs. However, since the current study tested its use in the axonal compartment, I was able to test its effect on HDAC6, which is the only HDAC expressed in this compartment. Besides its effect on acetylation, it is possible that trichostatin A could have other effects on axon degeneration. For example, trichostatin A has been shown to suppress TNF-α expression and signalling in a rat model of ischemic injury in the retina (Crosson et al., 2010). Trichostatin A can regulate the levels of interleukin-6 and TNF- α and thereby improve neurological performance in a rat model of permanent middle cerebral artery occlusion of stroke (Hyeon et al., 2007). In future *in vivo* studies, it would be useful to test other more specific HDAC6 inhibitors such as, MS-275, which also crosses the blood brain barrier, to determine if these would be suitable drugs for further therapeutic development (Yang et al., 2017a; Zhang and Schluesener, 2013).

The importance of acetylation in microtubule stability has been widely reported (Howes et al., 2014; Portran et al., 2017). It is known that acetylated tubulin protects microtubules against mechanical ageing and is also a marker of long-lived microtubules (Portran et al., 2017). Increasing microtubule acetylation using trichostatin A, has been shown to restore axonal transport in rat cortical neurons, following exposure to mutant leucine-rich repeat kinase (LRRK2; Godena et al., 2014). The same study showed that *in vivo*, trichostatin A treatment or knockdown of HDAC6 and Sir2-related protein (Sirt2), rescued axonal transport in a Drosophila model of mutant LRRK2. In cultured mouse cerebellar granule cells, levels of acetylation were compared between Wallerian degeneration slow (Wld^S) mice, which have a mutation that slows Wallerian degeneration (Lunn et al., 1989) and wildtype mice (Suzuki

and Koike, 2007). The authors found that base levels of acetylation were increased in *Wld*^{S} cells compared to wildtype. Furthermore, the authors showed that the deacetylating enzyme SIRT2 plays a key role in resistance of *Wld*^{S} cells to axon degeneration, whereby they found decreased SIRT2 in *Wld*^{S} granule cell cytoplasm. Additionally, SIRT2 knockdown enhanced microtubule acetylation and reduced axon degeneration in wildtype granule cells. These findings also highlight the importance of microtubule acetylation in axon degeneration.

This study also showed that tyrosinated tubulin is unchanged following kainic acid exposure. In contrast to acetylation, which is associated with long-lived microtubules, tyrosination is present in highly dynamic microtubules at the proximal end of the axon (Witte et al., 2008), and has been reported as a destabilising microtubule PTM (Khawaja et al., 1988; Kreis, 1987). This suggests that destabilising microtubules through tyrosination is not a key factor in driving excitotoxin-induced axon degeneration. In contrast to this, the absence of tubulin tyrosine ligase, which promoted tubulin tyrosination, has been shown to severely reduce axon regeneration (Song et al., 2015), suggesting that tubulin tyrosination may be more important for regeneration rather than degeneration. However, PTMs have also been described following developmental axon pruning, which can be modelled *in vitro* by trophic factor withdrawal (reviewed in Saxena and Caroni, 2007). Developmental axon pruning has been shown to involve decreases in both acetylation and tyrosination, with an accompanying increase in detyrosinated tubulin (Unsain et al., 2018).

In the current study, the influence of taxol, which has been investigated in a number of experimental axon degeneration paradigms (as review by Fukuda et al., 2017), and has been shown to protect against kainic acid-induced axon degeneration (King et al., 2013) was investigated on both acetylated tubulin and tyrosinated tubulin. Acetylated tubulin levels were significantly increased after taxol treatment, suggesting that the protective effect of taxol may

be through preventing deacetylation. Previous research in a mouse kidney ischemia model demonstrated that taxol treatment increased αTAT1 levels in the kidney, but did not change HDAC6 expression (Han et al., 2016). The acetylating enzyme, αTAT1 is still able to acetylate microtubules, even when stabilised by taxol (Howes et al., 2014), suggesting an overall promotion of acetylation in the presence of taxol. However, this thesis also showed that taxol decreased tubulin tyrosination. The down-stream effects of this modification on axonal health are unclear.

In addition to excitotoxic injury, alterations to microtubules have been demonstrated in other forms of axonal injury. For example, dynamic stretch injury of neuronal cultured cells induced axon degeneration, which was inhibited by taxol (Tang-Schomer et al., 2010). This is in line with earlier research in this area, suggesting that cytoskeletal changes begin as early as five minutes post fluid percussive injury (Povlishock and Pettus, 1996), indicating that changes to microtubules could be one of the earliest events to occur after initiating axonal injury and degeneration. Another study which investigated alpha-tubulin levels after optic nerve stretch injury found decreased alpha-tubulin levels between 0.5-4 hours post-injury, and a secondary decline after 72 hours post-injury (Serbest et al., 2007). This also suggests that microtubules may have an initial role after injury and another role in a secondary event post-injury.

One of the limitations of this study is that PTMs were investigated at 1 and 6 hours after kainic acid-induced axon degeneration. Future studies could investigate earlier timepoints, such as 0.5 hours, however, to target PTMs therapeutically, changes that occur at later timepoints, may not be effective targets. Future studies could also investigate the PTM glutamylation to identify any changes that may occur to glutamylation during excitotoxicity. As tyrosination was unchanged, drugs targeting tyrosination were not investigated in this

study, however, future studies could target tyrosination to determine if it affects the process of axon degeneration. Furthermore, it will be important to confirm these changes in animal models.

4.4.1 Conclusion

Together the data presented in this thesis, indicate that alterations to microtubule may be an early and modifiable event in several forms of axon degeneration. The key finding from this study was a significant decrease in acetylated tubulin following excitotoxin exposure, which was then targeted by the HDAC6 inhibitor, trichostatin A. With trichostatin A treatment to promote acetylation, axon degeneration was significantly reduced. Tyrosinated tubulin was unchanged suggesting axon degeneration pathways are not affected by changes to tyrosinated tubulin. Together these results demonstrate that altering microtubule acetylation can help prevent axon degeneration following excitotoxin exposure. Further deciphering microtubule PTMs and their interaction with degenerating pathways will be important in providing therapeutic treatment in several neurodegenerative diseases.

Chapter 5

Targeting microtubule-associated proteins in excitotoxin-induced axon degeneration

5 TARGETING MICROTUBULE-ASSOCIATED PROTEINS IN EXCITOTOXIN-INDUCED AXON DEGENERATION

5.1 INTRODUCTION

5.1.1 Microtubule-associated proteins

The previous chapter demonstrated that microtubule PTMs played an important role in the progression of axon degeneration. By altering the stabilising microtubule PTM, acetylated tubulin, axon degeneration was reduced to almost control levels. This suggests that microtubules may play a more integral role in axon degeneration pathways than previously hypothesised. To further investigate the role of microtubules in excitotoxin-induced axon degeneration, this chapter focuses on the potential role of MAPs. Microtubule PTMs influence the binding of MAPs (Magiera and Janke, 2014), therefore a loss of binding may escalate axon degeneration.

Dissociation of MAPs may be an early event in pathological conditions and may occur through altered PTMs or through altered phosphorylation. Dissociation of MAPs can drive microtubule instability, leading to degeneration (Baas et al., 2016). In addition, MAPs could also be involved in other pathways and may drive other events to cause degeneration, such as neuronal signalling and transport (Mietelska-Porowska et al., 2014).

Due to its role in AD and other neurodegenerative diseases, previous research has focussed on the MAP tau during axon degeneration (Dawson et al., 2010; Kneynsberg et al., 2017). Tau is located in the axonal compartment of a neuron, but in axon degeneration it migrates to the somatodendritic compartment. Research has shown that this may be due to initial damage to the axon initial segment (Yoshimura and Rasband, 2014), which normally keeps these regions separate and may suggest a general disruption to the normal localisation of proteins

in the neurons. Another MAP, which has an important role in regulating microtubule stability and has been implicated in neurodegenerative disease is collapsin response mediator 2 (CRMP2; Cole et al., 2007; Gu and Ihara, 2000; Hensley and Kursula, 2016; Isono et al., 2013; Soutar et al., 2009). CRMP2 has been proposed as a therapeutic target for AD due to it being phosphorylated by cdk5 and GSK3β (Yang et al., 2017b) and CRMP2 protects microtubules against depolymerisation with nocodazole (Hensley and Kursula, 2016). Previous research has shown that CRMP2 binding to microtubules is displaced when exposed to taxol or epothilone B, and suggests that it has a similar microtubule binding site to tau (Lin et al., 2011).

Another MAP of interest in neurodegeneration is MAP2, which is usually located in the dendrites. In disease, and particularly in excitotoxic conditions, MAP2 has been shown to be lost from the dendritic compartment (Hoskison et al., 2007). For example, there was an irreversible loss of MAP2 from the dendritic compartment in hippocampal slices when exposed to excessive NMDA (Hoskison et al., 2007), where MAP2 especially accumulated in CA1 hippocampal somata. Similarly, after excitotoxic neuronal damage via a glutamate transport inhibitor there was a loss of dendritic MAP2 immunoreactivity and the effects were restricted to the CA1 region (Arias et al., 1997). This suggests that MAP2 disruption may be a marker of excitotoxicity.

Activation of caspase-3 causes proteolysis of MAP1B and is also degraded by calpain, but degradation of MAP1B is prevented by antioxidants, suggesting that reactive oxygen species perturbs the microtubule network (Fifre et al., 2006). MAP1B is also widely distributed in both dendrites and axons. Although its role in axon regeneration is well-documented (Bouquet et al., 2004; Leibinger et al., 2017; Yang et al., 2012), its role in axon degeneration is currently unknown.

5.1.2 Phosphorylation of microtubule-associated proteins

Phosphorylation of MAPs is one of the key factors that determines how they bind to microtubules (Brugg and Matus, 1991) and it has been proposed that abnormal phosphorylation could be potentially a driver of neurodegenerative disease. In this regard, hyperphosphorylation of tau and CRMP2 have been reported as an early event in AD (Cole et al., 2007; Mondragón-Rodríguez et al., 2014; Rissman et al., 2004). Phosphorylation state is controlled by balance of kinase action to add phosphate groups and phosphatase action to remove phosphate groups. While there are a number of kinases implicated in neurodegenerative disease, which act specifically on the different MAPs, phosphatase activity is primarily performed by protein phosphatase PP2A, which removes phosphate groups from MAPs (Li et al., 2002; Van Kanegan and Strack, 2009). Protein phosphatase 2A specifically binds to tau and MAP2, which are both associated with microtubule stability (Sontag et al., 2012). This makes activating PP2A an attractive target for investigating MAP phosphorylation using drugs such as sodium selenate, which activates PP2A and removes phosphate groups (Corcoran et al., 2010). Pharmacological manipulation using sodium selenate has been shown to alter microtubule assembly in both *in vitro* and *in vivo* models (Shi et al., 2013). Therefore, determining whether MAPs are altered following an excitotoxic insult and whether altering their phosphorylation affects the degeneration process may lead to mechanistic insight in the role of microtubules in excitotoxin-induced axon degeneration.

5.1.3 Study outline

This study investigated the role of MAPs in an excitotoxin-induced model of axon degeneration. To investigate the potential changes to these MAPs, mouse cortical primary cell cultures were grown to 10 DIV in culture trays or in microfluidic chambers (as described

in section 2.7). To induce excitotoxicity, cultures were treated with kainic acid. Western blotting, ELISA and immunocytochemistry were used to determine alterations.

Firstly, the expression levels of some of the major axonally localised MAPs were investigated, including: MAP1B, CRMP2, and tau. The dendritic MAP, MAP2 was also investigated to determine if location is altered during degeneration. To examine the role of MAP phosphorylation, the PP2A activator sodium selenate was used to promote dephosphorylation of MAPs. Determining if MAP phosphorylation is an early event of axon degeneration can aid our understanding of degenerative mechanisms. Finally, since this research has demonstrated an effect of microtubule drugs taxol and trichostatin A on axon degeneration, I investigated the effect of these drugs on the expression levels of MAPs to determine whether these agents may be driving alterations in MAPs that could affect the microtubule cytoskeleton.

5.2 METHODS

5.2.1 Ethics and mice

All experiments and procedures were approved by the University of Tasmania Animal Ethics Committee (A12780 and A15121) and were in accordance with the Australian Guidelines for the Care and Use of Animals for Scientific Purposes. C57Bl/6 mice were used in cell culture experiments (see section 2.1).

5.2.2 Primary cortical culture

Mouse cortical neuron cultures were prepared as previously described (King et al., 2013). Cortical neurons were prepared from embryonic day 15.5 (E15.5) C57Bl/6 mice. Cortices were removed and transferred to 5 mL Hanks Balanced Salt Solution (HBSS, Gibco). Trypsin (0.0125%) was added for four minutes at 37ºC, followed by removal of HBSS and replaced with 1 mL of initial plating media (Neurobasal media (Gibco) v/v 2% B27 supplement, 0.5 mM glutamine, 25 µM glutamate, 10% v/v fetal calf serum and 1% v/v antibiotic/antimycotic) and mechanically triturated with a 1 mL pipette. Cells were plated either into the soma compartment of microfluidic chambers or directly into the wells of poly-L-lysine coated culture plates. Cells were allowed to adhere to the coverslip (Livingstone) at 37ºC for 30 minutes prior to adding initial plating media to the chambers. Cells were incubated at 37ºC overnight before initial media was replaced with subsequent plating media with no fetal calf serum and glutamate. Cells were grown to 10 days in vitro (DIV) at 37ºC in 5% CO_2 (see section 2.7.1, 2.7.2).

5.2.3 Pharmacological manipulation

Cells were treated with 0 µM, 10 µM or 25 µM of kainic acid (Sigma Aldrich, Lot#SLBD1491V) in DMSO (Sigma Aldrich, Lot#RNBF1056) at 10 DIV. Cells in 12-well

plates or the soma compartment of microfluidic chambers were exposed to kainic acid for 6 and 18 hours. For a set of experiments cells were treated with taxol (Calbiochem, Lot#B66835). Cells at 10 DIV in 12-well plates or axonal compartment of microfluidic chambers were treated with 10 nM or 100 nM trichostatin A (Sigma Aldrich, Lot#026M4036V) for 2 hours before 6 hours of kainic acid. For a subset of experiments cells were treated with sodium selenate. Cells at 10 DIV in axonal compartment of microfluidic chambers were treated with 100 µM of sodium selenate (Sigma Aldrich, Lot#BCBT2170) for 1 hour prior to 18 hours of kainic acid exposure (see section 2.8.1).

5.2.4 Live cell imaging and quantification of axonal degeneration

Microfluidic cultures were imaged on a Nikon TiE live cell microscope, with chambers maintained at 37ºC. Imaging was performed prior to treatment and 18 hours following treatment. Axonal side of the microfluidic chambers were imaged using 40x objective lens in identical regions before and after treatment. Axon degeneration was calculated by counting degenerated axons.

5.2.5 ELISA analysis of microtubule post-translational modifications and associated proteins

Cells were harvested with RIPA buffer with protease (cOmplete^{TM} Mini Protease Inhibitor Cocktail tablets, Roche) and phosphatase inhibitors (Phosphatase Inhibitor Cocktail, A.G. Scientific). Samples were diluted at 1:300 in 50 µL bicarbonate/carbonate coating buffer (AbCam), added to 96-well plate and incubated overnight at 4ºC. For the standard curve, protein samples were serially diluted at 1:100, 1:200, 1:400, and 1:800. A blank and no primary control were included to correct for ELISA results. Plate was washed with washing

buffer (0.01 M PBS with 0.05% v/v tween-20) prior to blocking with blocking buffer (0.01 M PBS with 5% v/v fetal bovine serum) and incubated at 37ºC for 30 minutes. Plates were incubated with detecting antibodies (tau 1:1000 rabbit, DAKO; CRMP2 1:1000 rabbit, Sigma Aldrich; MAP1B 1:500 mouse, AbCam) diluted in blocking buffer for 1 hour at room temperature (see section 2.8.4).

5.2.6 Immunocytochemistry

Immunocytochemistry was performed as previously described in section 2.9. After fixation cultures were blocked in diluent and incubated with primary antibody MAP2 (1:500, Millipore, MAB3418).

5.2.7 Statistical analysis

Differences for ELISA and axon degeneration counts were evaluated using one-way ANOVA, with Tukey's post-hoc test for multiple comparisons between groups. For kainic acid live-imaging experiments two coverslips on five separate culture days were analysed. For sodium selenate live-imaging experiments, 1-2 coverslips from four separate culture days were analysed. For whole cell kainic acid ELISAs, three coverslips per treatment from four separate culture days were used. For whole cell trichostatin A ELISAs, three coverslips per treatment from five separate culture days were used. For axon-only kainic acid ELISAs, cells were pooled from 2-3 chambers per treatment from four separate culture days. For axon-only trichostatin A and taxol ELISAs, cells were pooled from 2-3 chambers per treatment from five separate culture days. All statistical analysis and graphs were prepared in GraphPad Prism (v6.1). Values were reported as means ± standard error of the mean (SEM), with differences considered significant at $p<0.05$. For a list of all statistical analyses performed, see section 8.3.

5.3 RESULTS

5.3.1 The effect of kainic acid on axonal MAPs

The previous chapter showed kainic acid affected the microtubule PTM, acetylated tubulin. This chapter investigated the effect of kainic acid on MAPs. Neuronal cells were grown on 12-well trays to 10 DIV and were exposed to 25 μM kainic acid for 6 hours, followed by protein harvests. Firstly, the MAP tau was investigated. ELISA analysis demonstrated that treatment with 25 μM kainic acid significantly ($p<0.05$) increased tau levels after 6 hours (Figure 5.1 A). To further investigate the time-course of altered tau expression, the experiment was repeated and protein was harvested at one hour. Tau was also significantly ($p<0.05$) increased at 1-hour after 25 μM kainic acid treatment (Figure 5.1 B). Next CRMP2 and MAP1B levels were examined using ELISA in neurons following 6 hours kainic acid. Like tau, CRMP2 levels were significantly ($p<0.05$) increased following excitotoxicity (Figure 5.1 C). To further examine whether these changes were present specifically in axons, neurons were grown in microfluidic chambers, the somatodendritic compartment treated with 25 μM kainic acid and protein harvested from axons at 6 hours. Similar to the findings in whole neurons, axonal tau and CRMP2 were significantly ($p<0.05$) increased (Figure 5.1 D). ELISA analysis demonstrated neuronal MAP1B levels were unchanged (Figure 5.1 E), and MAP1B levels in axons were not altered (Figure 5.1 F). Together these data suggest that following an excitotoxic insult, expression levels of MAPs tau and CRMP2 are increased in the axon from as early as 1-hour post exposure.

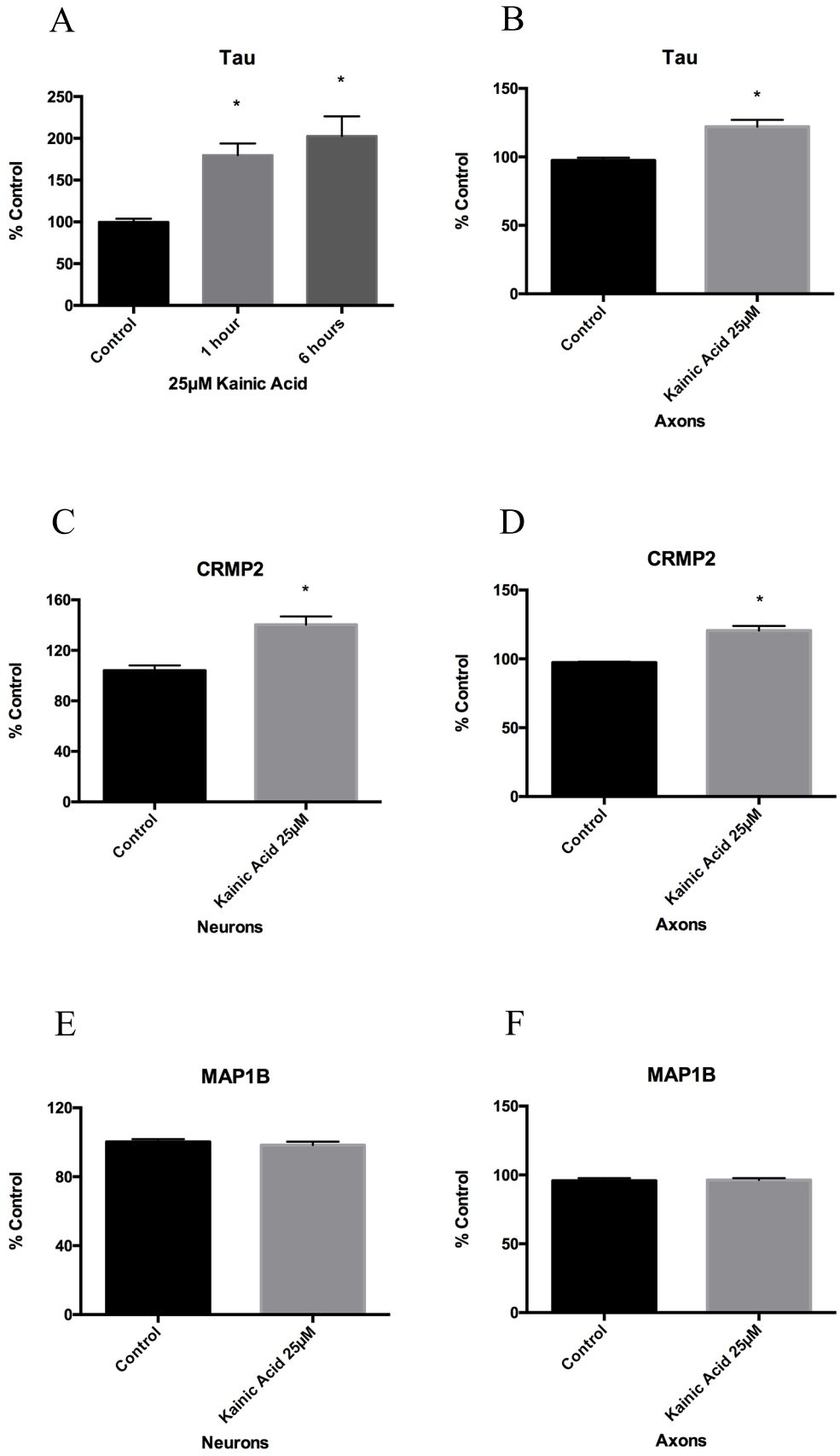
A
Tau
% Control
250
200
150
100
50
0
*
*
Control
1 hour
6 hours
25μM Kainic Acid
B
Tau
% Control
150
100
50
0
*
Control
Kainic Acid 25μM
Axons
C
CRMP2
% Control
160
120
80
40
0
*
Control
Kainic Acid 25μM
Neurons
D
CRMP2
% Control
150
100
50
0
*
Control
Kainic Acid 25μM
Axons
E
MAP1B
% Control
120
80
40
0
Control
Kainic Acid 25μM
Neurons
F
MAP1B
% Control
150
100
50
0
Control
Kainic Acid 25μM
Axons

Figure 5.1 The effect of kainic acid on MAPs

Levels of MAPs were quantitated by ELISA analysis in neurons and axons after 25 μM kainic acid treatment for 1 or 6 hours. Quantitation demonstrated that (A) tau was significantly increased ($p<0.05$) after 1 and 6 hours 25 μM kainic acid treatment in whole neurons. (B) Analysis of isolated axons from neurons grown in microfluidic chambers confirmed that 25 μM kainic acid treatment for 6 hours in the somatodendritic compartment significantly increased ($p<0.05$) axonal tau. CRMP2 levels in (C) neurons and (D) axons were significantly increased ($p<0.05$) relative to control following 6 hours kainic acid treatment. MAP1B levels in (E) neurons and (F) axons were unchanged compared to control after 25 μM kainic acid treatment for 6 hours. Bar graph represents mean ± SEM *$p < 0.05$ relative to control.

5.3.2 The effect of kainic acid treatment on MAP2

I next examined whether levels of the dendritic MAP, MAP2, were altered following excitotoxicity. Using an identical protocol as in section 5.3.1, I demonstrated using Western blotting that MAP2 levels in axons were significantly increased ($p<0.05$) at 1, 3 and 6 hours kainic acid exposure, compared to control (Figure 5.2 A). As MAP2 is a dendritic marker and levels were detected in the axon after kainic acid treatment with Western analysis, immunocytochemical labelling with an antibody against MAP2 was performed to confirm whether there was immunoreactivity in the axonal compartment. Cortical neurons grown in microfluidic chambers were treated in the somatodendritic compartment with kainic acid for 1, 3 and 6 hours with 100 μM kainic acid. Qualitative analysis demonstrated that while MAP2 was not detected in the axonal compartment at 0 hours, at 1-hour post kainic acid treatment, MAP2 immunoreactivity was present in the axonal compartment of the chamber (Figure 5.2 B). After 3 hours, MAP2 was still present, although the labelling was fragmented (Figure 5.2 C), potentially due to fragmentation of the axons with the higher concentration of kainic acid. After 6 hours, MAP2 immunolabelling was less intense relative to the 1 and 3-hour timepoints (Figure 5.2 D). These data suggest that excitotoxicity alters the localisation of MAP2 protein to the axon. Future studies will determine whether MAP2 mis-localisation is also present following lower concentrations of excitotoxin.

5.3.3 The effect of sodium selenate on excitotoxin-induced axon degeneration

Microfluidic chambers allow compartmentalised separation of axons from the somatodendritic compartment, which permits treatment to be applied exclusively to either compartment of the chamber. In the previous chapter, trichostatin A applied to axons protected them from kainic acid-induced axon loss and axon degeneration. In this study, I determined whether treatment of sodium selenate, which acts to increase activity of PP2A,

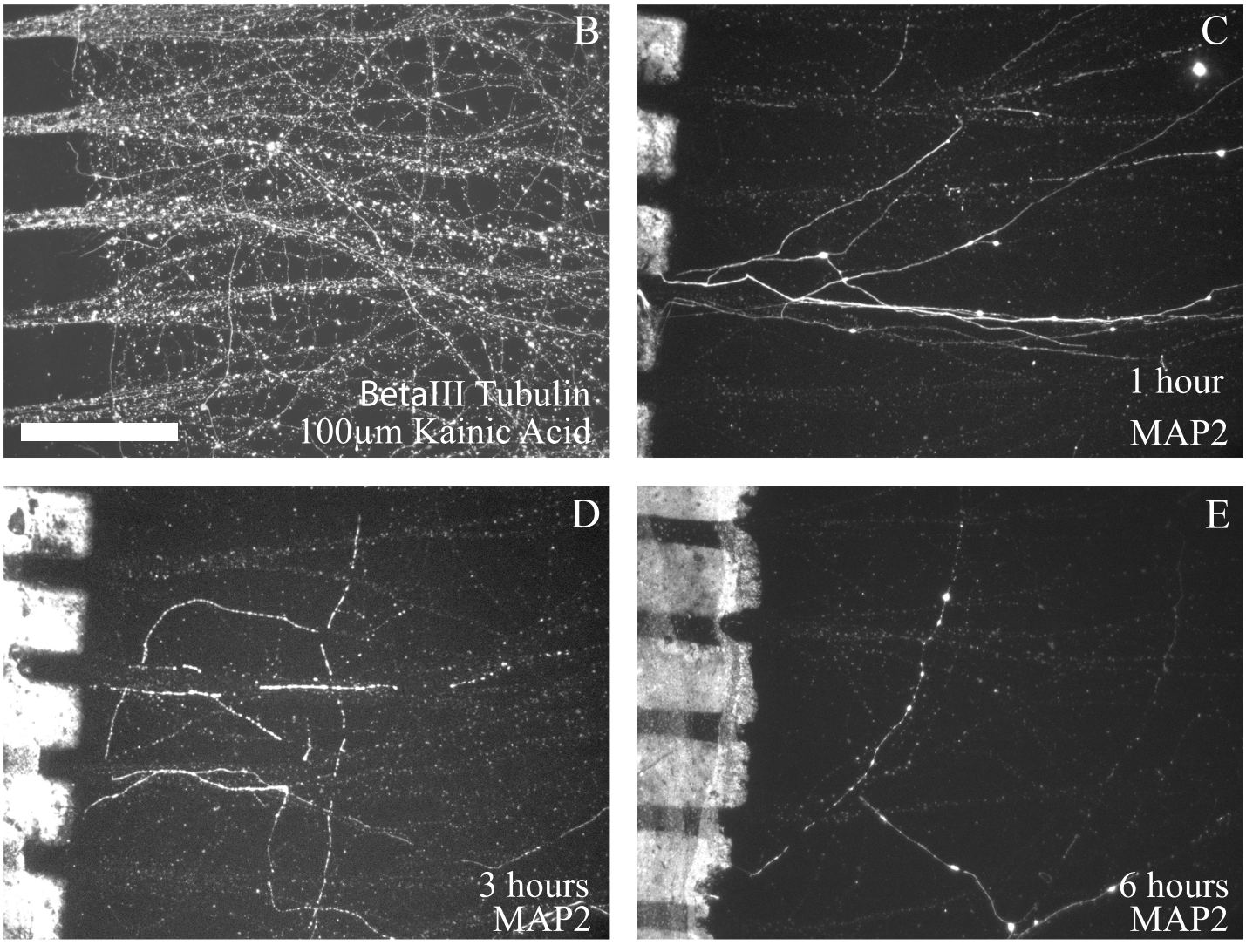
A
MAP2
*
10
8
6
4
2
0
KA 0 hour
KA 1 hour
KA 3 hour
KA 6 hour
B
BetaIII Tubulin
100µm Kainic Acid
C
1 hour
MAP2
D
3 hours
MAP2
E
6 hours
MAP2

Figure 5.2 Changes to MAP2 after excitotoxin exposure

MAP2 levels were quantitated in neurons following 100 μM kainic acid exposure (A) Western blot analysis demonstrated a significant ($p<0.05$) increase in neuronal MAP2 levels after 1, 3 and 6 hours kainic acid treatment relative to control. Representative images to show (B) control labelling with beta III tubulin after 6 hours of 100 μM kainic acid treatment. MAP2 labelling in the axon compartment of microfluidic chambers after (C) 1 hour, (D) 3 hours and (E) 6 hours of 100 μM kainic acid treatment. Bar graph represents mean ± SEM *$p < 0.05$ relative to control. Scale bar = 40 μm.

thus reducing phosphorylation of MAPs and promoting binding to microtubules, protected against axon degeneration. Mouse cortical neurons grown in microfluidic chambers to 10 DIV were exposed to 100 μM sodium selenate, which has previously been shown to activate PP2A in primary neuron culture (Alturkmani et al., 2012; van Eersel et al., 2010), in the axonal compartment of microfluidic chambers for 1 hour prior to treatment with 25 μm kainic acid in the somatodendritic compartment for 18 hours. Live-imaging of axons was performed immediately prior to and post-treatment to determine a degeneration index. Axon loss was significantly increased ($p<0.05$) at 25 μM kainic acid compared to vehicle control (Figure 5.3 A). However, addition of sodium selenate to the axonal compartment did not significantly alter kainic acid-induced axon loss and the combined treatment was still significantly ($p<0.05$) increased compared to vehicle control (Figure 5.3 A). Similarly, axonal sodium selenate did not have a protective effect on axon degeneration (Figure 5.3 B). Example live images showing axon loss and degeneration after 18 hours of all treatments (Figure 5.3 C-E).

5.3.4 The effect of trichostatin A on axonal MAPs following excitotoxin-induced axon degeneration

As the results show that tau and CRMP2 levels were increased by kainic acid, and I had previously shown that trichostatin A protects against kainic acid-induced axon degeneration, the effect of trichostatin A on these MAPs was investigated. Neurons were grown in 12-well culture trays and treated with trichostatin A for 2 hours followed by kainic acid treatment for 6 hours, prior to protein harvesting. ELISA analysis of neurons demonstrated that 10 nM trichostatin A treatment restored tau to control levels in the presence of kainic acid (Figure 5.4 A). To determine whether this effect was also present in axons, cortical neurons were grown in microfluidic chambers and the same treatment course was added as above before protein was harvested from axons. Similarly, 10 nM trichostatin A restored axonal tau levels

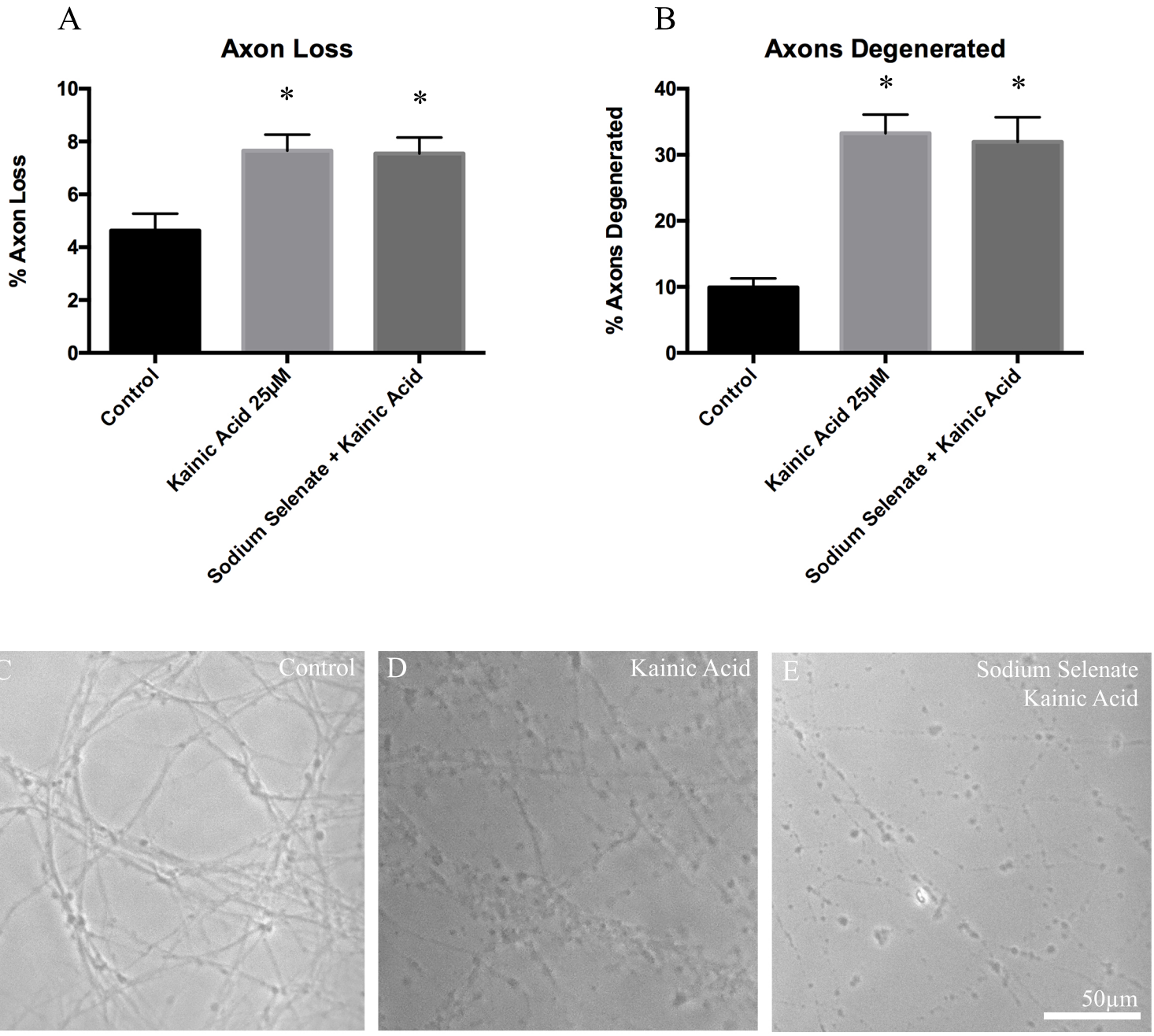
A
Axon Loss
% Axon Loss
10
8
6
4
2
0
*
*
Control
Kainic Acid 25μM
Sodium Selenate + Kainic Acid
B
Axons Degenerated
% Axons Degenerated
40
30
20
10
0
*
*
Control
Kainic Acid 25μM
Sodium Selenate + Kainic Acid
C
Control
D
Kainic Acid
E
Sodium Selenate
Kainic Acid
50μm

Figure 5.3 Axon degeneration and loss after sodium selenate treatment after kainic acid treatment

Live-imaging of the axonal compartment of microfluidic chambers were analysed for (A) axon loss and (B) axon degeneration index after treatment with 25 µM kainic acid (somatodendritic compartment) and 100 µM sodium selenate (axon compartment). Axon loss was significantly ($p<0.05$) increased after treatment with kainic acid. Combined treatment of sodium selenate and kainic acid, relative to control did not significantly alter kainic acid-induced axon loss and degeneration. Representative images of axonal compartment of (C) control, (D) kainic acid treatment, and (E) combined treatment of sodium selenate and kainic acid. Bar graph represents mean ± SEM *$p < 0.05$ relative to control. Scale bar is 50 µm.

A

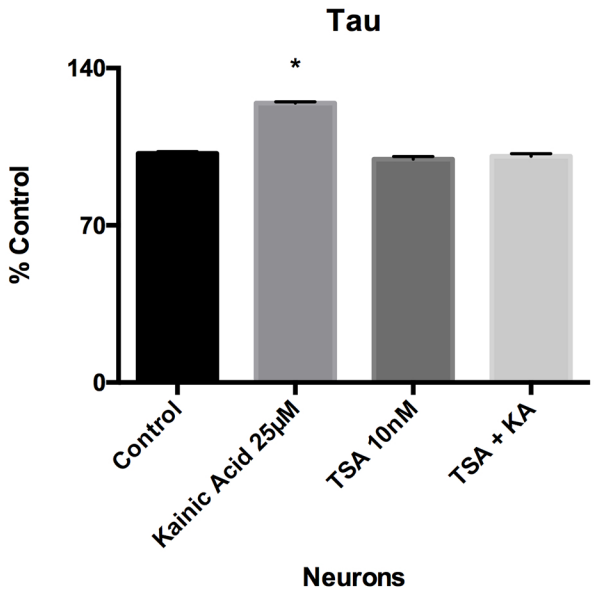
Tau
140
70
0
% Control
*
Control
Kainic Acid 25µM
TSA 10nM
TSA + KA
Neurons

B

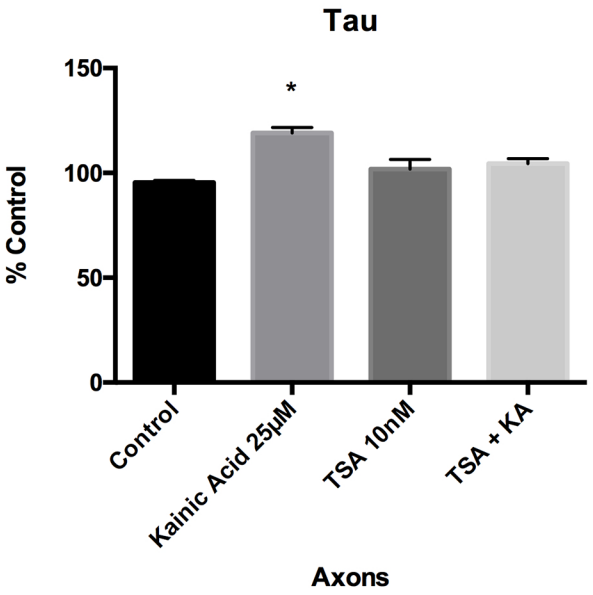
Tau
150
100
50
0
% Control
*
Control
Kainic Acid 25µM
TSA 10nM
TSA + KA
Axons

C

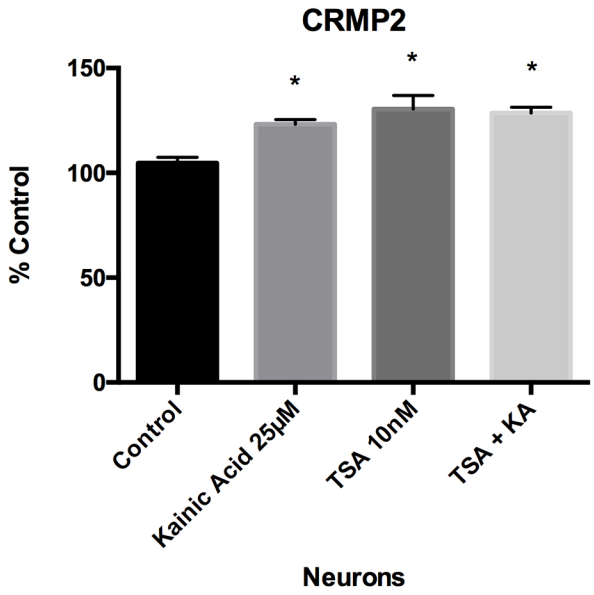
CRMP2
150
100
50
0
% Control
*
*
*
Control
Kainic Acid 25µM
TSA 10nM
TSA + KA
Neurons

D

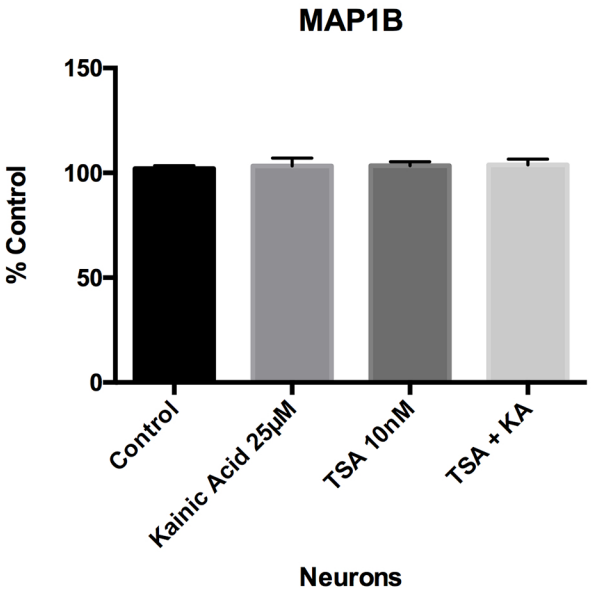
MAP1B
150
100
50
0
% Control
Control
Kainic Acid 25µM
TSA 10nM
TSA + KA
Neurons

Figure 5.4 Changes to MAPs following kainic acid treatment in the presence of trichostatin A

Changes to MAPs were investigated in neurons and isolated axons after treatment with 10 nM trichostatin A for 2 hours and 25 μM kainic acid for 6 hours. (A) ELISA analysis of tau in whole neurons demonstrated significantly increased levels ($p<0.05$) after kainic acid. In trichostatin A treated neurons levels of tau were not different from control. Levels of tau in kainic acid and trichostatin A treated neurons were not significantly different from control. (B) ELISA analysis of tau in isolated axons demonstrated significantly increased levels ($p<0.05$) after kainic acid treatment. In trichostatin A treated axons, levels of tau were not different from control. Levels of axonal tau in kainic acid treated neurons with trichostatin A were not significantly different from control. Levels of (C) CRMP2 were significantly increased ($p<0.05$) by either kainic acid or trichostatin A in neurons. Treatment of neurons with kainic acid in the presence of trichostatin A also resulted in significantly ($p<0.05$) increased CRMP2. Levels of (D) MAP1B in neurons were unchanged after kainic acid treatment but were significantly ($p<0.05$) increased after trichostatin A treatment and combined trichostatin A and kainic acid treatment, compared to control. Bar graph represents mean ± SEM *$p < 0.05$ relative to control.

following kainic acid treatments and they were no longer significantly different from vehicle control (Figure 5.4 B). However, 10 nM trichostatin A had no effect on neuronal CRMP2 levels, which remained significantly ($p<0.05$) higher following kainic acid in the presence of 10 nM trichostatin A (Figure 5.4 C). Neuronal MAP1B levels were unaffected by kainic acid and these were also unchanged at 10 nM trichostatin A treatment (Figure 5.4 D).

5.3.5 The effect of taxol on axonal MAPs following excitotoxin-induced axon degeneration

As it has been shown that taxol protects against kainic acid-induced axon degeneration, I next determined the effect of taxol on MAPs following kainic acid treatment. Neurons were grown in microfluidic chambers to 10 DIV and treated with taxol for 2 hours in the axonal compartment prior to 6 hours of kainic acid treatment in the somatodendritic compartment before axonal protein was harvested. As described previously, tau levels were significantly increased ($p<0.05$) after kainic acid treatment compared to vehicle control. When combined with treatment with axonal taxol, tau levels continued to be significantly increased ($p<0.05$) compared to vehicle control following kainic acid treatment, and did not differ from kainic acid treatment alone (Figure 5.5 A). As previously demonstrated, CRMP2 levels were significantly increased ($p<0.05$) after kainic acid treatment, and continued to be significantly increased ($p<0.05$) after taxol treatment and combined taxol and kainic acid treatment, compared to vehicle control (Figure 5.5 B). As demonstrated in previous results, MAP1B levels were not significantly increased after kainic acid treatment, compared to vehicle control. However, after taxol treatment alone and combined taxol and kainic acid treatment, MAP1B levels were significantly increased ($p<0.05$) compared to vehicle control (Figure 5.5 C).

A

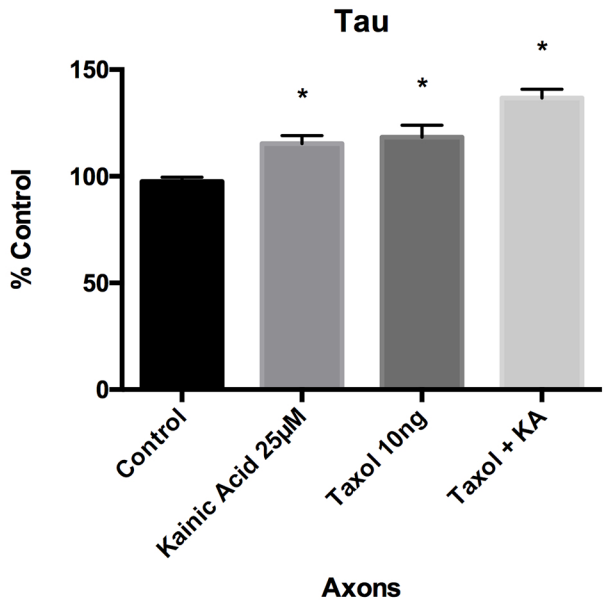
Tau
% Control
150
100
50
0
*
*
*
Control
Kainic Acid 25μM
Taxol 10ng
Taxol + KA
Axons

B

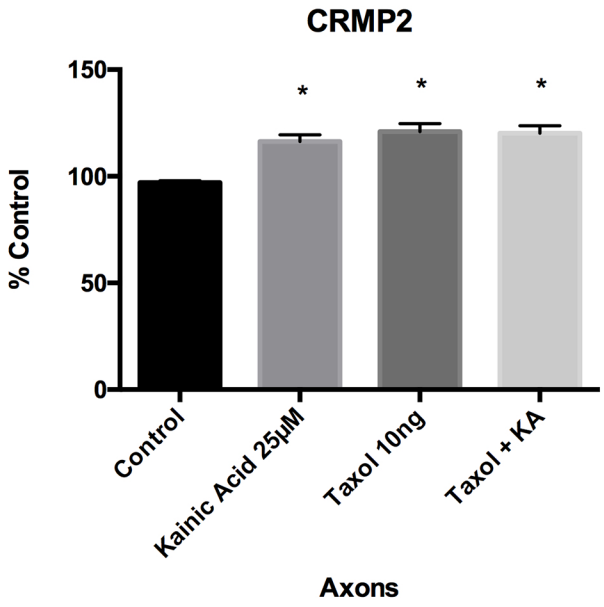
CRMP2
% Control
150
100
50
0
*
*
*
Control
Kainic Acid 25μM
Taxol 10ng
Taxol + KA
Axons

C

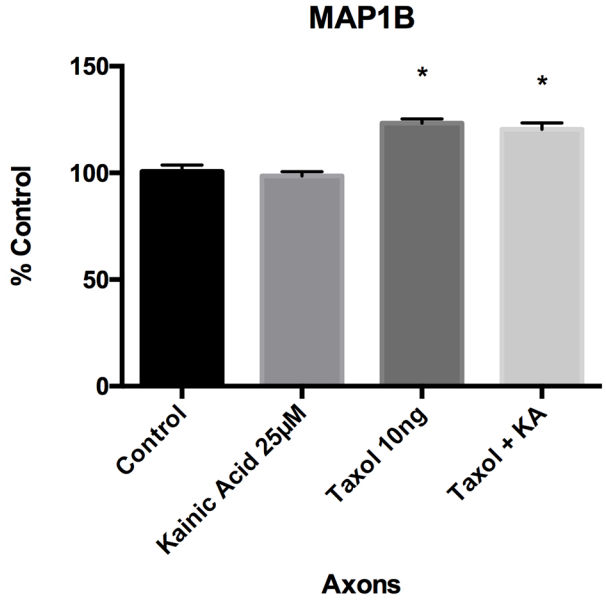
MAP1B
% Control
150
100
50
0
*
*
Control
Kainic Acid 25μM
Taxol 10ng
Taxol + KA
Axons

D

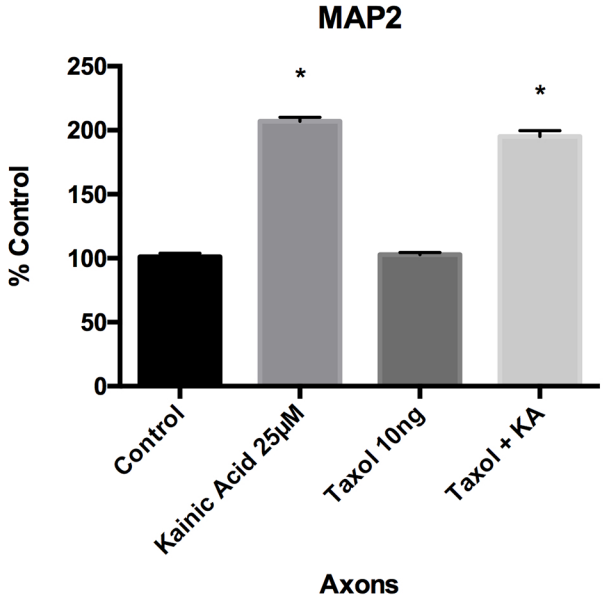
MAP2
% Control
250
200
150
100
50
0
*
*
Control
Kainic Acid 25μM
Taxol 10ng
Taxol + KA
Axons

Figure 5.5 Changes to MAPs following kainic acid treatment in the presence of taxol

Changes to MAPs were investigated in isolated axons after treatment with 10ng taxol for 2 hours and 25 μM kainic acid for 6 hours. (A) Tau was significantly increased in axons ($p<0.05$) in all treatment groups. (B) CRMP2 and (C) MAP1B levels were significantly increased in axons ($p<0.05$) after taxol treatment and combined taxol and kainic acid treatment in axons. (D) MAP2 levels were significantly ($p<0.05$) increased in axons compared to control after kainic acid treatment. MAP2 levels were unchanged by axonal taxol treatment with axonal taxol and somatodendritic kainic acid, MAP2 levels in axons were significantly ($p<0.05$) increased relative to control. MAP2 control levels of the axon were very low, and are expressed as 100%. Bar graph represents mean ± SEM *$p < 0.05$ relative to control.

5.3.6 The effect of taxol on MAP2 following excitotoxin-induced axon degeneration

As this thesis demonstrated the altered localisation of MAP2 following kainic acid treatment, the effect of taxol on axonal MAP2 was examined. MAP2 levels in untreated axons of cortical neurons grown in microfluidic chambers were very low, however, for data interpretation this was defined as 100%. ELISA analysis demonstrated that after 25 μM kainic acid treatment, axonal MAP2 levels were significantly increased ($p<0.05$) compared to vehicle control. Taxol alone applied to the axonal compartment did not significantly affect MAP2 levels. Furthermore, taxol did not significantly affect the increased axonal levels of MAP2 induced by kainic acid treatment and levels remained significantly increased ($p<0.05$) compared to vehicle control and taxol alone treatment (Figure 5.5 D).

Together these results suggest that targeting acetylation by trichostatin A can alter MAPs and prevent axon degeneration, suggesting that targeting microtubule PTMs which are altered during excitotoxicity, could be a potential therapeutic target in several neurodegenerative diseases.

5.4 DISCUSSION

The current study investigated the potential of targeting MAPs to protect against excitotoxin induced axon degeneration. Firstly, the expression levels of key axonal and somatodendritic MAPs were investigated. Microtubule-associated proteins play an important role in stabilising microtubules, so early changes to these proteins could enhance degeneration. Secondly, the effect of promoting MAP dephosphorylation through increasing activity of PP2A on axon degeneration was determined. I also determined how treatment with microtubule targeting drugs, which have been shown to protect axons following excitotoxicity, affected expression of MAPs following excitotoxicity. As microtubule alterations do not occur in isolation it is important to understand the downstream effects of any microtubule targeting drug. This study had a number of key findings that have increased our understanding of the role of MAPs following excitotoxicity. Firstly, following an excitotoxic insult there are changes in expression levels as well as a localisation of MAPs. Furthermore, treatment with trichostatin A or taxol has the capacity to prevent some of these changes to MAPs. I also showed that promoting dephosphorylation via PP2A is unlikely to protect against excitotoxin-induced axon degeneration.

In this study, I showed that excitotoxicity induced a significant increase in the expression of both tau and CRMP2. In the current study tau was shown to be increased as early as one hour after kainic acid treatment. It is currently unclear whether this increase in tau is through altered translation or reduced clearance of the protein. Kainic acid induced-excitotoxicity in a mouse model caused initial dephosphorylation of tau, followed by sustained hyperphosphorylation, possibly due to activation of cdk5 and down-regulation of PP2A (Liang et al., 2009). Overexpression of tau, induced by NMDA receptors, has been shown to mediate neuronal death by suppressing ERK phosphorylation (Sun et al., 2016). Since tau's

function is to stabilise microtubules, increased tau levels could be a compensatory mechanism, potentially to increase microtubule stability. However, research has increasingly investigated tau secretion into the extracellular space, increased tau expression could lead to increased release of tau, potentially leading to the spread of tau pathology and an increase in Aβ production (Dubal, 2018; Yamada, 2017). Levels of soluble and insoluble tau reflect the phosphorylation status of tau *in vivo* (Hirata-Fukae et al., 2009) and soluble tau has been shown to decrease the structural plasticity of hippocampal neurons (Bolós et al., 2017).

The effects of altered tau expression are currently debated. Tau knockdown results in learning and memory deficits in mouse models (Velazquez et al., 2018), whereas overexpression of tau results in increased phosphorylated tau, which has shown to protect against oxidative stress (Castellani et al., 2008), but is also implicated in neurodegenerative disease (Kadavath et al., 2015; Sontag et al., 1996). Furthermore, the phosphorylation state of tau, which was not investigated in the current study, is an important indicator of tau binding to microtubules, which is reported to inhibit axonal transport (Cox et al., 2016; Dubey et al., 2008), which can be rescued by changing tau's phosphorylation status (Kanaan et al., 2012). Interestingly, it has been shown that tau inhibits HDAC6 function (Perez et al., 2009), further supporting a protective role for the increased tau expression. However, it is currently unclear whether increased tau following excitotoxicity plays a protective or detrimental role.

The changes in tau prompted examination of expression levels of other MAPs and demonstrated that like tau, CRMP2 was significantly increased following excitotoxin exposure. The dysregulation and hyperphosphorylation of CRMP2 has been observed in AD (Hensley and Kursula, 2016; Williamson et al., 2011) and does not occur in other neurodegenerative diseases (Cole et al., 2007; Soutar et al., 2009; Williamson et al., 2011). CRMP2 is a MAP with a number of similarities to tau as it regulates microtubule stability, is

regulated by the same kinases as tau (Cole et al., 2008) and PTMs of CRMP2 may also contribute to disease (Hensley and Kursula, 2016). However, to date neuropathic mutations in CRMPs have not been reported. CRMP2 has been studied in an axon degeneration model of the optic nerve where CRMP2 is a downstream target of calpain, which cleaves CRMP2, leading to axon degeneration (Zhang et al., 2016). When calpain is inhibited and CRMP2 is overexpressed, it protects axons against acute axon degeneration (Zhang and Koch, 2017), suggesting that increased expression of CRMP2 may be a neuroprotective strategy in our model. Although CRMP2 phosphorylation was not investigated in the current study, previous research has shown that in contrast to our kainic acid induced excitotoxicity model, excitotoxicity through NMDA exposure reduces phosphorylation of CRMP2 and promotes CRMP2 cleavage after 6 hours (Yin et al., 2013). MAP1B levels, which are associated with microtubule stability (Riederer, 2007) were unchanged in this study, suggesting excitotoxin-induced axon degeneration does not affect microtubule stability thorough MAP1B alterations.

Phosphorylated MAP expression was not examined in the current study, although the effect of promoting MAP phosphorylation with sodium selenate was examined. In particular, PP2A, the target of sodium selenate, has been shown to bind to tau and MAP2 (Sontag et al., 2012). In this study, treatment with sodium selenate had no effect on axon loss or axon degeneration after kainic acid treatment.

Phosphorylation states of cytoskeletal proteins are regulated via protein kinase and phosphatase activity. Transduction of cellular signalling propagates through MAPK cascades and is mainly controlled by phosphorylation events (Nguyen et al., 2013). For example, neuronal MAP2 can regulate organelle transport within the axons and dendrites and the regulation of protein kinases for signal transduction (Sánchez et al., 2000). Other kinases such as MAP kinase kinases (MKK) can also activate kinases which regulate MAP

phosphorylation. For example, phosphorylation of tau by isoforms of MAPK p38, promotes microtubule assembly (Zarubin et al., 2005). Upstream signals by either extracellular stimuli such as inflammatory cytokines like TNF-α, or growth factors like CSF-1, can activate MAP kinases (Zarubin et al., 2005). Thus, phosphorylation in the microtubule-binding domain of MAPs by protein kinase p110 can regulate microtubule dynamics within neurons (Illenberger et al., 1996).

To more fully understand the role of MAP phosphorylation in excitotoxin-induced axon degeneration, further studies should examine the phosphorylation state of MAPs after kainic acid exposure, both with and without sodium selenate.

An unexpected finding of interest in the current study was the mis-localisation of MAP2 to the axon following excitotoxicity. It has been reported that during axon degeneration, axonal tau enters the dendritic compartment (Li et al., 2011), however, alterations to MAP2 localisation have not previously been reported. Previous research has shown that dendritic MAP2 is lost from the apical dendrites after NMDA-induced dendritic injury in hippocampal slices (Hoskison et al., 2007) and in a rat model of glutamate-induced excitotoxicity, immunoreactivity of MAP2 in the dendrites was reduced (Irving et al., 1996). Increased levels in MAP2 in aged wildtype mice have been associated with cognitive decline (Benice et al., 2006). In the current study, ELISA analysis demonstrated that MAP2 levels in axons were significantly increased after 25 μM kainic acid treatment. This was also confirmed with MAP2 immunolabelling in the axonal chamber after 100 μM kainic acid treatment. This supports the hypothesis that there may be breakdown of the axon initial segment, which separates MAPs to their respect compartments, after excitotoxicity (Clark et al., 2017; Evans et al., 2015; Leterrier, 2018).

This thesis investigated the downstream effects of microtubule-modifying drugs on MAPs. After promoting acetylation with trichostatin A, tau was unchanged compared to control, suggesting that increasing the PTM acetylation does not influence tau. However, trichostatin A increased CRMP2, which may promote microtubule stability through binding to tubulin heterodimers (Fukata et al., 2002). The relationship between acetylated tubulin and CRMP2 is currently not understood. Taxol treatment also increased CRMP2, and in an *in vivo* model taxol has been shown to abolish microtubule association of CRMPs (Lin et al., 2011). Inhibition of the tau phosphate kinase GSK3β has shown to improve CRMP's ability to promote microtubule polymerisation (Lin et al., 2011). This suggests that taxol could be potentially promoting microtubule stability via increasing CRMP2 expression. MAP1B was unchanged after trichostatin A treatment, which suggests that acetylation does not influence MAP1B expression, however, taxol does increase MAP1B expression. MAP1B has been shown to bind to taxol-stabilised microtubules (Ma et al., 2000; Pedrotti and Islam, 1996).

Taxol treatment increased tau expression, which could be due to competitive binding at the tau binding site, leading to tau dissociation from microtubules, and increasing tau secretion. Taxol has no effect on MAP2 expression, although taxol-induced flexibility of microtubules is decreased after the addition of MAP2 or tau (Dye et al., 1993).

This study has a number of limitations that could be addressed in future studies. Firstly, MAPs were investigated at six hours after kainic acid-induced excitotoxicity, and it would be of interest to examine earlier timepoints in future studies. Furthermore, it would be of interest to investigate the mechanism of MAP altered expression either through increased synthesis or decreased breakdown. Inhibiting phosphorylation of MAPs via sodium selenate treatment

was shown to not prevent axon degeneration, but the phosphorylation of specific MAPs was not investigated in the current study, and should be investigated in the future.

5.4.1 Conclusion

Together these data demonstrate that changes to the expression and localisation of MAPs are an early event in axon degeneration and that these can be modulated by a number of microtubule-targeting drugs, suggesting a complex interplay between microtubule modifying agents which needs to be considered in any therapeutic intervention. There has been much focus in neurodegenerative disease research around altered phosphorylation of MAPs. Although this data suggests that reducing phosphorylation of MAPs does not protect against degeneration, examining MAP phosphorylation as well as how proteins investigated in this study are altered by excitotoxic treatment, will be of interest in future studies.

Chapter 6

Final Discussion

6 FINAL DISCUSSION

This thesis sought to investigate the potential of microtubules as a therapeutic target in AD and to identify other more specific targets through understanding the mechanisms of axon degeneration. The pathological processes that occur in axons leading to their degeneration are under intense investigation. This thesis focussed on cellular and axonal changes following an excitotoxic insult, as this is implicated in many neurodegenerative diseases and injury. Specifically, the alterations to microtubules and associated proteins was investigated as well as the downstream consequences of these changes and how they can be target therapeutically to prevent axon degeneration. In addition, the effect of microtubule stabilisation on the pathological features of an AD model of amyloidosis was investigated. The data presented in chapters four and five demonstrate that following an excitotoxic insult the microtubule cytoskeleton undergoes a number of changes, some of which are directly related to axon degeneration. The data presented in this thesis also highlights the significant interplay between microtubule modifications, in that one modification cannot be targeted without causing changes to other parts of the cytoskeleton.

One of the major outcomes of this thesis, is the characterisation of microtubule alterations that occur after excitotoxin-induced axon degeneration in a primary cell culture model. The PTM, acetylation was significantly decreased, whereas the MAPs, tau and CRMP2 were significantly increased after excitotoxin-induced axon degeneration. Furthermore, targeting the PTM acetylation with an HDAC6 inhibitor, trichostatin A, not only promoted acetylation following excitotoxic insult, but also prevented axons from degenerating. This finding endorses microtubules as a therapeutic target in axon degeneration.

Hyperphosphorylation of MAPs, particularly tau, has been identified in AD. This thesis investigated whether phosphorylation of MAPs through the activation of the phosphatase PP2A can drive axon degeneration. In this *in vitro* study, activating PP2A via application of sodium selenate did not prevent axon degeneration or axon loss in a model of excitotoxin-induced axon degeneration. This suggests that phosphorylation status of MAPs may not have a driving role in excitotoxin-induced axon degeneration.

Finally, a number of microtubule-associated alterations were documented in the presence of microtubule-modulating drugs in this thesis. Of note, the microtubule-stabilising agent epothilone D significantly decreased phosphorylated neurofilament levels in the cortex and hippocampus of APP/PS1 and wildtype mice at 15-months of age. This finding highlights a potential compensatory mechanism within the cytoskeleton, whereby increased levels of stabilised microtubules, promotes decreased phosphorylated neurofilament levels. This result is also in accordance with previous research (Liu et al., 2012), which showed decreased neurofilament after promoting microtubule levels. Despite this effect on the cytoskeleton, there were no alterations in the number of dystrophic neurites surrounding plaques and no alteration in amyloid pathology, supporting safety of this drug for reduction of tau pathology in AD.

Can microtubule changes drive degeneration of the axon?

A hypothesis of this thesis was that microtubules undergo alterations during excitotoxin-induced axon degeneration, which can drive the fragmentation and loss of the axon. To determine potential changes to microtubule modifications and associated proteins, a model of axon degeneration was utilised. In this model, cultured neurons were grown in a

compartmentalised microfluidic chamber and changes to axons were determined following application of the excitotoxin kainic acid.

After kainic acid-induced axon degeneration, acetylated tubulin was significantly decreased in the axon. It was hypothesised that this reduction could drive axon degeneration as acetylated tubulin is associated with microtubule stability (Howes et al., 2014; Janke et al., 2017). To test this hypothesis, trichostatin A treatment was used to inhibit the activity of the de-acetylase HDAC6, and therefore promote acetylation. Treatment of axons with trichostatin A resulted in protection of the axon following excitotoxicity, demonstrating a key role for microtubule changes in axon fragmentation and loss following kainic acid. This result is in line with previous experiments suggesting that acetylated tubulin levels are affected before microtubule breakdown during axon degeneration (Neumann and Hilliard, 2014). This suggests that the PTM acetylation has a major role in preventing axon degeneration and that microtubule changes may drive degeneration of the axon. However, the role of acetylated tubulin in microtubule stability is not simple. For example, it has been documented that acetylated tubulin promotes the binding activity of the microtubule severing enzyme, katanin, which would potentially increase microtubule breakdown rather than decreasing it (Sudo and Baas, 2010). This suggests that other microtubule alterations promote microtubule breakdown in axon degeneration and it is not through enhanced severing by katanin. However, it would be of interest to rule out increased katanin binding and microtubule severing as a protective effect of acetylation in future studies.

Previous research has shown that the microtubule-stabilising drug taxol protects against kainic acid-induced axon degeneration (King et al., 2013). This prompted investigation into whether taxol also promotes microtubule acetylation. This thesis demonstrated that acetylated

tubulin was significantly increased in axons following taxol treatment, and this result is in line with previous research demonstrating that acetylated tubulin is significantly increased after taxol in non-neuronal cultured cells (Piperno et al., 1987; Webster et al., 1990) and in a kidney injury model (Han et al., 2016). Thus, increased tubulin acetylation in the presence of taxol is a potential protective mechanism for taxol following excitotoxic insult. The exact mechanism by which taxol protects axons from degeneration following excitotoxin exposure is currently unknown, however, it has been reported that other microtubule PTMs are also increased after taxol treatment. Detyrosinated tubulin has been demonstrated to be increased after treatment with taxol in cultured cells (Gundersen et al., 1987). In line with this data, tyrosinated tubulin was significantly decreased after treatment with taxol in this thesis. Tyrosinated tubulin is mainly located at the distal end of the axon, and at high levels, is associated with microtubule instability and can cause motor proteins to disassociate from microtubules. Tyrosination tubulin levels were unchanged after excitotoxin exposure, suggesting that tyrosinated tubulin does not have a driving role in microtubule breakdown during axon degeneration. Tyrosinated tubulin also recruits plus-end tracking proteins (+TIPs) that contain a CAP-Gly domain (Hammond et al., 2008) and as tyrosinated tubulin was unchanged by kainic acid treatment in this thesis, it could suggest that there was also no change to +TIPs bound to microtubule plus-ends, thus there is no consequential rapid depolymerisation. This could suggest a different mechanism for microtubule breakdown, so instead of rapid microtubule depolymerisation, severing protein activity could be enhanced by the other major microtubule severing enzyme spastin. Another PTM, glutamylation, enhances spastin severing activity, however, glutamylation expression during axon degeneration is widely disputed (Lacroix et al., 2010; Valenstein and Roll-Mecak, 2016).

To determine if targeting microtubules via replacement of tau can prevent axons from degenerating, taxol can be used, as it has the same microtubule binding site as tau. Previous research has shown that treatment with taxol followed by kainic acid-induced excitotoxicity prevents axon degeneration *in vitro* (King et al., 2013). To determine whether other microtubule changes can drive degeneration of axons, MAPs were also investigated in this thesis. Driving MAP dephosphorylation via PP2A activation, which should increase MAP binding to microtubules, did not provide a protective effect on axons in this study, suggesting altered MAP phosphorylation is not a driving factor in axon degeneration. However, a limitation of this study was that the phosphorylation of MAPs was not confirmed and concentrations of sodium selenate followed previous literature. Despite this, levels of some MAPs, including tau and CRMP2 were altered following excitotoxicity. Since CRMP2 and tau are reported to stabilise microtubules (Hensley and Kursula, 2016; Lin et al., 2011; Mokhtar et al., 2013), it could be hypothesised that increased levels of these proteins are neuroprotective at early stages of degeneration. In this regard, it has been shown that cleavage of CRMP2 occurs in axon degeneration after injury (Taghian et al., 2012). However, the role of tau and CRMP2 in axon degeneration is controversial as loss of tau has been shown to be neuroprotective (DeVos and Hyman, 2017; Zhang et al., 2009) and over-expression of CRMP2 can result in microtubule disassembly, as reported in dopamine-induced neuronal apoptosis (Hou et al., 2008). Although the role of CRMP2 and tau in axon degeneration are unclear, in the current study, trichostatin A and taxol significantly increased CRMP2 expression suggesting that increased tau and CRMP2 do not drive axon degeneration. Future studies will further investigate the cause of CRMP2 and tau alterations in kainic acid-induced axon degeneration and whether their role is protective or detrimental.

MAP1B levels were not altered following kainic acid-induced axon degeneration, although they were altered by treatment with trichostatin A. This suggests that MAP1B is not involved in this specific axon degeneration pathway. MAP1B regulates tyrosination of alpha-tubulin (Utreras et al., 2008), which was also unchanged. This suggests that tyrosinated microtubules, which are predominately located at the distal end of the axon, are not driving kainic acid-induced axon degeneration.

In summary, targeting microtubules via the PTM acetylation and the MAP tau, could prevent degeneration of axons, and may be useful therapeutic targets of neurodegenerative disease and injury.

Could pathological alterations in AD be explained by chronic excitotoxicity?

This thesis investigated the downstream effects of chronic excitotoxin exposure, a pathological process that has been implicated in AD (Hynd et al., 2004; Ong et al., 2013; Wang and Reddy, 2017). It is therefore of interest to examine whether alterations described in neurons in this thesis share any similarities with neuronal alterations in AD. In particular, one of the pathological alterations that occur in AD and other neurodegenerative diseases are aggregation of MAPs. The MAPs, tau and CRMP2 both undergo abnormal hyperphosphorylation prior to pathology (Soutar et al., 2009), resulting in aggregation (Watamura et al., 2016) and with likely downstream functional consequences such as the impairment of axonal transport (Mokhtar et al., 2018). Despite extensive research, there is still no consensus on the mechanisms by which tau and CRMP2 are altered in AD. This thesis demonstrated that excitotoxicity also has an effect on MAPs, and particularly on CRMP2 and tau. Although phosphorylation was not examined in this thesis, the results suggest that excitotoxicity could be driving pathological changes in AD. For example, previous studies

have shown that during glutamate excitotoxicity, CRMP2 is phosphorylated by calcium/calmodulin-dependent protein kinase II (CaMKII) and is associated with axonal varicosities, however, over-expression of CRMP2 increases axonal resistance to glutamate toxicity (Hou et al., 2009). This could suggest that excitotoxicity which occurs in AD (Hynd et al., 2004; Ong et al., 2013; Wang and Reddy, 2017), could lead to phosphorylation of CRMP2, in turn causing axon damage. In addition, CRMP2 interacts with NMDA receptors and regulates their function (Brustovetsky et al., 2014), indicating the relationship between CRMP2 and excitotoxicity.

Tau is a key aggregating protein, which causes pathology in several neurodegenerative diseases, including AD (Iqbal et al., 2010). Tau hyperphosphorylation is a well-studied pathology in AD (Gong and Iqbal, 2008; Šimić et al., 2016; Wang et al., 2013). Tau phosphorylation at multiple sites in the brain has been shown to be dysregulated during kainic acid excitotoxicity in a mouse model (Liang et al., 2009). This may suggest that excitotoxicity via glutamate receptors or Aβ-induced toxicity (Pallo et al., 2016) contributes to AD pathology by promoting abnormal phosphorylation of tau. The finding that tau is upregulated following excitotoxicity was an unexpected finding in this thesis. It is unclear whether tau is also upregulated in AD, however, recent research has highlighted novel roles for tau, including tau secretion, which may contribute to the pathological spread of tau pathology (Dubal, 2018).

Another unexpected finding in this thesis was that MAP2, a dendritic protein was observed in the axonal compartment after kainic acid-induced excitotoxicity. To my knowledge, this is the first time MAP2 has been described in the axonal compartment, although other research has shown that MAP2 expression is decreased in the dendrites after excitotoxicity in rat

hippocampus (Arias et al., 1997). Previous research has demonstrated that tau mis-localises to the dendrites in AD (Hoover et al., 2010). Together these data may suggest that in excitotoxic conditions, there is a general mis-localisation of MAPs, perhaps due to the breakdown of the axon initial segment (Leterrier, 2018; Sohn et al., 2016).

In summary, proteins associated with microtubules may be altered by excitotoxic mechanisms in AD, and contribute to pathology. Therefore, targeting MAPs may be a valid therapeutic approach for AD.

Could we safely target microtubules in neurodegenerative disease?

Microtubule-stabilising drugs have been proposed as a potential therapeutic target in AD due to the extensive tau pathology in the brains of AD patients. Although microtubule-stabilising drugs have been trialled in mutant tau models, the effects of microtubule stabilisation on the pathology associated with amyloidosis has not been investigated (Brunden et al., 2010; Zhang et al., 2012; Matsuoka et al., 2008; Barten et al., 2012). Thus, one of the aims of this study was to determine if the microtubule-stabilising drug epothilone D affects the deposition of plaques and associated pathology in the APP/PS1 mouse model of AD.

Maintaining the structural stability of the cytoskeleton during axon degeneration has been identified as a key stage in which to delay and/or prevent axon degeneration. The finding in chapter 3 that phosphorylated neurofilament protein is significantly reduced after epothilone D treatment in APP/PS1 and wildtype mice, suggests a direct link between the microtubule and neurofilament cytoskeleton (Zhao et al., 1994), that should be taken into consideration. In larger diameter axons, neurofilaments dominate microtubules by 10-fold (Lee and Cleaveland, 1996), however, in small diameter axons, fewer neurofilaments are present, and

a higher density of microtubules are present (Friede and Samorajski, 1970). Neurofilament accumulations have been implicated in a number of neurodegenerative diseases, including AD and it is unclear whether reducing neurofilaments would be a protective strategy in disease. In this thesis, epothilone D-induced reduction of phosphorylated neurofilament did not alter dystrophic neurite pathology in 15-month old APP/PS1 mice. However, a limitation of the current study, was the effect of epothilone D on overall levels of neurofilament proteins was not assessed and should be addressed in future studies. Despite the effects on the cytoskeleton induced by epothilone D, there were no alterations to other AD pathological features, such as amyloid plaque deposition and synaptic density suggesting that use of this drug to stabilise axons would not cause other detrimental effects. Epothilones have already been successfully used as therapeutics for various types of cancer and have undergone clinical trials (Beer et al., 2007; Eng et al., 2004; Lee et al., 2007). More recently, epothilones have also had success in mouse models of neurodegenerative disease, particularly tauopathies (Brizuela et al., 2014; Brunden et al., 2010; Fournet et al., 2012; Ruschel et al., 2015; Yu et al., 2018; Zhang et al., 2012a).

The current study identified a protective effect of the microtubule-stabilising drug trichostatin A on axons following kainic acid-induced excitotoxicity. This drug has previously been shown to be a successful therapeutic in several models of disease, including models of spinal muscular atrophy, arthritis and osteoclastogenesis (Avila and Burnett, 2007; Huber et al., 2007; Liu et al., 2014; Moreira et al., 2003; Nasu et al., 2008; Rahman et al., 2003; Williams et al., 2011; Yoo and Ko, 2011). However, although in this thesis, trichostatin A was used to target HDAC6 by application to the axonal compartment, trichostatin A is not specific for HDAC6. For example, trichostatin A has been shown to alter DNA replication in human cells (Kemp et al., 2005), and is a clastogen in human lymphoblasts *in vitro* (Olaharski et al., 2006).

It has also been shown to induce apoptosis in a human lung carcinoma cell line, suggesting that it has anti-cancer activity (Choi, 2005) and has been suggested to be a promising therapy for AD (as reviewed by Xu et al., 2011). Trichostatin A was shown to have no effect on removing plaques in an AD mouse model, however it was effective at preventing the formation of new amyloid deposits, although the size of existing plaques increased (Yang et al., 2014). Inhibition of another HDAC, HDAC3 reverses AD-related pathology *in vitro* and in an AD mouse model and alleviates memory impairment (Janczura et al., 2018). Trichostatin A has also been shown to ameliorate endotoxin-induced neuroinflammation and cognitive dysfunction in a endotoxin-induced mouse model (Hsing et al., 2015). In this thesis, treatment with trichostatin A significantly decreased axonal tau back to vehicle control levels following kainic acid exposure. This may suggest that trichostatin A has a beneficial effect on tau, although future studies will need to investigate this further. Based on the results of this thesis, and previous research, HDAC6 inhibitors warrant further investigate in the context of AD. However, although numerous HDAC6 inhibitors are FDA-approved for human use (as reviewed by Suraweera et al., 2018), blood brain barrier penetration needs to be considered.

The main limitations of this thesis include the use of cell culture models, and the use of an animal model of AD. Future studies should focus on confirming the cell culture results *in vivo*. Furthermore, the APP/PS1 mouse model of AD used in this thesis does not exhibit all AD pathology, in particular, there is no tau neurofibrillary tangle pathology present. Therefore, the results of the current study should be confirmed using a mouse model exhibiting neurofibrillary tau pathology. Other limitations of the APP/PS1 mouse model used include the over-expression of APP driven by the prion promoter, with expression likely far

higher than in familial AD. The mice also start developing pathology at a young age (3 months), which is not in the context of ageing.

In summary, research suggests that microtubules are able to be targeted safely as a therapeutic for neurodegenerative diseases and microtubule-targeting drugs have shown efficacious results in mouse models of neurodegenerative diseases. However, translation of these outcomes to humans has been challenging, with clinical trials being terminated at Phase II or Phase III. Increased understanding of the mechanisms of microtubule disruption that occur in neurodegenerative diseases, will identify more specific targets for intervention and improve the likelihood of successful treatment.

Conclusions

The studies undertaken in this thesis further our understanding of how microtubules are not only altered, but can also be targeted to prevent axon degeneration. Based on previous literature, the alterations of microtubules during axon degeneration were unclear, but the results presented in this thesis elucidated some of the unknown alterations. Future studies of axon degeneration will continue to investigate alterations to microtubules, specifically the role of phosphorylated tau, and if it is altered after treatment with trichostatin A or taxol. Furthermore, other microtubules PTMs such as detyrosination and glutamylation should be investigated, as their role in axon degeneration is currently unclear. The studies described in this thesis provide insight into the axonal changes that occur following kainic acid-induced excitotoxicity, provide a greater understanding of disease mechanisms in axon degeneration and highlights new potential therapeutic targets.

Chapter 7

References

7 REFERENCES

Adlard, P. A., King, C. E., and Vickers, J. C. (2000). The effects of taxol on the central nervous system response to physical injury. *Acta Neuropathol.* 100, 183–188.

Alonso-Nanclares, L., Merino-Serrais, P., Gonzalez, S., and DeFelipe, J. (2013). Synaptic changes in the dentate gyrus of APP/PS1 transgenic mice revealed by electron microscopy. *J Neuropathol Exp Neurol* 72, 386–395.

Alturkmani, H., Zgheib, C., Zouein, F., Alshaaer, N., Kurdi, M., and Booz, G. (2012). Selenate enhances STAT3 transcriptional activity in endothelial cells: differential actions of selenate and selenite on LIF cytokine signaling and cell viability. *J Inorg Biochem* 109, 9–15.

Alushin, G. M., Lander, G. C., Kellogg, E. H., Zhang, R., Baker, D., and Nogales, E. (2014). High-Resolution microtubule structures reveal the structural transitions in beta-tubulin upon GTP hydrolysis. *Cell* 157, 1117–1129.

Alzheimer, A. (1907). Über eine eigenartige Erkrankung der Hirnrinde. *Zeitschrift für Psychiatr. und Psych. Medizine* 64, 146–148.

Amos, L. A., and Lowe, J. (1999). How taxol® stabilises microtubule strucutre. *Chem. Biol.* 6, R65–R69.

Anand, R., Gill, K. D., and Mahdi, A. A. (2014). Therapeutics of Alzheimer's disease: past, present and future. *Neuropharmacology* 76, 27–50.

Andrieux, A., Salin, P., Schweitzer, A., Bégou, M., Pachoud, B., Brun, P., et al. (2006). Microtubule stabilizer ameliorates synaptic function and behavior in a mouse model for schizophrenia. *Biol Psychiatry* 60, 1224–1230.

Angoa-pérez, M., Kane, M. J., Briggs, D. I., Francescutti, D. M., and Kuhn, D. M. (2013). Marble burying and nestlet shredding as tests of repetitive, compulsive-like behaviors in mice. *J. Vis. Exp.* 82, e50978.

Arendt, T., Brückner, M. K., Gertz, H. J., and Marcova, L. (1998). Cortical distribution of neurofibrillary tangles in Alzheimer's disease matches the pattern of neurons that retain their capacity of plastic remodelling in the adult brain. *Neuroscience* 83, 991–1002.

Argyriou, A. A., Marmiroli, P., Cavaletti, G., and Kalofonos, H. P. (2011). Epothilone-induced peripheral neuropathy : a review of current knowledge. *J. Pain Symptom Manage.* 42, 931–940.

Arias, C., Arrieta, I., Massieu, L., and Tapia, R. (1997). Neuronal damage and MAP2 changes induced by the glutamate transport inhibitor dihydrokainate and by kainate in rat hippocampus in vivo. *Exp. Brain Res.* 116, 467–476.

Arimura, N., Hattori, A., Kimura, T., Nakamuta, S., Funahashi, Y., Hirotsune, S., et al. (2009). CRMP-2 directly binds to cytoplasmic dynein and interferes with its activity. *J. Neurochem.* 111, 380–390.

Arimura, N., Kawano, Y., Yoshimura, T., Kawabata, S., Hattori, A., Fukata, Y., et al. (2005). Phosphorylation by Rho kinase regulates CRMP-2 activity in growth cones. *Mol. Cell. Biol.* 25, 9973–9984.

Asthana, J., Kapoor, S., Mohan, R., and Panda, D. (2013). Inhibition of HDAC6 deacetylase activity increases its binding with microtubules and suppresses microtubule dynamic instability in MCF-7 cells. *J. Biol. Chem.* 288, 22516–22526.

Avila, A., and Burnett, B. (2007). Trichostatin A increases SMN expression and survival in a mouse model of spinal muscular atrophy. *J. Clin. …* 117, 659–671.

Baas, P., Rao, A., Matamoros, A., and Leo, L. (2016). Stability properties of neuronal microtubules. *Cytoskeleton (Hoboken).*, 1–19.

Bahi, A., and Dreyer, J. (2012). Hippocampus-specific deletion of tissue plasminogen activator "tPA" in adult mice impairs depression- and anxiety-like behaviors. *Eur. Neuropsychopharmacol.* 22, 672–682.

Bailey, M., Sackett, D., and Ross, J. (2015). Katanin severing and binding microtubules are inhibited by tubulin carboxy tails. *Biophys. J.* 109, 2546–2561.

Bakota, L., and Brandt, R. (2016). Tau biology and tau-directed therapies for Alzheimer's disease. *Drugs* 76, 301–313.

Ballatore, C., Brunden, K. R., Huryn, D. M., Trojanowski, J. Q., Lee, V. M. Y., and Smith, A. B. (2012). Microtubule stabilizing agents as potential treatment for Alzheimer's disease and related neurodegenerative tauopathies. *J. Med. Chem.* 55, 8979–8996.

Ballatore, C., Brunden, K. R., Piscitelli, F., James, M. J., Crowe, A., Yao, Y., et al. (2010). Discovery of brain-penetrant, orally bioavailable aminothienopyridazine inhibitors of tau aggregation. *J. Med. Chem.* 53, 3739–3747.

Barage, S. H., and Sonawane, K. D. (2015). Amyloid cascade hypothesis: pathogenesis and therapeutic strategies in Alzheimer's disease. *Neuropeptides* 52, 1–18.

Baron, R., Babcock, A. A., Nemirovsky, A., Finsen, B., and Monsonego, A. (2014). Accelerated microglial pathology is associated with Aβ plaques in mouse models of Alzheimer's disease. *Aging Cell* 13, 584–595.

Bassan, M., Zamostiano, R., Davidson, A., Pinhasov, A., Giladi, E., Perl, O., et al. (1999). Complete sequence of a novel protein containing a femtomolar-activity- dependent neuroprotective peptide. *J. Neurochem.* 72, 1283–1293.

Bateman, R. J., Munsell, L. Y., Morris, J. C., Swarm, R., Yarasheski, K. E., and Holtzman, D. M. (2006). Quantifying CNS protein production and clearance rates in humans using in vivo stable isotope labeling, immunoprecipitation, and tandem mass spectrometry. *Nat. Med.* 12, 856–861.

Bedard, P. L., di Leo, A., and Piccart-Gebhart, M. J. (2010). Taxanes: optimizing adjuvant chemotherapy for early-stage breast cancer. *Nat. Rev. Clin. Oncol.* 7, 22–36.

Beer, T. M., Higano, C. S., Saleh, M., Dreicer, R., Hudes, G., Picus, J., et al. (2007). Phase II

study of KOS-862 in patients with metastatic androgen independent prostate cancer previously treated with docetaxel. *Invest. New Drugs* 25, 565–570.

Benes, F. M., Todtenkopf, M. S., and Kostoulakos, P. (2001). GluR5,6,7 subunit immunoreactivity on apical pyramidal cell dendrites in hippocampus of schizophrenics and manic depressives. *Hippocampus* 11, 482-491.

Benice, T. S., Rizk, A., Kohama, S., Pfankuch, T., and Raber, J. (2006). Sex-differences in age-related cognitive decline in C57BL/6J mice associated with increased brain microtubule-associated protein 2 and synaptophysin immunoreactivity. *Neuroscience* 137, 413–423.

Benoy, V., Van Helleputte, L., Prior, R., D'Ydewalle, C., Haeck, W., Geens, N., et al. (2018). HDAC6 is a therapeutic target in mutant GARS-induced Charcot-Marie-Tooth disease. *Brain* 141, 673–687.

Beyreuther, K., and Masters, C. L. (1991). Amyloid precursor protein (APP) and beta A4 amyloid in the etiology of Alzheimer's disease: precursor-product relationships in the derangement of neuronal function. *Brain Pathol.* 1, 241–251.

Bi, M., Gladbach, A., Van Eersel, J., Ittner, A., Przybyla, M., Van Hummel, A., et al. (2017). Tau exacerbates excitotoxic brain damage in an animal model of stroke. *Nat. Commun.* 8, 1–14.

Bi, M., Ittner, A., Ke, Y. D., Götz, J., and Ittner, L. M. (2011). Tau-targeted immunization impedes progression of neurofibrillary histopathology in aged P301L tau transgenic mice. *PLoS One* 6, e26860.

Blazquez-Llorca, L., Valero-Freitag, S., Rodrigues, E. F., Merchán-Pérez, Á., Rodríguez, J. R., Dorostkar, M. M., et al. (2017). High plasticity of axonal pathology in Alzheimer's disease mouse models. *Acta Neuropathol. Commun.* 5, 14.

Bodaleo, F. J., Montenegro-Venegas, C., Henríquez, D. R., Court, F. A., and Gonzalez-

Billault, C. (2016). Microtubule-associated protein 1B (MAP1B)-deficient neurons show structural presynaptic deficiencies in vitro and altered presynaptic physiology. *Sci. Rep.* 6, 1–14.

Bollag, D. M., McQueney, P. A., Zhu, J., Hensens, O., Koupal, L., Liesch, J., et al. (1995). Epothilones, a new class of microtubule-stabilizing agents with a taxol-like mechanism of action. *Cancer Res.* 55, 2325–2333.

Bolmont, T., Haiss, F., Eicke, D., Radde, R., Mathis, C. A., Klunk, W. E., et al. (2008). Dynamics of the microglial/amyloid interaction indicate a role in plaque maintenance. *J. Neurosci.* 28, 4283–4292.

Bolós, M., Pallas-Bazarra, Terreros-Roncal, J., Perea, J., Jurado-Arjona, J., Ávila, J., et al. (2017). Soluble Tau has devastating effects on the structural plasticity of hippocampal granule neurons. *Transl. Psychiatry* 7, 1267.

Bömmel, H., Xie, G., Rossoll, W., Wiese, S., Jablonka, S., Boehm, T., et al. (2002). Missense mutation in the tubulin-specific chaperone E (Tbce) gene in the mouse mutant progressive motor neuronopathy, a model of human motoneuron disease. *J. Cell Biol.* 159, 563–569.

Bonnet, C., Boucher, D., Lazereg, S., Pedrotti, B., Islam, K., Denoulet, P., et al. (2001). Differential binding regulation of microtubule-associated proteins MAP1A, MAP1B, and MAP2 by tubulin polyglutamylation. *J. Biol. Chem.* 276, 12839–12848.

Bouquet, C., Soares, S., von Boxberg, Y., Ravaille-Veron, M., Propst, F., and Nothias, F. (2004). Microtubule-associated protein 1B controls directionality of growth cone migration and axonal branching in regeneration of adult dorsal root ganglia neurons. *J. Neurosci.* 24, 7204–7213.

Bowne-Anderson, H., Zanic, M., Kauer, M., and Howard, J. (2013). Microtubule dynamic instability: A new model with coupled GTP hydrolysis and multistep catastrophe.

BioEssays 35, 452–461.

Braak, H., Alafuzoff, I., Arzberger, T., Kretzschmar, H., and Tredici, K. (2006). Staging of Alzheimer disease-associated neurofibrillary pathology using paraffin sections and immunocytochemistry. *Acta Neuropathol.* 112, 389–404.

Brindisi, M., Cavella, C., Brogi, S., Nebbioso, A., Senger, J., Maramai, S., et al. (2016). Phenylpyrrole-based HDAC inhibitors: synthesis, molecular modeling and biological studies. *Futur. Med. Chem.* 8, 1573–1587.

Brindisi, M., Senger, J., Cavella, C., Grillo, A., Chemi, G., Gemma, S., et al. (2018). Novel spiroindoline HDAC inhibitors: synthesis, molecular modelling and biological studies. *Eur. J. Med. Chem.* 157, 127–138.

Brizuela, M., Blizzard, C. A., Chuckowree, J. A., Dawkins, E., Gasperini, R. J., Young, K. M., et al. (2014). The microtubule-stabilizing drug Epothilone D increases axonal sprouting following transection injury in vitro. *Mol. Cell. Neurosci.* 66, 129–140.

Broekkamp, C. L., Rijk, H. W., Joly-Gelouin, D., and Lloyd, K. L. (1986). Major tranquillizers can be distinguished from minor tranquillizers on the basis of effects on marble burying and swim-induced grooming in mice. *Eur. J. Pharmacol.* 126, 223–229.

Brouhard, G., and Rice, L. (2014). The contribution of αβ-tubulin curvature to microtubule dynamics. *J. Cell Biol.* 207, 323–334.

Brownlow, M. L., Benner, L., Agostino, D. D., Gordon, M. N., and Morgan, D. (2013). Ketogenic diet improves motor performance but not cognition in two mouse models of Alzheimer ' s pathology. *PLoS One* 8, 2–11.

Brugg, B., and Matus, A. (1991). Phosphorylation determines the binding of microtubule-associated protein 2 (MAP2) to microtubules in living cells. *J. Cell Biol.* 114, 735–743.

Brunden, K. R., Ballatore, C., Lee, V. M. Y., Smith, A. B., and Trojanowski, J. Q. (2012). Brain-penetrant microtubule-stabilizing compounds as potential therapeutic agents for

tauopathies. *Biochem. Soc. Trans.* 40, 661–666.

Brunden, K. R., Lee, V. M. Y., Smith, A. B., Trojanowski, J. Q., and Ballatore, C. (2017). Altered microtubule dynamics in neurodegenerative disease: therapeutic potential of microtubule-stabilizing drugs. *Neurobiol. Dis.* 105, 328–335.

Brunden, K. R., Yao, Y. M., Potuzak, J. S., Ferrer, N. I., Ballatore, C., James, M. J., et al. (2011). The characterization of microtubule-stabilizing drugs as possible therapeutic agents for Alzheimer's disease and related tauopathies. *Pharmacol. Res.* 63, 341–351.

Brunden, K. R., Zhang, B., Carroll, J., Yao, Y., Potuzak, J. S., Hogan, A. M., et al. (2010). Epothilone D improves microtubule density, axonal integrity, and cognition in a transgenic mouse model of tauopathy. *J. Neurosci.* 30, 13861–13866.

Brunden, K., Trojanowski, J., Smith 3rd, A. B., Lee, V. M. Y., and Ballatore, C. (2014). Microtubule-stabilizing agents as potential therapeutics for neurodegenerative disease. *Bioorg. Med. Chem.* 22, 1492–1501.

Brunholz, S., Sisodia, S., Lorenzo, A., Deyts, C., Kins, S., and Morfini, G. (2012). Axonal transport of APP and the spatial regulation of APP cleavage and function in neuronal cells. *Exp. Brain Res.* 217, 353–364.

Brustovetsky, T., Pellman, J. J., Yang, X. F., Khanna, R., and Brustovetsky, N. (2014). Collapsin response mediator protein 2 (CRMP2) interacts with N-methyl-D-aspartate (NMDA) receptor and Na+/Ca2+ exchanger and regulates their functional activity. *J. Biol. Chem.* 289, 7470–7482.

Burbank, K., and Mitchison, T. J. (2006). Microtubule dynamic instability. *Curr. Biol.* 16, R516.

Burgoyne, R. D., and Cumming, R. (1984). Ontogeny of microtubule-associated protein 2 in rat cerebellum: differential expression of the doublet polypeptides. *Neuroscience* 11, 156–167.

Busciglio, J., Lorenzo, A., Yeh, J., and Yankner, B. A. (1995). Beta-amyloid fibrils induce tau phosphorylation and loss of microtubule binding. *Neuron* 14, 879–888.

Cagnin, A., Brooks, D. J., Kennedy, A. M., Gunn, R. N., Myers, R., Turkheimer, F. E., et al. (2001). In-vivo measurement of activated microglia in dementia. *Lancet* 358, 461–467.

Carriedo, S. G., Yin, H. Z., and Weiss, J. H. (1996). Motor neurons are selectively vulnerable to AMPA/kainate receptor-mediated injury in vitro. *J. Neurosci.* 16, 4069–4079.

Cartelli, D., Casagrande, F., Busceti, C. L., Bucci, D., Molinaro, G., Traficante, A., et al. (2013). Microtubule alterations occur early in experimental parkinsonism and the microtubule stabilizer epothilone D is neuroprotective. *Sci. Rep.* 3, 1–10.

Cash, A. D., Aliev, G., Siedlak, S. L., Nunomura, A., Fujioka, H., Zhu, X., et al. (2003). Microtubule reduction in Alzheimer's disease and aging is independent of τ filament formation. *Am J Pathol* 162, 1623–1627.

Castellani, R., Nunomura, A., Lee, H., Perry, G., and Smith, M. (2008). Phosphorylated tau: toxic, protective, or none of the above. *J Alzheimers Dis* 14, 377–383.

Castro, A., and Martinez, A. (2000). Inhibition of tau phosphorylation: a new therapeutic strategy for the treatment of Alzheimer's disease and other neurodegenerative disorders. *Expert Opin. Ther. Pat.* 10, 1519–1527.

Ceccacci, E., and Minucci, S. (2016). Inhibition of histone deacetylases in cancer therapy: lessons from leukaemia. *Br. J. Cancer* 114, 605–611.

Chang, P. K., Verbich, D., and McKinney, R.A. (2012). AMPA receptors as drug targets in neurological disease--advantages, caveats, and future outlook. *Eur. J. Neurosci.* 35(12), 1908-1916.

Cheng, K. L., Bradley, T., and Budman, D. R. (2008). Novel microtubule-targeting agents - the epothilones. *Biologics* 2, 789–811.

Chiang, K., and Koo, E. H. (2014). Emerging therapeutics for Alzheimer's disease. *Annu.*

Rev. Pharmacol. Toxicol. 54, 381–405.

Choi, Y. (2005). Induction of apoptosis by trichostatin A, a histone deacetylase inhibitor, is associated with inhibition of cyclooxygenase-2 activity in human non-small cell lung cancer cells. *Int J Oncol* 27, 473–479.

Clark, J. A., Blizzard, C. A., Breslin, M. C., Yeaman, E. J., Lee, K. M., Chuckowree, J. A., et al. (2018). Epothilone D accelerates disease progression in the SOD1G93A mouse model of amyotrophic lateral sclerosis. *Neuropathol. Appl. Neurobiol.* 44, 590–605.

Clark, K., Sword, B., and Dupree, J. (2017). Oxidative stress induces disruption of the axon initial segment. *ASN Neuro* 9, 1759091417745426.

Cole, A. R., Noble, W., Aalten, L. Van, Plattner, F., Meimaridou, R., Hogan, D., et al. (2007). Collapsin response mediator protein-2 hyperphosphorylation is an early event in Alzheimer's disease progression. *J. Neurochem.* 103, 1132–1144.

Cole, A., Soutar, M., Rembutsu, M., van Aalten, L., Hastie, C., Mclaichlan, H., et al. (2008). Relative resistance of Cdk5-phosphorylated CRMP2 to dephosphorylation. *J Biol Chem* 283, 18227–18237.

Coleman, M. (2005). Axon degeneration mechanisms: commonality amid diversity. *Nat. Rev. Neurosci.* 6, 889–898.

Coleman, M. P., and Freeman, M. R. (2010). Wallerian degeneration, WldS, and Nmnat. *Annu. Rev. Neurosci.* 33, 245–267.

Conforti, L., Gilley, J., and Coleman, M. P. (2014). Wallerian degeneration: an emerging axon death pathway linking injury and disease. *Nat. Rev. Neurosci.* 15, 394–409.

Cook, C., Stankowski, J. N., Carlomagno, Y., Stetler, C., and Petrucelli, L. (2014). Acetylation: a new key to unlock tau's role in neurodegeneration. *Alzheimers. Res. Ther.* 6, 29.

Coombes, C., Yamamoto, A., McClellan, M., Reid, T., Plooster, M., Luxton, G., et al. (2016).

Mechanism of microtubule lumen entry for the α-tubulin acetyltransferase enzyme αTAT1. *PNAS* 113, E7176–E7184.

Corcoran, N. M., Martin, D., Hutter-Paier, B., Windisch, M., Nguyen, T., Nheu, L., et al. (2010). Sodium selenate specifically activates PP2A phosphatase, dephosphorylates tau and reverses memory deficits in an Alzheimer's disease model. *J. Clin. Neurosci.* 17, 1025–1033.

Cosenza, M., and Pozzi, S. (2018). The therapeutic strategy of HDAC6 inhibitors in lymphoproliferative disease. *Int. J. Mol. Sci.* 19, pii: E2337.

Cossart, R., Tyzio, R., Dinocourt, C., Esclapez, M., Hirsch, J. C., Ben Ari, Y., et al. (2001). Presynaptic kainate receptors that enhance the release of GABA on CA1 hippocampal interneurons. *Neuron* 29, 497–508.

Cox, K., Combs, B., Abdelmesih, B., Morfini, G., Brady, S. T., and Kanaan, N. M. (2016). Analysis of isoform-specific tau aggregates suggests a common toxic mechanism involving similar pathological conformations and axonal transport inhibition. *Neurobiol. Aging* 47, 113–126.

Crews, L., and Masliah, E. (2010). Molecular mechanisms of neurodegeneration in Alzheimer's disease. *Hum. Mol. Genet. Gen* 19, R12–R20.

Crosson, C. E., Mani, S. K., Husain, S., Alsarraf, O., and Menick, D. R. (2010). Inhibition of histone deacetylase protects the retina from ischemic injury. *Invest. Ophthalmol. Vis. Sci.* 51(7), 3639-3645.

Cusack, C. L., Swahari, V., Hampton Henley, W., Michael Ramsey, J., and Deshmukh, M. (2013). Distinct pathways mediate axon degeneration during apoptosis and axon-specific pruning. *Nat. Commun.* 4, 1876.

D'Souza, I., and Schellenberg, G. D. (2000). Determinants of 4-repeat tau expression. coordination between enhancing and inhibitory splicing sequences for exon 10

inclusion. *J. Biol. Chem.* 275, 17700–17709.

Da Silva, S. V., Haberl, M. G., Zhang, P., Bethge, P., Lemos, C., Gonçalves, N., et al. (2016). Early synaptic deficits in the APP/PS1 mouse model of Alzheimer's disease involve neuronal adenosine A2Areceptors. *Nat. Commun.* 7, 1–11.

Dale, J. M., and Garcia, M. L. (2012). Neurofilament phosphorylation during development and disease: which came first, the phosphorylation or the accumulation? *J. Amino Acids* 2012, Article ID 382107.

Dammermann, A., Desai, A., and Oegema, K. (2003). The minus end in sight. *Curr. Biol.* 13, R614–R624.

Dawson, H., Cantillana, V., Jansen, M., Wang, H., Vitek, M., Wilcock, D., et al. (2010). Loss of tau elicits axonal degeneration in a mouse model of Alzheimer's disease. *Neuroscience* 169, 516–531.

De Boer, S. F., and Koolhaas, J. M. (2003). Defensive burying in rodents: ethology, neurobiology and psychopharmacology. *Eur. J. Pharmacol.* 463, 145–161.

Deacon, R. M. J. (2006). Digging and marble burying in mice: simple methods for in vivo identification of biological impacts. *Nat. Protoc.* 1, 122–124.

Dehmelt, L., and Halpain, S. (2005). The MAP2/Tau family of microtubule-associated proteins. *Genome Biol.* 6, 204.

DeVos, S., and Hyman, B. (2017). Tau at the crossroads between neurotoxicity and neuroprotection. *Neuron* 94, 703–704.

Dickson, D. W. (1999). Microglia in Alzheimer's disease and transgenic models. How close the fit? *Am. J. Pathol.* 154, 1627–1631.

Dickson, T. C., King, C. E., McCormack, G. H., and Vickers, J. C. (1999). Neurochemical diversity of dystrophic neurites in the early and late stages of Alzheimer's disease. *Exp. Neurol.* 156, 100–110.

Doll, T., Meichsner, M., Riederer, B. M., Honegger, P., and Matus, A. (1993). An isoform of microtubule-associated protein 2 (MAP2) containing four repeats of the tubulin-binding motif. *J Cell Sci.* 106, 633–639.

Dompierre, J. P., Godin, J. D., Charrin, B. C., Cordelières, F. P., King, S. J., Humbert, S., et al. (2007). Histone deacetylase 6 inhibition compensates for the transport deficit in Huntington's disease by increasing tubulin acetylation. *J. Neurosci.* 27, 3571–3583.

Dong, X. X., Wang, Y., and Qin, Z. H. (2009). Molecular mechanisms of excitotoxicity and their relevance to pathogenesis of neurodegenerative diseases. *Acta Pharmacol. Sin.* 30, 379–387.

Doody, R. S., Thomas, R. G., Farlow, M., Iwatsubo, T., Vellas, B., Joffe, S., et al. (2014). Phase 3 trials of solanezumab for mild-to-moderate Alzheimer's disease. *N. Engl. J. Med.* 370, 311–321.

Drewes, G., Trinczek, B., Illenberger, S., Biernat, J., Schmitt-Ulms, G., Meyer, H. E., et al. (1995). Microtubule-associated protein/microtubule affinity-regulating kinase (p110mark): a novel protein kinase that regulates tau-microtubule interactions and dynamic instability by phosphorylation at the Alzheimer-specific site serine 262. *J. Biol. Chem.* 270, 7679–7688.

Dubal, D. (2018). The way of tau: secretion and synaptic dysfunction. *Trends Mol. Med.* 24, 595–597.

Dubey, J., Ratnakaran, N., and Koushika, S. P. (2015). Neurodegeneration and microtubule dynamics: death by a thousand cuts. *Front. Cell. Neurosci.* 9, 1–15.

Dubey, M., Chaudhury, P., Kabiru, H., and Shea, T. B. (2008). Tau inhibits anterograde axonal transport and perturbs stability in growing axonal neurites in part by displacing kinesin cargo: neurofilaments attenuate tau-mediated neurite instability. *Cell Motil. Cytoskeleton* 65, 89–99.

Dye, R., Fink, S., and Williams, R. (1993). Taxol-induced flexibility of microtubules and its reversal by MAP-2 and tau. *J Biol Chem* 268, 6847–6850.

Eira, J., Silva, C. S., Sousa, M. M., and Liz, M. A. (2016). The cytoskeleton as a novel therapeutic target for old neurodegenerative disorders. *Prog. Neurobiol.* 141, 61–82.

El Khoury, J., Hickman, S. E., Thomas, C. A., Cao, L., Silverstein, S. C., and Loike, J. D. (1996). Scavenger receptor-mediated adhesion of microglia to beta-amyloid fibrils. *Nature* 382, 716–719.

Encalada, S. E., Szpankowski, L., Xia, C.-H., and Goldstein, L. S. B. (2011). Stable kinesin and dynein assemblies drive the axonal transport of mammalian prion protein vesicles. *Cell* 144, 551–565.

Eng, C., Kindler, H. L., Nattam, S., Ansari, R. H., Kasza, K., Wade-Oliver, K., et al. (2004). A phase II trial of the epothilone B analog, BMS-247550, in patients with previously treated advanced colorectal cancer. *Ann. Oncol.* 15, 928–932.

Engmann, O., and Giese, K. P. (2009). Crosstalk between Cdk5 and GSK3beta: Implications for Alzheimer's Disease. *Front. Mol. Neurosci.* 2, 2.

Erez, H., Shemesh, O. A., and Spira, M. E. (2014). Rescue of tau-induced synaptic transmission pathology by paclitaxel. *Front Cell Neurosci* 8, 34.

Errico, A., Ballabio, A., and Rugarli, E. . (2002). Spastin, the protein mutated in autosomal dominant hereditary spastic paraplegia, is involved in microtubule dynamics. *Hum Mol Genet* 11, 153–163.

Erturk, A., Wang, Y., and Sheng, M. (2014). Local pruning of dendrites and spines by caspase-3-dependent and proteasome-limited mechanisms. *J. Neurosci.* 34, 1672–1688.

Evans, M., Dumitrescu, A., Kruijssen, D., Taylor, S., and Grubb, M. (2015). Rapid modulation of axon initial segment length influences repetitive spike firing. *Cell Rep.* 13, 1233–1245.

Fakata, Y., Itoh, T. J., Kimura, T., Ménager, C., Nishimura, T., Shiromizu, T., et al. (2002). CRMP-2 binds to tubulin heterodimers to promote microtubule assembly. *Nat. Cell Biol.* 4, 583–591.

Falcón-Moya, R., Sihra, T. S., and Rodríguez-Moreno, A. (2018). Kainate receptors: role in epilepsy. *Front. Mol. Neurosci.* 11, 217.

Fan, M., and Raymond, L. (2007). N-methyl-D-aspartate (NMDA) receptor function and excitotoxicity in Huntington's disease. *Prog. Neurobiol.* 81, 272–293.

Fanale, D., Bronte, G., Passiglia, F., Calò, V., Castiglia, M., Di Piazza, F., et al. (2015). Stabilizing versus destabilizing the microtubules: a double-edge sword for an effective cancer treatment option? *Anal. Cell. Pathol.* 2015, 690916.

Fawcett, D. W., and Porter, K. . (1954). A study of the fine structure of ciliated epithelia. *J. Morphol.* 94, 221–281.

Ferguson, S. A., Sarkar, S., and Schmued, L. C. (2013). Longitudinal behavioral changes in the APP/PS1 transgenic Alzheimer's Disease model. *Behav. Brain Res.* 242, 125–134.

Ferhat, L., Represa, A., Ferhat, W., Ben-Ari, Y., and Khrestchatisky, M. (2009). MAP2d mRNA is expressed in identified neuronal populations in the developing and adult rat brain and its subcellular distribution differs from that of MAP2b in hippocampal neurones. *Eur. J. Neurosci.* 10, 161–171.

Fernandez-Martos, C. M., King, A. E., Atkinson, R. a. K., Woodhouse, A., and Vickers, J. C. (2015). Neurofilament light gene deletion exacerbates amyloid, dystrophic neurite, and synaptic pathology in the APP/PS1 transgenic model of Alzheimer's disease. *Neurobiol. Aging* 36, 2757–2767.

Fernandez, M. A., Klutkowski, J. A., Freret, T., and Wolfe, M. S. (2014). Alzheimer presenilin-1 mutations dramatically reduce trimming of long amyloid β-peptides (Aβ) by γ-secretase to increase 42-to-40-residue Aβ. *J. Biol. Chem.* 289, 31043–31052.

Fiala, M., Restrepo, L., and Pellegrini, M. (2018). Immunotherapy of mild cognitive impairment by ω-3 supplementation: why are amyloid-β antibodies and ω-3 not working in clinical trials? *J. Alzheimer's Dis.* 62, 1013–1022.

Fifre, A., Sponne, I., Koziel, V., Kriem, B., Yen Potin, F. T., Bihain, B. E., et al. (2006). Microtubule-associated protein MAP1A, MAP1B, and MAP2 proteolysis during soluble amyloid beta-peptide-induced neuronal apoptosis: synergistic involvement of calpain and caspase-3. *J. Biol. Chem.* 281, 229–240.

Folch, J., Petrov, D., Ettcheto, M., Abad, S., Sanchez-Lopez, E., Garcia, M. L., et al. (2016). Current research therapeutic strategies for Alzheimer's disease treatment. *Neural Plast.* 2016, 8501693.

Fourest-Lieuvin, A., Peris, L., Gache, V., Garcia-Saez, I., Juillan-Binard, C., Lantez, V., et al. (2006). Microtubule regulation in mitosis: tubulin phosphorylation by the cyclin-dependent kinase Cdk1. *Mol. Biol. Cell* 17, 1041–1050.

Fournet, V., de Lavilleon, G., Schweitzer, A., Giros, B., Andrieux, A., and Martres, M. P. (2012). Both chronic treatments by epothilone D and fluoxetine increase the short-term memory and differentially alter the mood status of STOP/MAP6 KO mice. *J Neurochem* 123, 982–996.

Francis, P. T. (2005). The interplay of neurotransmitters in Alzheimer's disease. *CNS Spectr.* 10, 6–9.

Freeman, M. R. (2014). Signaling mechanisms regulating Wallerian degeneration. *Curr. Opin. Neurobiol.* 27, 224–231.

Fujiwara, T., Morimoto, K., Kakita, A., and Takahashi, H. (2012). Dynein and dynactin components modulate neurodegeneration induced by excitotoxicity. *J. Neurochem.* 122, 162–174.

Fukata, Y., Itoh, T., Kimura, T., Ménager, C., Nishimura, T., Shiromizu, T., et al. (2002).

CRMP-2 binds to tubulin heterodimers to promote microtubule assembly. *Nat Cell Biol* 4, 583–591.

Fukuda, Y., Li, Y., and Segal, R. (2017). A mechanistic understanding of axon degeneration in chemotherapy-induced peripheral neuropathy. *Front. Neurosci.* 11, 481.

Fumoleau, P., Coudert, B., Isambert, N., and Ferrant, E. (2007). Novel tubulin-targeting agents: anticancer activity and pharmacologic profile of epothilones and related analogues. *Ann. Oncol.* 18 Suppl 5, v9-15.

Galea, E., Morrison, W., Hudry, E., Arbel-Ornath, M., Bacskai, B. J., Gómez-Isla, T., et al. (2015). Topological analyses in APP/PS1 mice reveal that astrocytes do not migrate to amyloid-β plaques. *PNAS* 51, 15556–15561.

Garcia, E. P., Mehta, S., Blair, L. A., Wells, D. G., Shang, J., Fukushima, T., Fallon, J. R., Garner, C. C., and Marshall, J. (1998). SAP90 binds and clusters kainate receptors causing incomplete desensitization. *Neuron* 21, 727-739.

Geden, M. J., and Deshmukh, M. (2016). Axon degeneration: context defines distinct pathways. *Curr. Opin. Neurobiol.* 39, 108–115.

Gengler, S., Hamilton, A., and Holscher, C. (2010). Synaptic plasticity in the hippocampus of a APP/PS1 mouse model of Alzheimer's disease is impaired in old but not young mice. *PLoS One* 5, e9764.

Gerdts, J., Brace, E. J., Sasaki, Y., DiAntonio, A., and Milbrandt, J. (2015). SARM1 activation triggers axon degeneration locally via NAD(+) destruction. *Science (80-.).* 348, 453–457.

Ghosh, A. K., and Osswald, H. L. (2014). BACE1 (β-secretase) inhbitors for the treatment of Alzheimer's disease. *Chem. Soc. Rev.* 43, 6765–6813.

Gibson, S., and Bromberg, M. (2012). Amyotrophic lateral sclerosis: drug therapy from the bench to the bedside. *Semin Neurol* 32, 173–178.

Glenner, G. G., and Wong, C. W. (1984). Alzheimer's disease: initial report of the purification and characterization of a novel cerebrovascular amyloid protein. *Biochem. Biophys. Res. Commun.* 120, 885–890.

Godena, V. K., Brookes-Hocking, N., Moller, A., Shaw, G., Oswald, M., Sancho, R. M., et al. (2014). Increasing microtubule acetylation rescues axonal transport and locomotor deficits caused by LRRK2 Roc-COR domain mutations. *Nat. Commun.* 5, 5245.

Goedert, M., and Jakes, R. (2005). Mutations causing neurodegenerative tauopathies. *Biochim. Biophys. Acta - Mol. Basis Dis.* 1739, 240–250.

Goedert, M., and Spillantini, M. G. (2001). Tau gene mutations and neurodegeneration. *Biochem Soc Symp* 67, 59–71.

Goedert, M., Spillantini, M. G., Jakes, R., Rutherford, D., and Crowther, R. A. (1989). Multiple isoforms of human microtubule-associated protein tau: sequences and localization in neurofibrillary tangles of Alzheimer's disease. *Neuron* 3, 519–526.

Gong, C. X., and Iqbal, K. (2008). Hyperphosphorylation of microtubule-associated protein tau: a promising therapeutic target for Alzheimer disease. *Curr. Med. Chem.* 15, 2321–2328.

Gotz, J., Chen, F., Barmettler, R., and Nitsch, R. M. (2001). Tau filament formation in transgenic mice expressing P301L tau. *J. Biol. Chem.* 276, 529–534.

Gotz, J., Ittner, L. M., and Kins, S. (2006). Do axonal defects in tau and amyloid precursor protein transgenic animals model axonopathy in Alzheimer's disease? *J. Neurochem.* 98, 993–1006.

Govindarajan, N., Rao, P., Burkhardt, S., Sananbenesi, F., Schlüter, O. M., Bradke, F., et al. (2013). Reducing HDAC6 ameliorates cognitive deficits in a mouse model for Alzheimer's disease. *EMBO Mol. Med.* 5, 52–63.

Griffin, W. S., Stanley, L. C., Ling, C., White, L., MacLeod, V., Perrot, L. J., et al. (1989).

Brain interleukin 1 and S-100 immunoreactivity are elevated in Down syndrome and Alzheimer disease. *Proc. Natl. Acad. Sci.* 86, 7611–7615.

Grosheva, M., Guntinas-Lichius, O., Angelova, S. K., Kuerten, S., Alvanou, A., Streppel, M., et al. (2008). Local stabilization of microtubule assembly improves recovery of facial nerve function after repair. *Exp. Neurol.* 209, 131–144.

Gu, Y., and Ihara, Y. (2000). Evidence that collapsin response mediator protein-2 is involved in the dynamics of microtubules. *J Biol Chem* 275, 17917–17920.

Gunawardena, S., Yang, G., and Goldstein, L. S. B. (2013). Presenilin controls kinesin-1 and dynein function during APP-vesicle transport in vivo. *Hum. Mol. Genet.* 22, 3828–3843.

Gundersen, G. G., Khawaja, S., and Bulinski, J. C. (1987). Postpolymerization detyrosination of alpha-tubulin: a mechanism for subcellular differentiation of microtubules. *J. Cell Biol.* 105, 251–264.

Guo, T., Noble, W., and Hanger, D. P. (2017). Roles of tau protein in health and disease. *Acta Neuropathol.* 133, 665–704.

Habes, M., Janowitz, D., Erus, G., Toledo, J. B., Resnick, S. M., Doshi, J., et al. (2016). Advanced brain aging: relationship with epidemiologic and genetic risk factors, and overlap with Alzheimer disease atrophy patterns. *Transl. Psychiatry* 6, e775.

Halpain, S., and Dehmelt, L. (2006). The MAP1 family of microtubule-associated proteins. *Genome Biol.* 7, 224.

Hamel, E., del Campo, A. A., Lowe, M. C., and Lin, C. M. (1981). Interactions of taxol, microtubule-associated proteins, and guanine nucleotides in tubulin polymerization. *J. Biol. Chem.* 256, 11887–11894.

Han, S., Kim, J., Kim, J., and Park, K. (2016). Inhibition of microtubule dynamics impedes repair of kidney ischemia/reperfusion injury and increases fibrosis. *Sci. Rep.* 6, 27775.

Hardy, J. A., and Higgins, G. A. (1992). Alzheimer's disease: the amyloid cascade

hypothesis. *Science (80-.).* 256, 184–185.

Hasan, M. R., Kim, J. H., Kim, Y. J., Kwon, K. J., Shin, C. Y., Kim, H. Y., et al. (2013). Effect of HDAC inhibitors on neuroprotection and neurite outgrowth in primary rat cortical neurons following ischemic insult. *Neurochem. Res.* 38, 1921–1934.

Hellal, F., Hurtado, A., Ruschel, J., Flynn, K. C., Laskowski, C. J., Umlauf, M., et al. (2011). Microtubule stabilization reduces scarring and causes axon regeneration after spinal cord injury. *Science (80-.).* 331, 928–931.

Heneka, M. T., O'Banion, M. K., Terwel, D., and Kummer, M. P. (2010). Neuroinflammatory processes in Alzheimer's disease. *J. Neural Transm.* 117, 919–947.

Heneka, M. T., Sastre, M., Dumitrescu-Ozimek, L., Dewachter, I., Walter, J., Klockgether, T., et al. (2005). Focal glial activation coincides with increased BACE1 activation and precedes amyloid plaque deposition in APP[V717I] transgenic mice. *J. Neuroinflammation* 2, 22.

Hensley, K., and Kursula, P. (2016). Collapsin response mediator protein-2 (CRMP2) is a plausible etiological factor and potential therapeutic target in Alzheimer's disease: comparison and contrast with microtubule-associated protein tau. *J. Alzheimer's Dis.* 53, 1–14.

Hickman, S. E., Allison, E. K., and El Khoury, J. (2008). Microglial dysfunction and defective beta-amyloid clearance pathways in aging Alzheimer's disease mice. *J. Neurosci.* 28, 8354–8360.

Hirata-Fukae, C., Li, H., Ma, L., Hoe, H., Rebeck, G., Aisen, P., et al. (2009). Levels of soluble and insoluble tau reflect overall status of tau phosphorylation in vivo. *Neurosci. Lett.* 450, 51–55.

Holen, K., Syed, S., Hannah, A. L., Binger, K., Wood, L., Zhou, Y., et al. (2004). Phase I study using continuous intravenous (CI) KOS-862 (epothilone D) in patients with solid

tumors. *J. Clin. Oncol.* 22, 2024a.

Holland, R., McIntosh, A. L., Finucane, O. M., Mela, V., Rubio-Araiz, A., Timmons, G., et al. (2018). Inflammatory microglia are glycolytic and iron retentive and typify the microglia in APP/PS1 mice. *Brain. Behav. Immun.* 68, 183–196.

Homma, C., and Yamada, K. (2009). Physical properties of bedding materials determine the marble burying behavior of mice (C57BL/6J). *Open Behav. Sci. J.* 3, 34–39.

Hong, S., Beja-glasser, V. F., Nfonoyim, B. M., Frouin, A., Ramakrishnan, S., Merry, K. M., et al. (2016). Complement and microglia mediate early synapse loss in Alzheimer mouse models. *Science (80-.).* 352, 712–716.

Hoover, B. R., Reed, M. N., Su, J., Penrod, R. D., Kotilinek, L. A., Grant, M. K., et al. (2010). Tau mislocalization to dendritic spines mediates synaptic dysfunction independently of neurodegeneration. *Neuron* 68, 1067–1081.

Horio, T., Murata, T., and Damme, D. Van (2014). The role of dynamic instability in microtubule organization. *Plant Traffic Transp.* 5, 511.

Hosie, K. A., King, A. E., Blizzard, C. A., Vickers, J. C., and Dickson, T. C. (2012). Chronic excitotoxin-induced axon degeneration in a compartmented neuronal culture model. *ASN Neuro* 4, e00076.

Hoskison, M. ., Obata, Y. ., and Shuttleworth, C. . (2007). Calcium-dependent NMDA-induced dendritic injury and MAP2 loss in acute hippocampal slices. *Neuroscience* 145, 66–79.

Hoskison, M. M., and Shuttleworth, C. W. (2006). Microtubule disruption, not calpain-dependent loss of MAP2, contributes to enduring NMDA-induced dendritic dysfunction in acute hippocampal slices. *Exp. Neurol.* 202, 302–312.

Hou, S., Jiang, S., Aylsworth, A., Ferguson, G., Slinn, J., Hu, H., et al. (2009). CaMKII phosphorylates collapsin response mediator protein 2 and modulates axonal damage

during glutamate excitotoxicity. *J Neurochem* 111, 870–881.

Hou, S., Jiang, S., and Smith, R. (2008). Permissive and repulsive cues and signalling pathways of axonal outgrowth and regeneration. *Int. Rev. Cell Mol. Biol.* 267, 125–181.

Howes, S. C., Alushin, G. M., Shida, T., Nachury, M. V., and Nogales, E. (2014). Effects of tubulin acetylation and tubulin acetyltransferase binding on microtubule structure. *Mol. Biol. Cell* 25, 257–266.

Hsing, C., Hung, S., Chen, Y., Wei, T., Sun, D., Wang, J., et al. (2015). Histone deacetylase inhibitor trichostatin A ameliorated endotoxin-induced neuroinflammation and cognitive dysfunction. *Mediators Inflamm.* 2015, 163140.

Huber, L., Distler, J., Moritz, F., Hemmatazad, H., Hauser, T., Michel, B., et al. (2007). Trichostatin A prevents the accumulation of extracellular matrix in a mouse model of bleomycin-induced skin fibrosis. *Arthritis Rheum* 56, 2755–2764.

Huh, J. W., Raghupathi, R., Laurer, H. L., Helfaer, M. A., and Saatman, K. E. (2004). Transient loss of microtubule-associated protein 2 immunoreactivity after moderate brain injury in mice. *J. Neurotrauma* 20, 975–984.

Hyeon, J. K., Rowe, M., Ren, M., Hong, J. S., Chen, P. S., and Chuang, D. M. (2007). Histone deacetylase inhibitors exhibit anti-inflammatory and neuroprotective effects in a rat permanent ischemic model of stroke: multiple mechanisms of action. *J Pharmacol. Experiment. Therapeut.* 321(3), 892-901.

Hynd, M. R., Scott, H. L., and Dodd, P. R. (2004). Glutamate-mediated excitotoxicity and neurodegeneration in Alzheimer's disease. *Neurochem. Int.* 45, 583–95.

Ikonomidou, C., Stefovska, V., and Turski, L. (2000). Neuronal death enhanced by N-methyl-D-aspartate antagonists. *Proc Natl Acad Sci USA* 97, 12885–12890.

Illenberger, S., Drewes, G., Trinczek, B., Biernat, J., Helmut, E. M., and Joanna, B. O. (1996). Phosphorylation of microtubule-associated proteins MAP2 and MAP4 by the protein

kinase p110. *J. Biol. Chem.* 271, 10834–10843.

Iqbal, K., Liu, F., Gong, C.-X., and Grundke-Iqbal, I. (2010). Tau in Alzheimer disease and related tauopathies. *Curr Alzheimer Res* 7, 656–664.

Irving, E. A., McCulloch, J., and Dewar, D. (1996). Intracortical perfusion of glutamate in vivo induces alterations of tau and microtubule-associated protein 2 immunoreactivity in the rat. *Acta Neuropathol.* 92, 186–196.

Isono, T., Yamashita, N., Obara, M., Araki, T., Nakamura, F., Kamiya, Y., et al. (2013). Amyloid-β25-35 induces impairment of cognitive function and long-term potentiation through phosphorylation of collapsin response mediator protein 2. *Neurosci. Res.* 77, 180–185.

Ittner, A., Bertz, J., Suh, L. S., Stevens, C. H., Götz, J., and Ittner, L. M. (2015). Tau-targeting passive immunization modulates aspects of pathology in tau transgenic mice. *J. Neurochem.* 132, 135–145.

Janczura, K. J., Volmar, C.-H., Sartor, G. C., Rao, S. J., Ricciardi, N. R., Lambert, G., et al. (2018). Inhibition of HDAC3 reverses Alzheimer's disease-related pathologies in vitro and in the 3xTg-AD mouse model. *Proc. Natl. Acad. Sci.* 115, E11148–E11157.

Jang, E. H., Sim, A., Im, S. K., and Hur, E. M. (2016). Effects of microtubule stabilization by epothilone B depend on the type and age of neurons. *Neural Plast.* 2016, 5056418.

Janke, C., and Montagnac, G. (2017). Causes and consequences of microtubule acetylation. *Curr. Biol.* 27, R1287–R1292.

Jankowsky, J. L., Slunt, H. H., Ratovitski, T., Jenkins, N. A., Copeland, N. G., and Borchelt, D. R. (2001). Co-expression of multiple transgenes in mouse CNS: a comparison of strategies. *Biomol. Eng.* 17, 157–165.

Jankowsky, J., and Zheng, H. (2017). Practical considerations for choosing a mouse model of Alzheimer's disease. *Mol. Neurodegener.* 12, 89.

Jean, D. C., and Baas, P. W. (2013). It cuts two ways: microtubule loss during Alzheimer disease. *EMBO J* 32, 2900–2902.

Jennings, S., Chenevert, M., Liu, L., Mottamal, M., Wojcik, E. J., and Huckaba, T. M. (2017). Characterization of kinesin switch I mutations that cause hereditary spastic paraplegia. *PLoS One* 12, 1–19.

Jin, N., Zhu, H., Liang, X., Huang, W., Xie, Q., Xiao, P., et al. (2017). Sodium selenate activated Wnt/β-catenin signaling and repressed amyloid-β formation in a triple transgenic mouse model of Alzheimer's disease. *Exp. Neurol.* 297, 36–49.

Job, D., Valiron, O., and Oakley, B. (2002). Microtubule nucleation. *Curr. Opin. Cell Biol.* 15, 111–117.

Jochems, J., Boulden, J., Lee, B. G., Blendy, J. A., Jarpe, M., Mazitschek, R., et al. (2014). Antidepressant-like properties of novel HDAC6-selective inhibitors with improved brain bioavailability. *Neuropsychopharmacology* 39, 389–400.

Jung, K., Chu, K., Lee, S., Park, H., Kim, J., Kang, K., et al. (2009). Augmentation of nitrite therapy in cerebral ischemia by NMDA receptor inhibition. *Biochem Biophys Res Commun* 378, 507–512.

Kadavath, H., Hofele, R. V, Biernat, J., Kumar, S., Tepper, K., Urlaub, H., et al. (2015). Tau stabilizes microtubules by binding at the interface between tubulin heterodimers. *Proc. Natl. Acad. Sci.* 112, 7501–7506.

Kadowaki, T., Fujita-Yamaguchi, Y., Nishida, E., Takaku, F., Akiyama, T., Kathuria, S., et al. (1985). Phosphorylation of tubulin and microtubule-associated proteins by the purified Insulin receptor kinas. *J. Biol. Chem.* 260, 4016–4020.

Kalebic, N., Martinez, C., Perlas, E., Hublitz, P., Bilbao-Cortes, D., Fiedorczuk, K., et al. (2013). Tubulin acetyltransferase TAT1 destabilizes microtubules independently of its acetylation activity. *Mol. Cell. Biol.* 33, 1114–1123.

Kamal, A., Almenar-Queralt, A., LeBlanc, J. F., Roberts, E. A., and Goldstein, L. S. (2001). Kinesin-mediated axonal transport of a membrane compartment containing beta-secretase and presenilin-1 requires APP. *Nature* 414, 643–648.

Kamphuis, W., Mamber, C., Moeton, M., Kooijman, L., Sluijs, J. A., Jansen, A. H. P., et al. (2012). GFAP isoforms in adult mouse brain with a focus on neurogenic astrocytes and reactive astrogliosis in mouse models of Alzheimer disease. *PLoS One* 7, e42823.

Kanaan, N. M., Morfini, G., Pigino, G., LaPointe, N. E., Andreadis, A., Song, Y., et al. (2012). Phosphorylation in the amino terminus of tau prevents inhibition of anterograde axonal transport. *Neurobiol. Aging* 33, 826.e15–826.e30.

Kandalepas, P. C., Sadleir, K. R., Eimer, W. A., Zhao, J., Nicholson, D. A., and Vassar, R. (2013). The Alzheimer's ??-secretase BACE1 localizes to normal presynaptic terminals and to dystrophic presynaptic terminals surrounding amyloid plaques. *Acta Neuropathol.* 126, 329–352.

Kaur, U., Banerjee, P., Bir, A., Sinha, M., Biswas, A., and Chakrabati, S. (2015). Reactive oxygen species, redox signaling and neuroinflammation in Alzheimer's disease: the NF-κB connection. *Curr. Top. Med. Chem.* 15.

Kemp, M., Ghosh, M., Liu, G., and Leffak, M. (2005). The histone deacetylase inhibitor trichostatin A alters the pattern of DNA replication origin activity in human cells. *Nucleic Acids Res.* 33, 325–336.

Ketter, N., Brashear, H. R., Bogert, J., Di, J., Miaux, Y., Gass, A., et al. (2017). Central review of amyloid-related imaging abnormalities in two phase III clinical trials of Bapineuzumab in mild-to-moderate Alzheimer's disease patients. *J. Alzheimer's Dis.* 57, 557–573.

Khawaja, S., Gundersen, G. G., and Bulinski, J. C. (1988). Enhanced stability of microtubules enriched in detyrosinated tubulin is not a direct function of detyrosination level. *J. Cell*

Biol. 106, 141–149.

Khazaei, M. R., Girouard, M. P., Alchini, R., Tone, S. O., Shimada, T., Bechstedt, S., et al. (2014). Collapsin response mediator protein 4 regulates growth cone dynamics through the actin and microtubule cytoskeleton. *J. Biol. Chem.* 289, 30133–30143.

Kim, J., Onstead, L., Randle, S., Price, R., Smithson, L., Zwizinski, C., et al. (2007). A 40 inhibits amyloid deposition in vivo. *J. Neurosci.* 27, 627–633.

Kim, T.-K., Han, H.-E., Kim, H., Lee, J.-E., Choi, D., Park, W. J., et al. (2012). Expression of the plant viral protease NIa in the brain of a mouse model of Alzheimer's disease mitigates Aβ pathology and improves cognitive function. *Exp. Mol. Med.* 44, 740–8.

King, A., Brain, A., Hanson, K., Dittmann, J., Vickers, J., and Fernandez-martos, C. (2018). Disruption of leptin signalling in a mouse model of Alzheimer ' s disease. *Metab. Brain Dis.* 2.

King, A. E., Southam, K. A., Dittmann, J., and Vicker, J. C. (2013). Excitotoxin-induced caspase-3 activation and microtubule disintegration in axons is inhibited by taxol. *Acta Neuropathol.* 1, 59.

King, A. E., Woodhouse, A., Kirkcaldie, M. T. K., and Vickers, J. C. (2016). Excitotoxicity in ALS: overstimulation, or overreaction? *Exp. Neurol.* 275, 162–171.

King, M. E., Kan, H. M., Baas, P. W., Erisir, A., Glabe, C. G., and Bloom, G. S. (2006). Tau-dependent microtubule disassembly initiated by prefibrillar beta-amyloid. *J Cell Biol* 175, 541–546.

Kneynsberg, A., Combs, B., Christensen, K., Morfini, G., and Kanaan, N. (2017). Axonal degeneration in tauopathies: Disease relevance and underlying mechanisms. *Front. Neurosci.* 11, 572.

Koffie, R. M., Meyer-luehmann, M., Hashimoto, T., Adams, K. W., Mielke, M. L., Garcia-alloza, M., et al. (2009). Oligomeric amyloid beta associates with postsynaptic densities

and correlates with excitatory synapse loss near senile plaques. *PNAS* 106, 4012–4017.

Koivisto, H., Leinonen, H., Puurula, M., and Hafez, H. S. (2016). Chronic pyruvate supplementation increases exploratory activity and brain energy reserves in young and middle-aged mice. *Front. Aging Neurosci.* 8.

Konner, J., Grisham, R. N., Park, J., O'Connor, O. A., Cropp, G., Johnson, R., et al. (2012). Phase I clinical, pharmacokinetic, and pharmacodynamic study of KOS-862 (epothilone D) in patients with advanced solid tumors and lymphoma. *Invest. New Drugs* 30, 2294–2302.

Koo, E. H., and Squazzo, S. L. (1994). Evidence that production and release of amyloid β-protein involves the endocytic pathway. *J. Biol. Chem.* 269, 17386–17389.

Kraft, A. W., Hu, X., Yoon, H., Yan, P., Xiao, Q., Wang, Y., et al. (2013). Attenuating astrocyte activation accelerates plaque pathogenesis in APP/PS1 mice. *FASEB J* 27, 187–198.

Kreis, T. E. (1987). Microtubules containing detyrosinated tubulin are less dynamic. *EMBO J.* 6, 2597–2606.

Kull, F. J., and Sloboda, R. D. (2014). A slow dance for microtubule acetylation. *Cell* 157, 1255–1256.

Kumar, N., and Flavin, M. (1981). Preferential action of a brain detyrosinolating carboxypeptidase on polymerized tubulin. *J. Biol. Chem.* 256, 7678–7686.

Kurd, D. D., and Saxton, W. M. (1996). Kinesin mutations cause motor neuron disease phenotypes by disrupting fast axonal transport in Drosophila. *Genetics* 144, 1075–1085.

Kuznetsov, S. A., Rodionov, V. I., and Rosenblat, V. A. (1984). MAP2 competes with MAP1 for binding to microtubules. *Biochem. Biophys. Res. Commun.* 119, 173–178.

Lacroix, B., Van Dijk, J., Gold, N. D., Guizetti, J., Aldrian-Herrada, G., Rogowski, K., et al. (2010). Tubulin polyglutamylation stimulates spastin-mediated microtubule severing. *J.*

Cell Biol. 189, 945–954.

Lai, T., Zhang, S., and Wang, Y. (2014). Excitotoxicity and stroke: identifying novel targets for neuroprotection. *Prog. Neurobiol.* 115, 157–188.

Lammich, S., Kojro, E., Postina, R., Gilbert, S., Pfeiffer, R., Jasionowski, M., et al. (1999). Constitutive and regulated alpha-secretase cleavage of Alzheimer's amyloid precursor protein by a disintegrin metalloprotease. *Proc. Natl. Acad. Sci.* 96, 3922–3927.

Layton, M. E., and Pazdernik, T. L. (1999). Reactive oxidant species in piriform cortex extracellular fluid during seizures induced by systemic kainic acid in rats. *J. Mol. Neurosci.* 13, 63–68.

Lazarov, O., Morfini, G., Lee, E., Farah, M., Szodorai, A., DeBoer, S., et al. (2005). Axonal transport, amyloid precursor protein, kinesin-1, and the processing apparatus: revisited. *J. Neurosci.* 25, 2386–2395.

Lazic, S. E. (2015). Analytical strategies for the marble burying test: avoiding impossible predictions and invalid p-values. *BMC Res Notes* 8, 141.

Lazo-Gómez, R., Ramírez-Jarquín, U. N., Tovar-y-Romo, L. B., and Tapia, R. (2013). Histone deacetylases and their role in motor neuron degeneration. *Front. Cell. Neurosci.* 7, 243.

Lee, C. Y., and Landreth, G. E. (2010). The role of microglia in amyloid clearance from the AD brain. *J. Neural Transm.* 117, 949–960.

Lee, J. H., Shin, S. K., Jiang, Y., Choi, W. H., Hong, C., Kim, D.-E., et al. (2015). Facilitated tau degradation by USP14 aptamers via enhanced proteasome activity. *Sci. Rep.* 5, 10757.

Lee, S. H., Son, S. M., Son, D. J., Kim, S. M., Kim, T. J., Song, S., et al. (2007). Epothilones induce human colon cancer SW620 cell apoptosis via the tubulin polymerization independent activation of the nuclear factor-kappaB/IkappaB kinase signal pathway.

Mol Cancer Ther 6, 2786–2797.

Leibinger, M., Andreadaki, A., Golla, R., Levin, E., Hilla, A., Diekmann, H., et al. (2017). Boosting CNS axon regeneration by harnessing antagonistic effects of GSK3 activity. *PNAS* 114, E5454–E5463.

Leterrier, C. (2018). The axon initial segment: an updated viewpoint. *J Neurosci* 38, 2135–2145.

Lewerenz, J., and Maher, P. (2015). Chronic glutamate toxicity in neurodegenerative diseases-what is the evidence? *Front. Neurosci.* 9, 469.

Lewis, J., Dickson, D. W., Lin, W. L., Chisholm, L., Corral, A., Jones, G., et al. (2001). Enhanced neurofibrillary degeneration in transgenic mice expressing mutant tau and APP. *Science (80-.).* 293, 1487–1491.

Ley, S. C., Verbi, W., Pappin, D. J. C., Druker, B., Davies, A. A., and Crumpton, M. J. (1994). Tyrosine phosphorylation of α tubulin in human T lymphocytes. *Eur. J. Immunol.* 24, 99–106.

Li, H., Zhu, Y. H., Chi, C., Wu, H. W., and Guo, J. (2014). Role of cytoskeleton in axonal regeneration after neurodegenerative diseases and CNS injury. *Rev. Neurosci.* 25, 527–542.

Li, J. M., Zeng, Y. J., Peng, F., Li, L., Yang, H. T., Hong, Z., Lei, D., Chen, Z., and Zhou, D. (2010). Aberrant glutamate receptor 5 expression in temporal lobe epilepsy lesions. *Brain Res* 1311, 166-174.

Li, L., and Yang, X.-J. (2015). Tubulin acetylation: responsible enzymes, biological functions and human diseases. *Cell. Mol. Life Sci.* 72, 4237–4255.

Li, X., Kumar, Y., Zempel, H., Mandelkow, E.-M., Biernat, J., and Mandelkow, E. (2011). Novel diffusion barrier for axonal retention of tau in neurons and its failure in neurodegeneration. *EMBO J.* 30, 4825–4837.

Li, X., Scuderi, A., Letsou, A., and Virshup, D. (2002). B56-associated protein phosphatase 2A is required for survival and protects from apoptosis in drosophila melanogaster. *Mol Cell Biol* 22, 3674–3684.

Liang, Z., Liu, F., Iqbal, K., Grundke-Iqbal, I., and Gong, C. (2009). Dysregulation of tau phosphorylation in mouse brain during excitotoxic damage. *J Alzheimers Dis* 17, 531–539.

Lin, P. C., Chan, P. M., Hall, C., and Manser, E. (2011). Collapsin response mediator proteins (CRMPs) are a new class of microtubule-associated protein (MAP) that selectively interacts with assembled microtubules via a taxol-sensitive binding interaction. *J. Biol. Chem.* 286, 41466–41478.

Lingor, P., Koch, J. C., Tonges, L., and Bahr, M. (2012). Axonal degeneration as a therapeutic target in the CNS. *Cell Tissue Res.* 349, 289–311.

Liu, C. C., Kanekiyo, T., Xu, H., and Bu, G. (2013). Apolipoprotein E and Alzheimer disease: risk, mechanisms and therapy. *Nat. Rev. Neurol.* 9, 106–118.

Liu, H., Yazdani, A., Murray, L., Beauvais, A., and Kothary, R. (2014). The Smn-independent beneficial effects of trichostatin A on an intermediate mouse model of spinal muscular atrophy. *PLoS One* 9, e101225.

Liu, N., Xiong, Y., Li, S., Ren, Y., He, Q., Gao, S., et al. (2015a). New HDAC6-mediated deacetylation sites of tubulin in the mouse brain identified by quantitative mass spectrometry. *Sci. Rep.* 5, 16869.

Liu, Q., Xie, F., Siedlak, S. L., Nunomura, A., Honda, K., Moreira, P. I., et al. (2004a). Neurofilament proteins in neurodegenerative diseases. *Open Neurol. J.* 61, 3057–3075.

Liu, T., Perry, G., Chan, H. W., Verdile, G., Martins, R. N., Smith, M. A., et al. (2004b). Amyloid-β-induced toxicity of primary neurons is dependent upon differentiation-associated increases in tau and cyclin-dependent kinase 5 expression. *J. Neurochem.* 88,

554–563.

Liu, X.-A., Rizzo, V., and Puthanveettil, Sathyanarayanan, V. (2012). Pathologies of axonal transport in diseases. *Transl. Neurosci.* 3, 355–372.

Liu, Y., Lee, J. W., and Ackerman, S. L. (2015b). Mutations in the microtubule-associated protein 1A (Map1a) gene cause Purkinje cell degeneration. *J. Neurosci.* 35, 4587–4598.

Lopez-Rodriguez, A. B., Hennessy, E., Murray, C., Lewis, A., Barra, N. de, Fagan, S., et al. (2018). Microglial and astrocyte priming in the APP/PS1 model of Alzheimer's disease: increased vulnerability to acute inflammation and cognitive deficits. *Cold Spring Harb Lab* Epub ahead.

Low, L. K., and Cheng, H. J. (2006). Axon pruning: an essential step underlying the developmental plasticity of neuronal connections. *Philos. Trans. R. Soc. B Biol. Sci.* 361, 1531–1544.

Lu, C. Y., Chang, Y. C., Hua, C. H., Chuang, C., Huang, S. H., Kung, S. H., et al. (2017). Tubacin, an HDAC6 selective inhibitor, reduces the replication of the Japanese encephalitis virus via the decrease of viral RNA synthesis. *Int. J. Mol. Sci.* 18.

Lunn, E. R., Perry, V. H., Brown, M. C., Rosen, H., and Gordon, S. (1989). Absence of Wallerian degeneration does not hinder regeneration in peripheral nerve. *Eur. J. Neurosci.* 1, 27–33.

Luo, Y., Bolon, B., Kahn, S., Bennett, B. D., Babu-Khan, S., Denis, P., et al. (2001). Mice deficient in BACE1, the Alzheimer's β-secretase, have normal phenotype and abolished β-amyloid generation. *Nat. Neurosci.* 4, 231–232.

Lye, T. C., and Shores, E. A. (2000). Traumatic brain injury as a risk factor for Alzheimer's disease : a review. *Neuropsychology* 10, 1–15.

Ma, D., Himes, B., Shea, T., and Fischer, I. (2000). Axonal transport of microtubule-associated protein 1B (MAP1B) in the sciatic nerve of adult rat: distinct transport rates

of different isoforms. *J Neurosci* 20, 2112–2120.

Ma, R. hong, Zhang, Y., Hong, X. yue, Zhang, J. fei, Wang, J. Z., and Liu, G. ping (2017). Role of microtubule-associated protein tau phosphorylation in Alzheimer's disease. *J. Huazhong Univ. Sci. Technol. - Med. Sci.* 37, 307–312.

Maas, C., Belgardt, D., Lee, H. K., Heisler, F. F., Lappe-Siefke, C., Magiera, M. M., et al. (2009). Synaptic activation modifies microtubules underlying transport of postsynaptic cargo. *Proc. Natl. Acad. Sci. U. S. A.* 106, 8731–6.

Magiera, M., and Janke, C. (2014). Post-translational modifications of tubulin. *Curr Biol* 24, R351-354.

Magiera, M. M., Singh, P., Gadadhar, S., and Janke, C. (2018). Tubulin posttranslational modifications and emerging links to human disease. *Cell* 173, 1323–1327.

Malmanche, N., Dourlen, P., Gistelinck, M., Demiautte, F., Link, N., Dupont, C., et al. (2017). Developmental expression of 4-repeat-tau induces neuronal aneuploidy in drosophila tauopathy models. *Sci. Rep.* 7, 1–14.

Malpas, C. B., Vivash, L., Genc, S., Saling, M. M., Desmond, P., Steward, C., et al. (2016). A phase IIa randomized control trial of VEL015 (sodium selenate) in mild-moderate Alzheimer's disease. *J. Alzheimer's Dis.* 54, 223–232.

Mandelkow, E. M., Stamer, K., Vogel, R., Thies, E., and Mandelkow, E. (2003). Clogging of axons by tau, inhibition of axonal traffic and starvation of synapses. *Neurobiol. Aging* 24, 1079–1085.

Manocha, G. D., Floden, A. M., Rausch, K., Kulas, J. A., McGregor, B. A., Rojanathammanee, L., et al. (2016). APP regulates microglial phenotype in a mouse model of Alzheimer's disease. *J. Neurosci.* 36, 8471–8486.

Manoharan, S., Guillemin, G. J., Abiramasundari, R. S., Essa, M. M., Akbar, M., and Akbar, M. D. (2016). The role of reactive oxygen species in the pathogenesis of Alzheimer's

disease, Parkinson's disease, and Huntington's disease: a mini review. *Oxid. Med. Cell. Longev.* 2016, 8590578.

Manton, I., and Clarke, B. (1952). An electron microscope study of the spermatozoid of sphagnum. *J. Exp. Bot.* 3, 368–75.

Mao, C.-X., Wen, X., Jin, S., and Zhang, Y. Q. (2017). Increased acetylation of microtubules rescues human tau-induced microtubule defects and neuromuscular junction abnormalities in Drosophila. *Dis Model Mech* 10, 1245–1252.

Martin, N., Jaubert, J., Gounon, P., Salido, E., Haase, G., Szatanik, M., et al. (2002). A missense mutation in Tbce causes progressive motor neuronopathy in mice. *Nat. Genet.* 32, 443–447.

Masliah, E., Mallory, M., Hansen, L., Alford, M., DeTeresa, R., and Terry, R. (1993). An antibody against phosphorylated neurofilaments identifies a subset of damaged association axons in Alzheimer's disease. *Am J Pathol* 142, 871–882.

Masliah, E., Terry, R. D., Mallory, M., Alford, M., and Hansen, L. A. (1990). Diffuse plaques do not accentuate synapse loss in Alzheimer's disease. *Am J Pathol* 137, 1293–1297.

Matsuoka, Y., Jouroukhin, Y., Gray, A. J., Ma, L., Hirata-Fukae, C., Li, H. F., et al. (2008). A neuronal microtubule-interacting agent, NAPVSIPQ, reduces tau pathology and enhances cognitive function in a mouse model of Alzheimer's disease. *J. Pharmacol. Exp. Ther.* 325, 146–153.

McCarran, W. J., and Goldberg, M. P. (2007). White matter axon vulnerability to AMPA/kainate receptor-mediated ischemic injury Is developmentally regulated. *J. Neurosci.* 27, 4220–4229.

Meda, L., Cassatella, M. A., Szendrei, G. I., Otvos Jr., L., Baron, P., Villalba, M., et al. (1995). Activation of microglial cells by beta-amyloid protein and interferon-gamma. *Nature* 374, 647–650.

Medina, M. (2018). An overview on the clinical development of tau-based therapeutics. *Int. J. Mol. Sci.* 19, 1160.

Menéndez, M., Rivas, G., Díaz, J. F., and Andreu, J. M. (1998). Control of the structural stability of the tubulin dimer by one high affinity bound magnesium ion at nucleotide N-site. *J. Biol. Chem.* 273, 167–176.

Menting, K. W., and Claassen, J. A. H. R. (2014). β-secretase inhibitor; a promising novel therapeutic drug in Alzheimer's Disease. *Front. Aging Neurosci.* 6, 165.

Merriam, E. B., Millette, M., Lumbard, D. C., Saengsawang, W., Fothergill, T., Hu, X., et al. (2013). Synaptic regulation of microtubule dynamics in dendritic spines by calcium, F-Actin, and drebrin. *J. Neurosci.* 33, 16471–16482.

Micheva, K. D., Busse, B., Weiler, N. C., O'Rourke, N., and Smith, S. J. (2010). Single-synapse analysis of a diverse synapse population: proteomic imaging methods and markers. *Neuron* 68, 639–653.

Miedel, C. J., Patton, J. M., Miedel, A. N., Miedel, E. S., and Levenson, J. M. (2017). Assessment of spontaneous alternation, novel object recognition and limb clasping in transgenic mouse models of amyloid-β and tau neuropathology. *J. Vis. Exp.* 123, e55523.

Mietelska-Porowska, A., Wasik, U., Goras, M., Filipek, A., and Niewiadomska, G. (2014). Tau protein modifications and interactions: their role in function and dysfunction. *Int. J. Mol. Sci.* 15, 4671–4713.

Mietto, B. S., Mostacada, K., and Martinez, A. M. B. (2015). Neurotrauma and inflammation: CNS and PNS responses. *Mediators Inflamm.* 2015, 251204.

Millecamps, S., Gowing, G., Corti, O., Mallet, J., and Julien, J.-P. (2007). Conditional NF-L transgene expression in mice for in vivo analysis of turnover and transport rate of neurofilaments. *J. Neurosci.* 27, 4947–4956.

Millet, L. J., and Gillette, M. U. (2012). Over a century of neuron culture : from the hanging

drop to microfluidic devices. *Yale J. Biol. Med.* 85, 501–521.

Min, S.-W., Chen, X., Tracy, T. E., Li, Y., Zhou, Y., Wang, C., et al. (2015). Critical role of acetylation in tau-mediated neurodegeneration and cognitive deficits. *Nat. Med.* 21, 1154–1162.

Mitew, S., Kirkcaldie, M. T., Dickson, T. C., and Vickers, J. C. (2013a). Altered synapses and gliotransmission in Alzheimer's disease and AD model mice. *Neurobiol. Aging* 34, 2341–2351.

Mitew, S., Kirkcaldie, M. T., Dickson, T. C., and Vickers, J. C. (2013b). Neurites containing the neurofilament-triplet proteins are selectively vulnerable to cytoskeletal pathology in Alzheimer's disease and transgenic mouse models. *Front. Neuroanat.* 7, 30.

Mo, J. J., Li, J. Y., Yang, Z., Liu, Z., and Feng, J. S. (2017). Efficacy and safety of anti-amyloid-β immunotherapy for Alzheimer's disease: a systematic review and network meta-analysis. *Ann. Clin. Transl. Neurol.* 4, 931–942.

Mohri, H. (1968). Amino-acid composition of "tubulin" constituting microtubules of sperm flagella. *Nature* 217, 1053–1054.

Mokhtar, S. H., Bakhuraysah, M. M., Cram, D. S., and Petratos, S. (2013). The beta-amyloid protein of Alzheimer's disease: communication breakdown by modifying the neuronal cytoskeleton. *Int J Alzheimers Dis* 2013, 910502.

Mokhtar, S. H., Kim, M. J., Magee, K. A., Aui, P. M., Thomas, S., Bakhuraysah, M. M., et al. (2018). Amyloid-beta-dependent phosphorylation of collapsin response mediator protein-2 dissociates kinesin in Alzheimer's disease. *Neural Regen. Res.* 13, 1066–1080.

Mondragón-Rodríguez, S., Perry, G., Luna-Muñoz, J., Acevedo-Aquino, M., and Williams, S. (2014). Phosphorylation of tau protein at sites Ser(396-404) is one of the earliest events in Alzheimer's disease and Down syndrome. *Neuropathol Appl Neurobiol* 40, 121–135.

Moreira, J., Scheipers, P., and Sørensen, P. (2003). The histone deacetylase inhibitor trichostatin A modulates CD4+ T cell responses. *BMC Cancer* 3, 30.

Moritz, M., Braunfeld, M. B., Guénebaut, V., Heuser, J., and Agard, D. A. (2000). Structure of the γ-tubulin ring complex: a template for microtubule nucleation. *Nat. Cell Biol.* 2, 365–370.

Morris, M., Knudsen, G. M., Maeda, S., Trinidad, J. C., Ioanoviciu, A., Burlingame, A. L., et al. (2015). Tau post-translational modifications in wild-type and human amyloid precursor protein transgenic mice. *Nat. Neurosci.* 18, 1183–9.

Mukhtar, E., Adhami, V. M., and Mukhtar, H. (2014). Targeting microtubules by natural agents for cancer therapy. *Mol. Cancer Therpy* 13, 275–284.

Nasu, Y., Nishida, K., Miyazawa, S., Komiyama, T., Kadota, Y., Abe, N., et al. (2008). Trichostatin A, a histone deacetylase inhibitor, suppresses synovial inflammation and subsequent cartilage destruction in a collagen antibody-induced arthritis mouse model. *Osteoarthr. Cartil.* 16, 723–732.

Nava-Mesa, M. O., Jiménez-Dí-az, L., Yajeya, J., and Navarro-Lopez, J. D. (2014). GABAergic neurotransmission and new strategies of neuromodulation to compensate synaptic dysfunction in early stages of Alzheimer's disease. *Front. Cell. Neurosci.* 8, 167.

Ndountse, L., and Chan, H. (2009). Role of N-methyl-D-aspartate receptors in polychlorinated biphenyl mediated neurotoxicity. *Toxicol Lett* 184, 50–55.

Neukomm, L. ., and Freeman, M. R. (2014). Diverse cellular and molecular modes of axon degeneration. *Trends Cell Biol.* 24, 515–523.

Neumann, B., and Hilliard, M. A. (2014). Loss of MEC-17 leads to microtubule instability and axonal degeneration. *Cell Rep.* 6, 93–103.

Nguyen, L. K., Kolch, W., and Kholodenko, B. N. (2013). When ubiquitination meets

phosphorylation: a systems biology perspective of EGFR/MAPK signalling. *Cell. Commun. Signal*. 11, 52.

Nicolas, L. B., Kolb, Y., and Prinssen, E. P. (2006). A combined marble burying-locomotor activity test in mice: a practical screening test with sensitivity to different classes of anxiolytics and antidepressants. *Eur. J. Pharmacol.* 547, 106–115.

Nisbet, R. M., Van Der Jeugd, A., Leinenga, G., Evans, H. T., Janowicz, P. W., and Götz, J. (2017). Combined effects of scanning ultrasound and a tau-specific single chain antibody in a tau transgenic mouse model. *Brain* 140, 1220–1230.

Niwa, S., Nakamura, F., Tomabechi, Y., Aoki, M., Shigematsu, H., Matsumoto, T., et al. (2017). Structural basis for CRMP2-induced axonal microtubule formation. *Sci. Rep.* 7, 1–17.

Njung'e, K., and Handley, S. L. (1991). Evaluation of marble-burying behavior as a model of anxiety. *Pharmacol Biochem Behav* 38, 63–67.

Noble, M., Lewis, S. A., and Cowan, N. J. (1989). The microtubule binding domain of microtubule-associated protein MAP1B contains a repeated sequence motif unrelated to that of MAP2 and Tau. *J. Cell Biol.* 109, 3367–3376.

Nogales, E., Whittaker, M., Milligan, R. A., and Downing, K. H. (1999). High-resolution model of the microtubule. *Cell* 96, 79–88.

Nogales, E., Wolf, S. G., and Downing, K. H. (1998). Structure of the alpha beta tubulin dimer by electron crystallography. *Nature* 391, 199–203.

Nogales, E., Wolf, S. G., Khan, I. ., Ludueña, R. F., and Downing, K. H. (1995). Structure of tubulin at 6.5 A and location of the taxol-binding site. *Nature* 375, 424–427.

Nunez, J. (1988). Immature and mature variants of MAP2 and tau proteins and neuronal plasticity. *Trends Neurosci.* 11, 477–479.

O'Mara, A. R., Collins, J. M., King, A. E., Vickers, J. C., and Kirkcaldie, M. . T. K. (2018).

Accurate and unbiased Quantitation of amyloid-β fluorescence images using imageSURF. *Curr. Alzheimer Res.* Epub ahead.

Okello, A., Edison, P., Archer, H. A., Turkheimer, F. E., Kennedy, J., Bullock, R., et al. (2009). Microglial activation and amyloid deposition in mild cognitive impairment: A PET study. *Neurology* 72, 56–62.

Olaharski, A., Ji, Z., Woo, J., Lim, S., Hubbard, A., Zhang, L., et al. (2006). The histone deacetylase inhibitor trichostatin a has genotoxic effects in human lymphoblasts in vitro. *Toxicol Sci* 93, 341–347.

Olivares, D., Deshpande, V. K., Shi, Y., Lahiri, D. K., Greig, N. H., Rogers, J. T., et al. (2012). N-Methyl D-Aspartate (NMDA) receptor antagonists and memantine treatment for Alzheimer's disease, vascular dementia and Parkinson's disease. *Curr Alzheimer Res* 9, 746–758.

Ong, W. Y., Tanaka, K., Dawe, G. S., Ittner, L. M., and Farooqui, A. A. (2013). Slow excitotoxicity in Alzheimer's disease. *J. Alzheimer's Dis.* 35, 643–668.

Ordóñez-Gutiérrez, L., Antón, M., and Wandosell, F. (2015). Peripheral amyloid levels present gender differences associated with aging in AβPP/PS1 mice. *J. Alzheimer's Dis.* 44, 1063–1068.

Pachima, Y. I., Zhou, L. Y., Lei, P., and Gozes, I. (2016). Microtubule-tau interaction as a therapeutic target for Alzheimer's disease. *J. Mol. Neurosci.* 58, 145–152.

Pallo, S. P., DiMaio, J., Cook, A., Nilsson, B., and Johnson, G. V. W. (2016). Mechanisms of tau and Aβ-induced excitotoxicity. *Brain Res* 1634, 119–131.

Papa, L., Robicsek, S. A., Brophy, G. M., Wang, K. K. W., Hannay, H. J., Heaton, S., et al. (2017). Temporal profile of microtubule-associated protein 2: a novel indicator of diffuse brain injury severity and early ortality after brain trauma. *J. Neurotrauma* 35, 32–40.

Parness, J., and Horwitz, S. B. (1981). Taxol binds to polymerized tubulin in vitro. *J. Cell Biol.* 91, 479–487.

Pedersen, J. T., and Sigurdsson, E. M. (2015). Tau immunotherapy for Alzheimer's disease. *Trends Mol. Med.* 21, 394–402.

Pedrotti, B., and Islam, K. (1996). Dephosphorylated but not phosphorylated microtubule associated protein MAP1B binds to microfilaments. *FEBS Lett* 388, 131–133.

Perez-Nievas, B. G., and Serrano-Pozo, A. (2018). Deciphering the astrocyte reaction in Alzheimer's disease. *Front. Aging Neurosci.* 10, 114.

Perez, M., Santa-Maria, I., De Barreda, E. G., Zhu, X., Cuadros, R., Cabrero, J. R., et al. (2009). Tau - an inhibitor of deacetylase HDAC6 function. *J. Neurochem.* 109, 1756–1766.

Perez, Y., Bar-Yaacov, R., Kadir, R., Wormser, O., Shelef, I., Birk, O. S., et al. (2019). Mutations in the microtubule-associated protein MAP11 (C7orf43) cause microcephaly in humans and zebrafish. *Brain*, 1–12.

Peris, L., Wagenbach, M., Lafanechère, L., Brocard, J., Moore, A. T., Kozielski, F., et al. (2009). Motor-dependent microtubule disassembly driven by tubulin tyrosination. *J. Cell Biol.* 185, 1159–1166.

Perlmutter, L. S., Barron, E., and Chui, H. C. (1990). Morphologic association between microglia and senile plaque amyloid in Alzheimer's disease. *Neurosci. Lett.* 119, 32–36.

Perrot, R., and Julien, J.-P. (2010). Maldistribution of neurofilaments, disease pathogenesis, and amyotrophic lateral sclerosis. *US Neurol.* 05, 30.

Peters, O., Schipke, C. G., Philipps, A., Haas, B., Pannasch, U., Wang, L. P., et al. (2009). Astrocytes function is modified by Alzheimer's disease-like pathology in aged mice. *J. Alzheimer's Dis.* 18, 177–189.

Pianu, B., Lefort, R., Thuiliere, L., Tabourier, E., and Bartolini, F. (2014). Amyloid beta1-42

peptide regulates microtubule stability independently of tau. *J Cell Sci*.

Pigino, G., Morfini, G., Pelsman, A., Mattson, M. P., Brady, S. T., and Busciglio, J. (2003). Alzheimer's presenilin 1 mutations impair kinesin-based axonal transport. *J. Neurosci.* 23, 4499–4508.

Piperno, G., LeDizet, M., and Chang, X. J. (1987). Microtubules containing acetylated alpha-tubulin in mammalian cells in culture. *J. Cell Biol.* 104, 289–302.

Pitts, M. W. (2018). Barnes maze procedure for spatial learning and memory in mice. *Bio Protoc* 8, e2744.

Plummer, S., Van den Heuvel, C., Thornton, E., Corrigan, F., and Cappai, R. (2016). The neuroprotective properties of the amyloid precursor protein following traumatic brain injury. *Aging Dis.* 7, 163.

Portran, D., Schaedel, L., Xu, Z., Théry, M., and Nachury, M. V. (2017). Tubulin acetylation protects long-lived microtubules against mechanical ageing. *Nat. Cell Biol.* 19, 391–398.

Povlishock, J., and Pettus, E. (1996). Traumatically induced axonal damage: evidence for enduring changes in axolemmal permeability with associated cytoskeletal change. *Acta Neurochir Suppl* 66, 81–86.

Praprotnik, D., Smith, M. A., L., R. P., Vinters, H. V, and Perry, G. (1996). Filament heterogeneity within the dystrophic neurites of senile plaques suggests blockage of fast axonal transport in Alzheimer's disease. *Acta Neuropathol.* 91, 226–235.

Prezel, E., Elie, A., Delaroche, J., Stoppin-Mellet, V., Bosc, C., Serre, L., et al. (2018). Tau can switch microtubule network organizations: from random networks to dynamic and stable bundles. *Mol. Biol. Cell* 29, 154–165.

Priller, C., Bauer, T., Mitteregger, G., Krebs, B., Kretzschmar, H. A., and Herms, J. (2006). Synapse formation and function is modulated by the amyloid precursor protein. *J. Neurosci.* 26, 7212–7221.

Qiang, L., Yu, W., Andreadis, A., Luo, M., and Baas, P. W. (2006). Tau protects microtubules in the axon from severing by katanin. *J. Neurosci.* 26, 3120–3129.

Qin, W., Zhang, M., Piao, Y., Guo, D., Zhu, Z., Tian, X., et al. (2012). Wallerian degeneration in central nervous system: Dynamic associations between diffusion indices and their underlying pathology. *PLoS One* 7, 1–10.

Qiu, C., Kivipelto, M., and Von Strauss, E. (2009). Epidemiology of Alzheimer's disease: occurrence, determinants, and strategies toward intervention. *Dialogues Clin. Neurosci.* 11, 111–128.

Rahman, M., Kukita, A., Kukita, T., Shobuike, T., Nakamura, T., and Kohashi, O. (2003). Two histone deacetylase inhibitors, trichostatin A and sodium butyrate, suppress differentiation into osteoclasts but not into macrophages. *Blood* 101, 3451–3459.

Rankin, C. A., Sun, Q., and Gamblin, T. C. (2007). Tau phosphorylation by GSK-3β promotes tangle-like filament morphology. *Mol. Neurodegener.* 2, 12.

Ransohoff, R. M., and Brown, M. A. (2012). Innate immunity in the central nervous system. *J. Clin. Investig.* 122, 1164–1171.

Rao, A. N., Patil, A., Brodnik, Z. D., Qiang, L., Rodrigo, A., Sullivan, K. A., et al. (2017). Pharmacologically increasing microtubule acetylation corrects stress-exacerbated effects of organophosphates on neurons. *Traffic* 18, 433–441.

Rao, S., He, L., Chakravarty, S., Ojima, I., Orr, G. A., and Horwitz, S. B. (1999). Characterization of the taxol binding site on the microtubule. *J. Biol. Chem.* 274, 37990–37994.

Rapoport, M., Dawson, H. N., Binder, L. I., Vitek, M. P., and Ferreira, A. (2002). Tau is essential to β-amyloid-induced neurotoxicity. *PNAS* 99, 6364–6369.

Reed, N., Cai, D., Blasius, T., Jih, G., Meyhofer, E., Gaertig, J., et al. (2006). Microtubule acetylation promotes kinesin-1 binding and transport. *Curr. Biol.* 16, 2166–2172.

Reis, G. F., Yang, G., Szpankowski, L., Weaver, C., Shah, S. B., Robinson, J. T., et al. (2012). Molecular motor function in axonal transport in vivo probed by genetic and computational analysis in Drosophila. *Mol. Biol. Cell* 23, 1700–1714.

Riederer, B. M. (2007). Microtubule-associated protein 1B, a growth-associated and phosphorylated scaffold protein. *Brain Res. Bull.* 71, 541–558.

Rissman, R., Poon, W., Blurtin-Jones, M., Oddo, S., Torp, R., Vitek, M., et al. (2004). Caspase-cleavage of tau is an early event in Alzheimer disease tangle pathology. *J Clin Invest* 114, 121–130.

Rizzu, P., Van Swieten, J. C., Joosse, M., Hasegawa, M., Stevens, M., Tibben, A., et al. (1999). High prevalence of mutations in the microtubule-associated protein tau in a population study of frontotemporal dementia in the netherlands. *Am. J. Hum. Genet.* 64, 414–421.

Roberson, E. D., Scearce-Levie, K., Palop, J. J., Yan, F., Cheng, I. H., Gerstein, H., et al. (2007). Reducing endogenous tau ameliorates amyloid beta-induced deficits in an Alzheimer's disease mouse model. *Science (80-.).* 316, 750–754.

Robert, J., Button, E. B., Yuen, B., Gilmour, M., Kang, K., Bahrabadi, A., et al. (2017). Clearance of beta-amyloid is facilitated by apolipoprotein E and circulating highdensity lipoproteins in bioengineered human vessels. *Elife* 6, 1–24.

Rodrigues, E. M., Weissmiller, A. M., and Goldstein, L. S. (2012). Enhanced beta-secretase processing alters APP axonal transport and leads to axonal defects. *Hum Mol Genet* 21, 4587–4601.

Rohrer, J. D., Paviour, D., Vandrovcova, J., Hodges, J., de Silva, R., Rossor, M. N. (2011). Novel L284R MAPT mutation in a family with an autosomal dominant progressive supranuclear palsy syndrome. *Neurodegen Dis* 8, 149-152.

Rohrer Bley, C., Furmanova, P., Orlowski, K., Grosse, N., Broggini-Tenzer, A., McSheehy,

P. M. J., et al. (2013). Microtubule stabilising agents and ionising radiation: Multiple exploitable mechanisms for combined treatment. *Eur. J. Cancer* 49, 245–253.

Rosenfeld, C. S., and Ferguson, S. A. (2014). Barnes maze testing strategies with small and large rodent models. *J. Vis. Exp.* 84, e51194.

Rosenmann, H., Grigoriadis, N., Karussis, D., Boimel, M., Touloumi, O., Ovadia, H., et al. (2006). Tauopathy-like abnormalities and neurologic deficits in mice immunized with neuronal tau protein. *Arch. Neurol.* 63, 1459–1467.

Ross, J. L., Santangelo, C. D., Makrides, V., and Fygenson, D. K. (2004). Tau induces cooperative Taxol binding to microtubules. *Proc. Natl. Acad. Sci.* 101, 12910–12915.

Roy, S., Zhang, B., Lee, V. M., and Trojanowski, J. Q. (2005). Axonal transport defects: a common theme in neurodegenerative diseases. *Acta Neuropathol.* 109, 5–13.

Rubin, E. H., Rothermel, J., Tesfaye, F., Chen, T., Hubert, M., Ho, Y. Y., et al. (2005). Phase I dose-finding study of weekly single-agent patupilone in patients with advanced solid tumors. *J. Clin. Oncol.* 23, 9120–9129.

Ruschel, J., Hellal, F., Flynn, K. C., Dupraz, S., Elliott, D. A., Tedeschi, A., et al. (2015). Systemic administration of epothilone B promotes axon regeneration after spinal cord injury. *Science (80-.).* 348, 347–352.

Sadleir, K. R., Kandalepas, P. C., Buggia-Prévot, V., Nicholson, D. A., Thinakaran, G., and Vassar, R. (2016). Presynaptic dystrophic neurites surrounding amyloid plaques are sites of microtubule disruption, BACE1 elevation, and increased Aβ generation in Alzheimer's disease. *Acta Neuropathol.* 132, 1–22.

Salazar, S. V., Gallardo, C., Kaufman, A. C., Herber, C. S., Haas, L. T., Robinson, S., et al. (2017). Conditional deletion of Prnp rescues behavioral and synaptic deficits after disease onset in transgenic Alzheimer's disease. *J. Neurosci.* 37, 0722-17.

Salloway, S., Sperling, R., Fox, N. C., Blennow, K., Klunk, W., Raskind, M., et al. (2014).

Two phase 3 trials of bapineuzumab in mild-to-moderate Alzheimer's disease. *N. Engl. J. Med.* 370, 322–333.

Salvadores, N., Sanhueza, M., Manque, P., and Court, F. A. (2017). Axonal degeneration during aging and its functional role in neurodegenerative disorders. *Front. Neurosci.* 11, 451.

Sánchez-Elexpuru, G., Serratosa, J., and Sánchez, M. P. (2017). Sodium selenate treatment improves symptoms and seizure susceptibility in a malin-deficient mouse model of Lafora disease. *Epilepsia* 58, 467–475.

Sánchez, C., Diaz-Nido, J., and Avila, J. (2000). Phosphorylation of microtubule-associated protein 2 (MAP2) and its relevance for the regulation of the neuronal cytoskeleton function. *Prog. Neurobiol.* 61, 133–168.

Saxena, S., and Caroni, P. (2007). Mechanisms of axon degeneration: From development to disease. *Prog. Neurobiol.* 83, 174–191.

Scales, T. M. E., Lin, S., Kraus, M., Goold, R. G., and Gordon-Weeks, P. R. (2009). Nonprimed and DYRK1A-primed GSK3β-phosphorylation sites on MAP1B regulate microtubule dynamics in growing axons. *J. Cell Sci.* 122, 2424–2435.

Schiff, P. B., and Horwitz, S. B. (1981). Taxol assembles tubulin in the absence of exogenous guanosine 5'-triphosphate or microtubule-associated proteins. *Biochemistry* 20, 3247–3252.

Selkoe, D. J. (1991). The molecular pathology of Alzheimer's disease. *Neuron* 6, 487–498.

Selkoe, D. J., and Hardy, J. (2016). The amyloid hypothesis of Alzheimer's disease at 25 years. *EMBO Mol. Med.* 8, 595–608.

Selvaraj, B. T., Frank, N., Bender, F. L. P., Asan, E., and Sendtner, M. (2012). Local axonal function of STAT3 rescues axon degeneration in the pmn model of motoneuron disease. *J. Cell Biol.* 199, 437–451. doi:10.1083/jcb.201203109.

Sengottuvel, V., and Fischer, D. (2011). Facilitating axon regeneration in the injured CNS by microtubules stabilization. *Commun. Integr. Biol.* 4, 391–393.

Sengottuvel, V., Leibinger, M., Pfreimer, M., Andreadaki, A., and Fischer, D. (2011). Taxol facilitates axon regeneration in the mature CNS. *J. Neurosci.* 31, 2688–2699.

Sengupta, A., Novak, M., Grundke-Iqbal, I., and Iqbal, K. (2006). Regulation of phosphorylation of tau by cyclin-dependent kinase 5 and glycogen synthase kinase-3 at substrate level. *Fed. Eur. Biochem. Soc. Lett.* 580, 5925–5933.

Serbest, G., Burkhardt, M., Siman, R., Raghupathi, R., and Saatman, K. (2007). Temporal profiles of cytoskeletal protein loss following traumatic axonal injury in mice. *Neurochem. Res.* 32, 2006–2014.

Serrano-Pozo, A., Frosch, M. P., Masliah, E., and Hyman, B. T. (2011). Neuropathological alterations in Alzheimer disease. *Cold Spring Harb. Perspect. Med.* 1, a006189.

Seto, E., and Yoshida, M. (2014). Erasers of histone acetylation: the histone deacetylase enzymes. *Cold Spring Harb Perspect Biol* 6, a018713.

Sevigny, J., Chiao, P., Bussière, T., Weinreb, P. H., Williams, L., Maier, M., et al. (2016). The antibody aducanumab reduces Aβ plaques in Alzheimer's disease. *Nature* 537, 50–56.

Sharp, D. J., and Ross, J. L. (2012). Microtubule-severing enzymes at the cutting edge. *J. Cell Sci.* 125, 2561–2569.

Shi, K., Jiang, Q., Li, Z., Shan, L., Li, F., An, J. J., et al. (2013). Sodium selenite alters microtubule assembly and induces apoptosis in vitro and in vivo. *J. Hematol. Oncol.* 6, 7.

Shultz, S. R., Wright, D. K., Zheng, P., Stuchbery, R., Liu, S. J., Sashindranath, M., et al. (2015). Sodium selenate reduces hyperphosphorylated tau and improves outcomes after traumatic brain injury. *Brain* 138, 1297–1313.

Siemers, E. R., Sundell, K. L., Carlson, C., Case, M., Sethuraman, G., Liu-Seifert, H., et al. (2016). Phase 3 solanezumab trials: secondary outcomes in mild Alzheimer's disease patients. *Alzheimer's Dement.* 12, 110–120.

Sigurdsson, E. M. (2016). Tau immunotherapy. *Neurodegener. Dis.* 16, 34–38.

Šimić, G., Leko, M., Wray, S., Harrington, C., Delalle, I., Jovanov-Milošević, N., et al. (2016). Tau protein hyperphosphorylation and aggregation in Alzheimer's disease and other tauopathies, and possible neuroprotective strategies. *Biomolecules* 6, 6.

Simões-Pires, C., Zwick, V., Nurisso, A., Schenker, E., Carrupt, P.-A., and Cuendet, M. (2013). HDAC6 as a target for neurodegenerative diseases: what makes it different from the other HDACs? *Mol. Neurodegener.* 8, 7.

Simon, D. J., Weimer, R. M., McLaughlin, T., Kallop, D., Stanger, K., Yang, J., et al. (2012). A caspase cascade regulating developmental axon degeneration. *J. Neurosci.* 32, 17540–17540.

Snyder, J. P., Nettles, J. H., Cornett, B., Downing, K. H., and Nogales, E. (2001). The binding conformation of Taxol in β-tubulin: A model based on electron crystallographic density. *PNAS* 98, 5312–5316.

Sohn, P. D., Tracy, T. E., Son, H.-I., Zhou, Y., Leite, R. E. P., Miller, B. L., et al. (2016). Acetylated tau destabilizes the cytoskeleton in the axon initial segment and is mislocalized to the somatodendritic compartment. *Mol. Neurodegener.* 11, 47.

Solito, E., and Sastre, M. (2012). Microglia function in Alzheimer's disease. *Front. Pharmacol.* 3, 14.

Song, W., Cho, Y., Watt, D., and Cavalli, V. (2015). Tubulin-tyrosine ligase (TTL)-mediated increase in tyrosinated α-tubulin in injured axons is required for retrograde injury signaling and axon regeneration. *J. Biol. Chem.* 290, 14765–14775.

Song, Y., and Brady, S. T. (2015). Posttranslational modifications of tubulin: pathways to

functional diversity of microtubules. *Trends Cell Biol* 25, 125–136.

Song, Y., Kirkpatrick, L. L., Schilling, A. B., Helseth, D. L., Chabot, N., Keillor, J. W., et al. (2013). Transglutaminase and polyamination of tubulin: posttranslational modification for stabilizing axonal microtubules. *Neuron* 78, 109–123.

Sontag, E., Nunbhakdi-Craig, V., Lee, G., Bloom, G. S., and Mumby, M. C. (1996). Regulation of the phosphorylation state and microtubule-binding activity of tau by protein phosphatase 2A. *Neuron* 17, 1201–1207.

Sontag, J.-M., and Sontag, E. (2014). Protein phosphatase 2A dysfunction in Alzheimer's disease. *Front. Mol. Neurosci.* 7, 1–10.

Sontag, J. M., Nunbhakdi-Craig, V., White, C. L., Halpain, S., and Sontag, E. (2012). The protein phosphatase PP2A/Bα binds to the microtubule-associated proteins tau and MAP2 at a motif also recognized by the kinase fyn: implications for tauopathies. *J. Biol. Chem.* 287, 14984–14993.

Soutar, M. P., Thornhill, P., Cole, A. R., and Sutherland, C. (2009). Increased CRMP2 phosphorylation is observed in Alzheimer's disease; does this tell us anything about disease development? *Curr. Alzheimer Res.* 6, 269–278.

Spires-Jones, T. L., and Hyman, B. T. (2014). The intersection of amyloid beta and tau at synapses in Alzheimer's disease. *Neuron* 82, 756–771.

Spriggs, D., Dupont, J., Pezzulli, S., Larkin, J., Johnson, R. G., Hannah, A. L., et al. (2003). KOS-862 (epothilone D): Phase I dose escalating and pharmacokinetic (PK) study in patients with advanced malignancies. *Proc. Am. Soc. Clin. Oncol.* 22, 894a.

Stamer, K., Vogel, R., Thies, E., Mandelkow, E., and Mandelkow, E. M. (2002). Tau blocks traffic of organelles, neurofilaments, and APP vesicles in neurons and enhances oxidative stress. *J. Cell Biol.* 156, 1051–1063.

Stanford, P. M., Halliday, G. M., Brooks W. S., Kwok, J. B., Storey, C. E., Creasy H., Morris,

J. G., Fulham, M. J., Schofield, P.R. (2000). Progressive supranuclear palsy pathology caused by a novel silent mutation in exon 10 of the tau gene: expansion of the disease phenotype caused by tau gene mutations. *Brain* 123 (part 5), 880-893.

Stokin, G. B., and Goldstein, L. S. (2006). Axonal transport and Alzheimer's disease. *Annu. Rev. Biochem.* 75, 607–627.

Stokin, G. B., Lillo, C., Falzone, T. L., Brusch, R. G., Rockenstein, E., Mount, S. L., et al. (2005). Axonopathy and transport deficits early in the pathogenesis of Alzheimer's disease. *Science (80-.).* 307, 1282–1288.

Sudo, H., and Baas, P. W. (2010). Acetylation of microtubules influences their sensitivity to severing by katanin in neurons and fibroblasts. *J. Neurosci.* 30, 7215–26.

Sudo, H., and Baas, P. W. (2011). Strategies for diminishing katanin-based loss of microtubules in tauopathic neurodegenerative diseases. *Hum. Mol. Genet.* 20, 763–778.

Sun, X., Tuo, Q., Liuyang, Z., Xie, A., Feng, X., Yan, X., et al. (2016). Extrasynaptic NMDA receptor-induced tau overexpression mediates neuronal death through suppressing survival signaling ERK phosphorylation. *Cell Death Dis.* 7, e2449.

Suraweera, A., O'Byrne, K., and Richard, D. (2018). Combination therapy with histone deacetylase inhibitors (HDACi) for the treatment of cancer: achieving the full therapeutic potential of HDACi. *Front. Oncol.* 8, 92.

Suzuki, K., and Koike, T. (2007). Mammalian Sir2-related protein (SIRT) 2-mediated modulation of resistance to axonal degeneration in slow Wallerian degeneration mice: a crucial role of tubulin deacetylation. *Neuroscience* 147, 599–612.

Taft, W. C., Yang, K., Dixon, E., and Hayes, R. L. (1992). Microtubule-associated protein 2 levels decrease in hippocampus following traumatic brain injury. *J. Neurotrauma*.

Taghian, K., Lee, J. Y., and Petratos, S. (2012). Phosphorylation and cleavage of the family of collapsin response mediator proteins may play a central role in neurodegeneration

after CNS trauma. *J. Neurotrauma* 29, 1728–1735.

Tan, M., Cha, C., Ye, Y., Zhang, J., Li, S., Wu, F., et al. (2015). CRMP4 and CRMP2 interact to coordinate cytoskeleton dynamics, regulating growth cone development and axon elongation. *Neural Plast.* 2015.

Tang-Schomer, M. D., Patel, A. R., Baas, P. W., and Smith, D. H. (2010). Mechanical breaking of microtubules in axons during dynamic stretch injury underlies delayed elasticity, microtubule disassembly, and axon degeneration. *FASEB J.* 24, 1401–1410.

Tao, J., Feng, C., and Rolls, M. M. (2016). The microtubule-severing protein fidgetin acts after dendrite injury to promote their degeneration. *J. Cell Sci.* 129, 3274 LP-3281.

Taylor, A. M., Blurton-Jones, M., Rhee, S. W., Cribbs, D. H., Cotman, C. W., and Jeon, N. L. (2005). A microfluidic culture platform for CNS axonal injury, regeneration and transport. *Nat. Methods* 2, 599–605.

Taylor, A., Rhee, S., and Jeon, N. (2006). Microfluidic chambers for cell migration and neuroscience research. *Methods Mol Biol* 321, 167–177.

Taylor, G. T., Lerch, S., and Chourbaji, S. (2017). Marble burying as compulsive behaviors in male and female mice. *Acta Neuropathol. Exp.* 77, 254–260.

Terry, R. D., Masliah, E., Salmon, D. P., Butters, N., DeTeresa, R., Hill, R., et al. (1991). Physical basis of cognitive alterations in Alzheimer's disease: synapse loss is the major correlate of cognitive impairment. *Ann. Neurol.* 30, 572–580.

Thomas, A., Burant, A., Bui, N., Graham, D., Yuva-Paylor, L. A., and Paylor, R. (2009). Marble burying reflects a repetitive and perseverative behavior more than novelty-induced anxiety. *Psychopharmacology (Berl).* 204, 361–373.

Trojanowski, J. Q., Smith, A. B., Huryn, D., and Lee, V. M. (2005). Microtubule-stabilising drugs for therapy of Alzheimer's disease and other neurodegenerative disorders with axonal transport impairments. *Expert Opin. Pharmacother.* 6, 683–686.

Uchida, S., and Shumyatsky, G. (2016). Deceivingly dynamic: learning-dependent changes in stathmin and microtubules. *Neurobiol. Learn. Mem.* 33, 557–573.

Ulloa, L., Montejo de Garcini, E., Gómez-Ramos, P., Morán, M. A., and Avila, J. (1994). Microtubule-associated protein MAP1B showing a fetal phosphorylation pattern is present in sites of neurofibrillary degeneration in brains of Alzheimer's disease patients. *Mol. Brain Res.* 26, 113–122.

Unsain, N., Bordenave, M. D., Martinez, G. F., Jalil, S., Von Bilderling, C., Barabas, F. M., et al. (2018). Remodeling of the Actin/Spectrin Membrane-associated Periodic Skeleton, Growth Cone Collapse and F-Actin Decrease during Axonal Degeneration. *Sci. Rep.* 8, 1–16.

Uribe, V., Wong, B. K. Y., Graham, R. K., Cusack, C. L., Skotte, N. H., Pouladi, M. A., et al. (2012). Rescue from excitotoxicity and axonal degeneration accompanied by age-dependent behavioral and neuroanatomical alterations in caspase-6-deficient mice. *Hum. Mol. Genet.* 21, 1954–1967.

Utreras, E., Jiménez-Mateos, E., Contreras-Vallejos, E., Tortosa, E., Pérez, M., Rojas, S., et al. (2008). Microtubule-associated protein 1B interaction with tubulin tyrosine ligase contributes to the control of microtubule tyrosination. *Dev Neurosci* 30, 200–210.

Valdinocci, D., Grant, G. D., Dickson, T. C., and Pountney, D. L. (2018). Epothilone D inhibits microglia-mediated spread of alpha-synuclein aggregates. *Mol Cel Neuro* 89, 80-94.

Valenstein, M. L., and Roll-Mecak, A. (2016). Graded control of microtubule severing by tubulin glutamylation. *Cell* 164, 911–921.

Van Den Bosch, L., Van Damme, P., Bogaert, E., and Robberecht, W. (2006). The role of excitotoxicity in the pathogenesis of amyotrophic lateral sclerosis. *Biochim. Biophys. Acta - Mol. Basis Dis.* 1762, 1068–1082.

van Eersel, J., Ke, Y. D., Liu, X., Delerue, F., Kril, J. J., Gotz, J., et al. (2010). Sodium selenate mitigates tau pathology, neurodegeneration, and functional deficits in Alzheimer's disease models. *Proc. Natl. Acad. Sci.* 107, 13888–13893.

Van Kanegan, M., and Strack, S. (2009). The protein phosphatase 2A regulatory subunits B'beta and B'delta mediate sustained TrkA neurotrophin receptor autophosphorylation and neuronal differentiation. *Mol Cell Biol* 29, 662–674.

Vandenberghe, R., Rinne, J. O., Boada, M., Katayama, S., Scheltens, P., Vellas, B., et al. (2016). Bapineuzumab for mild to moderate Alzheimer's disease in two global, randomized, phase 3 trials. *Alzheimers. Res. Ther.* 8, 18.

Vargas, M. E., and Barres, B. A. (2007). Why Is Wallerian degeneration in the CNS so slow? *Annu. Rev. Neurosci.* 30, 153–179.

Varidaki, A., Hong, Y., and Coffey, E. T. (2018). Repositioning microtubule stabilizing drugs for brain disorders. *Front. Cell. Neurosci.* 12, 226.

Vassar, R. (2014). BACE1 inhibitor drugs in clinical trials for Alzheimer's disease. *Alzheimer's Res. Ther.* 6, 1–14.

Velazquez, R., Ferreira, E., Tran, A., Turner, E., Belfiore, R., Branca, C., et al. (2018). Acute tau knockdown in the hippocampus of adult mice causes learning and memory deficits. *Aging Cell* 10, e12775.

Vemu, A., Szczesna, E., Zehr, E., Spector, J., Grigorieff, N., Deaconescu, A., et al. (2018). Severing enzymes amplify microtubule arrays through lattice GTP-tubulin incorporation. *Science (80-.).* 361, pii: eaau1504.

Verghese, P. B., Castellano, J. M., Garai, K., Wang, Y., Jiang, H., Shah, A., et al. (2013). ApoE influences amyloid- (A) clearance despite minimal apoE/A association in physiological conditions. *Proc. Natl. Acad. Sci.* 110, E1807–E1816.

Verstraelen, P., Detrez, J., Verschuuren, M., Kuijlaars, J., Nuydens, R., Timmermans, J., et

al. (2017). Dysregulation of microtubule stability impairs morphofunctional connectivity in primary neuronal networks. *Front. Cell. Neurosci.* 11, 173.

Vickers, J. C., Chin, D., Edwards, A. M., Sampson, V., Harper, C., and Morrison, J. (1996). Dystrophic neurite formation associated with age-related beta amyloid deposition in the neocortex: clues to the genesis of neurofibrillary pathology. *Exp Neurol* 141, 1–11.

Vickers, J. C., King, A. E., Woodhouse, A., Kirkcaldie, M. T. K., Staal, J. A., McCormack, G. H., et al. (2009). Axonopathy and cytoskeletal disruption in degenerative diseases of the central nervous system. *Brain Res. Bull.* 80, 217–223.

Vogelsberg-Ragaglia, V., Schuck, T., Trojanowski, J. Q., and Lee, V. M. Y. (2001). PP2A mRNA expression is quantitatively decreased in Alzheimer's disease hippocampus. *Exp. Neurol.* 168, 402–412.

Voronkov, M., Braithwaite, S. P., and Stock, J. B. (2011). Phosphoprotein phosphatase 2A: a novel druggable target for Alzheimer's disease. *Futur. Med. Chem.* 3, 821–833.

Vossel, K. A., Tartaglia, M. C., Nygaard, H. B., Zeman, A. Z., and Miller, B. L. (2017). Epileptic activity in Alzheimer's disease: causes and clinical relevance. *Lancet. Neurol.* 16(4), 311-322.

Vu, H. T., Akatsu, H., Hashizume, Y., Setou, M., and Ikegami, K. (2017). Increase in α-tubulin modifications in the neuronal processes of hippocampal neurons in both kainic acid-induced epileptic seizure and Alzheimer's disease. *Sci. Rep.* 7, 1–14.

Walters, G. B., Gustafsson, O., Sveinbjornsson, G., Eiriksdottir, V. K., Agustsdottir, A. B., Jonsdottir, G. A., et al. (2018). MAP1B mutations cause intellectual disability and extensive white matter deficit. *Nat. Commun.* 9.

Wang, J. T., Medress, Z. A., and Barres, B. A. (2012). Axon degeneration: molecular mechanisms of a self-destruction pathway. *J. Cell Biol.* 196, 7–18.

Wang, J., Tung, Y. C., Wang, Y., Li, X. T., Iqbal, K., and Grundke-Iqbal, I. (2001).

Hyperphosphorylation and accumulation of neurofilament proteins in Alzheimer disease brain and in okadaic acid-treated SY5Y cells. *FEBS Lett.* 507, 81–87.

Wang, J., Xia, Y., Grundke-Iqbal, I., and Iqbal, K. (2013). Abnormal hyperphosphorylation of tau: sites, regulation, and molecular mechanism of neurofibrillary degeneration. *J Alzheimers Dis* 33, S123-139.

Wang, Q., Yu, S., Simonyl, A., Sun, G., and Sun, A. (2005). Kainic acid-mediated excitotoxicity as a model for neurodegeneration. *Mol Neurobiol* 31, 3–16.

Wang, R., and Reddy, P. (2017). Role of glutamate and NMDA receptors in Alzheimer's disease. *J Alzheimers Dis* 57, 1041–1048.

Wang, Y., Gu, Z., Cao, Y., Liang, Z., Han, R., Bennett, M., et al. (2006). Lysosomal enzyme cathepsin B is involved in kainic acid-induced excitotoxicity in rat striatum. *Brain Res* 107, 245–249.

Wang, Y., Han, R., Liang, Z., Wu, J., Zhang, X., Gu, Z., et al. (2008). An autophagic mechanism is involved in apoptotic death of rat striatal neurons induced by the non-N-methyl-D-aspartate receptor agonist kainic acid. *Autophagy* 4, 214–226.

Wang, Z., Leng, Y., Wang, J., Liao, H.-M., Bergman, J., Leeds, P., et al. (2016). Tubastatin A, an HDAC6 inhibitor, alleviates stroke-induced brain infarction and functional deficits: potential roles of α-tubulin acetylation and FGF-21 up-regulation. *Sci. Rep.* 6, 19626.

Wani, M. C., Taylor, H. L., Wall, M. E., Coggon, P., and McPhail, A. T. (1971). Plant antitumor agents. VI. The isolation and structure of taxol, a novel antileukemic and antitumor agent from Taxus brevifolia. *J. Am. Chem. Soc.* 93, 2325–2327.

Watamura, N., Toba, J., Yoshii, A., Nikkuni, M., and Oshima, T. (2016). Colocalization of phosphorylated forms of WAVE1, CRMP2, and tau in Alzheimer's disease model mice: Involvement of Cdk5 phosphorylation and the effect of ATRA treatmen. *J Neurosci Res*

94, 15–26.

Watts, R. J., Hoopfer, E. D., and Luo, L. (2003). Axon pruning during Drosophila metamorphosis: evidence for local degeneration and requirement of the ubiquitin-proteasome system. *Neuron* 38, 871–885.

Watts, R. J., Schuldiner, O., Perrino, J., Larsen, C., and Luo, L. (2004). Glia engulf degenerating axons during developmental axon pruning. *Curr. Biol.* 14, 678–684.

Webster, D., Wehland, J., Weber, K., and Borisy, G. (1990). Detyrosination of alpha tubulin does not stabilize microtubules in vivo. *J. Cell Biol.* 111, 113–122.

Weller, R. ., Massey, A., Juo, Y.-M., and Roher, A. E. (2000). Cerebral amyloid angiopathy: accumulation of Abeta in interstitial fluid drainage pathways in Alzheimer's disease. *Ann. N. Y. Acad. Sci.* 153, 725–733.

West, T., Hu, Y., Verghese, P. B., Bateman, R. J., Braunstein, J. B., Fogelman, I., et al. (2017). Preclinical and clinical development of ABBV-8E12, a humanized anti-tau antibody, for treatment of Alzheimer's disease and other tauopathies. *J. Prev. Alzheimer's Dis.* 4, 236–241.

Wilden, P. A., and Kahn, C. R. (1994). The level of insulin receptor tyrosine kinase activity modulates the activities of phosphatidylinositol 3-kinase. *Mol. Endocirnology* 8, 558–567.

Williams, P., Nishu, K., and Rahman, M. (2011). HDAC inhibitor trichostatin A suppresses osteoclastogenesis by upregulating the expression of C/EBP-β and MKP-1. *Ann N Y Acad Sci* 1240, 18–25.

Williamson, R., Van Aalten, L., Mann, D. M. A., Platt, B., Plattner, F., Bedford, L., et al. (2011). CRMP2 hyperphosphorylation is characteristic of Alzheimer's disease and not a feature common to other neurodegenerative diseases. *J. Alzheimer's Dis.* 27, 615–625.

Wirths, O., and Bayer, T. A. (2010). Neuron loss in transgenic mouse models of Alzheimer's

disease. *Int. J. Alzheimers. Dis.* 2010, 6–11.

Wischik, C. M., Harrington, C. R., and Storey, J. M. D. (2014). Tau-aggregation inhibitor therapy for Alzheimer's disease. *Biochem. Pharmacol.* 88, 529–539.

Witte, H., Neukirchen, D., and Bradke, F. (2008). Microtubule stabilization specifies initial neuronal polarization. *J. Cell Biol.* 180, 619.

Wloga, D., and Gaertig, J. (2010). Post-translational modifications of microtubules. *J. Cell Sci.* 123, 3447–3455.

Wolfe, M. S. (2009). Tau mutations in neurodegenerative diseases. *J. Biol. Chem.* 284, 6021–6025.

Wu, H. Y., Hudry, E., Hashimoto, T., Kuchibholta, K., Rozkalne, A., Fan, Z., et al. (2010). Amyloid β induces the morphological neurodegenerative triad of spine loss, dendritic simplification, and neuritic dystrophies through calcineurin activation. *J. Neurosci.* 30, 2636–2649.

Wyss-Coray, T., and Rogers, J. (2012). Inflammation in Alzheimer disease—a brief review of the basic science and clinical literature. *Cold Spring Harb. Perspect. Med.* 2, a006346.

Xie, R., Nguyen, S., Mckeehan, W. L., and Liu, L. (2010). Acetylated microtubules are required for fusion of autophagosomes with lysosomes. *BMC Cell Biol.* 11, 89.

Xu, K., Dai, X., Huang, H., and Jiang, Z. (2011). Targeting HDACs: a promising therapy for Alzheimer's disease. *Oxid. Med. Cell. Longev.* 2011, 143269.

Xu, Z., Schaedel, L., Portran, D., Aguilar, A., Gaillard, J., Marinkovich, M. P., et al. (2017). Microtubules acquire resistance from mechanical breakage through intralumenal acetylation. *Science (80-.).* 356, 328–332.

Yabe, I., Sasaki, H., Tashiro, K., Matsuura, T., Takegami, T., and Satoh, T. (2002). Spastin gene mutation in Japanese with hereditary spastic paraplegia. *J Med Genet* 39, e46.

Yadav, P., Selvaraj, B. T., Bender, F. L. P., Behringer, M., Moradi, M., Sivadasan, R., et al.

(2016). Neurofilament depletion improves microtubule dynamics via modulation of Stat3/stathmin signaling. *Acta Neuropathol.* 132, 93–110.

Yamada, K. (2017). Extracellular tau and its potential role in the propagation of tau pathology. *Front. Neurosci.* 11, 667.

Yan, X. X., Ma, C., Gai, W. P., Cai, H. B., and Luo, X. G. (2014). Can BACE1 inhibition mitigate early axonal pathology in neurological diseases? *J. Alzheimers Dis.* 38, 705–718.

Yang, M., Wu, M., Xia, P., Wang, C., Yan, P., Gao, Q., et al. (2012). The role of microtubule-associated protein 1B in axonal growth and neuronal migration in the central nervous system. *Neural Regen. Res.* 7, 842–848.

Yang, S., Zhang, R., Wang, G., and Zhang, Y. (2017a). The development prospection of HDAC inhibitors as a potential therapeutic direction in Alzheimer's disease. *Transl Neurodegener* 6, 19.

Yang, W., Chauhan, A., Wegiel, J., Kuchna, I., Gu, F., and Chauhan, V. (2014). Effect of trichostatin A on gelsolin levels, proteolysis of amyloid precursor protein, and amyloid beta-protein load in the brain of transgenic mouse model of Alzheimer's disease. *Curr Alzheimer Res* 11, 1002–1011.

Yang, Z., Kuboyama, T., and Tohda, C. (2017b). A systematic strategy for discovering a therapeutic drug for Alzheimer's disease and its target molecule. *Front. Pharmacol.* 8, 340.

Yin, Y., Wang, Y., Chen, L., Han, S., Zhao, L., Luo, Y., et al. (2013). Tat-collapsin response mediator protein 2 (CRMP2) increases the survival of neurons after NMDA excitotoxity by reducing the cleavage of CRMP2. *Neurochem. Res.* 38, 2095–2104.

Yoo, Y.-E., and Ko, C.-P. (2011). Treatment with trichostatin A initiated after disease onset delays disease progression and increases survival in a mouse model of amyotrophic

lateral sclerosis. *Exp. Neurol.* 231, 147–159.

Yoon, S. S., and Jo, S. A. (2012). Mechanisms of amyloid-β peptide clearance: potential therapeutic targets for Alzheimer's disease. *Biomol. Ther.* 20, 245–255.

Yoshimura, T., and Rasband, M. (2014). Axon initial segments: diverse and dynamic neuronal compartments. *Curr Opin Neurobiol* 27, 96–102.

Yoshiyama, Y., Higuchi, M., Zhang, B., Huang, S. M., Iwata, N., Saido, T. C., et al. (2007). Synapse loss and microglial activation precede tangles in a P301S tauopathy mouse model. *Neuron* 53, 337–351.

Yu, D., Pessino, V., Kuei, S., and Valentine, M. T. (2013). Mechanical and functional properties of epothilone-stabilized microtubules. *Cytoskeleton* 70, 74–84.

Yu, F., and Schuldiner, O. (2014). Axon and dendrite pruning in Drosophila. *Curr. Opin. Neurobiol.* 27, 192–198.

Yu, W., Qiang, L., Solowska, J., Karabay, A., Korulu, S., and Baas, P. (2008). The microtubule-severing proteins spastin and katanin participate differently in the formation of axonal branches. *Mol. Biol. Cell* 19, 1485–1498.

Yu, Z., Yang, L., Yang, Y., Chen, S., Sun, D., Xu, H., et al. (2018). Epothilone B benefits nigral dopaminergic neurons by attenuating microglia activation in the 6-hydroxydopamine lesion mouse model of Parkinson's disease. *Front. Cell. Neurosci.* 12, 324.

Yuan, A., and Nixon, R. A. (2016). Specialized roles of neurofilament proteins in synapses: relevance to neuropsychiatric disorders. *Brain Res. Bull.* 126, 334–346.

Yuan, J., Lipinski, M., and Degterev, A. (2003). Diversity in the mechanisms of neuronal cell death. *Neuron* 40, 401–413.

Zajkowski, T., Nieznanska, H., and Nieznanski, K. (2015). Stabilization of microtubular cytoskeleton protects neurons from toxicity of N-terminal fragment of cytosolic prion

protein. *Biochim. Biophys. Acta* 1853, 2228–2239.

Zarubin, T., and Han, J. (2005). Activation and signaling of the p38 MAP kinase pathway. *Cell. Res.* 15(1), 11-18.

Zempel, H., Luedtke, J., Kumar, Y., Biernat, J., Dawson, H., Mandelkow, E., et al. (2013). Amyloid-β oligomers induce synaptic damage via tau-dependent microtubule severing by TTLL6 and spastin. *EMBO J.* 32, 2920–37.

Zempel, H., and Mandelkow, E.-M. (2015). Tau missorting and spastin-induced microtubule disruption in neurodegeneration: Alzheimer disease and Hereditary Spastic Paraplegia. *Mol. Neurodegener.* 10, 68.

Zhai, Q., Wang, J., Kim, A., Liu, Q., Watts, R., Hoopfer, E., et al. (2003). Involvement of the ubiquitin-proteasome system in the early stages of Wallerian degeneration. *Neuron* 39, 217–225.

Zhang, B., Carroll, J., Trojanowski, J. Q., Yao, Y., Iba, M., Potuzak, J. S., et al. (2012a). The microtubule-stabilizing agent, epothilone D, reduces axonal dysfunction, neurotoxicity, cognitive deficits, and Alzheimer-like pathology in an interventional study with aged tau transgenic mice. *J. Neurosci.* 32, 3601–3611.

Zhang, B., Maiti, A., Shively, S., Lakhani, F., McDonald-Jones, G., Bruce, J., et al. (2005). Microtubule-binding drugs offset tau sequestration by stabilizing microtubules and reversing fast axonal transport deficits in a tauopathy mode. *Proc. Natl. Acad. Sci.* 102, 227–231.

Zhang, B., Yao, Y., Cornec, A. S., Oukoloff, K., James, M. J., Koivula, P., et al. (2018). A brain-penetrant triazolopyrimidine enhances microtubule-stability, reduces axonal dysfunction and decreases tau pathology in a mouse tauopathy model. *Mol. Neurodegener.* 13, 59.

Zhang, F., Su, B., Wang, C., Siedlak, S. L., Mondragon-Rodriguez, S., Lee, H., et al. (2015a).

Posttranslational modifications of α-tubulin in Alzheimer disease. *Transl. Neurodegener.* 4, 9.

Zhang, H., Dai, X., Qi, Y., He, Y., Du, W., and Pang, J. (2015b). Histone deacetylases inhibitors in the treatment of retinal degenerative diseases: overview and perspectives. *J Ophthalmol* 2015, 250812.

Zhang, H., Ma, Q., Zhang, Y., and Xu, H. (2012b). Proteolytic processing of APP. *J Neurochem.* 120, 9–21.

Zhang, J.-N., and Koch, J. (2017). Collapsin response mediator protein-2 plays a major protective role in acute axonal degeneration. *Neural Regen. Res.* 12, 692.

Zhang, J.-N., Michel, U., Lenz, C., Friedel, C. C., Köster, S., D'Hedouville, Z., et al. (2016). Calpain-mediated cleavage of collapsin response mediator protein-2 drives acute axonal degeneration. *Sci. Rep.* 6, 37050.

Zhang, Y., Tian, Q., Zhang, Q., Zhou, X., Liu, S., and Wang, J. (2009). Hyperphosphorylation of microtubule-associated tau protein plays dual role in neurodegeneration and neuroprotection. *Pathophysiology* 16, 311–316.

Zhang, Z. Y., and Schluesener, H. J. (2013). Oral administration of histone deacetylase inhibitor MS-275 Ameliorates neuroinflammation and cerebral amyloidosis and improves behavior in a mouse model. *J. Neuropathol. Exp. Neurol.* 72, 178–185.

Zhao, Y., Mu, X., and Du, G. (2016). Microtubule-stabilizing agents: new drug discovery and cancer therapy. *Pharmacol. Ther.* 162, 134–143.

Zhu, J., Zheng, X. Y., Zhang, H. L., and Luo, Q. (2011). Kainic acid-induced neurodegenerative model: potentials and limitations. *J. Biomed. Biotechnol.* 2011, Article ID 457079.

Zilberman, Y., Ballestrem, C., Carramusa, L., Mazitschek, R., Khochbin, S., and Bershadsky, A. (2009). Regulation of microtubule dynamics by inhibition of the tubulin deacetylase

HDAC6. *J. Cell Sci.*

Chapter 8

Appendices

8 APPENDICES

8.1 COMMON LABORATORY REAGENTS

0.01 M Phosphate Buffered Saline (PBS) – 1.0 L

850 mL MilliQ® water

100 mL 90.0 gL^{-1} Sodium chloride

40 mL 28.0 gL^{-1} Di-sodium hydrogen orthophosphate

10 mL 31.2 gL^{-1} Sodium di-hydrogen orthophosphate ($NaH_2PO_4.2H_2O$; Ajax, Australia)

4% Paraformaldehyde – 1.0 L

40 g granulated paraformaldehyde (PFA)

500 mL MilliQ® water

400 mL 28.0 gL^{-1} Na_2HPO

100 mL 31.2 gL^{-1} $NaH_2PO_4.2H_2O$

1.0 M NaOH & 1.0 M HCl to pH

Heat MilliQ® to 80°C, add granulated PFA and 5 drops of NaOH. Stir until PFA dissolved, add $NaH_2PO_4.H_2O$ and Na_2HPO. Filter and pH to 7.4.

Tissue Storage Solution – 500 mL

500 mL 0.01 M PBS

0.5 g sodium azide

Cryoprotectant Solution (30% sucrose) – 500 mL

500 mL 0.01 M PBS

150 g sucrose

0.02% sodium azide

Initial Plating Media – 500 mL

500 mL Neurobasal medium
2% v/v B27 supplement
10% v/v fetal calf serum
0.5 mM glutamine
25 mM glutamate
1% v/v antibiotic/antimycotic

Subsequent Plating Media – 500 mL

500 mL Neurobasal medium
2% v/v B27 supplement
0.5 mM glutamine
1% v/v antibiotic/antimycotic

8.2 STATISTICAL ANALYSIS

Table 8.1 Statistical analysis for chapter 3

Figure Number	Figure Name	Panel	n	Statistics	p-value	95% Confidence Interval for Mean	
Figure 3.1	The effect of epothilone D treatment on weight in APP/PS1 mice	A	9 per group	Two-way ANOVA	0.0684		
Figure 3.2	The effect of epothilone D treatment on behaviour and cognition in APP/PS1 mice	A	9 per group	Two-way ANOVA	0.0937		
		B	9 per group	Two-way ANOVA, Tukey's post hoc test	0.0370	-2.680	-0.07161
		C	9 per group	Two-way ANOVA, Tukey's post hoc test	0.0367	-1607	-43.18
		D	9 per group	Two-way ANOVA	0.6550		
		F	9 per group	Two-way ANOVA	0.2846		
		G	9 per group	Two-way ANOVA	0.3820		
Figure 3.3	The effect of epothilone D treatment on	A	9 per group	Two-way ANOVA	0.1137		

Figure Number	Figure Name	Panel	n	Statistics	p-value	95% Confidence Interval for Mean	
	cognition in APP/PS1 mice						
		B	9 per group	Two-way ANOVA	0.2367		
		C	9 per group	Two-way ANOVA	0.9506		
		D	9 per group	Two-way ANOVA	0.7370		
Figure 3.4	Axonal pathology in epothilone D treated 15-month old APP/PS1 mice	A	6-7 per group	Unpaired t-test, two-tailed	0.7853		
		B	6-7 per group	Unpaired t-test, two-tailed	0.6419		
		C	6-7 per group	Unpaired t-test, two-tailed	0.5528		
Figure 3.5	Axonal pathology in epothilone D treated 15-month old APP/PS1 mice	A	3-4 per group	Non-parametric Kruskal-Wallis test, Dunn's multiple comparisons test	0.0204		
		B	3-4 per group	Non-parametric Kruskal-Wallis test, Dunn's multiple comparisons test	0.2654		
		C	3-4 per group	Non-parametric Kruskal-Wallis test, Dunn's multiple comparisons test	0.4812		

Figure Number	Figure Name	Panel	n	Statistics	p-value	95% Confidence Interval for Mean	
Figure 3.6	Synapse pathology in epothilone D treated 15-month-old APP/PS1 mice	B	7-8 per group	Unpaired t-test, two-tailed	0.6482		
		C	7-8 per group	Unpaired t-test, two-tailed	0.2995		
		D	7-8 per group	Unpaired t-test, two-tailed	0.7967		
		F	7-8 per group	Unpaired t-test, two-tailed	0.9438		
		G	7-8 per group	Unpaired t-test, two-tailed	0.5462		
		H	7-8 per group	Unpaired t-test, two-tailed	0.7086		
Figure 3.7	Western blot analysis of synapses in epothilone D treated 15-month-old APP/PS1 mice	A	3-4 per group	Non-parametric Kruskal-Wallis test, Dunn's multiple comparisons test	0.0176		
		B	3-4 per group	Non-parametric Kruskal-Wallis test, Dunn's multiple comparisons test	0.1191		
		C	3-4 per group	Non-parametric Kruskal-Wallis test, Dunn's multiple comparisons test	0.1322		
		D	3-4 per group	Non-parametric Kruskal-Wallis test,	0.6919		

Figure Number	Figure Name	Panel	n	Statistics	p-value	95% Confidence Interval for Mean	
				Dunn's multiple comparisons test			
Figure 3.8	The effect of epothilone D on amyloid pathology in 15-month-old APP/PS1 mice	C	7-8 per group	Unpaired t-test, two-tailed	0.7475		
		D	7-8 per group	Unpaired t-test, two-tailed	0.5603		
		E	7-8 per group	Unpaired t-test, two-tailed	0.8623		

Table 8.2 Statistical analysis for chapter 4

Figure Number	Figure Name	Panel	n	Statistics	p-value	Mean Difference	95% Confidence Interval for Mean	
Figure 4.1	Axon degeneration and loss in microfluidic chambers after kainic acid treatment	A	2 coverslips from 5 culture days per treatment	One-way ANOVA, Tukey's post hoc test	0.0002	-6.744 4.331 7.721	-10.90 0.1766 3.567	-2.589 8.486 11.88
		B	2 coverslips from 5 culture days per treatment	One-way ANOVA, Tukey's post hoc test	0.0003	-20.85 -26.66	-34.57 -40.37	-7.139 -12.94
Figure 4.2	Changes to microtubule post-translational modifications after kainic acid treatment	A	3 coverslips from 4 culture days per treatment	One-way ANOVA, Tukey's post hoc test	0.0005	41.25 47.05	14.66 20.46	67.84 73.64
		B	3 coverslips from 4 culture days per treatment	One-way ANOVA	0.6014			
		C	Pooled from 2-3 chambers per treatment from 4 culture days	Unpaired t-test, two-tailed	0.0422	-19.53	-38.10	-0.9581
		D	Pooled from 2-3 chambers per	Unpaired t-test, two-tailed	0.3913	4.244	-6.997	15.48

Figure Number	Figure Name	Panel	n	Statistics	p-value	Mean Difference	95% Confidence Interval for Mean	
			treatment from 4 culture days					
		E	Pooled from 2-3 chambers per treatment from 4 culture days	Unpaired t-test, two-tailed	0.0164	-49.95	-87.00	-12.90
Figure 4.3	Effect of trichostatin A on microtubule acetylation following kainic acid treatment	A	2-3 coverslips from 5 culture days per treatment	Non-parametric Kruskal-Wallis test, Dunn's multiple comparisons test	0.0001	-30.00 -21.86		
		B	2-3 coverslips from 5 culture days per treatment	Non-parametric Kruskal-Wallis test, Dunn's multiple comparisons test	0.0005	18.72 25.06		
		C	3 coverslips from 5 culture days per treatment	Non-parametric Kruskal-Wallis test, Dunn's multiple comparisons test	0.2401			
Figure 4.4	Effect of trichostatin A on microtubule acetylation following kainic acid treatment	A	3 coverslips from 5 culture days per treatment	Two-way ANOVA, Tukey's post hoc test	0.0001	26.22 -19.17 -45.39 -29.36 16.04	16.22 -29.17 -55.40 -39.36 6.030	36.23 -9.163 -35.39 -19.35 26.04

Figure Number	Figure Name	Panel	n	Statistics	p-value	Mean Difference	95% Confidence Interval for Mean	
		B	Pooled from 2-3 chambers per treatment from 5 culture days	Two-way ANOVA, Tukey's post hoc test	0.0001	24.67 -17.88 -42.55 -22.42 20.13	13.76 -28.78 -53.45 -33.33 9.222	35.57 -6.976 -31.64 -11.52 31.03
		C	Pooled from 2-3 chambers per treatment from 5 culture days	Two-way ANOVA, Tukey's post hoc test	0.0001	39.43 -45.49 -84.92 -32.34 52.58	23.71 -61.21 -100.6 -48.06 36.86	55.15 -29.77 -69.20 -16.62 68.30
Figure 4.5	Effect of trichostatin A on microtubule tyrosination following kainic acid treatment	A	3 coverslips from 5 culture days per treatment	Two-way ANOVA	0.3252			
		B	Pooled from 2-3 coverslips per treatment from 5 culture days	Two-way ANOVA	0.8608			
Figure 4.6	Axon degeneration and axon loss after kainic acid treatment in the presence of trichostatin A	A	1-2 coverslips from 4 culture days per treatment	Two-way ANOVA, Tukey's post hoc test	0.0002	-6.744 4.331 7.865	-10.97 0.1066 3.640	-2.519 8.556 12.09

Figure Number	Figure Name	Panel	n	Statistics	p-value	Mean Difference	95% Confidence Interval for Mean	
		B	1-2 coverslips from 4 culture days per treatment	Two-way ANOVA, Tukey's post hoc test	<0.0001 1 1	-17.30 12.46 16.68	-25.41 4.349 8.570	-9.190 20.57 24.79
Figure 4.7	The effect of taxol on microtubule post-translational modifications	A	3 coverslips from 5 culture days per treatment	Two-way ANOVA	<0.0001 1 1	33.59 -11.54 -19.45 -53.04	24.20 -20.94 -28.85 -62.44	42.99 -2.149 -10.06 -43.65
		B	3 coverslips from 5 culture days per treatment	Two-way ANOVA, Tukey's post hoc test	<0.0001 1 1	17.39 35.64 12.02 30.27 18.25	12.01 30.26 6.637 24.88 12.86	22.78 41.02 17.40 35.65 23.63

Table 8.3 Statistical analysis of chapter 5

Figure Number	Figure Name	Panel	n	Statistics	p-value	Mean Differences	95% Confidence Interval for Mean	
Figure 5.1	The effect of kainic acid on microtubule-associated proteins	A	Pooled from 2-3 coverslips per treatment from 4 culture days	One-way ANOVA, Tukey's post hoc test	0.0002	-79.86 -102.9	-144.0 -157.6	-15.75 -48.25
		B	Pooled from 2-3 coverslips per treatment from 4 culture days	Unpaired t-test, two-tailed	0.0043	24.56	11.11	38.02
		C	3 coverslips from 4 culture days per treatment	Unpaired t-test, two-tailed	0.0036	36.39	17.09	55.70
		D	3 coverslips from 4 culture days per treatment	Unpaired t-test, two-tailed	0.4826			
		E	Pooled from 2-3 coverslips per treatment from 4 culture days	Unpaired t-test, two-tailed	0.0005	23.21	14.99	31.43

Figure Number	Figure Name	Panel	n	Statistics	p-value	Mean Differences	95% Confidence Interval for Mean	
		F	Pooled from 2-3 coverslips per treatment from 4 culture days	Unpaired t-test, two-tailed	0.8351			
Figure 5.2	Changes to MAP2 after excitotoxin exposure	A	2 coverslips per treatment from 4 culture days	One-way ANOVA, Tukey's post hoc test	0.0001 0.0001 0.0001 0.0001	-3.112 -2.422 2.380 1.690	-4.442 -3.752 1.050 0.3606	-1.782 -1.093 3.710 3.020
Figure 5.3	Axon degeneration and loss after sodium selenate treatment after kainic acid treatment	A	2 coverslips per treatment from 4 culture days	One-way ANOVA, Tukey's post hoc test	0.0115 0.0115	-3.024 -2.917	-5.477 -5.370	-0.5707 -0.4644
		B	2 coverslips per treatment from 4 culture days	One-way ANOVA, Tukey's post hoc test	0.0004 0.0004	-23.34 -22.04	-34.41 -33.11	-12.26 -10.96
Figure 5.4	Changes to microtubule-associated proteins with trichostatin A treatment after kainic acid treatment	A	3 coverslips from 5 culture days per treatment	Two-way ANOVA, Tukey's post hoc test	<0.0001 <0.0001 <0.0001	-22.41 24.90 23.62	-26.65 20.66 19.38	-18.17 29.14 27.86

Figure Number	Figure Name	Panel	n	Statistics	p-value	Mean Differences	95% Confidence Interval for Mean	
		B	Pooled from 2-3 coverslips per treatment from 5 culture days	Two-way ANOVA	0.0003	-23.70 17.29 14.67	-34.78 6.206 3.592	-12.62 28.36 25.75
		C	3 coverslips from 5 culture days per treatment	Two-way ANOVA, Tukey's post hoc test	0.0009	-18.44 -25.75 -23.81	-33.26 -40.57 -38.62	-3.625 -10.94 -8.990
		D	3 coverslips from 5 culture days per treatment	Two-way ANOVA	0.9695			
Figure 5.5	Changes to microtubule-associated proteins with trichostatin A treatment after kainic acid treatment	A	Pooled from 2-3 coverslips per treatment from 5 culture days	Two-way ANOVA	<0.0001	-17.74 -20.71 -39.10 -21.36 -18.39	-29.81 -32.78 -51.17 -33.43 -30.46	-5.672 -8.642 -27.03 -9.290 -6.320
		B	Pooled from 2-3 coverslips per treatment from 5 culture days	Two-way ANOVA, Tukey's post hoc test	<0.0001	-19.26 -23.84 -23.15	-30.10 -34.68 -33.99	-8.422 -13.00 -12.31

Figure Number	Figure Name	Panel	n	Statistics	p-value	Mean Differences	95% Confidence Interval for Mean	
		C	Pooled from 2-3 coverslips per treatment from 5 culture days	Two-way ANOVA, Tukey's post hoc test	<0.0001	-22.63 -19.67 -24.81 -21.85	-31.06 -28.10 -33.24 -5.465	-14.20 -11.24 -16.38 -13.42
		D	Pooled from 2-3 coverslips per treatment from 5 culture days	Two-way ANOVA, Tukey's post hoc test	<0.0001	-105.7 -93.88 104.2 11.84 -92.39	-114.4 -102.6 95.52 3.128 -101.1	-97.01 -85.17 112.9 20.55 -83.68

8.3 PDF VERSION OF THE HDAC6 INHIBITOR TRICHOSTATIN A ACETYLATES MICROTUBULES AND PROTECTS AXONS FROM EXCITOTOXIN-INDUCED DEGENERATION IN A COMPARTMENTED CULTURE MODEL

frontiers in Neuroscience

ORIGINAL RESEARCH
published: 29 November 2018
doi: 10.3389/fnins.2018.00872

The HDAC6 Inhibitor Trichostatin A Acetylates Microtubules and Protects Axons From Excitotoxin-Induced Degeneration in a Compartmented Culture Model

Kelsey Hanson, Nan Tian, James C. Vickers and Anna E. King*

Wicking Dementia Research and Education Centre, College of Health, University of Tasmania, Hobart, TAS, Australia

Axon degeneration has been implicated as a pathological process in several neurodegenerative diseases and acquired forms of neural injury. We have previously shown that stabilizing microtubules can protect axons against excitotoxin-induced fragmentation, however, the alterations of microtubules following excitotoxicity that results in axon degeneration are currently unknown. Hence, this study investigated whether excitotoxicity affects the post-translational modifications of microtubules and microtubule-associated proteins, and whether reversing these changes has the potential to rescue axons from degeneration. To investigate microtubule alterations, primary mouse cortical neurons at 10 days *in vitro* were treated with 10 or 25 μM kainic acid to induce excitotoxicity and axon degeneration. Post-translational modifications of microtubules and associated proteins were examined at 6 h following kainic acid exposure, relative to axon degeneration. While there were no changes to tyrosinated tubulin or MAP1B, acetylated tubulin was significantly ($p < 0.05$) decreased by 40% at 6 h post-treatment. To determine whether increasing microtubule acetylation prior to kainic acid exposure could prevent axon fragmentation, we investigated the effect of reducing microtubule deacetylation with the HDAC6 inhibitor, trichostatin A. We found that trichostatin A prevented kainic acid-induced microtubule deacetylation and significantly ($p < 0.05$) protected axons from fragmentation. These data suggest that microtubule acetylation is a potential target for axonal protection where excitotoxicity may play a role in neuronal degeneration.

Keywords: microtubule acetylation, trichostatin A, axon degeneration, HDAC6, excitotoxicity

OPEN ACCESS

Edited by:
Irving E. Vega,
Michigan State University,
United States

Reviewed by:
Simone Brogi,
Università degli Studi di Siena, Italy
Franklin David Rumjanek,
Universidade Federal do Rio de Janeiro, Brazil

****Correspondence:***
Kelsey Hanson
kelsey.hanson@utas.edu.au

Specialty section:
This article was submitted to Neurodegeneration, a section of the journal Frontiers in Neuroscience

Received: *31 August 2018*
Accepted: *08 November 2018*
Published: *29 November 2018*

Citation:
Hanson K, Tian N, Vickers JC and King AE (2018) The HDAC6 Inhibitor Trichostatin A Acetylates Microtubules and Protects Axons From Excitotoxin-Induced Degeneration in a Compartmented Culture Model. Front. Neurosci. 12:872. doi: 10.3389/fnins.2018.00872

INTRODUCTION

Axon degeneration is a pathological process that occurs in several neurodegenerative diseases, and acquired forms of brain injury, and can occur independently of cell death (Lingor et al., 2012). The best described mechanisms of axon degeneration are axonal pruning, which occurs during development and Wallerian degeneration, which occurs following axon severing (Coleman, 2005; Coleman and Freeman, 2017). In contrast, the cellular process underlying axon degeneration in a

range of neurodegenerative diseases and following brain injury are less well understood and are unlikely to be linked to direct axonal severing, but rather to a gradual series of biochemical changes following specific disease-associated pathological insults.

One such pathological insult, excitotoxicity, is a result of excessive stimulation by the excitatory neurotransmitter glutamate, leading to, for example, increased intracellular calcium and a cascade of harmful calcium-dependent events (Dong et al., 2009). Excitotoxic mechanisms have been implicated in Alzheimer's disease, traumatic brain injury, stroke, and amyotrophic lateral sclerosis, which all undergo some form of axon degeneration (as reviewed by Gibson and Bromberg, 2012; Lai et al., 2014; Siedler et al., 2014; Lewerenz and Maher, 2015). Our previous studies in compartmentalized cultured neurons have shown that excitotoxicity directed to the neuronal soma results in fragmentation of the unexposed axon (Hosie et al., 2012). This was significantly attenuated by treatment of the axons with the microtubule stabilizing drug, taxol, implicating microtubule disruption in the breakdown of the axon (King et al., 2013).

Microtubules are highly dynamic polymers of alpha and beta tubulin. Their ability to undergo rapid changes in polymerization state (termed dynamic instability) is essential for their function and is controlled by the binding of associate proteins (MAPs) as well as by their post-translational modifications (PTMs) (Horio and Murata, 2014). The microtubule disruption that occurs following excitotoxin exposure and leads to axon degeneration could result from depolymerization, potentially relating to changes to PTM or from altered MAP binding. However, microtubule PTMs and MAP binding are not independent, and some MAP binding capacity to microtubules can be influenced by microtubule PTMs (Howes et al., 2014). PTMs of microtubules include glutamylation, tyrosination, and acetylation. Acetylation, glutamylation and detyrosination are associated with stable microtubules, whereas tyrosination is associated with unstable and more dynamic areas of microtubules (Uchida and Shumyatsky, 2015). Thus, microtubule PTMs may be a potential target for therapeutic intervention. In this regard, drugs targeting acetylation such as HDAC6 (histone deacetylase 6) inhibitors have been investigated for the treatment of depression, cancer, stroke, environmental stress and Huntington's disease (Dompierre et al., 2007; Lazo-Gómez et al., 2013; Simoes-Pires et al., 2013; Jochems et al., 2014; Brindisi et al., 2016, 2018; Ceccacci and Minucci, 2016; Wang et al., 2016; Rao et al., 2017).

In this study we have investigated the temporal changes to microtubule PTMs and MAPs following an excitotoxic insult with a view to modifying microtubule stability to prevent axon degeneration. Furthermore, we also investigated the effect of the HDAC6 inhibitor, trichostatin A, on axon degeneration.

MATERIALS AND METHODS

Ethics and Mice

All experiments and procedures were approved by the University of Tasmania Animal Ethics Committee (A12780 and A15121) and were in accordance with the Australian Guidelines for the Care and Use of Animals for Scientific Purposes. C57Bl/6 mice were housed in optiMICE cages on a 12-h light/dark cycle with free access to food and water.

Primary Cortical Cell Culture

Mouse cortical neuron cultures were prepared as previously described (King et al., 2013). Cortical neurons were prepared from embryonic day 15.5 (E15.5) C57Bl/6 mice. Females were sacrificed using CO_2 and embryos were removed and decapitated. Heads were kept on ice during dissection to prevent tissue degradation. Cortices were removed using a dissecting microscope (Leica), dissociated from the meningeal layers and transferred to 5 ml Hanks Balanced Salt Solution (HBSS, Gibco). Trypsin (0.0125%) was added for 4 min at 37°C, followed by removal of HBSS and replaced with 1 ml of initial plating media [Neurobasal media (Gibco) containing 2% B27 supplement, 0.5 mM glutamine, 25 μM glutamate, 10% fetal calf serum and 1% antibiotic/antimiotic] and mechanically triturated with a 1 ml pipette. Cell density was assessed using a trypan blue exclusion assay and 200,000 cells were plated either into the soma compartment of microfluidic chambers (450 μm long, 10 μm wide, and 3 μm high barrier grooves, Xona Microfluidics), which allows fluidic isolation of cells from the axon (Taylor et al., 2006), or directly into the wells of poly-L-lysine coated culture plates. Cells were allowed to adhere to the coverslip (Livingstone) at 37°C for 30 min prior to adding initial plating media to the chambers and were incubated at 37°C overnight before initial media was replacement with subsequent plating media with no fetal calf serum and glutamate. Cells were grown to 10 days *in vitro* (DIV) at 37°C in 5% CO_2.

Pharmacological Manipulation

Cells were treated with 0, 10, or 25 μM of kainic acid (Sigma, lot #SLBD1491V) in DMSO (Sigma, Lot # RNBF1056) at 10 DIV, a timepoint which corresponds to dense axonal growth in the axon compartment of microfluidic chambers (Hosie et al., 2012; Millet and Gillette, 2012). Cells in 12-well plates or the soma compartment of microfluidic chambers were exposed to kainic acid for 1, 6, and 18 h. For a set of experiments cells were treated with trichostatin A, an inhibitor of the deacetylating enzyme HDAC6, which promotes microtubule acetylation. Cells at 10 DIV in 12-well plates or axonal compartment of microfluidic chambers were treated with 10 or 100 nM trichostatin A (Sigma, Lot # 026M4036V) for 2 h before 6 h of kainic acid exposure prior to ELISA analysis for acetylated tubulin. The health of cells following TSA treatment was not significantly different from vehicle control, as determined using an alamarBlue assay (**Supplementary Figure 1**). For all pharmacological manipulations vehicle controls were performed and are reported. No significant difference was found in any measure for vehicles to untreated cells.

Live Cell Imaging and Quantitation of Axonal Degeneration

Microfluidic cultures were imaged on a Nikon TiE live cell microscope, with chambers maintained at 37°C. Imaging was performed prior to treatment and 18 h following treatment.

Axonal side of the microfluidic chambers were imaged using 40× objective lens to measure axon fragmentation and degeneration. A quantitative measure of axonal degeneration was obtained from five random regions of interest (200 × 200 μm) in the axonal chamber, at least 40 μm away from the microgrooves. Identical regions were imaged before and after treatment. Axon degeneration was calculated by counting degenerated axons. A degeneration index (DI) was determined by the following equation.

$$DI = \left(\frac{\left(\frac{axons\ degenerated\ before}{axons\ degenerated\ after} \right)}{total\ number\ of\ axons} \right) \times 100 \quad (1)$$

The percentage fragmentation refers to the percentage of axons the have fragmented after treatment, compared to the total number of axons before treatment. In our experiments we also analyzed 35, 50, and 100 μM of kainic acid in the cell culture using live imaging, however the axons were too degenerated to be able to target therapeutically.

ELISA Analysis of Microtubule Post-translational Modifications

Plating media was removed from cells plated in 12-well trays, and cultures were rinsed with HBSS. Cells were harvested with RIPA buffer with protease (Complete^{TM} Mini Protease Inhibitor Cocktail tablets, Roche) and phosphatase inhibitors (Phosphatase Inhibitor Cocktail, A.G. Scientific). Samples were centrifuged at 13,000 rpm for 1 min and pellets were discarded. Samples were diluted at 1:300 in 50 μl bicarbonate/carbonate coating buffer (AbCam), added to 96-well plate and incubated overnight at 4°C. For the standard curve, protein samples were serially diluted at 1:100, 1:200, 1:400, and 1:800. A blank and no primary control were included to correct for ELISA results. Plate was washed with washing buffer (0.01M PBS with 0.05% tween-20) prior to blocking with blocking buffer (0.01M PBS with 5% fetal bovine serum) and incubated at 37°C for 30 min. Plates were washed prior to incubation with detecting antibodies (acetylated tubulin 1:500 mouse, Sigma; tyrosinated tubulin 1:500 rabbit, Millipore; tau 1:1,000 rabbit, DAKO; CRMP2 1:1,000 rabbit, Sigma; MAP1B 1:500 mouse, AbCam) diluted in blocking buffer for 1 h at room temperature. Plates were washed and incubated with species-specific HRP secondary antibody (DAKO) diluted in blocking buffer at 1:2,000 and incubated at room temperature for 45 min. Plates were washed and incubated with room temperature tetramethylbenzidine (TMB) substrate (Thermo Scientific, Lot # SA2328991) for 15 min. The reaction was stopped 0.1M H_2SO_4. Plate was read using plate reader at 450 nm.

Western Blot Analysis of Microtubule Post-translational Modifications

Plating media was removed from microfluidic chambers and culture was rinsed with HBSS. Axons were harvested with RIPA buffer with protease (Complete^{TM} Mini Protease Inhibitor Cocktail tablets, Roche) and phosphatase inhibitors (Phosphatase Inhibitor Cocktail, A.G. Scientific), with protein pooled from 2 to 4 chambers per treatment group. Denatured protein samples (20 μg) were electrophoresed into Bolt® 4–12% Bis-Tris gels (Invitrogen), transferred to PVDF membrane (Bio-Rad) and incubated overnight with primary antibodies acetylated tubulin (1:1,000 mouse, Sigma), tyrosinated tubulin (1:1,000 rabbit, Millipore), MAP1B (1:1,000 mouse, AbCam). The corresponding anti-rabbit or anti-mouse horseradish peroxidase conjugated secondary antibody (1:7,000, DAKO) was used as previously described (King et al., 2018). GAPDH (1:5,000 mouse, Millipore) was used as a loading control. Bands were visualized with enhanced chemiluminescence (ECL) solution-Luminata Forte Western horseradish peroxidase (HRP) substrate (Millipore) and images acquired with a Chemi-Smart 5000 Imaging System (Vilber Lourmat) equipped with Chemi-Capt 5000 software. Band intensity was measured as the integrated intensity using Fiji software. After standardizing to GAPDH, each value was calculated as a percentage of control samples (See **Supplementary Figure 1**).

Statistical Analysis

Values were reported as means ± standard error of the mean (SEM), with differences considered significant at $p < 0.05$. Differences for ELISA and axon degeneration counts were evaluated using one-way ANOVA, with Tukey's *post-hoc* test for multiple comparisons between groups. For kainic acid live imaging experiments two coverslips on five separate culture days were analyzed. For trichostatin A live imaging experiments, 1–2 coverslips from four separate culture days were analyzed. For whole cell kainic acid ELISAs, three coverslips per treatment from four separate culture days were used. For whole cell trichostatin A ELISAs, three coverslips per treatment from five separate culture days were used. For axon-only kainic acid ELISAs, cells were pooled from 2 to 3 chambers per treatment from four separate culture days. For axon-only trichostatin A ELISAs, cells were pooled from 2 to 3 chambers per treatment from five separate culture days. All statistical analysis and graphs were prepared in GraphPad Prism (v6.1).

RESULTS

Model of Excitotoxin-Induced Axon Degeneration

Microfluidic chambers allow compartmentalized separation of axons from the somatodendritic compartment, which permits treatment to be applied exclusive to either compartment of the chamber. To establish an acute model of excitotoxin-induced axon degeneration, mouse cortical neurons at 10 DIV were exposed to 10 and 25 μM kainic acid in the somatodendritic compartment for 18 h. Live imaging of axons was performed immediately prior to and post-treatment to determine a degeneration index. Axon loss was significantly increased ($p < 0.05$) at 25 μM kainic acid compared to control (**Figure 1A**). Axonal degeneration at both 10 and 25 μM kainic acid was significantly increased ($p < 0.05$) compared to control (**Figure 1B**).

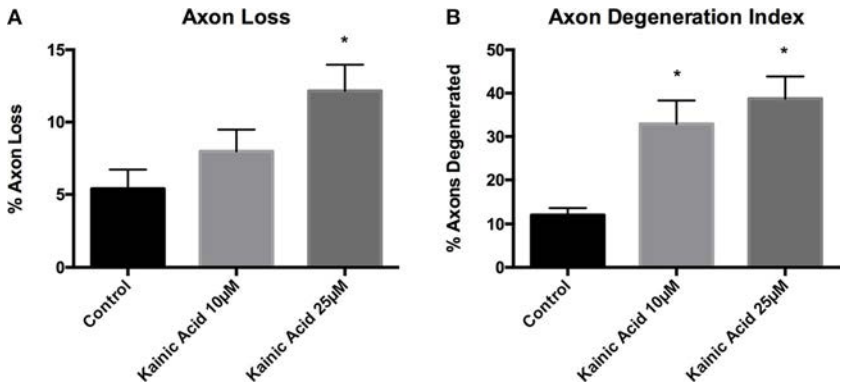

FIGURE 1 | Axon degeneration and loss in microfluidic chambers after kainic acid treatment. Live imaging of the axonal compartment of microfluidic chambers were analyzed for **(A)** axon loss and **(B)** axon degeneration index after treatment with 10 or 25 μM kainic acid. Axon loss was significantly increased ($p < 0.05$) following 25 μM kainic acid treatment relative to control, whereas, 10 μM kainic acid did not cause significant axon loss compared to control. The axon degeneration index was significantly increased ($p < 0.05$) following either 10 or 25 μM doses of kainic acid compared to control. Bar graph represents mean ± SEM *$p < 0.05$ relative to control.

Microtubule Alterations After Excitotoxin-Induced Axon Degeneration

We next determined whether there were changes in microtubule PTMs and the microtubule-associated protein, tau, following 25 μM kainic acid exposure at 1 and 6 h, and whether these changes were related to downstream degeneration (**Figure 2**). Neuronal cells grown on 12-well trays and cells grown in the somatodendritic compartment of microfluidic chambers were exposed to 25 μM kainic acid for 6 h. ELISA analysis of neurons demonstrated that, at 1 h after 25 μM kainic acid treatment, acetylated and tyrosinated tubulin levels were unchanged, however the microtubule associated protein tau was significantly ($p < 0.05$) increased, compared to control (**Figures 2A–C**). At 6 h after 25 μM kainic acid treatment in both neurons and axons, acetylated tubulin levels were significantly ($p < 0.05$) decreased (**Figure 2D**). Tyrosinated tubulin levels were unchanged (**Figure 2E**), whereas, tau levels were also significantly ($p < 0.05$) increased (**Figure 2F**). Western blot analysis of acetylated tubulin levels in axons confirmed these were also significantly ($p < 0.05$) decreased (**Figure 2G**).

Since 25 μM kainic acid treatment affected levels of the microtubule associated protein tau, we examined whether other microtubule associated proteins were altered at 6 h post treatment. Neuronal cells grown on 12-well trays and cells grown in somatodendritic compartment of microfluidic chambers were exposed to 25 μM kainic acid for 6 h. CRMP2 and MAP1B levels in neurons and axons were examined using ELISA. Like tau, CRMP2 was significantly ($p < 0.05$) increased following excitotoxicity (**Figures 3A,C**) and MAP1B was unchanged in both neurons and axons (**Figures 3B,D**).

Trichostatin A and Microtubule Alterations

Since our data showed significantly reduced acetylated tubulin levels in the axon after 25 μM kainic acid treatment (**Figure 2**), we hypothesized that promoting microtubule acetylation could rescue these changes and prevent axon degeneration. To promote microtubule acetylation, trichostatin A was used to inhibit the de-acetylating enzyme HDAC6.

We first determined the concentrations of trichostatin A required to promote acetylation in our primary mouse cortical cultures. ELISA analysis demonstrated that acetylated tubulin levels after 10 and 100 nM trichostatin A were significantly ($p < 0.05$) increased compared to control at 2 h post-treatment (**Figure 4A**).

We next determined whether HDAC6 inhibition with trichostatin A could rescue acetylated tubulin following excitotoxin exposure. Neuronal cells grown on 12-well trays and the axonal compartment of microfluidic chambers were pre-treated with low (10 nM) trichostatin A for 2 h prior to exposure to 25 μM kainic acid. ELISA analysis demonstrated that 10 nM trichostatin A restored acetylated tubulin levels after kainic acid exposure, as compared to control, in both neurons and axons (**Figures 4B,C**). Western blot analysis also demonstrated that 10 nM trichostatin A restored acetylated tubulin levels after excitotoxicity in axons (**Figure 4D**).

Since our results had shown that tau and CRMP2 levels were increased by kainic acid, we examined the effect of trichostatin A on these MAPs. ELISA analysis of neurons demonstrated that 10 nM trichostatin A treatment restored tau to control levels in the presence of kainic acid (**Figure 5B**). However, CRMP2 levels remained significantly ($p < 0.05$) higher following kainic acid in the presence of 10 nM trichostatin A (**Figure 5D**). As we had previously shown, tyrosinated tubulin and MAP1B levels were unaffected by kainic acid and these were also unchanged at 10 nM trichostatin A treatment (**Figures 5A,C**). ELISA analysis of axons also demonstrated that tau levels were restored after 10 nM trichostatin A, and tyrosinated tubulin levels were unchanged (**Figures 5E,F**).

Trichostatin A and Axon Degeneration

We next determined if the rescue of acetylation by trichostatin A treatment following excitotoxin exposure was also protective

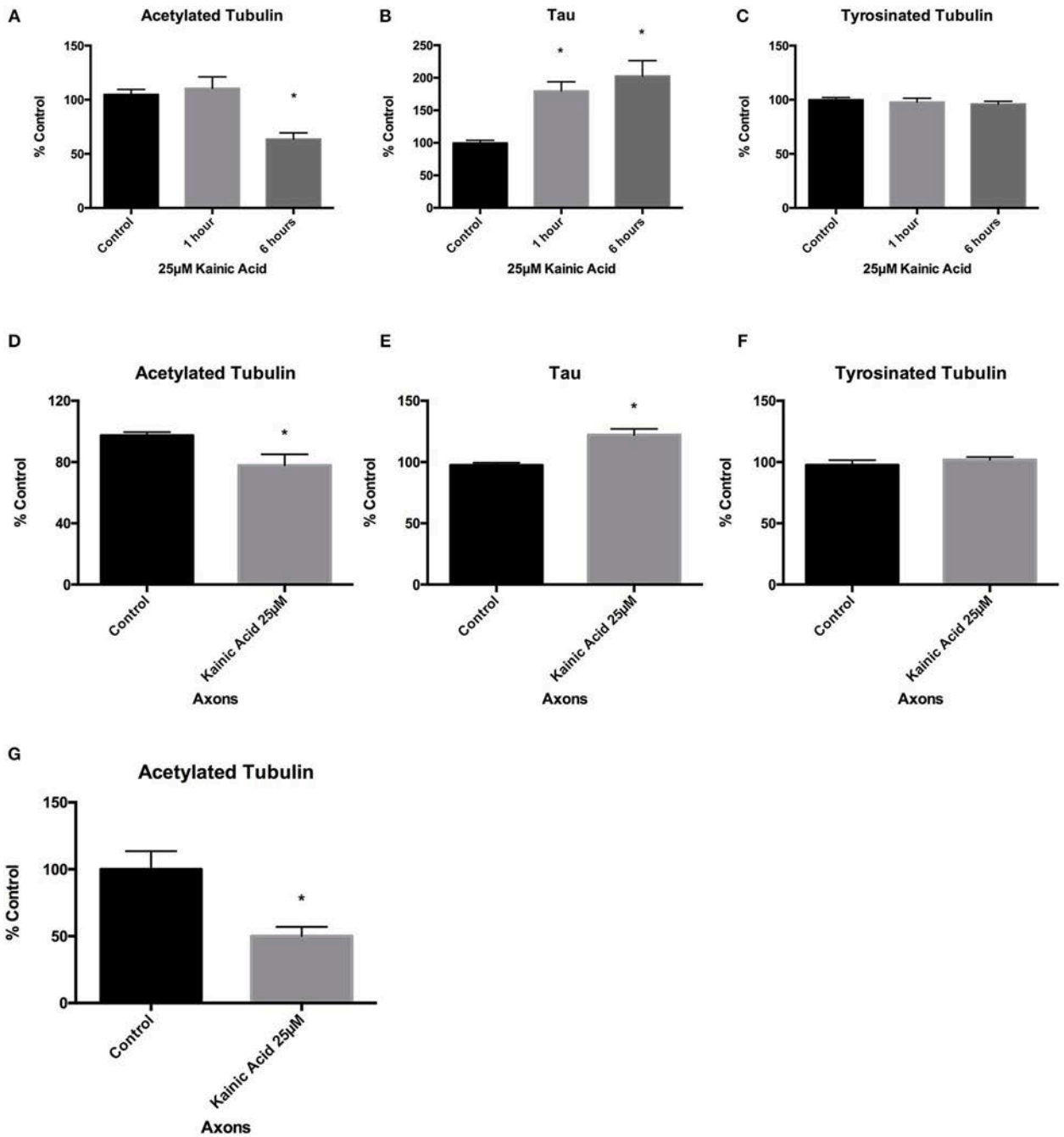

FIGURE 2 | Changes to microtubules after kainic acid treatment. Changes to microtubule post-translational modifications and the microtubule-associated protein tau were investigated in both whole cultured neurons and isolated axons after treatment with 25 μM kainic acid. ELISA analysis of neurons at 1 and 6 h after 25 μM kainic acid treatment showed **(A)** a significant decrease ($p < 0.05$) in acetylated tubulin levels after 6 h and **(B)** a significant decrease ($p < 0.05$) in tau levels at both 1 and 6 h, relative to control. **(C)** Tyrosinated tubulin levels were unchanged compared to control. ELISA analysis of axons at 6 h post treatment with 25 μM kainic acid demonstrated **(D)** significantly decreased ($p < 0.05$) levels of acetylated tubulin, whereas **(E)** tau axonal levels were significantly increased ($p < 0.05$) at this timepoint relative to control. Axonal levels of **(F)** tyrosinated tubulin were unchanged compared to control. To confirm the effect of 25 μM kainic acid on acetylated tubulin in axons Western blot analysis was performed **(G)** demonstrating a significant decrease ($p < 0.05$). Bar graph represents mean ± SEM *$p < 0.05$ relative to control.

against axonal degeneration (**Figure 6**). Neurons were grown in microfluidic chambers and axons exposed to low (10 nM) and high (100 nM) trichostatin A for 2 h prior to somatodendritic treatment with 25 μM kainic acid. Axon degeneration was quantitated from images acquired before and 18 h after kainic acid treatment. In the presence of 10 and 100 nM trichostatin A,

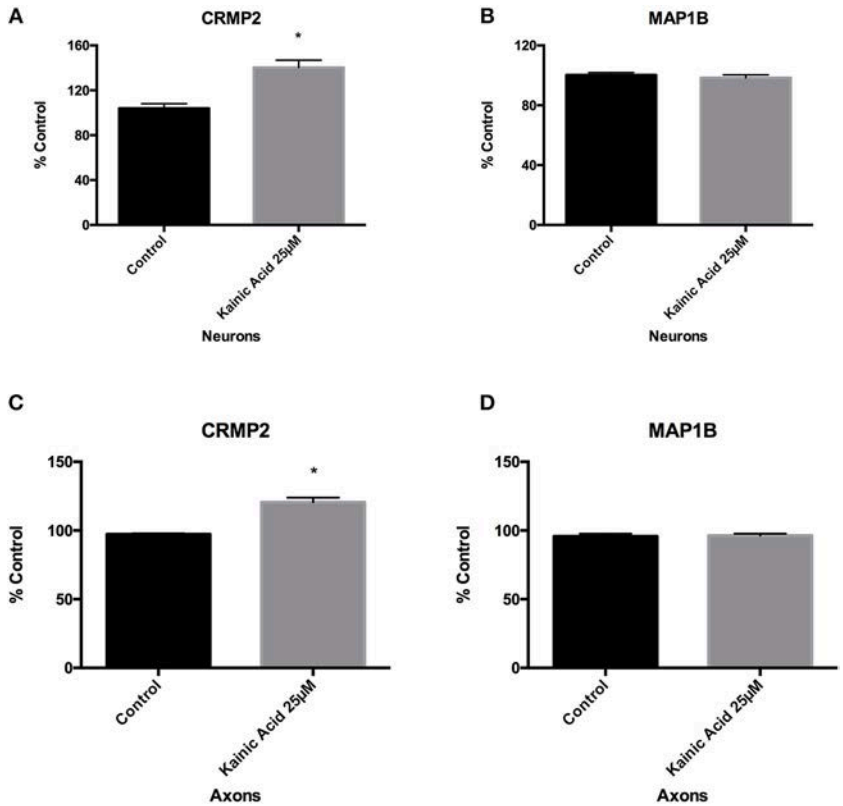

FIGURE 3 | Changes to microtubules associated proteins after kainic acid treatment. Microtubule-associated proteins, CRMP2 and MAP1B levels were analyzed in neurons and axons after 25 μM kainic acid treatment for 6 h. ELISA analysis demonstrated that CRMP2 levels in **(A)** neurons and **(C)** axons were significantly increased ($p < 0.05$) relative to control. ELISA analysis of MAP1B levels in **(B)** neurons and **(D)** axons were unchanged compared to control after 25 μM kainic acid treatment. Bar graph represents mean ± SEM $^*p < 0.05$ relative to control.

axon degeneration (**Figure 6B**) and axon loss (**Figure 6A**) were significantly reduced ($p < 0.05$) after exposure to 25 μM kainic acid.

DISCUSSION

Understanding the mechanisms underlying the relationship between microtubule alterations and axon degeneration can potentially lead to a better understanding of neurodegenerative changes linked to excitotoxicity. The current study investigated whether excitotoxin-induced axon degeneration caused alterations in the post-translational modifications of microtubules and the expression of microtubule-associated protein, tau, and whether inhibition of these biochemical changes to these cytoskeletal proteins can protect axons.

The main finding of this study was that, following excitotoxin exposure, there were changes to both microtubule PTMs and to the levels of MAPs expressed by neurons and that these changes occurred within 6 h of treatment. The key change to PTMs was the acetylation of tubulin which occurred by 6 h and was present in both whole neuron analysis as well as within the axons. The major enzyme involved in tubulin acetylation state in mammals is alpha-tubulin acetyltransferase 1 (αTAT1; Coombes et al., 2016). It is currently unclear whether loss of tubulin acetylation in the current project results from increased deacetylation or from decreased acetylation. Furthermore, downstream processes following kainic acid exposure that result in loss of acetylation are currently not known but will be the subject of future investigations.

In the current study, treatment with trichostatin A prevented decreases in acetylated tubulin levels after kainic acid exposure, consequently reducing axonal fragmentation and axon loss, suggesting that tubulin deacetylation is a key event in excitotoxin induced axon degeneration. Trichostatin A is a HDAC6 inhibitor, which has been investigated in motor neuron degeneration (Yoo et al., 2011; Lazo-Gómez et al., 2013) and used to treat retinal degenerative diseases (reviewed in Zhang et al., 2015). The importance of acetylation in microtubule stability has been widely reported (Howes et al., 2014; Portran et al., 2017). It is known that acetylated tubulin protects microtubules against mechanical aging and is also a marker of long-lived microtubules (Portran et al., 2017). Increasing microtubule acetylation using trichostatin A, has been shown to restore axonal transport in rat cortical neurons, following exposure to mutant leucine-rich repeat kinase (LRRK2) (Godena et al.,

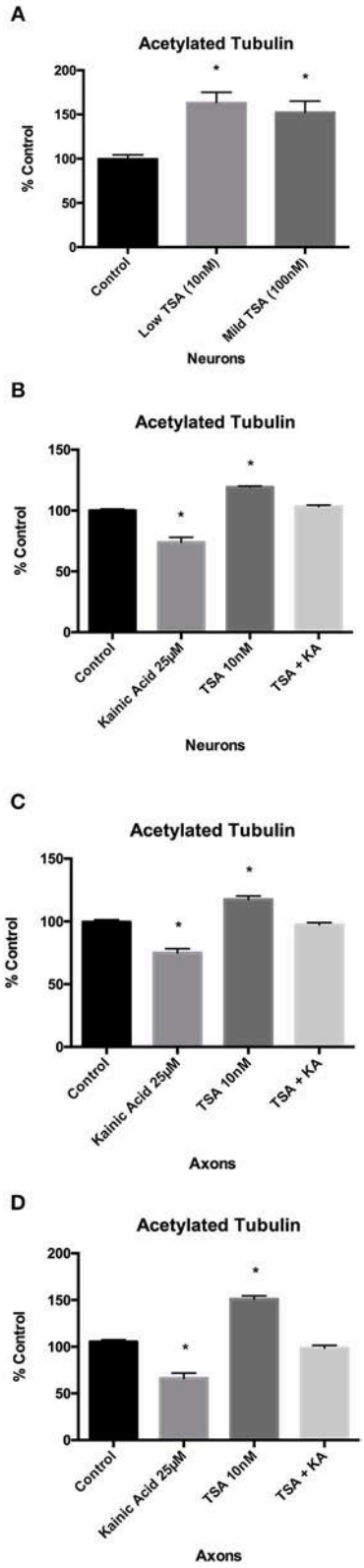

FIGURE 4 | Effect of trichostatin A on microtubule acetylation following kainic acid treatment. Acetylated tubulin levels in whole cultured neurons were analyzed after 10 and 100 nM of trichostatin A treatment for 2 h. **(A)** ELISA analysis of acetylated tubulin levels after 10 or 100 nM trichostatin A demonstrated a significant increase ($p < 0.05$) compared to control. ELISA analysis demonstrated that in **(B)** whole cultured neurons and **(C)** isolated axons, 10 nM trichostatin A inhibited the effect of 25 μM kainic acid on acetylated tubulin levels, and the levels of acetylated tubulin levels in kainic acid treated neurons which had been treated with trichostatin A were not significantly different from control, despite the significant decrease ($p < 0.05$) in acetylated tubulin in cells treated with kainic acid alone. **(D)** To confirm the ELISA analysis of acetylated tubulin levels a Western blot was performed of harvested isolated axons from neurons treated with 25 μM kainic acid in the presence of absence of axonal trichostatin A (10 nM). This confirmed that trichostatin A rescued the decrease in acetylation resulting from kainic acid treatment. Bar graph represents mean ± SEM *$p < 0.05$ relative to control. TSA, trichostatin A; KA, kainic acid.

2014). The same study showed that *in vivo*, trichostatin A treatment or knockdown of HDAC6 and Sir-related protein (SIRT) 2 (Sirt2), rescued axonal transport in a Drosophila model of mutant LRRK2. In cultured mouse cerebellar granule cells, levels of acetylation were compared between Wallerian degeneration slow (Wld^S) mice, which have a mutation that slows Wallerian degeneration (Lunn et al., 1989) and wildtype mice (Suzuki and Koike, 2007). The authors found that base levels of acetylation were increased in Wld^S cells compared to wildtype. Furthermore, the authors showed that the deacetylating enzyme SIRT2 plays a key role in resistance of Wld^S cells to axon degeneration, whereby they found decreased SIRT2 in Wld^S granule cell cytoplasm. Additionally, SIRT2 knockdown enhanced microtubule acetylation and reduced axon degeneration in wildtype granule cells. These findings also highlight the importance of microtubule acetylation in axon degeneration.

Our study also showed that tyrosinated tubulin is unchanged following kainic acid exposure. In contrast to acetylation, which is associated with long-lived microtubules, tyrosination is present in highly dynamic microtubules at the proximal end of the axon (Witte et al., 2008), and has been reported as a destabilizing microtubule PTM (Kreis, 1987; Khawaja et al., 1988). This suggests that destabilizing microtubules through tyrosination is not the key factor in driving excitotoxin-induced axon degeneration. However, in axon regeneration studies, absence of tubulin tyrosine ligase, which promoted tubulin tyrosination, has been shown to severely reduce axon regeneration (Song et al., 2015), suggesting that tubulin tyrosination may be more important for regeneration rather than degeneration. However, PTMs have also been described following developmental axon pruning, which can be modeled *in vitro* by trophic factor withdrawal (reviewed in Saxena and Caroni, 2007). Developmental axon pruning has been shown to involve decreases in both acetylation and tyrosination, with an accompanying increase in detyrosinated tubulin (Unsain et al., 2018).

The microtubule-associated protein, tau, has been implicated in neurodegenerative disease, particularly Alzheimer's disease (AD) and was therefore of interest in this study. In AD, tau has been reported to dissociate from microtubules; thereby

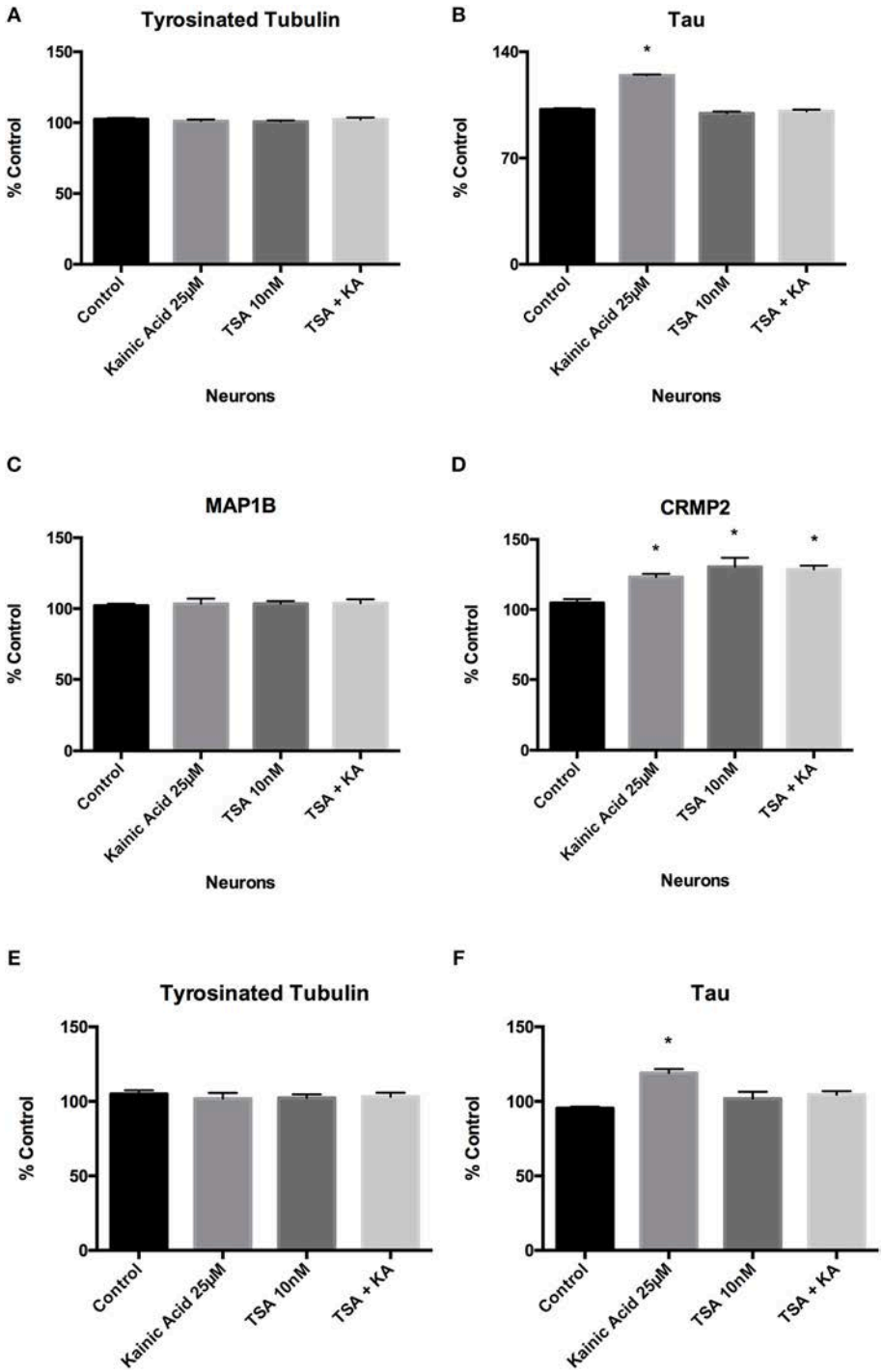

FIGURE 5 | Effect of trichostatin A on tyrosinated tubulin and microtubule-associated proteins following kainic acid treatment. ELISA analysis demonstrated that **(A)** trichostatin A had no effect on neuronal tyrosinated tubulin levels following kainic acid treatment relative to control. **(B)** Trichostatin A rescued kainic acid-induced increases in tau, with no significant difference in tau levels for kainic acid treated cells in the presence of trichostatin A. **(C)** MAP1B levels were unchanged compared to control with any of the treatments. **(D)** CRMP2 levels were significantly increased ($p < 0.05$) relative to control by either treatment with kainic acid or trichostatin A or by kainic acid in the presence of trichostatin A. Tyrosinated tubulin and tau levels were also analyzed in isolated axons after treatment of the neurons with 25 μM kainic acid in the presence or absence of axonal 10 nM trichostatin A. **(E)** Tyrosinated tubulin levels were not significantly different between treatment groups. **(F)** As expected, tau levels were significantly increased ($p < 0.05$) after 25 μM kainic acid treatment, compared to control and this effect was prevented by trichostatin A treatment. Bar graph represents mean ± SEM *$p < 0.05$ relative to control. TSA; trichostatin A, KA; kainic acid.

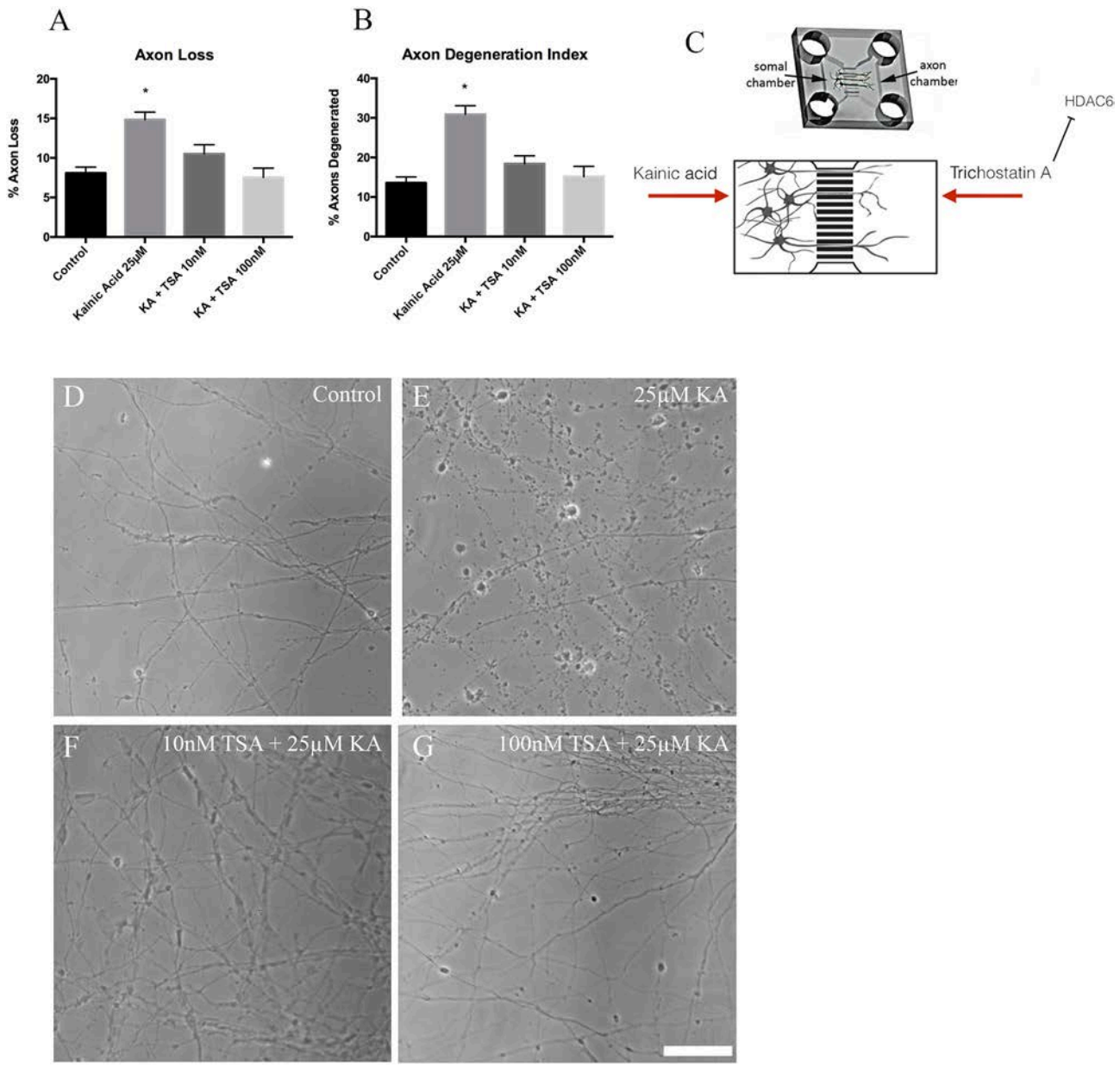

FIGURE 6 | Axon degeneration and axon loss after kainic acid treatment in the presence of trichostatin A. Live images of the axonal compartments of microfluidic chambers were analyzed for **(A)** axon loss and **(B)** axon degeneration after treatment of the neurons with 25 μM kainic acid in the presence or absence of 10 or 100 nM axonal trichostatin A. Both axon loss and axon degeneration were significantly increased ($p < 0.05$) with 25 μM kainic acid treatment, however, this effect was rescued by treatment with either concentration of trichostatin A. In the presence of trichostatin A, axonal loss and degeneration were not significantly different from controls. **(C)** Figure to show how trichostatin A and kainic acid treatment is administered to microfluidic chamber compartments. Representative images for **(D)** control, **(E)** 25 μM kainic acid, **(F)** 10 nM trichostatin A + 25 μM kainic acid and **(G)** 100 nM trichostatin A + 25 μM kainic acid. Bar graph represents mean ± SEM *$p < 0.05$ relative to control. Scale bar = 50 μm. TSA, trichostatin A; KA, kainic acid.

reducing microtubule stability (Sontag et al., 1996; Kadavath et al., 2015). The dissociated tau then aggregates to form tau neurofibrillary tangles; a major hallmark of Alzheimer's disease. However, the exact function of tau in binding to microtubules is not clear. In this study, we showed that tau expression levels were increased following excitotoxicity. Tau was shown to be increased as early as 1 h after kainic acid treatment, suggesting it could be a compensatory mechanism, potentially to increase microtubule stability. The changes in tau prompted us to examine expression levels of other MAPs and we demonstrated that like tau, CRMP2 was increased following excitotoxin exposure. The dysregulation and hyperphosphorylation of CRMP2 has been observed in Alzheimer's disease (Williamson et al., 2011; Hensley and Kursula, 2016). Examining phosphorylation of these MAPs

as well as how these proteins are altered by excitotoxic treatment, will be of interest in future studies.

Alterations to microtubules have also been demonstrated in other forms of axonal injury. For example, dynamic stretch injury of neuronal cultured cells induced axon degeneration, which was inhibited by taxol (Tang-Schomer et al., 2010). This strengthens earlier research in this area, suggesting that cytoskeletal changes begin as early as 5 min post fluid percussive injury (Pettus and Povlishock, 1996), indicating that changes to microtubules could be one of the earliest events to occur after initiating axonal injury and degeneration. Another study which investigated alpha tubulin levels after optic nerve stretch injury found decreased alpha tubulin levels between 0.5 and 4 h post-injury, and a secondary decline after 72 h post-injury (Serbest et al., 2007). This also suggests that microtubules may have an initial role after injury and another role in a secondary event post-injury.

CONCLUSION

Together these data indicate that alterations to microtubule may be an early and modifiable event in several forms of axon degeneration. The earliest change detected, after 1 h of kainic acid treatment, was a significant increase in tau, which was followed by 6 h by a significant decrease in acetylated tubulin and significant increase in CRMP2. These MAPs and PTM are associated with dynamic instability of the microtubules, however tyrosinated tubulin, and MAP1B levels, which are also linked to microtubule stability were unaffected. Together these results suggest that microtubule alterations were specific to the insult. Promotion of microtubule acetylation with trichostatin A treatment, in some cases restored altered levels of PTMs and MAPs to control levels. The current study demonstrates that altering microtubule acetylation can help prevent axon degeneration through excitotoxin exposure. Further deciphering microtubule post-translational modifications and their interaction with degenerating pathways will be important in providing therapeutic treatment in several neurodegenerative diseases.

AUTHOR CONTRIBUTIONS

KH, JV, and AK conceived and designed the experiments; KH and NT performed the experiments; KH analyzed the data; JV and AK contributed reagents, materials, analysis tools, KH, AK, and JV wrote the paper.

FUNDING

NHMRC grant number APP1085221.

ACKNOWLEDGMENTS

JO and JR Wicking Trust (Equity Trustees). Yulgilbar Foundation.

SUPPLEMENTARY MATERIAL

The Supplementary Material for this article can be found online at: https://www.frontiersin.org/articles/10.3389/fnins.2018.00872/full#supplementary-material

Supplementary Figure 1 | (A) Western blots of axons from microfluidic chambers after treatment with 2 h trichostatin A and 6 h somal kainic acid. The Western blots were quantitated in **Figure 4D**. **(B)** alamarBlue cell viability assay after treatment with trichostatin A for 2 h and **(C)** after 6 h kainic acid treatment. Bar graph represents mean ± SEM $^{**}p < 0.01$; $^{****}p < 0.001$ relative to control. TSA, trichostatin A; KA, kainic acid.

REFERENCES

Brindisi, M., Cavella, C., Brogi, S., Nebbioso, A., Senger, J., Maramai, S., et al. (2016). Phenylpyrrole-based HDAC inhibitors: synthesis, molecular modelling and biological studies. *Future Med. Chem.* 8, 1573–1587. doi: 10.4155/fmc-2016-0068

Brindisi, M., Senger, J., Cavella, C., Grillo, A., Chemi, G., Gemma, S., et al. (2018). Novel spiroindoline HDAC inhibitors: synthesis, molecular modelling and biological studies. *Eur. J. Med. Chem.* 157, 127–138. doi: 10.1016/j.ejmech.2018.07.069

Ceccacci, E., and Minucci, S. (2016). Inhibition of histone deacetylases in cancer therapy: lessons from leukaemia. *Br. J. Cancer* 114, 605–611. doi: 10.1038/bjc.2016.36

Coleman, M. (2005). Axon degeneration mechanisms: commonality amid diversity. *Nat. Rev. Neurosci.* 6, 889–898. doi: 10.1038/nrn1788

Coleman, M. P., and Freeman, M. R. (2017). Wallerian degeneration, $Wlds^S$ and nmnat. *Annu. Rev. Neurosci.* 33, 245–267. doi: 10.1146/annurev-neuro-060909-153248

Coombes, C., Yamamoto, A., McClellan, M., Reid, T. A., Plooster, M., Luxton, G. W. G., et al. (2016). Mechanism of microtubule lumen entry for the α-tubulin acetyltransferase enzyme αTAT1. *Proc. Natl. Acad. Sci. U.S.A.* 113, E7176–E7184. doi: 10.1073/pnas.1605397113

Dompierre, J. P., Godin, J. D., Charrin, B. C., Cordelières, F. P., King, S. J., Humbert, S., et al. (2007). Histone deacetylase 6 inhibition compensates for the transport deficit in Huntington's disease by increasing tubulin acetylation. *J. Neurosci.* 27, 3571–3583. doi: 10.1523/JNEUROSCI.0037-07.2007

Dong, X. P., Wang, Y., and Qin, Z. H. (2009). Molecular mechanisms of excitotoxicity and their relevance to pathogenesis of neurodegenerative diseases. *Acta Pharmacol. Sin.* 30, 379–387. doi: 10.1038/aps.2009.24

Gibson, S. B., and Bromberg, M. B. (2012). Amyotrophic lateral sclerosis: drug therapy from the bench to the bedside. *Semin. Neurol.* 32, 173–178. doi: 10.1055/s-0032-1329193

Godena, V. K., Brookes-Hocking, N., Moller, A., Shaw, G., Oswald, M., Sancho, R. M., et al. (2014). Increasing microtubule acetylation rescues axonal transport and locomotor deficits caused by LRRK2 Roc-COR domain mutations. *Nat. Commun.* 5:5245. doi: 10.1038/ncomms6245

Hensley, K., and Kursula, P. (2016). Collapsin response mediator protein-2 (CRMP2) is a plausible etiological factor and potential therapeutic target in Alzheimer's disease: comparison and contrast with microtubule-associated protein tau. *J. Alzheimer's Dis.* 53: 1–14. doi: 10.3233/JAD-160076

Horio, T., and Murata, T. (2014). The role of dynamic instability in microtubule organization. *Front. Plant Sci.* 5:511. doi: 10.3389/fpls.2014.00511

Hosie, K. A., King, A. E., Blizzard, C. A., Vickers, J. C., and Dickson, T. C. (2012). Chronic excitotoxin-induced axon degeneration in a compartmented neuronal culture model. *ASN Neuro.* 4, 47–57. doi: 10.1042/AN20110031

Howes, S. C., Alushin, G. M., Shida, T., Nachury, M. V., and Nogales, E. (2014). Effects of tubulin acetylation and tubulin acetyltransferase binding on microtubule structure. *Mol. Biol. Cell*. 25, 257–266. doi: 10.1091/mbc.e13-07-0387

Jochems, J., Boulden, J., Lee, B. G., Blendy, J. A., Jarpe, M., Mazitschek, R., et al. (2014). Antidepressant-like properties of novel HDAC6-selective inhibitors with improved brain bioavailability. *Neuropsychopharmacology* 39, 389–400. doi: 10.1038/npp.2013.207

Kadavath, H., Hofele, R. V., Biernat, J., Kumar, S., Tepper, K., Urlaub, H., et al. (2015). Tau stabilizes microtubules by binding at the interface between tubulin heterodimers. *Proc. Natl. Acad. Sci. U.S.A.* 112, 7501–7506. doi: 10.1073/pnas.1504081112

Khawaja, S., Gundersen, G. G., and Bulinkski, J. C. (1988). Enhanced stability of microtubules enriched in detyrosinated tubulin is not a direct function of detyrosination level. *J. Cell Biol.* 106, 141–149. doi: 10.1083/jcb.106.1.141

King, A., Brain, A., Hanson, K., Dittmann, J., Vickers, J., and Fernandez-Martos, C. (2018). Disruption of leptin signalling in a mouse model of Alzheimer's disease. *Metab. Brain Dis.* 33, 1097–1110. doi: 10.1007/s11011-018-0203-9

King, A. E., Southam, K. A., Dittmann, J., and Vickers, J. C. (2013). Excitotoxin-induced caspase-3 activation and microtubule disintegration in axons is inhibited by taxol. *Acta Neuropathol. Commun.* 1:59. doi: 10.1186/2051-5960-1-59

Kreis, T. E. (1987). Microtubules containing detyrosinated tubulin are less dynamic. *EMBO J.* 6, 2597–2606. doi: 10.1002/j.1460-2075.1987.tb02550.x

Lai, T. W., Zhang, S., and Wang, Y. T. (2014). Excitotoxicity and stroke: identifying novel targets for neuroprotection. *Prog. Neurobiol.* 115, 157–188. doi: 10.1016/j.pneurobio.2013.11.006

Lazo-Gómez, R., Ramírez-Jarquín, U. N., Tovar-y-Romo, L. B., and Tapia, R. (2013). Histone deacetylases and their role in motor neuron degeneration. *Front. Cell. Neurosci.* 7:243. doi: 10.3389/fncel.2013.00243

Lewerenz, J., and Maher, P. (2015). Chronic glutatmate toxicity in neurodegenerative diseases – what is the evidence? *Front. Neurosci.* 9:469. doi: 10.3389/fnins.2015.00469

Lingor, P., Kock, J. C., Tönges, L., and Bähr, M. (2012). Axonal degeneration as a therapeutic target in the CNS. *Cell Tissue Res.* 349, 289–311. doi: 10.1007/s00441-012-1362-3

Lunn, E. R., Perry, V. H., Brown, M. C., Rosen, H., and Gordon, S. (1989). Absence of Wallerian degeneration does not hinder regeneration in peripheral nerve. *Euro. J. Neurosci.* 1, 27–33. doi: 10.1111/j.1460-9568.1989.tb00771.x

Millet, L. J., and Gillette, M. U. (2012). New perspectives on neuronal development via microfluidic environments. *Trends Neurosci.* 35, 752–761. doi: 10.1016/j.tins.2012.09.001

Pettus, E. H., and Povlishock, J. T. (1996). Characterization of a distinct set of intra-axonal ultrastructural changes associated with traumatically induced alteration in axolemmal permeability. *Brain Res.* 722, 1–11. doi: 10.1016/0006-8993(96)00113-8

Portran, D., Schaedel, L., Xu, Z., Théry, M., and Nachury, M. V. (2017). Tubulin acetylation protects long-lived microtubules against mechanical aging. *Nat. Cell Biol.* 19, 391–398. doi: 10.1038/ncb3481

Rao, A. N., Patil, A., Brodnik, Z. D., Qiang, L., Espana, R. A., Sullivan, K. A., et al. (2017). Pharmacologically increasing microtubule acetylation corrects stress-exacerbated effects of organophosphates on neurons. *Traffic* 18, 433–441. doi: 10.1111/tra.12489

Saxena, S., and Caroni, P. (2007). Mechanisms of axon degeneration: from development to disease. *Prog. Neurobiol.* 83, 174–191. doi: 10.1016/j.pneurobio.2007.07.007

Serbest, G., Burkhardt, M. F., Siman, R., Raghupathi, R., and Saatman, K. E. (2007). Temporal profiles of cytoskeletal protein loss following traumatic axonal injury in mice. *Neurochem. Res.* 32, 2006–2014. doi: 10.1007/s11064-007-9318-9

Siedler, D. G., Chuah, M. I., Kirkcaldie, M. T. K., Vickers, J. C., and King, A. E. (2014). Diffuse axonal injury in brain trauma: insights from alterations in neurofilaments. *Front. Cell. Neurosci.* 8:429. doi: 10.3389/fncel.2014.00429

Simoes-Pires, C., Zwick, V., Nurisso, A., Schenker, E., Carrupt, P. A., and Cuendet, M. (2013). HDAC6 as a target for neurodegenerative diseases: what makes it different from the other HDACs? *Mol. Neurodegener.* 8:7. doi: 10.1186/1750-1326-8-7

Song, W., Yongcheol, C., Watt, D., and Cavalli, V. (2015). Tubulin-tyrosine ligase (TTl)-mediated increase in tyrosinated alpha-tubulin in injured axons is required for retrograde injury signaling and axon regeneration. *J. Biol. Chem.* 290, 14765–14775. doi: 10.1074/jbc.M114.622753

Sontag, E., Nunbhakdi-Craig, V., Lee, G., Bloom, G. S., and Mumby, M. C. (1996). Regulation of the phosphorylation state and microtubule-binding activity of tau by protein phosphatase 2A. *Neuron* 17, 1201–1207. doi: 10.1016/S0896-6273(00)80250-0

Suzuki, K., and Koike, T. (2007). Mammalian sir2-related protein (SIRT) 2-mediated modulation of resistance to axonal degeneration in slow Wallerian degeneration mice: a crucial role of tubulin deacetylation. *Neuroscience* 147, 599–612. doi: 10.1016/j.neuroscience.2007.04.059

Tang-Schomer, M. D., Patel, A. R., Baas, P. W., and Smith, D. H. (2010). Mechanical breaking of microtubules in axons during dynamic stretch injury underlies delayed elasticity, microtubule disassembly, and axon degeneration. *FASEB J.* 24, 1401–1410. doi: 10.1096/fj.09-142844

Taylor, A. M., Rhee, S. W., and Jeon, N. L. (2006). Microfluidic chambers for cell migration and neuroscience research. *Methods Mol. Biol.* 321, 167–177. doi: 10.1385/1-59259-997-4:167

Uchida, S., and Shumyatsky, G. P. (2015). Deceivingly dynamic: learning-dependent changes in stathmin and microtubules. *Neurobiol. Learn. Mem.* 214, 52–61. doi: 10.1016/j.nlm.2015.07.011

Unsain, N., Bordenave, M. D., Martinez, G. F., Jalil, S., von Bilderling, C., Barabas, F. M., et al. (2018). Remodeling of the actin/spectrin membrane-associated periodic skeleton, growth cone collapse and F-actin decrease during axonal degeneration. *Sci. Rep.* 8:3007. doi: 10.1038/s41598-018-21232-0

Wang, Z., Hu, P., Tang, F., Lian, H., Chen, X., Zhnag, Y., et al. (2016). HDAC6 promotes cell proliferation and confers resistance to temozolomide in glioblastoma. *Cancer Lett.* 379, 134–142. doi: 10.1016/j.canlet.2016.06.001

Williamson, R., van Aalten, L., Mann, D. M., Platt, B., Plattner, F., Bedford, L., et al. (2011). CRMP2 hyperphosphorylation is characteristic of Alzheimer's disease and not a feature common to other neurodegenerative diseases. *J. Alzheimer's Dis.* 27, 615–625. doi: 10.3233/JAD-2011-110617

Witte, H., Neukirchen, D., and Bradke, F. (2008). Microtubules stabilization specifies initial neuronal polarization. *J. Cell Biol.* 180, 619–632. doi: 10.1083/jcb.200707042

Yoo, D. Y., Kim, W., Nam, S. M., Kim, D. W., Chung, J. Y., Choi, S. Y., et al. (2011). Synergistic effects of sodium butyrate, a histone deacetylase inhibitor, on increase of neurogenesis induced by pyridoxine and increase of neural proliferation in the mouse dentate gyrus. *Neurochem. Res.* 36, 1850–1857. doi: 10.1007/s11064-011-0503-5

Zhang, F., Su, B., Wang, C., Siedlak, S. L., Mondragon-Rodriguez, S., Lee, H. G., et al. (2015). Posttranslational modifications of alpha-tubulin in Alzheimer's disease. *Transl. Neurodegener.* 4:9. doi: 10.1186/s40035-015-0030-4

Conflict of Interest Statement: The authors declare that the research was conducted in the absence of any commercial or financial relationships that could be construed as a potential conflict of interest.